APPENDIX 1 – the project

Daniel Fritch, Jörg Baumgärtner, Nicolas Cuenot, Jean-Jacques Graff, Albert Genter, 2008, The Soultz EGS pilot plant: energy heat and power from deep Enhanced Geothermal Systems, presented at *3rd. International Conference on Ecological Vehicles and Renewable Energies*, Monaco, 27-30 March, 2008.

EVER MONACO 2008
March 27 - 30

Third International Conference on
Ecological Vehicles & Renewable Energies

The Soultz EGS pilot plant: energy heat and power from deep Enhanced Geothermal Systems

Daniel Fritsch
EEIG Heat Mining
Route de Soultz, BP38, F-67250 Kutzenhausen, France
E-mail: fritsch@soultz.net

Jörg Baumgaertner
Bestec GmbH
Landauer Str. 28, D-76870 Kandel, Germany
E-mail: baumgaertner@bestec-for-nature.com

Nicolas Cuenot
EEIG Heat Mining
E-mail: cuenot@soultz.net

Jean-Jacques Graff
EEIG Heat Mining
E-mail: graff@soultz.net

Albert Genter
EEIG Heat Mining
E-mail: genter@soultz.net

Abstract: *This paper reports a multinational approach to develop an Enhanced Geothermal System reservoir (EGS) which is a promising way for the production of geothermal heat and power. The pilot site is located at the French-German border in Soultz-sous-Forêts. Over two decades research and development have been carried out with governmental and European funding, as well as with France and Germany. The deep wells system today consists of three wells with more than 5000 m depth each. Stimulation and circulation tests with three wells have been completed successfully from 2000 to 2005 and hydraulic performance has been improved in the year 2006. Partners of the Soultz consortium today are EDF, Electricité de Strasbourg, EnBW Energie Baden-Württemberg AG, Pfalzwerke AG and Evonik AG. Associated within an EEIG (European Economic Interest Grouping) called "Exploitation Minière de la Chaleur" the partners now are going to install a geothermal power plant and start generation of geothermal power in 2008.*

Keywords: Enhanced Geothermal Systems, Geothermal power plant, Electricity production, Upper Rhine Valley.

1. Introduction

Today, the geothermal resource is already locally exploited in some favourable places where three conditions are superimposed: (1) the demand of local consumers, (2) temperature increasing with depth fast enough to reach at minimum cost the value corresponding to the

consumers' demand and (3) a water productive aquifer system called also a natural geothermal reservoir lying at the required depth.
Even if the two first conditions coincide on a large proportion of inhabited regions, the third one is only fulfilled with a quality high enough in few places. Consequently today the challenge is to develop geothermal exploitation in the large regions where there is both an economic demand and where the required temperatures are accessible at minimum depth, despite a random distribution of the local water productive features within the highly heterogeneous regional natural reservoirs lying in these regions.
The basic common observation leading to solve this apparently difficult equation is the fact these temperature increases with depth faster than "normal" in vast European regions (fig.1). This phenomenon implies that deep regional water convective loops are transferring the heat towards surface faster than normal in that regions and consequently that deep permeable fracture fields are existing here and could be economic targets.
Unfortunately it was also observed that except in some locally highly favourable situation, the drainage of that relatively dispersed water resources towards surface plants was not an easy task and required a special technology.

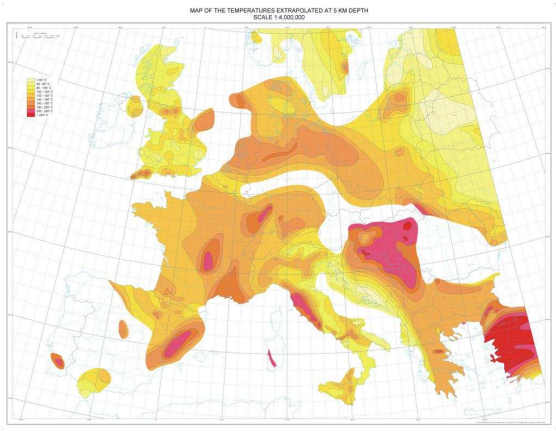

Figure 1: Expected temperatures at 5 km depth in Western Europe [1]. Several hot spots occur.

2. The EGS concept

The technology today under promising developments in Europe at Soultz (France) or in Landau (Germany), in USA, in Australia and through other local experiences is named EGS (Enhanced Geothermal Systems). The EGS concept consists simply of drilling at least two boreholes into deep fractured rocks, extracting hot fluid from a production well and injecting the cooled fluid back into the fractured reservoir through an injection well. Generally both boreholes have been stimulated permitting to connect the two wells to the natural surrounding geothermal fractured reservoir by enhancing the permeability [2]. This may imply some direct connections between the wells through natural fractures. Contrary to conventional hydrothermal reservoirs, Enhanced Geothermal Systems require stimulation, since the rock mass permeability in the vicinity of the boreholes is generally too low for economic heat recovery.

3. The EGS potential capacities

A- Evaluation of the EGS potential

Using the temperature map extrapolated to depths of 5 km, an estimation of the EGS potential in Europe has been calculated [1]. The hottest surfaces, that are those where the temperature is higher than 180ºC, have been determined for 16 countries. In Europe, it is Hungary, France, Serbia, Italy and Croatia which top the list of nations with high geothermal potential. Although the estimation for Turkey has only been done for its Western part, it has a very high geothermal potential. As far as the EGS potentialities are concerned, countries like Romania, Germany, Austria, Slovakia and Bosnia come next in the list of European countries. However, their potential is probably underestimated because the temperature map is not systematically documented, for example for the perimeter of the Pannonian Basin (Hungary).

B- EGS power production

From the estimated potential values considered as renewable reserves, it is possible to estimate the permanent power production capacities. As an example, we can consider that the Western European EGS potential (without Turkey) is estimated at ~ 21 500 GW year or 180 000 TWh. Assuming we could exploit during around 20 years a first series of plants addressing around 10% of that reserve, i.e. 18 000 TWh, it could be possible to get a yearly base load electricity production capacity of around 900 TWh for Western Europe. After 20 years, the plant costs being amortised, other units could be deployed on the most favourable sites selected within the 90% remaining surfaces.

4. The Soultz EGS project

A- The motivations and the related organisation

The Soultz site was selected on the base of studies previously performed [3, 4] showing a typical thermal effect generated by convective water loops in that area. Deep conditions on that place were considered as being representative enough for the "Rhine graben" region to propose a feasibility study [5] aiming at the recognition of the deep natural fractures network and of its hydraulic properties [6, 7]. The programme included the validation of the required technologies for drilling and for the development of the connections between the wells and the neighbouring permeable fractures [8, 9, 10]. That study was carried out through a first series of tests up to 2001 as they are summarised on the table 1.

Table 1: Milestones in the implementation of the Soultz EGS project between 1984 and 2000.

Year	Milestones
1984	First formal draft of the Soultz project.
1987	Drilling of the first well (GPK1) to 2000 m.
1990	Creation of a network of medium depth (~ 1500 m) observation wells using old oil wells and detailed exploration down to 2250 m by deepening and continuous coring of an existing well (EPS1).
1992	Deepening of GPK1 to 3600 m; temperature measured: 165°C.
1995	Drilling of the second well (GPK2) to 3878 m (horizontal distance between wells: 450 m).
1997	Successful circulation test (25 kg/s) between GPK1-GPK2 wells over a four-month period (production temperature ~140°C).
2000	Deepening of GPK2 to 5010 m; temperature: 203°C. Open-hole stimulation between 4.5 km and 5 km.

The results of these tests demonstrated clearly that:
- It is possible to develop the productivities of the wells in that region up to values making possible to expect a balance positive enough between the power produced and the power required for pumping to provide a large net energy output;
- Temperatures high enough for economic power steam or heat productions are reachable in that kind of terrain within a depth range 1500 - 5000 m by reasonably cheap and safe conventional drilling technologies.

Consequently, five industrial partners (EDF, Electricité de Strasbourg, Shell, ENEL and Pfalzwerke) associated within an EEIG (European Economic Interest Grouping) called "Exploitation Minière de la Chaleur", supported by three public funding agencies (EC, ADEME for France and BMU for Germany) and eight scientific partners (or groups of partners such as CNRS) decided to build a pilot plant at the same location at Soultz. This pilot plant aims at the validation of the technologies at their highest difficulty level (-5000 m depth) but also being the most promising for a future general exploitation of the geothermal resources through plants locally optimised depending from the users' requirements. The pilot plant programme includes two phases (see table 2):
- the first one (2001-2004) was mostly consisting in building and preliminary testing of the deep underground equipment;
- the second one (2004-2008) is still undergoing and it aims at a full mastering of the geothermal production and power generations technologies towards their future industrial deployment.

At Phase I termination (2001-2004), Shell and ENEL left the EEIG, but it still includes five members because it was joined by EnBW and Evonik for participation within Phase II (2004-2008).

Table 2: Milestones in the implementation of the Soultz EGS project between 2001 and 2008.

Year	Milestones
2001	Decision to build an EGS Pilot Plant at Soultz.
2002	Drilling to 5 km of well GPK3, in the immediate vicinity of GPK2. Horizontal distance between open holes GPK2-GPK3: about 650 m.
2003/2004	Open-hole stimulation in GPK3 and circulation tests between GPK3 and GPK2. Drilling to 4985 m of well GPK4.
2004/2005	Open-hole stimulation in GPK4, followed by circulation tests between the central injection well (GPK3) and the two lateral production wells GPK2 and GPK4.
2006	Improvement of the wells hydraulic performances (chemical stimulation).
2006/2008	Geothermal production and power generation.

B- The present status of the EGS pilot plant

5 deep boreholes were drilled at the geothermal site into the granite basement (Tables 1, 2). One is 3600 m deep, one is 2200 m deep and the three others reach 5000 m depth (fig. 2). All have been at least once stimulated to improve their connection to the fractures network.

GPK2 (in blue), GPK3 (in red) and GPK4 (in purple) reach a depth of around 5 km and form the geothermal triplet. GPK2 and GPK4 are set as production boreholes and GPK3 is used to re-inject the cooled water, once its calories have been collected. The wellheads of the GPK-2, -3 and -4 are only 6 m far apart from each other, while there is a horizontal distance of roughly 650 m between each bottom hole: this allows the water circulating on rather long pathways in contact with hot crystalline rocks, so that it could be reheated before being pumped again. Such requirements implied that the boreholes' trajectories have to be deviated from the vertical (fig. 2).

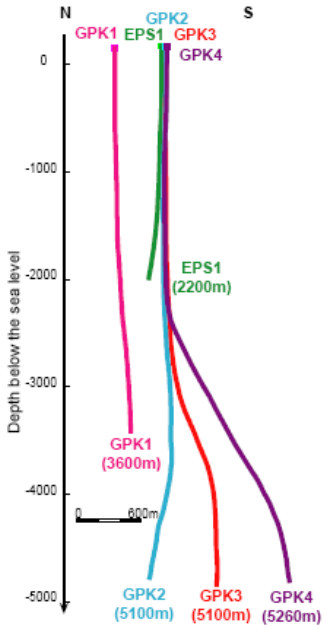

Figure 2: Vertical N-S cross-section of the borehole trajectories at Soultz from [7].

In order to develop the permeability at depth, two kinds of stimulations were tested at Soultz to enhance the hydraulic performance of the geothermal system. The "classical" treatment is the hydraulic stimulation. More recently we also tried to perform chemical stimulations. Hydraulic stimulations consist in injecting large volume of water (several thousands of cubic meters) at high flow rates (generally, more than 40 l/s). After each drilling operation, a hydraulic stimulation was performed in order to improve the connection of the borehole to the network of fractures. The direct consequence of hydraulic stimulation is induced microseismicity. On one hand, this could have a negative impact on the population, as some of the earthquakes of larger magnitude (generally higher than 2) can be felt in the surroundings, but on the other hand, induced microseismicity is a mean to monitor the effectiveness of the treatment. The highest density of microseismic events is observed in the vicinity of the bottom holes, meaning that hydraulic stimulations are mostly effective in that area [11, 12]. As the hydraulic performances of the boreholes were not at the expected level after all hydraulic stimulations, so that further improvement was necessary, and taking into account that we had to limit the seismic activity, we performed several chemical stimulations [13, 14]. The goal is to try to dissolve the natural hydrothermal deposits sealing the fractures. Therefore a small proportion of chemicals is added to the injected water. After all hydraulic and chemical stimulation tests, improvements of hydraulic performances of the boreholes have been made mainly in the production wells (GPK2, GPK4). Even though the productivity index of GPK3 does not reach the expected value, it was decided to continue with the building of the power plant and perform the next circulation test with a power output.

5. Power Production at Soultz

Based on the above exploration and developments, it was decided to test a first conversion module of 1.5 MWe. The different components of the power plant are installed by the end of 2007 and power production should begin in April 2008.

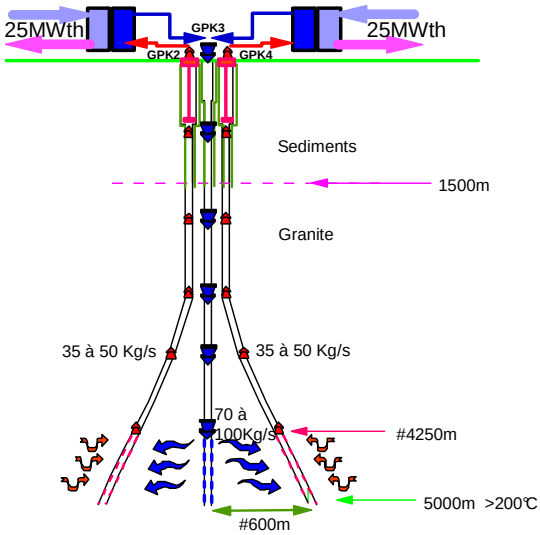

Figure 3: Principle of the geothermal power plant developed at Soultz.

Figure 3 presents the basic concept of the geothermal pilot plant as it is expected to run. If a production flow rate of 70-100 l/s is reached, corresponding to a maximal thermal power

output of roughly 50 MW, the power plant could deliver around 5 MW of electrical power. To reach this goal, it is necessary to install production pumps into the boreholes, because the artesian flow rates are not sufficient. 2 types of production pumps will be tested: a Line Shaft Pump (LSP) and a Electro-Submersible Pump (ESP). With the LSP, the pump itself is in the well, the motor is at surface and the connection is done through a line shaft. The main advantage is to avoid installing the motor in hot brine, but there are mechanical risks with the line shaft, which has to be perfectly aligned. Issues related to corrosion/scaling and lubrication of the shaft should also be carefully studied. The pump should be installed at 350 m depth into GPK2, which presents good verticality and is the best producer. With the ESP, both the pump and its motor are installed into the well. The technology is well-known for standard conditions, but the problem is to adapt the pump to geothermal conditions at rather high temperatures (200°C): metallurgy and resistance to corrosion require a specific design. Another crucial issue is the cooling of the motor, which can only be done by the hot geothermal fluid. The pump should be installed at 500 m depth in GPK4, which is the lower productive well.

Figure 4: Installation of the air cooling system.

Due to the quality of the geothermal brine (high salt content and corrosive compounds), it cannot be vaporized and thus cannot feed directly the turbine. The produced heat shall be transferred to a secondary circuit which involves a low boiling point working fluid. This is the principle of binary cycles. Two kinds of binary cycles were studied for the case of the Soultz-sous-Forêts project: Organic Rankine Cycle (ORC) and Kalina Cycle. Even though Kalina cycle has a higher efficiency, the technology is far more complex than ORC cycles. As the purpose of the project is first to demonstrate the feasibility of power production with such a system, the ORC technology has been preferred. In ORC binary plants, the working fluids are mostly organic fluids. Here isobutane was proposed by the supplier of the ORC system. As there is no easily accessible shallow aquifer around the geothermal site, an air-cooling system was required for the power plant, which also limits the impact on environment. It consists in a 9-fans system. Figure 4 shows the air cooling system. The turbine (fig. 5) is radial and should operate at around 13000 rpm. The generator (fig. 6) is asynchronous and is running at around 1500 rpm. A gearbox is installed between the two. The generator shall deliver 11 kV and the produced power will be injected into the 20 kV local network.

Figure 5: View inside the turbine.

Figure 6: Generator aligned with the turbine.

The system is built so that the production coming from each well or both can easily be used to feed either the power production loop or the testing loop. If the sustainability of the production is established, then one ORC unit could be added to increase the power production of the plant.

6. Conclusions

After 20 years of extensive research, the Soultz project is about to deliver its first power production. The success of the demonstration power plant could open the way for a new kind of geothermal power plants using the heat stored in deep, fractured crystalline rocks. The lessons learnt at Soultz can be used in other places but have already been applied for commercial geothermal projects. For example a geothermal project has just started in the Upper Rhine valley (Germany) with power production in Landau, whose development took benefits from the experience gained at Soultz [15].

Acknowledgements

This project is supported by public funding from the European Commission, ADEME (French agency for environment and energy), BMU (German ministry of environment) and private funding from EDF and Electricité de Strasbourg (France), Pfalzwerke AG, EnBW AG and Evonik Industries AG (Germany).

References

[1] A Genter, L. Guillou-Frottier, J. Feybesse, N. Nicol, Ch. Dezayes, and S. Schwartz, “Typology of potential Hot Fractured Rock resources in Europe,” Geothermics, pp. 701-710, 2003.

[2] A. Gérard, A. Genter, Th. Kohl, Ph. Lutz, P. Rose, and F. Rummel, “The deep EGS (Enhanced Geothermal System) project at Soultz-sous-Forêts (Alsace, France),” Geothermics, pp. 473-483, 2006.

[3] F. Munck, K. Sauer, F. Walgenwitz, Ph. Maget, and R. Tietze, “Synthése géothermique du Fossé Rhénan Supérieur,” Internal report BRGM-Geologisches Landesamt in Bade-Wurtemberg Commission of the European Communities, 100 pp. 21 maps at 1:250,000, 1979.

[4] A. Gérard, A. Menjoz, and P. Schwoerer, “L’anomalie thermique de Soultz sous Forêts“, Géothermie Actualités 3, pp. 35-42, 1984.

[5] A. Gérard, and O. Kappelmeyer, “The Soultz-sous-Forêts project“, Geothermics 16, pp. 393-399, 1987.

[6] A. Genter, C. Castaing, C. Dezayes, H. Tenzer, H. Traineau, and T. Villemin, “Comparative analysis of direct (core) and indirect (borehole imaging tools) collection of fracture data in the Hot Dry Rock Soultz reservoir (France)”, J. Geophys. Res., 102 (B7), pp. 15419-15431, 1997.

[7] C. Dezayes, P. Chevremont, B. Tourlière, G. Homeier, and A. Genter, “Geological study of the GPK4 HFR borehole and correlation with the GPK3 borehole (Soultz-sous-Forêts, France)”, BRGM/RP-53697-FR, 94 pp, 2005.

[8] A. Gérard, J. Baumgartner, R. Baria, R. Jung, S. Gentier, and A. Genter, ”Elements for a conceptual model of the underground heat exchanger at Soultz-sous-Forêts, France. Situation, beginning 1998”, in Proceedings *of the 4th Int. HDR Forum*. Geologische Jahrbuch Reihe E Geophysics Heft SE1 Hannover 2002, pp. 291-290, Strasbourg, 2002.

[9] L. André, V. Rabemanana, and F.D. Vuataz., “Influence of water-rock interactions on fracture permeability of the deep reservoir at Soultz-sous-Forêts, France“, Geothermics, pp. 507-531, 2006.

[10] N. Cuenot, J. Charléty, L. Dorbath, and H. Haessler, “Faulting mechanisms and stress regime at the European HDR site of Soultz-sous-Forêts, France“, Geothermics, pp. 561-575, 2006.

[11] R. Baria, R. Jung, T. Tischner, J. Nicholls, S. Michelet, B. Sanjuan, N. Soma, H. Asanuma, B. Dyer, and J. Garnish, “Creation of an HDR/EGS reservoir at 5000 m depth at the European HDR project”, in Proceedings *31st Workshop on Geothermal Reservoir Engineering*, Stanford, California 2006.

[12] T. Tischner, M. Schindler, R. Jung, and P. Nami, “HDR project in Soultz: hydraulic and seismic observations during stimulations of the 3 deep wells by massive water injections”, in Proceedings *32nd Workshop on Geothermal Reservoir Engineering*, Stanford, California, 2007.

[13] S. Portier, L. André, and F.-D Vuataz, “Review of chemical stimulation techniques in oil industry and applications to geothermal systems”, Technical Report, Centre for Geothermal Research, Neuchâtel University, Switzerland, 2007.

[14] P. Nami, M. Schindler, T. Tischner, R. Jung, and D. Teza, “Evaluation of stimulation operations and current status of the deep Soultz wells prior to power production”, in Proceedings *EHDRA Scientific Conference*, Soultz-sous-Forêts, France, 2007.

[15] J. Baumgärtner , H. Menzel, and P. Hauffe. “The geox GmbH Project in Landau - The first geothermal power project in Palatinate / Upper Rhine Valley”, in Proceedings *First European Geothermal Review, Geothermal Energy for Electric Power Production*, p. 33, Mainz, Rhineland Palatinate, Germany, 2007.

APPENDIX 2 (a)

Keith Evans, Stefan Baisch, Nicolas Cuenot, Louis Dorbath and Reinhard Jung, 2008, Milestone events & key observations in seismics at Soultz, *paper presented at the EHDRA Scientific Conference, Soultz-sous-Forêts,* September 24-25, 2008.

List of milestone events and observations in Seismics

EC Contract SES6-CT-2003-502706

PARTICIPANT ORGANIZATION NAME: ETH Zurich

Related with Work Package 5+

Related with Working Group 4

MILESTONE EVENTS & KEY OBSERVATIONS IN SEISMICS AT SOULTZ

Keith Evans[1], Stefan Baisch[2], Nicolas Cuenot[3], Louis Dorbath[4], Reinhard Jung[5]

1) Dept. of Earth Sciences, ETH-Zürich, Switzerland
2) Q-Con GmbH, Bad Bergzabern, Germany
3) EEIG Heat Mining, Kutzenhausen, France
4) EOST/IPGS, Strasbourg, France
5) JUNG-GEOTHERM, Isernhagen, Germany
e-mail: keith.evans@erdw.ethz.ch

ABSTRACT

In 2007 EHDRA decided that the Workgroups should produce timeline-structured summaries of key events and milestones in their area of expertise that have impacted the Soultz project since its inception. This work remains in progress. Here we present the base-level listing of events and observations from which this document will be expanded.

EVENTS & MILESTONES

1988: GPK1 drilled to 2002 (582 m open hole) and stimulated

- 400 microseismic events observed that defined a cloud elongated in the NNW-SSE direction

1992 GPK1 extended to 3590 m and stimulated

- Methods of high-resolution location of events were developed and indicates the vast majority of events occur on and define planar or linear large-scale structures.
- Multiplets occurring within large structures indicate structural widths of tens of metres. The failure planes of the individual multiplets have dimensions of up to several tens of metres, and have orientations that scatter about that of the parent structure. This is consistent with failure on fractures within the damage zone of fracture zones.
- Stress derived from focal mechanism inversion is inconsistent with drilling-induced tension fractures observations.
- Dislocations of up to 2 cm seen on fractures in the well with relatively little nearby moment release suggest aseismic slip is occurring, as does changes in well injectivity during periods of negligible seismic activity.
- Cloud growing with time during stimulation
- Maximum magnitude was around 2
- Seismic event rate depends on the injected flow rate (moment versus volume, needs to be checked!!)
- Straight, sharp boundaries on the seismic cloud
- Development of downhole seismic sensors
- Soma's imaging method
- Distribution of events density versus distribution of moment density (needs to be checked!!)

1995 GPK2 extended to 3876 m (365 m open hole) and stimulated

- Use of the seismic cloud to target the new well
- Only a slight overlap with GPK1 cloud
- With GPK1 open, the seismic cloud did not move towards GPK1 but around. When the well was closed, the seismic cloud did approach GPK1.
- More spherical shape of the seismic cloud compared to GPK1 cloud. Might be related to the pumping schedule (GPK1 only well stimulated with step rates).
- Upward growth of the seismic cloud was more limited than for GPK1, perhaps because of the use of brine.

1997 4 month circulation tests (97Jul12)

- No significant seismic activity (?)
- Maximum magnitude below 1 (?)

2000 Extend GPK2 to 5000 m TVD and stimulate (00Jun30)

- Downward migration during injection, but upward migration during shut in
- Preferred growth to the North-West in the first phase of the stimulation, then sudden migration to the South (lower density)
- Maximum magnitude: 2.6, event occurred during the post-stimulation test
- Clear lower boundary for the upper stimulated volume and upper boundary for this stimulated area (gap in between)
- Released moment increased linearly with injected volume
- Average level of magnitude higher than for upper reservoir
- From downhole sensors, some events have high stress drop
- From surface sensors, events have normal stress drop, source size is bigger
- Focal mechanisms indicate mainly normal faulting, but also strike-slip and are consistent with the stress tensor.

2003 Drill GPK3 to 5000 m TVD and stimulate (03May27) with simultaneous injection into GPK2 for the latter part

- Onset of microseismicity started after 6h of injection (pressure 6 MPa higher than the downhole ambient pressure)
- Maximum magnitude observed during shut-in to date: 2.9
- General direction North-South (different from GPK2)
- Very large extension of the stimulated volume
- Large growth of seismic cloud during shut-in in comparison to GPK2
- Large upward growth
- Concentration of seismic events between the wells during dual injection
- Large magnitude events on the border of the cloud

2004 Drill GPK4 to 5000 m TVD and stimulate (04Sep13 & 05Feb04)

- Acidization improvements in injectivity and communication with GPK3.
- Almost no overlapping with GPK3 seismic cloud
- General trend NNE-SSW
- Maximum magnitude: 2.3
- During the second stimulation, no seismicity until pressure reached the same pressure as during the first stimulation
- During the second stimulation, seismicity occurred after an injected volume only the half of the total volume injected during the first stimulation (not complete refilling of the previous stimulated volume)
- No overlapping between the September and the February seismicity
- Microseismicity clustered around top casing leak during post HCl step rate test in March 2005
- Microseismicity only around top casing leak during RMA test in May 2006
- No microseismicity during NTA test in October 2006
- Microseismicity around top casing leak during the OCA test in February 2007

2005 Circulation test (July to December 2005)

- No serious microseismicity
- Events were deep and below GPK4
- Maximum event size is (cf. Nicolas)
- Microseismicity increases with flow rate

APPENDIX 2 (b)

Sophie Michelet, Roy Baria, Jörg Baumgärtner, André Gérard, Steven Oates, Thomas Hettkamp and Dimitra Teza, 2004, Seismic source parameter evaluation and its importance in the development of an HDR/EGS system, *Proc. 29th Workshop on Geothermal Reservoir Engineering*, Stanford University, Stanford, Cal., Jan 26-28, 2004.

Twenty-Ninth Workshop on Geothermal Reservoir Engineering
Stanford University, Stanford, California, January 26-28, 2004

SEISMIC SOURCE PARAMETER EVALUATION AND ITS IMPORTANCE IN THE DEVELOPMENT OF AN HDR/EGS SYSTEM

S. Michelet[1], R. Baria[1], J. Baumgaertner[2], A. Gérard[1], S. Oates[3], T. Hettkamp[2], D. Teza[4]

1 EEIG „Heat Mining", 67250 Kutzenhausen, France, eeig@soultz.net

2 BESTEC Gmbh, 76870 Kandel, Germany, bestec@bestec-for-nature.com

3 Shell international, 2288 Rijswijk, steve.oates@shell.com

4 BGR, Hanover, teza@soultz.net

ABSTRACT

In 2000 and 2003, massive hydraulic stimulations were carried out at the European Geothermal Hot Dry Rock (or EGS) site at Soultz-sous-Forêts, France. These stimulations were performed in the 5000 m deep wells in the crystalline basement. The objective was to create a dense network of enhanced permeability fractures, which would form the heat exchanger. The injection of water in the fractured rock generated a high level of microseismic activity. Around 30,000 and 90,000 micro-earthquakes were triggered during the injection of 2000 and 2003 respectively. From this around 14,000 and 9,000 events were then located and processed. Source parameters for these events were calculated using Brune's model on acceleration traces. An automatic process based on a genetic algorithm was developed to calculate source parameters such as seismic moments, moment magnitudes, stress drops. Large events were induced during the shut-in period and the spatial distribution of stress drops suggests that a redistribution of stresses may be occurring in the reservoir. Some of these big events may be caused by the release of locked up stress on specific fractures. Events in the range of up to 2.9 Ml have been generated during these periods and it is felt that the detailed understanding of the source parameters may be a way forward for reducing these larger events by revaluating the stimulation strategy.

INTRODUCTION

In 2000 and 2003, massive hydraulic stimulations were carried out at the European Geothermal Hot Dry Rock (or EGS) site at Soultz-sous-Forêts, France. These stimulations were performed in the 5000 m deep wells in the crystalline basement. The objective was to create a dense network of enhanced permeability fractures, which would form the heat exchanger. The injection of water in the fractured rock generated a high level of microseismic activity. Around 30,000 and 90,000 micro-earthquakes were triggered during the injection of 2000 and 2003 respectively. From this around 14,000 and 9,000 events were then located respectively and processed. Source parameters for these events were calculated using Brune's model (1970) on acceleration traces.

MICROSEISMIC NETWORK

A comprehensive seismic monitoring system was set up and operated during operations in 2003 (see figure 1). Seismometers were deployed in wells GPK-1, 4616, EPS1 (depths 3500m, 1480m and 2017m respectively) and 4-axis accelerometer tools in wells 4550, OPS4, 4601 (depths 1482m, 1484m and 1539m respectively) as shown in figure 1. The frequency band of the acquisition system was from 10Hz to 1 kHz. The sampling rate was 0.5 ms and the total duration of the recorded signal was 5 seconds. P and S arrivals on the triggered events were picked automatically. The hypocenter locations shown here were calculated by **Semore Seismic** [http://www.seismics.net/].

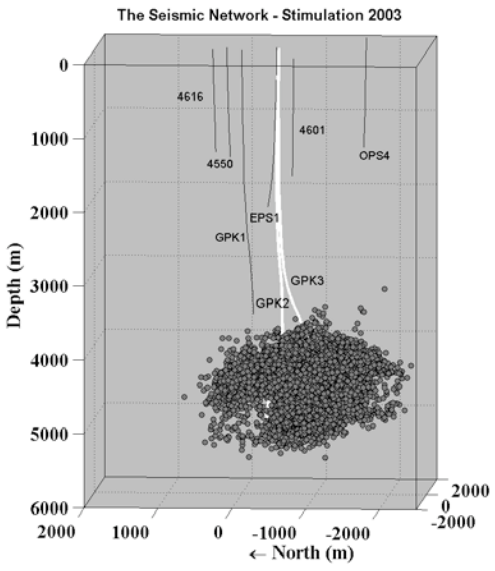

Figure 1: the seismic network – stimulation 2003

Monitoring the reservoir creation

Between 30th June and 6th July 2000, a total volume of 23,400 m^3 of water was injected into the openhole section of the well GPK-2 (See figure 2). The initial flow rate was 31 l/s, this one was increased up to 41 and then 51 l/s. After the stimulation, a test of injectivity was also done from 13th July to 15th July 2000 with 4,500 m^3 of water injected. During the monitoring period, 31,511 triggers were recorded on the down-hole network from which 13,954 events were located. The seismic activity was high throughout the entire experiment: roughly 150 events per hour. After shut-in, it decayed rapidly but a significant event rate persisted (more than 20 events/h). We observed that the seismic cloud was trended North West of the well GPK2 (figure 3) and that events occurred between the casing-shoe (4430m) and a depth of 5500m. The moment magnitudes of events were ranging between –2 and 2.6. The greatest, 2.6 occurred the 16th July 2000 i.e. one day after the end of the operations.

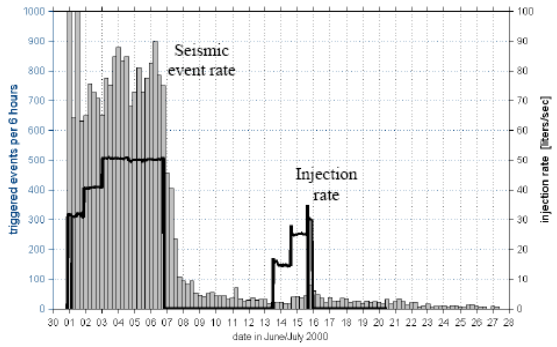

Figure 2: Distribution of events per 6 hours and injection rate (l/s) in 2000 at Soultz (Weidler et al., 2002)

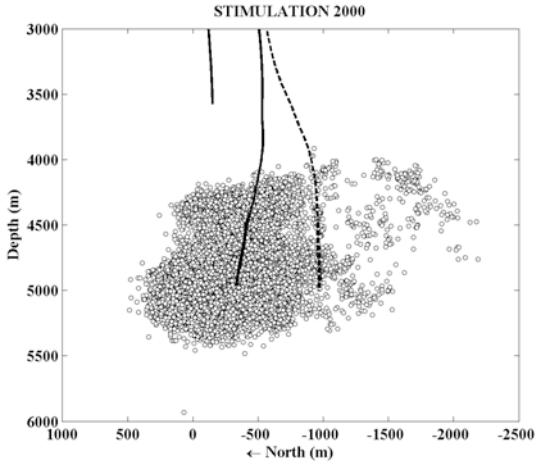

Figure 3: The seismic cloud viewed from the West – stimulation 2000

The most recent stimulation test at the site was carried out in the summer of 2003. Between 27th May and 7th June a total volume of 34,000 m^3 of water was injected into the open-hole section of GPK-3 and between 2nd June and 4th June, 3,300 m3 of water was injected into the open-hole section of GPK-2. Moreover, between 11th June and 17th June, a venting test in the GPK-2 well was performed.
The injection in GPK-3 started the 27th May; different steps of rate followed as can be seen on figure 4. In the middle of the experiment, a dual injection between the GPK2 and GPK3 wells was undertaken. The shut-in in GPK-3 was performed the 6th June: the flow rate was decreased progressively in three steps in order to avoid large seismic activity caused by rapid pressure drops. After this, the GPK-2 well was put in production on the 11th June. This test was stopped on the 17th June.

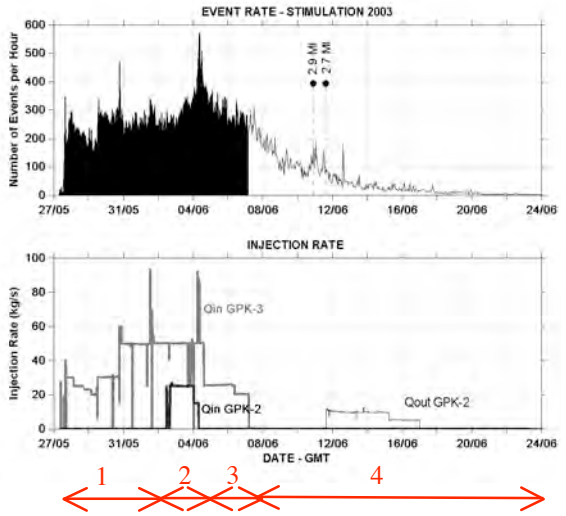

Figure 4: the seismic activity & the injection rate – stimulation 2003

During the stimulation test, 90,648 triggers were recorded on the down-hole network from which 8,354 events were auto-located (See figures 5 & 6). The seismic activity was high throughout the entire experiment i.e. an average of 300 events per hour and a maximum rate of 580 events per hour just after the flow rate of 93 l/s. The seismic rate during the 2000 stimulation was not that high because the threshold trigger was higher than in 2003. During this test, the seismic activity was very well correlated to changes in flow rates: each time the flow rate is increased the number of events per hour increased. After the shut-in of the well GPK-3 (the 6th June 2003), the number of events per hour decreased but the seismic activity was still high (more than 100 events per hour). The 10th June and the 11th June, two microseismic events of local magnitude 2.9 and 2.7 respectively occurred just before the venting test in the GPK-2 well. An increase in the seismic activity is observed just before each of these two large microearthquakes. This

behavior can be seen as a pre-shock crisis in reference to aftershock sequences following an earthquake. The venting test was held in response to this high seismic activity in order to decrease the over-pressure within the stimulated zone.

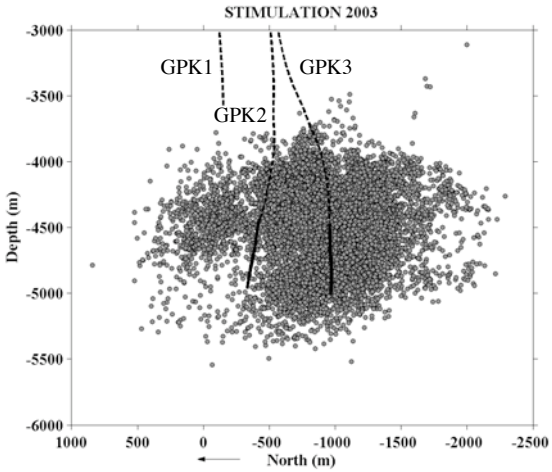

Figure 5: the seismic cloud viewed from the West – stimulation 2003

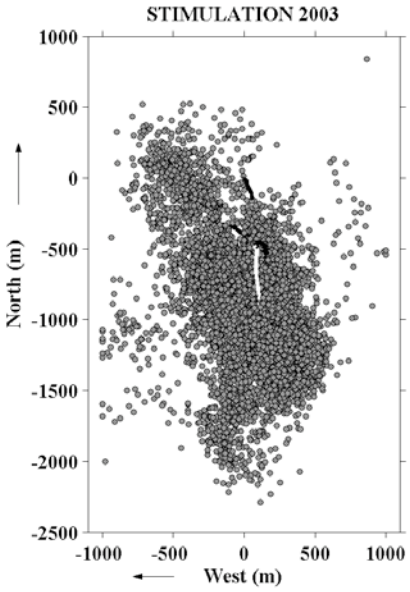

Figure 6: top view of the seismic cloud – stimulation 2003

The seismic cloud has an approximate volume of 3 km^3, striking N30W which is in accordance with orientation of the acting major horizontal stress (Hettkamp, 1998).

We also looked at the distribution of the depth with the time (Figure 7). A migration upward of the microseismic events is observed starting with the dual injection (2nd June 2003). At the same time, instead of having a change of pressure in the GPK-3 well, stabilization is seen. This stabilization of the pressure and its independence to the flow rate indicate that at least some portion of the fractures was completely mechanically opened (Cornet F.H. and Berard Th., 2003).

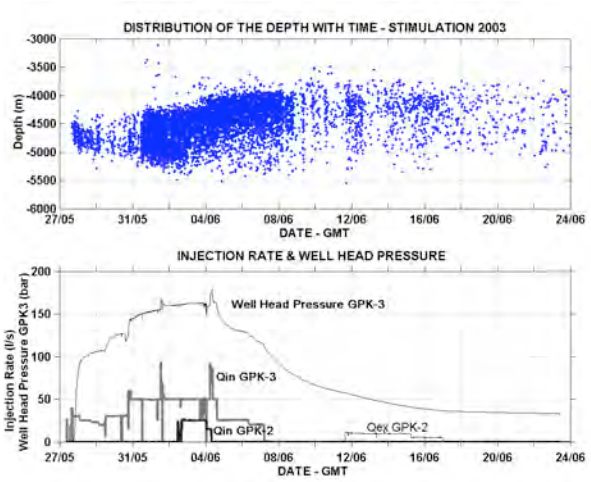

Figure 7: Distribution of the microseismic event depth with time (top part of the figure) and injection rate and wellhead pressure in GPK3 with time

Source parameter calculation: method

We only processed the records of the sensor in the well 4550 because the system used an amplitude threshold trigger on the accelerometer sensor in this well to detect and acquire potential microseismic events. We only worked on the P arrivals on the vertical sensor traces because we assume that the P-wave has vertical angle of incidence (the sources are at 5 km depth and the sensor at 1.5 km above). We didn't process the S arrivals on the sub-horizontal sensor traces at present. The vertical trace from each station was then windowed with a window of 300ms containing the P pulse and beginning at the picked P-wave arrival time and then Fourier transformed to give the corresponding acceleration spectrum. We worked in the Fourier domain in order to characterize the mechanism of the seismic source. We have first corrected the spectrum from attenuation. To do so, we used a least squared method and calculated the attenuation factor Q value that gives a zero-slope for the corrected data A_0 for frequencies between 140 and 260 Hz:

$$A\_0 = data \times \exp(\pi \times \mathrm{K} \times f)$$

Where K=R/(Q.α) is in second (Anderson, 1991), R is the distance between the source and the sensor (m), Q is the attenuation factor and α is the P-wave velocity (m/s).

Then, we used a genetic algorithm (Gordy, 1996) applied to the Brune's model (1970) to find the best combination of {corner frequency, seismic

moment} that fit the spectrum at *low frequencies* (16 to 120 Hz) with:

$$S_1 = \Omega_0 \times (2 \times \pi \times f)^2$$

and at *high frequencies* (120 to 260 Hz) with (see figure 8):

$$S_2 = \Omega_0 \frac{(2 \times \pi \times f)^2}{\left(\frac{f}{f_c}\right)^2}$$

where f_c is the corner frequency (Hz), Ω_0 is the low frequency limit (N.m).

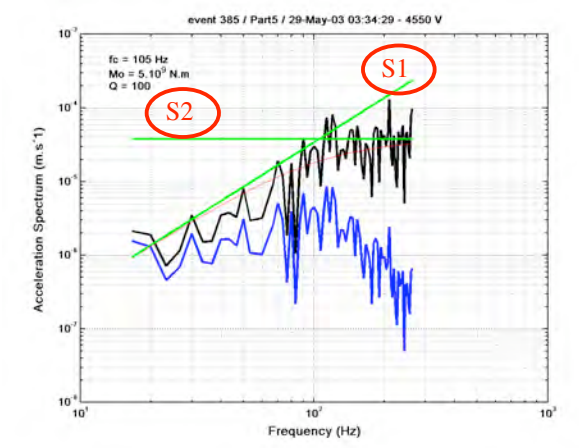

Figure 8: Fitting of the inversion for a typical event

From these parameters, it is possible to deduce the seismic moment M_0, related to the low-frequency limit of the acceleration spectrum Ω_0 by the following expression:

$$M_o = \frac{4\pi \times \rho \times \alpha^3 \times R}{0.39} \times \Omega_0$$

Where ρ is the density (2640 kg/m^3), α is the P wave velocity (5950 m/s), R is the source to sensor distance (m).

The estimates of source radius r assumed Madariaga's (1976) quasi-dynamic circular model:

$$r = \frac{1.97 \times \beta}{2 \times \pi \times f_0}$$

Where β is the S wave velocity (3400 m/s).

Estimates of stress drop Δσ and average slip Δu can be derived from the moment using relations appropriate for a circular crack with uniform stress drop:

$$\Delta\sigma = \frac{7 \times M_0}{16 \times r^3} \text{ and } \Delta u = \frac{M_0}{\mu \times \pi \times r^2}$$

where μ is the shear modulus (1.2.10^{10} Pa).

In this study, seismic moment was converted to moment magnitude M using the following relation from Pearson (1982):

$$M = (\log_{10}(M_0) - 10.2) \times 1.298$$

Where M_o is in N.m.

Source parameter: results & discussions

On figure 9 is shown the histogram of moment magnitudes for the 2003 data. Most magnitude values lie in the range between -2 and 2.1 but the largest event was 2.9Ml, unfortunately not located by our network because the signal is saturated on downhole sensors for microearthquakes greater than 2.

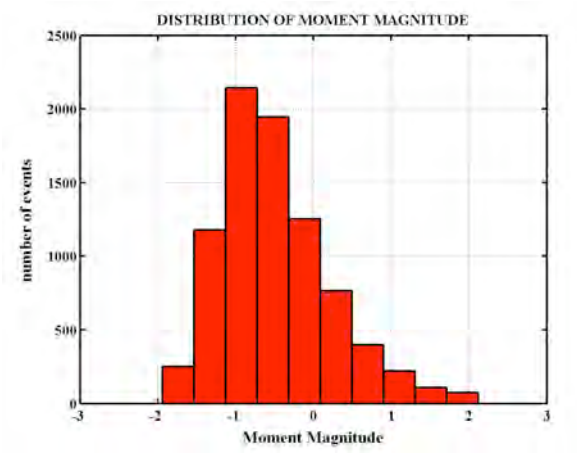

Figure 9: distribution of moment magnitude values

We will now focus on the source parameters that we computed for the 2000 and 2003 data. The first important parameter is the seismic moment because it allows quantifying the intensity of the earthquake. We decided to study the after shut-in events (figure 10) because during this period, the two largest microseismic events occurred. We observed that the seismic activity is confined to two zones: the first one is around the GPK-3 well at 4000 m depth; the second zone is in the northward part of the cloud at 4400 m depth. In 2000, large after shut-in seismic moments were also observed in this second zone (this zone is indicated by a red circle in figure 11). It seems therefore that this zone is seismically very active and that the fractures are there close to rupture. Besides, stress accumulations seem to be considerable in this area as the 2.6Ml event occurred here in 2000.

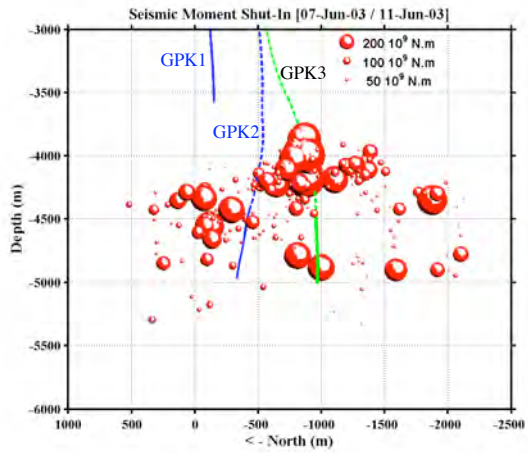

Figure 10: spatial distribution of the seismic moment after the shut-in – East view – stimulation 2003

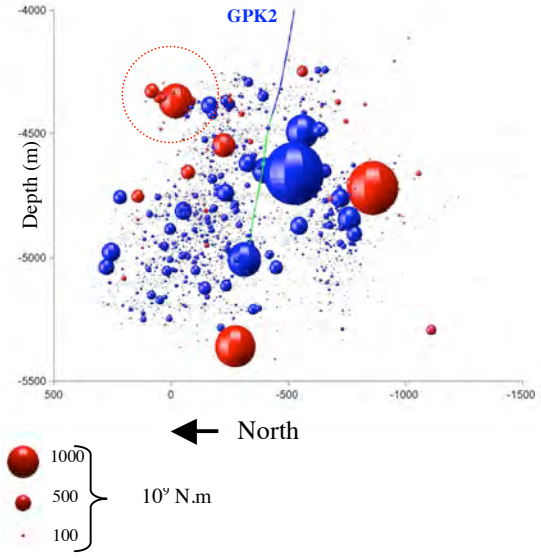

Figure 11: spatial distribution of the seismic moment - blue = during stimulation; red = after the shut-in – East view – stimulation 2000

The second key parameter is the stress drop because it depends on the stress field and the geometry of the fracture. For the 2003 stimulation, we have represented on vertical section the distribution of stress drops (see figure 12) for four periods of time indicated on figure 4: (1) injection only in the GPK-3 well, (2) dual injection in the GPK-2 and GPK-3 wells, (3) injection only in GPK-3 well with the shut-in in the GPK-2 well and at last, (4) shut-in in GPK-3 well and venting in the well GPK-2. During the first phase (1), the events with large stress drops are located all around the GPK-3 well but during the following phase (2), (3) and (4), these events are migrating to the boundaries of the seismic cloud. Thus, at the end of the stimulation, large stress drops happen in the upper part of the stimulated reservoir and around one kilometer away from GPK-2 and GPK-3. The same observation was done in 2000, especially for the after shut-in events (figure 13). These observations suggest that a stress front is propagating from the well out into the reservoir. Fehler and Phillips (1991) also found that events with the largest stress drops occurred near the edges of the seismically active zone where newly activated faults may be expected rather than in the interior of the seismic zone, which has already been fractured.

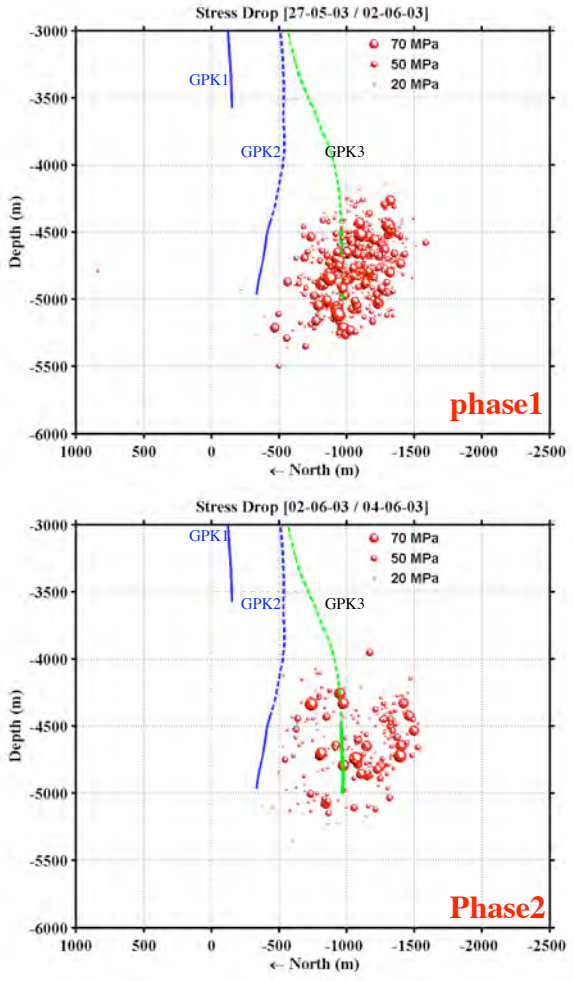

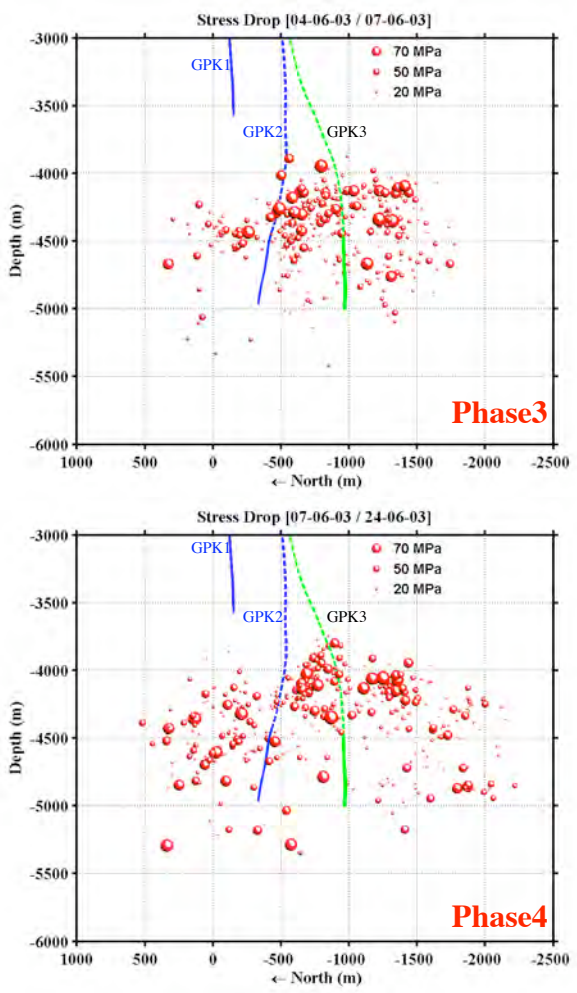

Figure 12: time evolution of stress drop during the stimulation 2003

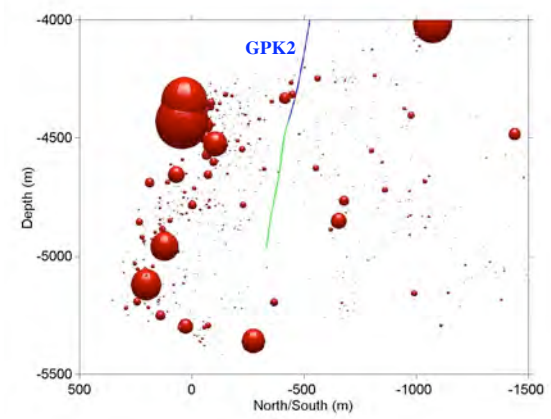

Figure 13: spatial distribution of the seismic moment after the shut-in – East view – stimulation 2000

We also observed that after shut-in, these zones with large stress drops (figure 13 and 12 (4)) coincides with the location of the largest events (magnitude > 2.5). The migration of large stress drop events may therefore indicate when zones of high seismic risk are situated.

CONCLUSION

In 2000 and 2003, two stimulations took place at the Hot Dry Rock site in Soultz-sous-Forêts (France). We triggered more than 30,000 and 90,000 microearthquakes respectively each time. From these, 14,000 and 9,000 microseismic events were located and processed in order to characterize the geometry of the reservoir. We then computed automatically the source parameters of these events, especially their seismic moment and stress drops. We found that the events with the largest seismic moments occur predominantly where the M > 2.5 events occur. It seems therefore possible to use this information to delineate the zones of seismic risk. Besides, we found that events with large stress drops are migrating to the boundaries of the stimulated zone and where the M > 2.5 events occur. This suggests that the monitoring of stress drops during stimulation operations may allow the determination of zones of high seismic risk.

REFERENCES

Anderson J.G. and Humphrey J.R. (1991), A Least Squares Method for Objective Determination of Earthquake Source Parameters, Seismological Research Letters, 62, No 3-4, 201-209

Anderson J.G. (1986), Implications of Attenuation for Studies of the Earthquake source, in S. Das, J. Boatwright, and C.H. Scholz, eds, Earthquake source Mechanics, Maurice Ewing Volume 6, Geophysical Monograph 37, American Geophys. Union, Washington, D.C, 311-318

Brune J.N. (1970), Tectonic stress and the spectra of seismic shear waves from earthquakes, J.Geophys .Res. 75, 4997-5009

Cornet F.H, Berard Th. (2003), A case example of integrated stress profile evaluation, Rock Stress, Sugarawa, Obara & Sato, 2003, Swets & Zeitlinger, Lisse ISBN 9058096394

Fehler M., and Phillips W.S. (1991), Simultaneous Inversion for Q and source parameters of microearthquakes accompanying hydraulic fracturing in granitic rock, Bull. Seism. Soc. Am. 81, 553-575

Gordy (1996), Genetic Algorithms toolbox for Matlab, http://www.geatbx.com/links/genetic_maximization_matlab_m_gordy.html

Madariaga R. (1976), Dynamics of an expanding circular fault, Bull. Seism. Soc. Am., 66, 639-666

Pearson C. (1982), Parameters and a magnitude moment relationship from small earthquakes observed during hydraulic fracturing experiments in crystalline Rocks, Geophysical Research Letters, vol. 9, no4, 404-407

Weidler R. et al. (2002), Integrated Microseismic and Hydraulic Monitoring of HDR Reservoir Stimulation, Soultz 2000, EAGE 64th Conference & Exhibition, Florence.

FUNDING

Work at Soultz is funded and supported by the European Commission Directorate–General Research, the French Ministère délégué à la Recherche et aux Nouvelles Technologies, the French Agence de l'Environnement et de la Maîtrise de l'Energie, the German Bundesministerium für Umwelt, Naturschutz und Reaktorsicherheit within the frame of the "Zukunftsinvestitionsprogramm", the Projektträ-ger of the Forschungszentrum Jülich in Germany and by the Members of the EEIG "Exploitation Minière de la Chaleur".

ACKNOWLEDGEMENT

During the stimulation program discussed here, major contributions were also made by the following: Ben Dyer (Semore Seismics), Jonathan Nicholls, Terry Gandy and his staff (SII). I would like to thank Mathieu Darnet (Institut de Physique du Globe de Strasbourg) for fruitful discussions.

APPENDIX 2 (c)

Roy Baria, Sophie Michelet, Jörg Baumgärtner, Ben Dyer, André Gérard, Jonathan Nicholls, Thomas Hettkamp, Dimitra Teza, Nobukazu Soma, Hiroshi Asanuma, John Garnish and Thomas Mégel, 2006, Microseismic monitoring of the World's largest potential HDR reservoir, *Proc. 29th Workshop on Geothermal Reservoir Engineering*, Stanford University, Stanford, Cal., Jan 26-28, 2004.

PROCEEDINGS, Twenty-Ninth Workshop on Geothermal Reservoir Engineering
Stanford University, Stanford, California, January 26-28, 2004

MICROSEISMIC MONITORING OF THE WORLD'S LARGEST POTENTIAL HDR RESERVOIR

R.Baria[1], S.Michelet[1], J.Baumgaertner [1, 2], B.Dyer[3], A.Gerard [1], J.Nicholls, T.Hettkamp [1,3], D.Teza [4], N.Soma [5], H.Asanuma [6], J. Garnish, T.Megel[7]

[1)]EEIG "Heat Mining", Kutzenhausen, France.
[2)]BESTEC GmbH, Kandel, Germany.
[3)]Semore Seismic, Falmouth, UK.
[4)]BGR, Hanover, Germany.
[5)] National Institute of Advanced Industrial Science and Technology (AIST) Tsukuba, Japan.
[6)]Tohoku University, Sendai Japan., [7)] GEOWATT AG, Dohlenweg 28, CH-8050, Zurich.

ABSTRACT:

The current phase of the European Hot Dry Rock Project at Soultz-sous-Forêts requires the drilling of two additional deep wells to 5000 m depth into the crystalline basement, to form a module consisting of a central injector and two producers. The first well GPK-2 was drilled to 5000 m in 1999 and stimulated in 2000. The well GPK-3 (the injector) was drilled in 2002 and targeted using microseismic and other data. The bottom hole temperature was 200.6 ºC and separation between the two wells at the bottom is around 600 m. GPK3 was then stimulated to enhance the permeability between the wells. A number of stimulation techniques were tried including "***focused"*** stimulation, a novel method of injecting simultaneously in two wells. Microseismic monitoring, flow logging and other diagnostic methods were used during these injections.

The ***"sparse"*** microseismic network at the Soultz site consists of a number of seismic sensors deployed in wells between 1500 m and 3600 m deep with bottom hole temperatures of 130-160 ºC. A 48 channel, 22 bit data digitizing unit was used for data acquisition in conjunction with proprietary software to carry out automatic timing and location in real time. This gave a real time decision-making possibility and control of the reservoir. This was the first time that such an interactive method had been carried out at this site.

Around 90 000 micro-earthquakes were triggered during these injections and about 9 000 events were automatically timed and located in real time. These stimulations created a total reservoir volume in excess of 3 km^3. This is the largest stimulated volume in the development of HDR technology to date.

The data suggest that "focused" stimulation may have a significant advantage over a single well stimulation technique and may be a way forward for efficient stimulation of larger separations between wells, thus improving the economic viability and acceptance of HDR/HFR/EGS systems.

It is recognized that the reservoir creation process generates microseismic events but generation of bigger events (30 events approaching 2ML & one up to 2.9ML during this campaign) may retard the acceptance of this technology in an urban environment. This needs further studies to understand the processes and find a procedure to reduce the incidence of larger events.

INTRODUCTION

It has taken over 30 years of research for the concept of Hot Dry Rock (HDR) formulated in Los Alamos (USA) to approach reality at Soultz-sous-Forêts (France). The concept has evolved over that time, and various names have been proposed from Hot Wet Rock, Enhanced Geothermal System, Hot Fractured Rock etc. Different terms apply to different geological and tectonic settings but the principle still remains the same i.e. getting heat out of the deep and hot underground rock mass following permeability enhancement using hydraulic stimulations.

The research at the European HDR site at Soultz started in 1988 following the encouragement of the European Commission to pool the limited available national funds to form a coordinated multi-national team. The main task was to develop the technology needed to access the vast environmentally-friendly HDR energy resource. The European HDR research site is situated at Soultz-sous-Forêts on the western edge of the Rhine Graben, about 50 km north of Strasbourg (Fig. 1). Baria et al (1993), Garnish et al (1994), Baria et al (1995), Baumgaertner et al (1995), & Baumgaertner et al (1998) give a brief summary of the various stages of the development of this technology at Soultz since 1987.

The present phase started in April 2001 and will last until September 2004. It is called a Scientific Pilot Plant (Phase 1). The brief is to drill two additional deviated 5000 m deep wells to form a three-well system and to create an enhanced permeability fractured rock reservoir by hydraulic stimulations. It also includes use of various diagnostic techniques to understand and quantify various properties of the stimulated reservoir. The program also includes the establishment of a database of the potential HDR resource in the Western Europe.

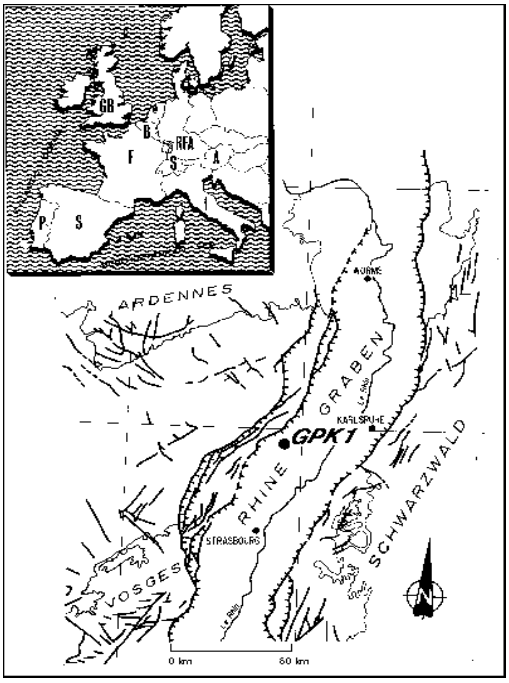

Figure 1: The location of the European HDR site at Soultz-sous-Forêts

BASIC CHARACTERISTICS OF THE SITE

Geology

The European HDR test site is in the Northern flank of the Rhine Graben, which is part of the Western European rift system (Villemin, 1986). The rift extends approximately N-S for 300 km from Mainz (central Germany) to Basel (Switzerland). The Soultz granite is part of the same structural rocks that form the crystalline basement in the Northern Vosges, and intrudes into Devonian - Early Carboniferous rocks.

The geology of the Soultz site and its tectonic setting have been described by Cautru (1987). The pre-Oligocene rocks that form the graben have slipped down a few hundred meters during the formation phase of the graben. The Soultz granitic horst (above which the site is located) has subsided less than the graben. The graben is about 320 million years old (Köhler, 1989) and is covered by sedimentary layers about 1400 m thick at the Soultz site.

Boreholes

The eight boreholes available at the site are shown in Fig. 2. They range in depth from 1400 m to 5000 m. The five boreholes #4601, #4550, #4616 and EPS-1 are old oil wells that have been extended to 1600 m, 1500 m, 1420 m and 2850 m respectively in order to deploy seismic sondes in the basement rock. Additionally, the well OPS4 was drilled in 2000 to a depth of 1800 m.

The first purpose-drilled well (GPK1) was extended from 2000 m to 3590 m in 1993 (Baumgärtner et al., 1995) and has a 6-1/4" open hole of about 780 m. GPK1 was used for large-scale hydraulic injection and production tests in 1993, 1994 and 1997 but presently it is used as a deep seismic observation well. GPK2 is about 450 m south of GPK1 and was drilled in late 1994 to a depth of 3890 m and subsequently deepened to 5000 m in 1999. GPK3 is a 5000m deviated well with the bottom hole located about 600 m south of GPK2 (Fig. 2).

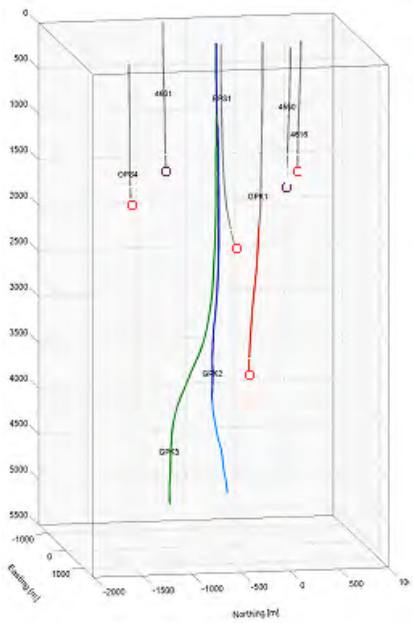

Figure 2: layout of the boreholes

Temperature gradient

In the Soultz area the temperature trend has been determined using numerous measurements in the boreholes. The variation in temperature gradient can be roughly described as 10.5°C/100 m for the first 900 m, reducing to 1.5°C/100 m down to 2350 m (Schellschmidt & Schultz, 1991) then increasing to 3°C/100 m from around 3500 m to the maximum depth measured (5000 m).

This irregular gradient suggests that there is a zone of enhanced circulation between the granite basement and the sedimentary cover. The reduction in the temperature gradient and its subsequent increase suggests that there are convective cells present which may extend to greater depth. Thermal modeling and the available data (geochemical and hydraulics) both support this view.

Joint network

Information on the joint network at the Soultz site has been obtained from continuous cores in EPS1 and borehole imaging logs in GPK1 (Genter and Traineau (1992a) and (1992b)). The observations suggest that there are two principal joint sets striking N10E and N170E and dipping 65°W and 70°E respectively (Genter and Dezayes, 1993). The granite is pervasively fractured with a mean joint spacing of about 3.2 joints/m but with considerable variations in joint density.

Stress regime

At the Soultz site, the stress regime was obtained using the hydrofracture stress measurement method (Klee and Rummel, 1993). The stress magnitude at Soultz as a function of depth (for 1458-3506 m depth) can be summarized as:

(Min. horizontal stress) $S_h = 15.8 + 0.0149 \cdot (Z - 1458)\}$

(Max. horizontal stress) $S_H = 23.7 + 0.0336 \cdot (Z - 1458)\}$

(Overburden) $S_V = 33.8 + 0.0255 \cdot (Z - 1377)\}$

S_h, S_H, S_V in MPa and Z = depth (m)

Note that this implies a cross-over between S_V and S_H around 3000 – 4000 m depth, with a consequent transition in failure mode from normal faulting to strike-slip.

Microseismic network

A microseismic network has been installed at the site for detecting microseismic events during fluid injections and locating their origins (Fig. 2). The equipment consists of three 4-axis accelerometer sondes and 3-axis geophone sondes (Calidus Electronics), linked to a fast seismic data acquisition (Perseids, IFP) and processing system (DIVINE, Semore Seismic). The sondes were deployed at the bottoms of wells #4550, #4601, EPS1, OPS4 and GPK1. Additionally, the teams from Tohoku University and AIST, Japan, carried out continuous digital recording.

In addition, a surface network consisting of around 35 stations was installed by EOST in order to be able to characterize larger events.

REAL TIME RESERVOIR CONTROL SYSTEM

The seismic activity generated during the stimulation was monitored continuously using a dedicated system based on subsurface sensors. The seismic data from the monitoring wells were continuously transmitted to the acquisition room by a combination of landline and radio telemetry. During the stimulation and subsequent circulation test the acquisition system detected in excess of 90 000 potential seismic events. The event rate was typically around 250 events/hour. The peak rate was just in excess of 580 events/hour, one event every seven seconds.

The seismic trace data were transferred continuously to an automatic timing and event location package, (Divine, Semore Seismic), to obtain real time event locations. The network at the site is ***sparse*** and around 9 000 events were located in this way using auto-picked P and S timing. The event locations could be viewed in the hydraulic control room and other sites remote from the acquisition room over the network. This was the first time at this site that seismic data have been available in real time.

In parallel, Tohoku University & AIST group also carried out auto locations in a batch process to confirm the real time location by Divine.

HYDRAULIC STIMULATIONS OF GPK2 & GPK3

GPK2 was stimulated first in 2000. Subsequently GPK3 was targeted on the basis of the information gathered from various methods including microseismic, hydraulic, stress, jointing etc. GPK3 was drilled to 5000 m depth with the casing shoe set at 4556 m depth.

Although the primary objective of the hydraulic injection was to stimulate the new well GPK3, a number of variations in the stimulation techniques were also carried out. The seismic data are therefore presented in four parts of the hydraulic history (Phases 1 to 4) as shown in Fig. 3. Phase 1 consists of injection in GPK3 of up to 60 l/s, Phase 2 consists of simultaneous injection in GPK2 & 3, Phase 3 consists of shutting in GPK2 and continued injection in GPK3 and then shut-in, and Phase 4 consists of shutting in both wells initially but venting GPK2 at around 10 l/s for 5 days.

First Phase

The stimulation commenced on 27th June with the injection of heavy brine (density around 1.2 kg/l) at a rate of 30 l/s. When the supply of brine was exhausted the stimulation proceeded with cold fresh water. The purpose of the brine was to stimulate preferentially the deeper and so hotter part of the openhole.

This practice had been shown to be successful during previous stimulation of GPK2. The injection rate was increased to 50 l/s on 30th May with one short period at up to 90 l/s.

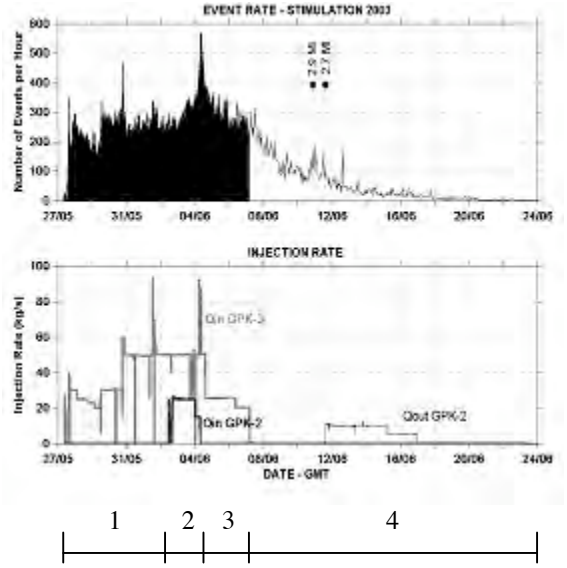

Figure 3: Event rate and injection rate during the stimulation in 2003

The onset of seismicity occurred at around 3 MPa overpressure, which was consistent with the observations in 2000, and suggests that the state of stress on the stimulated joints may be close to critical (just as has been seen at every other HDR site investigated; this is probably not a coincidence (Pine and Batchelor (1984))). The seismicity at the start of the GPK3 injection was located around the main flowing zone at 4760 m detected on the flow log (Figure 4). The events developed towards GPK2 in a downward direction. Over the period of this phase of the injection the event distribution continued to develop north and south of the GPK3 openhole but the progress slowed towards GPK2 (Figure 5a).

Second Phase

The concept of "focused" stimulation was based on the experience and observation in 1995. During the initial stimulation of GPK2 in 1995, when the well was only 3600 m deep, it was observed that the seimicity moved from GPK2 towards GPK1 but started to bypass the well GPK1. GPK1 was used at the time to produce in-situ brine needed to inject in GPK2. It became apparent that the production from GPK1 was causing a reduction in the in-situ pore pressure near the well and therefore inhibiting the shearing of the joints. The production from GPK1 was stopped and almost immediately seismicity started to migrate towards GPK1.

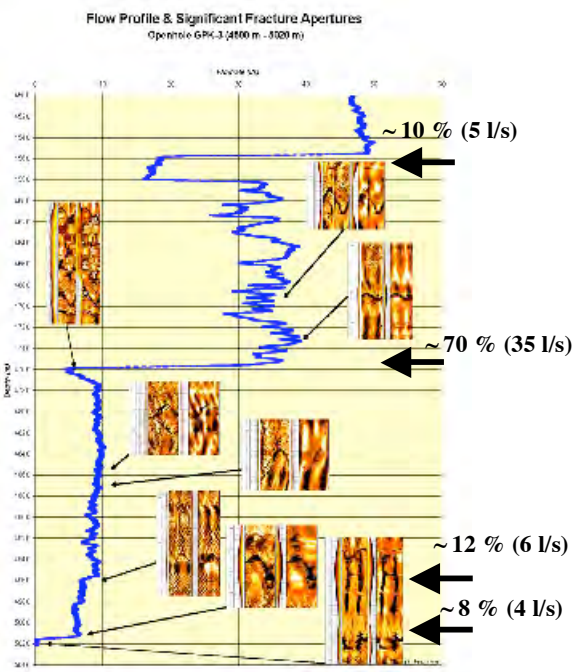

Figure 3: Flow profile and significant fracture apertures (Courtesy of Glen Homeier and Jonathan Nicholls)

This implied that if stimulations were carried out in both wells simultaneously then the overpressure in the reservoir between the wells would be the result of superposition of the injection pressures. This would elevate the pressure between the wells significantly more than that from a single well stimulation; in other words this would help to stimulate or shear the joints in the area which has always been traditionally difficult to manipulate. Although this seemed a reasonable approach, the infrastructure needed and the logistics of stimulating both wells at the same time was daunting.

Due to better planning and restructuring of the available resource in 2003, it was possible to inject in both wells simultaneously for a limited period. This type of stimulation had never been tried in the HDR environment and it was decided to name it as "focused" stimulation. This technique may facilitate selective stimulation of certain part of the reservoir between the wells by manipulating the injection pressure in each.

In an effort to stimulate the region south of GPK2 it was decided to inject simultaneously into GPK2 and GPK3. The separation at the bottom of the two wells is in excess of 600 m. During this phase around 50 l/s was being injected in GPK3 and injection of about 20 l/s was started in GPK2.

The distribution of events due to the relatively short GPK2 injection developed significantly towards the upper part of the reservoir (figure 5b). A deep region of seismicity also developed. These new regions of seismicity are indicated by the red dash ellipses in Figure 5b. There is very little seismicity immediately adjacent to the GPK2 openhole as this region was previously stimulated in 2000. It is a characteristic of the stimulations at Soultz that the

seismicity is concentrated in unstimulated parts of the reservoir, as would be expected.

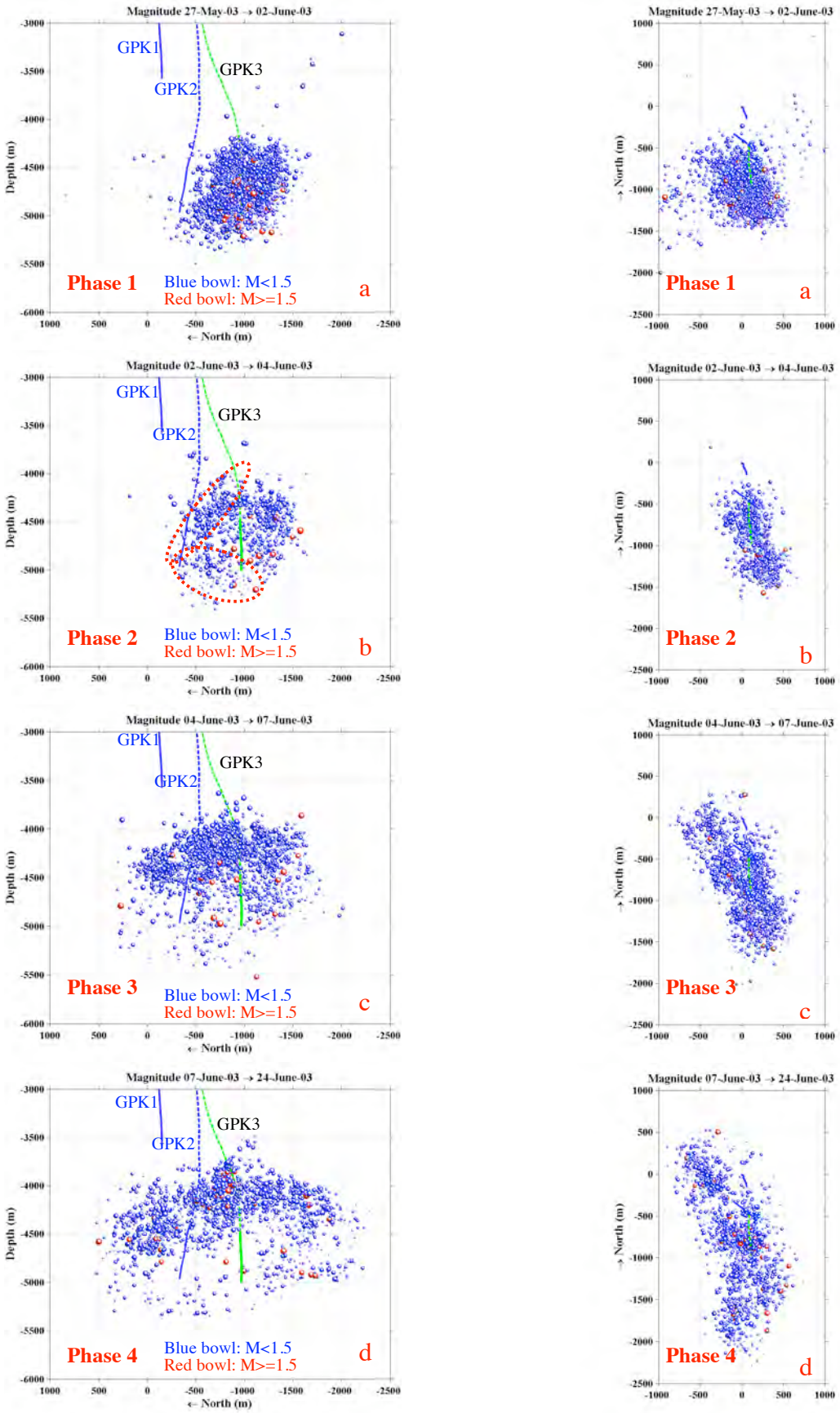

Figure 4: Vertical North to South sections through the seismic event distributions during the GPK3 stimulations phases.

Third Phase

In the third phase of the stimulation (Figure 5c), GPK2 was shut-in and the injection into GPK3 was increased to 90 l/s for 3 hrs and then progressively reduced in three steps in order to avoid larger seismic events, which were believed to be caused by rapid pressure drop.

Nonetheless, the event distribution demonstrates that the reservoir continued to develop to the north of GPK3, predominantly at the top of the reservoir. There is also a distinct zone of seismicity beneath GPK2 and GPK3, suggesting that a deep flowing zone has been stimulated.

Fourth Phase

In the fourth phase (Figure 5d), initially when GPK3 was also shut-in, the microseismic events continued to be generated instead of decaying rapidly as occurred during the stimulation at 3600 m depth. This observation, in conjunction with the slower decay in the shut-in curve, suggests that the leak-off was not as large and therefore the system was relative tight compared to that at 3600 m depth.

Secondly, two large events (2.9 and 2.7 ML) were generated on 11th June 2003. As these could be felt at surface, some measures to reduce such events were required. GPK2 was vented at around 10 l/s to reduce the pressure in the reservoir.

The seismic events were generated on the periphery of the reservoir with the majority of them (including the larger events) concentrated at the top of the reservoir (Figure 5d). This may be due to a thermal effect as the cold injection water heats up within the reservoir causing an upward pressure due to the buoyancy effect. The seismicity continued to be generated but with a gradual decline for at least two months after the venting test.

During the 2000 stimulation of GPK2, it was observed that there was no pressure response in GPK1. Seismic events migrated upwards during this stimulation but the microseismic cloud appeared to stop as if there were some upper barrier. During the stimulation of GPK3 (2003) there *was* a pressure response in GPK1, indicating that this barrier may have been breached. It is worth stating that the events did not develop sufficiently upwards to connect into the region of the reservoir created previously at the bottom of GPK1. This suggests that the stimulated region of the GPK3/2 reservoir has remained isolated in the deeper, hotter granite where the potential geothermal resource is greatest.

Following the stimulation a circulation test was performed. This demonstrated that the target productivity of GPK2 of 1 l/s/bar had been reached. The injectivity of GPK3 was 0.3 l/s/bar. This is less than desired but it is expected that this value will improve following cleaning operations and the stimulation of the new well GPK4.

MODELLING

A numerical scope calculation for the following two cases has been performed (Geowatt AG, Zurich) to highlight the possible hydraulic behavior under stimulation condition:

1) Stimulation in a single borehole
2) Simultaneous stimulation in two boreholes

Therefore, a 3D hydraulic model was set up assuming typical conditions of the Soultz reservoir at 5.0 km depth (i.e. initial far-field permeability = 10mD ($10^{-14}m^2$), initial near borehole permeability = 1D ($10^{-12}m^2$) and the stimulation rates of GPK3 (i.e. 100 l/s). The 3D model used two boreholes at 500 m apart, each borehole with a 500 m open hole section. The model consisted of ~40,000 nodes and was especially refined near the two boreholes.

The results of these calculations are illustrated on the pressure field along the direct line between the boreholes (Figures. 6 & 7) and on the shape of the pressure isosurface (1 MPa, 3 MPa, 5 MPa, see Figures 8 & 9).

Clearly, the pressure contour of case 1(Figure 6) is on a much lower level than that of case 2 (Figure 7). In these settings, the critical 3 MPa will not be reached in the center. However, in the two-borehole stimulation (case 2) this pressure level is already reached after 3 hrs.

PRELIMINARY OBSERVATIONS & CONCLUSIONS

1. The onset of shearing was observed at around 3MPa overpressure.

2. Around 90 000 microseismic events were recorded and about 9 000 were automatically located in real time during the stimulation.

3. The availability of microseismic event data in real time provided a significant benefit in monitoring and controlling the hydraulic operations during the stimulation of GPK3.

4. The seismic event rate follows the injection pressure/flow but only decayed slowly after the shut-in compared to the rate observed in 2000.

5. Broadly, the seismicity started at around 4700 m depth in GPK3 and migrated approximately N-S.

6 On average, the large events are distributed throughout the seismic cloud.

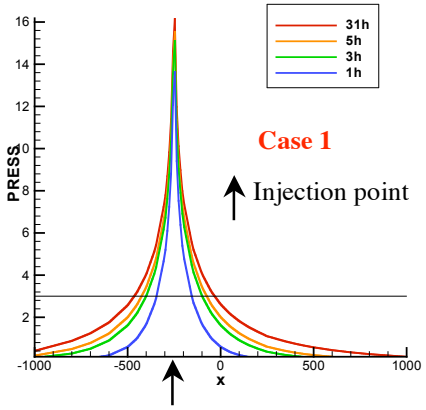

Figure 6: Pressure evolution along the direct connection of the open borehole sections with time of run 1

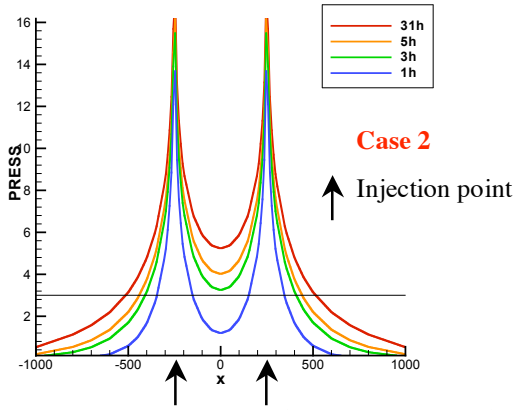

Figure 7: Pressure evolution along the direct connection of the open borehole sections with time of run 2

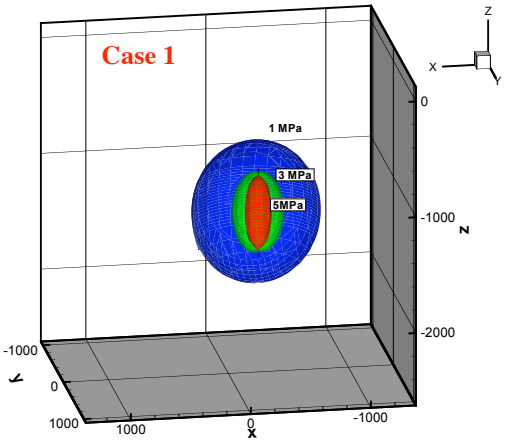

Figure 8: Isobars (1 MPa, 3 MPa, 5 MPa) after 30 h (nearly steady-state) of run 1.

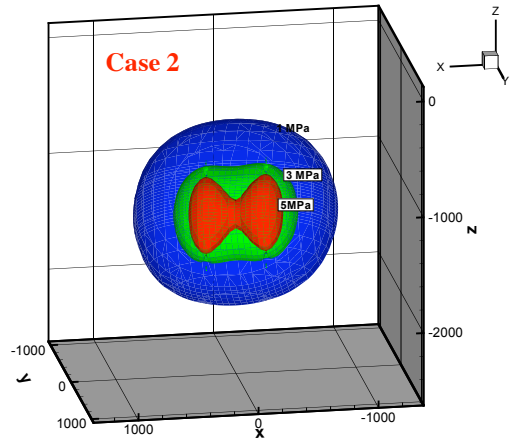

Figure 9: Isobars (1 MPa, 3 MPa, 5 MPa) after 30 h (nearly steady-state) of run 2 (right). The stimulated volume marked by the 3 MPa case is significantly larger (~10 times) than that one of run 1.

7. During the "focused" injection, the seismicity is distributed evenly between the wells and predominantly below the GPK2/GPK3 casing shoes.

8. Subsequently, the seismicity continued to expand N – S and structures above the casing shoes developed strongly, probably caused by the buoyancy effect of the injected fluid.

9. The successful extension of the reservoir to encompass the previously stimulated region around GPK2 created a total of reservoir volume in excess of 3 km^3. This is the largest ever stimulated volume in the development of HDR technology in conjunction with the largest separation between the injection and production well to date (over 650 m).

10. The apparently near critical state of stress in the reservoir region may also have been an important factor in the successful stimulation of a large reservoir volume. It should be stressed, however, that this effect has been seen at every HDR site tested to date and may be the norm.

11. In excess of 400 events were above 1.0 ML and around 30 events were above 2.0 ML.

12. The largest 2.9 ML event was recorded on the 10th June 2003 at 22:54 (GMT time).

13. Although stimulations were considered to be successful, the generation of large events needs further investigation into stress migration and lockup. Subsequently, a stimulation and circulation strategy must be developed to reduce bigger seismic events if this technology is to be acceptable in an urban environment.

FUNDING

Work at Soultz is funded and supported by the European Commission Directorate–General Research, the French Ministère délégué à la Recherche et aux Nouvelles Technologies, the French Agence de l'Environnement et de la Maîtrise de l'Energie, the German Bundesministerium für Umwelt, Naturschutz und Reaktorsicherheit within the frame of the "Zukunftsinvestitionsprogramm", the Projektträ-ger of the Forschungszentrum Jülich in Germany and by the Members of the EEIG "Exploitation Minière de la Chaleur".

ACKNOWLEDGEMENTS

The authors would like to thank all the teams who contributed to the success of the project at Soultz. Special thanks go to all participants and contractors who were actively involved during the summer hydraulic program (GI, ENEL, MeSy, GTC, IPG (Strasbourg). W. Reich (BGR), J-P Fath, J-L Riff & V. Can.

The authors would like to give special acknowledgement to Perry Moore (SII) who died on 21st March 2003 in Kazakhstan. He was a friend and had an absolute faith in the HDR concept from his Los Alamos days. He supported the program with tremendous drive & enthusiasm, and his expertise will be sorely missed.

We would also like to thank T.Megel & T.Kohl (Geowatt AG, Zurich) for helpful discussion and production of the model at such a short notice.

REFERENCES

Baria R, Baumgärtner J and Gérard A, 1993; Heat mining in the Rhinegraben; Socomine Internal project report.

Baria R, Garnish J, Baumgartner J, Gerard A, Jung R, 1995. Recent development in the European HDR research program at Soultz-Sous-Forets (France). Proceeding of the World Geothermal Congress, Florence, Italy, International Geothermal Association, Vol. 4, 2631-2637, ISBN 0-473-03123-X.

Baumgärtner J, Moore P and Gérard A, 1995. Drilling of hot and fractured granite at Soultz - Proceeding of the World Geothermal Congress, Florence, Italy, International Geothermal Association, Vol. 4, 2657-26663, ISBN 0-473-03123-X.

Baumgärtner, J., Gérard, A., Baria, R., Jung, R., Tran-Viet, T., Gandy, T., Aquilina, L., Garnish, J., 1998. Circulating the HDR reservoir at Soultz: maintaining production and injection flow in complete balance. Proceedings of the 23rd Workshop on. Geothermal Reservoir Engineering, Stanford University, California

Cautru JP, 1987; Coupe géologique passant par le forage GPK1 calée sur la sismique réflexion; BRGM/IMRG document.

Garnish J, Baria R, Baumgärtner J, and Gérard A, 1994. The European Hot Dry Rock Programme 1994-1995, GRC Trans.

Genter A, and Dezayes C, 1993; Fracture evaluation in GPK1 borehole by using FMI data; field report, BRGM Orléans.

Genter A, and Traineau H, 1992a; Hydrothermally altered and fractured granite in an HDR reservoir in the EPS1 borehole, Alsace, France, 17th Workshop on geothermal reservoir engineering, Stanford Univ., Jan. 29-31, 1992; preprint.

Genter A, and Traineau H, 1992b; Borehole EPS1, Alsace, France; Preliminary geological results from granite core analyses for Hot Dry Rock research; Scientific drilling 3; pp 205-214.

Klee G, and Rummel F, 1993; Hydraulic data from the European HDR Research Project test site, Soults sous Forets. Int. J. Rock Mech. Min Sci & Geomech. Abstr.,Vol 30, No 7, 973-976, 1993..

Köhler H, 1989; Geochronology on the granite core material from GPK1, Soultz-sous-Forêts; Ruhr Universität Bochum report 70844.

Pine R, and Batchelor A, (1984), Downward migration of shearing in jointed rock during hydraulic injections, Int. Journal of Rock Mechanics and Mining Science, Vol 21, No 5, 249-263.

Schellschmidt R, and Schulz R, 1991; Hydrothermic studies in the Hot Dry Rock Project at Soultz-sous-Forêts; Geothermal Science and Technology, vol. 3(1-4), Bresee (Ed), Gordon and Breach Science Publishers, pp. 217-238.

Villemin T, 1986; Tectonique en extension, fracturation et subsidence: le Fossé Rhénan et le Bassin de Sarre-Nahe; Thèse de doctorat de l'univ. Pierre et Marie Curie, Paris VI.

APPENDIX 2 (d)

Marion Schindler, Patrick Nami, Rüdiger Schellschmidt, Dimitra Teza and Torsten Tischner, 2008, Correlation of hydraulic and seismic observations during stimulation experiments in the 5 km deep crystalline reservoir at Soultz, *paper presented at the EHDRA Scientific Conference, Soultz-sous-Forêts*, September 24-25, 2008.

EC Contract SES6-CT-2003-502706

PARTICIPANT ORGANIZATION NAME: BGR

Working Group: WG4

Related with Work Package: WP1/WP5

CORRELATION OF HYDRAULIC AND SEISMIC OBSERVATIONS DURING STIMULATION EXPERIMENTS IN THE 5 KM DEEP CRYSTALLINE RESERVOIR AT SOULTZ

M. Schindler[1], P. Nami[2], R. Schellschmidt[2], D. Teza[3], T. Tischner[1]

1 Federal Institute for Geosciences and Natural Resources (BGR), Stilleweg 2, D-30655 Hannover, Germany
2 Leibniz Institute for Applied Geosciences (GGA-Institute), Stilleweg 2, D-30655 Hannover, Germany
3 BESTEC GmbH, Landauer Straße 28, D-76870 Kandel, Germany
e-mail: Marion.Schindler@bgr.de

ABSTRACT

Between 2000 and 2005, each of the three 5000 m deep wells (GPK2, GPK3, and GPK4) of the European HDR/EGS project at Soultz (Upper Rhine Graben, France) was hydraulically stimulated through massive water injections. A microseismic network of up to 6 downhole sensors allowed to monitor the stimulation operations and to locate the hypocenter distribution.
The stimulation of GPK2 resulted in a 20-fold increase in productivity and created a rather narrow distribution of microseismic events with a strike direction around N145°E. It appears that this zone has for a great part governed the stimulation.
A similar flow rate (50 l/s) was applied to stimulate GPK3. Although the stimulation created significantly more events which are widely dispersed, it did not improve much the productivity. A flow zone at 4760 m MD, which was already permeable before the stimulation, might explain this behaviour.
The stimulation of GPK4 was performed in two stages, each with a lower flow rate (30 l/s) in order to reduce the risk of higher magnitude seismicity. The spatial density of the corresponding seismic events is comparable to the stimulation of GPK2, again indicating an effective stimulation and a significant productivity enhancement. In the second stage performed in 2005, a slightly higher volume of water than before was injected. The seismic activity was comparable low and spatially much more dispersed than in the first step. Consequently, the productivity of the well was not improved much.
We conclude that the effect of the stimulation in terms of productivity enhancement can be qualitatively derived from the seismic density distribution. A high seismic density correlates with a significant productivity enhancement whereas a more dispersed distribution results from a less effective stimulation.

INTRODUCTION

Hydraulic stimulation is the most recognized means to improve the permeability of rock formations in a large scale and to connect boreholes over several hundreds of meters. For the targeting of the wells as well as for the control of stimulation, the monitoring of microseismicity - induced either by fracturing the rock or by shearing the preexisting fractures – is the only tool which gives insight into the underground away from the borehole.
In the European HDR/EGS project in Soultz, hydraulic stimulations and microseismic monitoring are carried out since the beginning in 1987. The site is located in the Rhine Graben, some 50 km north of Strasbourg near the German boundary (Fig. 1, left). The project aims to develop a subsurface heat exchanger in granite for geothermal power production. For this purpose, a borehole triplet was drilled and stimulated hydraulically after the drilling to connect the wells to the surrounding fracture network and to enhance the permeability of the reservoir. The triplet consists of one injector (GPK3) and two producers (GPK2 and GPK4) which reach a total depth of 5000 m and a formation temperature of 200 °C.

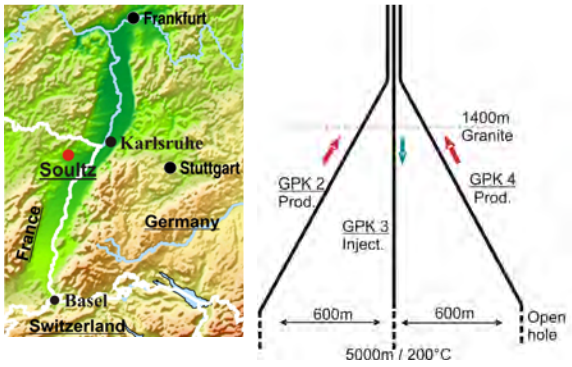

Figure 1: Location of Soultz-sous-Forêts (left) and scheme of the borehole triplet (right).

A huge data base of hydraulic and seismic data developed in the course of time and many researchers have analyzed the different stimulation processes, but the work is not consistently performed for all the stimulations. The purpose of this paper is to review systematically all hydraulic stimulations with a focus on the seismic events reflecting the temporal and spatial reservoir development. By comparing stimulation pressures, hydraulic results and microseismic behaviour, we deduce different hydraulic behaviour of the activated structures. Moreover, we intend to correlate the spatial seismic intensity to the productivity enhancement of the single stimulations.

SEISMIC NETWORK AND STIMULATION OPERATIONS

Each of the three wells has a 500 m long non cased open hole section to access the formation (Fig. 2) from 4500 to

5000 m. Their bottom hole horizontal distance is about 600 m each. GPK2 was deepened in 1999 and stimulated in 2000; GPK3 was then drilled into the edge of the stimulated area and stimulated in 2003. Targeting, drilling and stimulation of GPK4 was performed in 2004 and 2005. Resulting from stress measurements and the orientation of microseismicity observed during the stimulations, the open hole sections of the wells are aligned along an azimuth of N170°-N180° which represents both the direction of maximum horizontal stress (SH=169° N from Valley&Ev ans, 2006) and main direction of microseismicity.

The seismic data we present in this paper are collected with the downhole network which was deployed to monitor the microseismicity during hydraulic experiments. It consists of six observation wells GPK1, EPS1, 4616, 4501, 4601 and OPS4 (Fig. 2) equipped with 4-component accelerometer sensors and geophones or hydrophones. The data were transmitted in analogue by landline and radio telemetry to the data acquisition room where they were band pass filtered and digitized. The data acquisition system used an amplitude threshold trigger to detect and record the potential microseismic events. The microseismic event location was performed automatically and manually (Dyer, 2001, 2004, 2005).

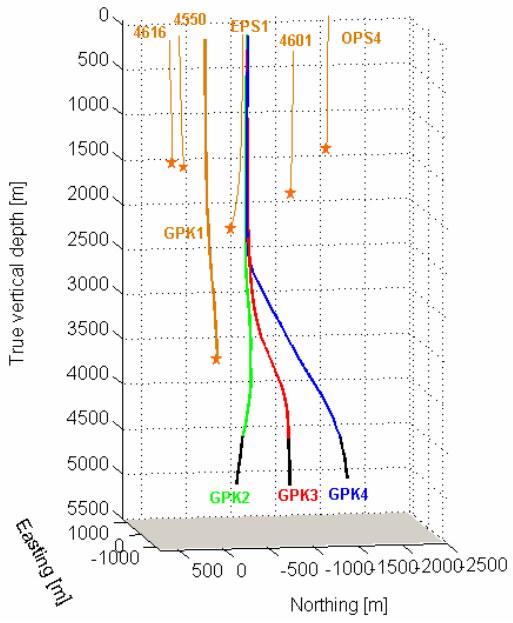

Figure 2: *Sketch of the geothermal borehole triplet: GPK2 and GPK4 are producing wells, GPK3 an injector. The open hole sections are illustrated in black. The surrounding observation wells are orange, the stars indicate the depth level of the installed downhole seismic sensors.*

For our interpretations, we use located seismic events provided by Ben Dyer (Dyer, 2001, 2004, 2005) in order to work with consistent data files for the analysis of temporal and spatial effects. Magnitudes or seismic moments are not to our disposal in a consistent way for all operations so that we interpret the peak amplitudes of the vertical component of sensor 4601 for GPK2 and 4550 for GPK3 and GPK4 as a proxy for the released energy.

The hydraulic data we present in this paper are from the surface hydraulic data acquisition system which was operational during all stimulations. The detailed analysis of the hydraulic tests was performed, if possible, with data from downhole tools.

HYDRAULIC STIMULATIONS AND SEISMIC OBSERVATIONS

In general, the hydraulic stimulations were performed using solely fresh water. Prior to the fresh water, heavy brine with a density up to 1.2 g/cm³ was injected to initiate the opening of fractures at the deeper borehole section. The single stimulations are briefly described below.

GPK2 (2000)

The initial productivity of GPK2 was around 0.02 l/(s*bar). The well was hydraulically stimulated during 6 days by the injection of 2300 m³ of fresh water at increasing flow rates of 31, 41, and 51 l/s (Fig. 3, blue line in upper graph). A rather flat but continuous pressure increase (green line) in the main injection phase indicates that no constant pressure boundary or infinitely conductive structure was connected to the well by this operation. The differential pressure of about 15 MPa in this phase is lower than expected and shows that the reservoir is close to a critical state. The productivity determined during and after the stimulation is 0.4 l/(s*bar), which means a 20-fold increase in productivity. A more detailed analysis of the stimulation in GPK2 can be found in Weidler et al., (2002), and Tischner et al., (2006).

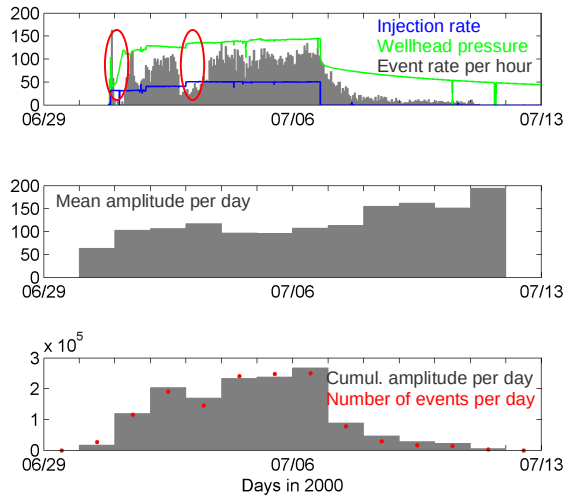

Figure 3: *Summary of hydraulic and seismic parameters during the stimulation of GPK2 in 2002. Upper: wellhead pressure [bar], flow rate [l/s], event rate per hour. Red circles indicate change of trigger level or missing data. Middle: Mean amplitude [cV] per day at sensor 4601V. Lower: Cumulative amplitude [mV] per day and number of events per day, multiplied by a factor of 100 to match amplitude scale.*

During this stimulation, about 31500 triggers were recorded of which 14000 seismic events were located. The latter are shown as event rate per hour in Fig. 3. Due to trigger level changes, the onset of seismicity at the start of the injection is masked by the two spikes, but it seems that the event rate depends on the flow rate. A rather stable rate of 100 events per hour occurred at a constant flow rate which means that fractures continued to be generated. The seismicity as well as the pressure decreased slowly once the well was shut in. The magnitudes of the located events range in magnitude between -0.9 and 2.6; the largest event occurred during the shut-in of GPK2. The mean amplitudes of sensor 4601V are illustrated in the middle part of Fig. 3 and indicate a small increase in event strength during the injection and a significant increase in event size during shut-in, although the number of events per day is decreasing after the injection (Fig. 3, lower). The lower graph allows to infer the

distribution of event strength during each day: assuming a constant strength distribution of events for each day, the cumulative amplitude is proportional to the event number. In the case of GPK2, we see a rather constant relation between cumulative amplitude and cumulative event number meaning that the strength distribution of events did not change with time. In contrast, the cumulative amplitude would increase relative to the event number when the strength distribution contains relatively more strong events. When the partition of smaller events is growing, the amplitude would decrease in relation to the event number.

GPK3 (2003)

GPK3 as the future injection well had an initial productivity of 0.2 l/(s*bar). The fracturing operation in 2003 consumed 37500 m³ of fresh water (Fig. 4, blue line). During the first 6 days, the injection rate was 30 and 50 l/s with two peaks of 60 and 90 l/s. The following simultaneous injection into GPK3 and GPK2, the 'focused stimulation', (Hettkamp et al., 2004, Baria et al., 2006) aimed at concentrating the fracturing process between the wells GPK2 and GPK3. The injection stopped with a stepwise decrease of injection rate in GPK3 in order to avoid a too fast pressure change in the reservoir, as recognized from the GPK2 stimulation. After the occurrence of bigger events in this shut-in phase, the well GPK2 was discharged at 10 l/s to depressurize the reservoir. The pressure during the stimulation of GPK3 (Fig. 4, upper graph, green line) is characterized by a flow rate-dependent trend and a low overall pressure level. An almost stable pressure is observed only after the fifth day of operation, supposing therefore an effective stimulation only for the last 4 – 5 days at the onset of the 50 l/s injection. The productivity obtained during stimulation was 0.3 l/(s*bar) (Tischner et al., 2007) and is confirmed by post-stimulation injection tests.

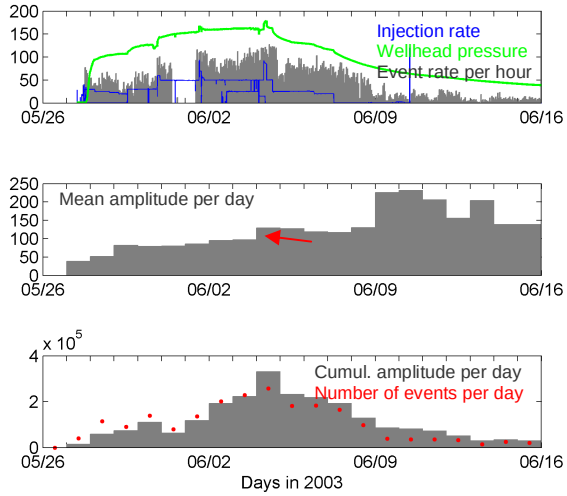

Figure 4: *Summary of hydraulic and seismic parameters during the stimulation of GPK3 in 2003. Upper: wellhead pressure [bar], flow rate [l/s], event rate per hour. Middle: Mean amplitude [cV] per day at sensor 4550V. Lower: Cumulative amplitude [mV] per day and number of events per day, multiplied by a factor of 100 to match amplitude scale.*

The stimulation triggered 92980 seismic records of which about 22000 could be located. The event rate per hour (Fig. 4, top) shows a correlation to the flow rate and reaches its maximum of 130 events per hour in dual injection where the absolute flow rate (GPK2+GPK3 injection) is highest. The mean amplitude per day (Fig. 4, middle) is slightly masked by a clipping of amplitudes at 2.3 V corresponding to roughly a magnitude of 2.3. Nevertheless, the mean amplitude seems to be correlated to flow rate changes but increases only slightly during the stimulation. One points seem to be non-proportional: a step is observed during the dual stimulation (06/04) when the overpressure reaches it maximum (Fig. 4, middle, red arrow). A strong increase of amplitudes occurs again during the shut-in phase. The lower graph in Fig. 4 indicates that the fraction of stronger events in the strength distribution of all events per day in increasing with time, shown by the changing relation between cumulative amplitude and cumulative event number. The strongest events of magnitude 2.6 to 2.9 occurred again in the shut-in phase, although the strategy of a 'stepwise' shut-in was chosen.

GPK4 (2004 and 2005)

The initial productivity of the well GPK4 was ~ 0.01 l/(s*bar). In order to avoid the development of stronger microseismic events, the stimulation of GPK4 was split in two parts with each a small volume and short duration. The first stimulation in September 2004 used 9400 m³ of fresh water in 3.5 days. A flow rate of 30 l/s, with peaks of 40 to 45 l/s for a few hours each, was applied. In spite of the lower flow rate, the pressure level was higher than during the stimulations of GPK3 and GPK2 and increased very rapidly by 170 bar and decreased slowly to ~165 bar. The high pressure level as well as the slow decrease are typical for the creation of an artificial fracture (Tischner et al., 2006). A weak overpressure was observed in GPK3 (~1.5 bar) and GPK2 (~1.1 bar) as well.
About 5700 seismic events were located during the first stimulation with a maximum magnitude of 2.3 (Dyer, 2005) and are shown in Fig. 5. The observed event rate is low with about 70 events per hour and the fraction of larger events decreases faster during the shut-in compared to GPK3. Only a few microseismic events saturated the sensor. Again the mean sensor amplitude per day (Fig. 5 middle) increases only slightly with time and shows a significant change in the shut-in.

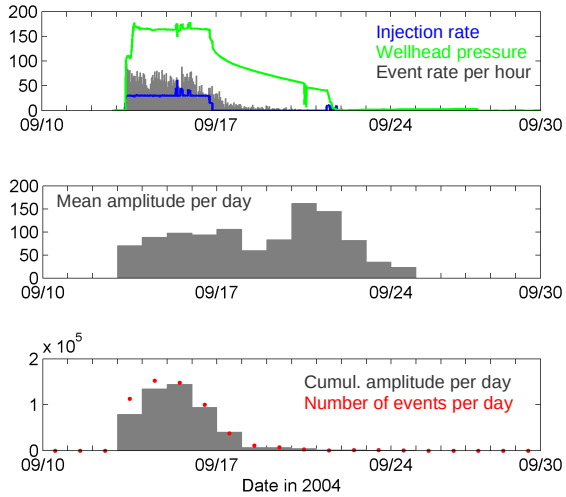

Figure 5: *Summary of hydraulic and seismic parameters during the first stimulation of GPK4 in 2004. Upper: wellhead pressure [bar], flow rate [l/s], event rate per hour. Middle: Mean amplitude [cV] per day at sensor 4550V. Lower: Cumulative amplitude [mV] per day and number of events per day, multiplied by a factor of 100 to match amplitude scale.*

The second stimulation (Fig. 6) began in February 2005 with the injection of 12300 m³ of water with flow rates of 30, 45, and 25 l/s. The highest overpressure (180 bar) of all stimulations was reached and indicates rather a refilling of the already stimulated rock mass instead of an efficient stimulation. Moreover, analysis of the shut-in curves of both stimulations of GPK4 indicates that the second stimulation did not further improve the productivity of GPK4. Weak pressure responses in GPK3 (~3.5 bar) and GPK2 (~1.7 bar) were observed during the stimulation of GPK4. The productivity amounts to 0.2 l/(s*bar) at the end of the second stimulation and is retained during the post-injection tests (Tischner et al., 2007).

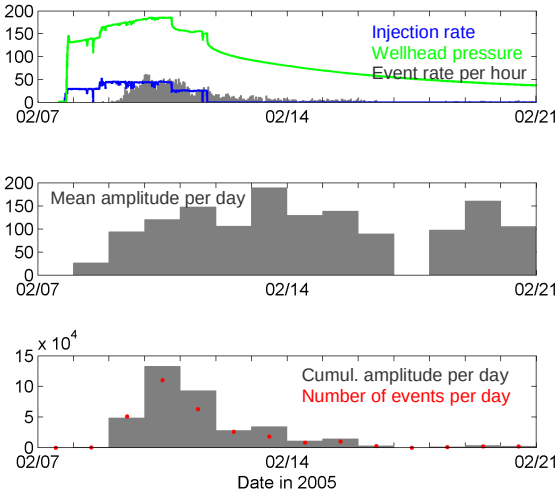

Figure 6: *Summary of hydraulic and seismic parameters during the second stimulation of GPK4 in 2005. Upper: wellhead pressure [bar], flow rate [l/s], event rate per hour. Middle: Mean amplitude [cV] per day at sensor 4601V. Lower: Cumulative amplitude [mV] per day and number of events per day, multiplied by a factor of 100 to match amplitude scale.*

The seismicity (Fig. 6) was less pronounced than during the first stimulation of GPK4 in spite of the higher flow rate and pressure. Only 3000 event were located with an event rate of about 50 events per hour. The onset of seismicity occurs only after about 4000 m² have been injected and corresponds to the thesis that the first part of the injection, as described above, only filled the reservoir instead of having a fracturing effect ('Kaiser-Effect').

DISCUSSION

Seismicity

In all stimulations, the seismic event rate depends on the flow rate, and decreases fast during shut-in. During the stimulation, only a little increase in event strength with duration of injection is observed. The amplitudes rise rapidly during shut-in and are located at the outer boundary of the reservoir since the stimulated area grows outward rapidly after shut-in.
This relation between radius of stimulated area measured from the well and time of investigation is shown exemplary for the stimulation of GPK2 in Fig. 7. The growth of the outer boundary seems to follow a parabolic law and becomes faster as soon as the well is shut-in. Although the seismic propagation is not only governed by diffusion but by a fracturing process, the process might be described by a 'pseudo-diffusivity' D which should be comparable to the one yielded from hydraulic test analysis. After Streltsova (1988), the 'radius of investigation', for which we take the front of seismic events, is described by:

$$r \approx 2 \cdot \sqrt{D \cdot t} = 2 \cdot \sqrt{\frac{k}{n \cdot c_t \cdot \mu} \cdot t}$$

Where
r: Distance of pressure (here seismic) front from well
t: time
n: porosity (0.03)
ct: total compressibility (1*10-9 Pa^{-1})
μ: viscosity (2*10-4 Pa*s)
(Parameters taken from Tischner et al., 2006)

Using these parameters and assuming an initial permeability of k= 9*10-17 m² (Nami, pers. comm., 2008) yields the lower boundary with D= 0.015 m²/s, indicated in red in Fig. 7. After the stimulation, the reservoir had a permeability of 2*10-15 m² (Nami, pers. comm. 2008) which is presented by the orange line (D=0.33 m²/s). This line roughly encloses the seismic front during the stimulation and therefore we suspect whether the permeability **after** stimulation can be estimated from the spatio-temporal development of the microseismicity **during** stimulation.
A similar result was obtained by Tischner (2007) for a comparison of productivities during and after the stimulation. The authors concluded that the target productivity of the wells can be steered during the stimulation by adjusting the flow rate. The productivity during the stimulation is then proven to pertain also after the stimulation. Since productivity is governed by permeability, the same mechanism might explain our observations here but has to be clarified by analyzing systematically the other stimulations.

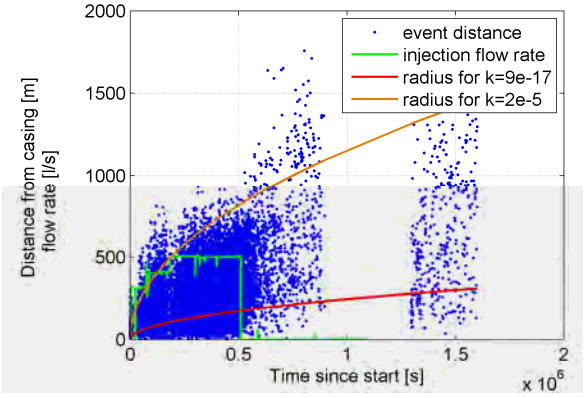

Figure 7: *Radial distance of microseismic events from the casing during the stimulation of GPK2. It is clearly seen that the seismic events spread out from the well, especially after shut-in, when the inner region of the stimulated area becomes void of events*.

Baisch et al. (2006) analysed the above illustrated accelerated movement of the microseismic events far from the well and the occurrence of the strongest events during the shut-in phase. They suggested that the spatial gradients of the fluid overpressure are small on the outer boundaries of the stimulated area so that only relative small stress-diffusions are sufficient to make many patches overcritical for slipping at a time.

Hydraulic Characteristics

Table 1summarizes the main stimulation parameters flow rate, improvement in productivity and the number of located seismic events.

Well	Inj. Volume [m³]	improvement	Events	Stim. Volume [km³]	Stim. Volume per inj. volume (m³/ m³)
GPK2	23000	0.02 0.4	31500/ 14000	0.468	20300
GPK3	37500	0. 2 0.3	93000/ 22000	1.013	27000
GPK4 2004	9400	0.01 0.2	36536/ 5700	0.164	17400
GPK4 2005	12200	0.2	3000	0.179	14700

Table 1: *Summary of main stimulation parameters for the stimulations in GPK2, GPK3, and GPK4.*

The following hydraulic characterizations as results of post-stimulation tests are taken from Tischner et al., (2006), and give insight into these observations.
It is striking that the stimulations of GPK2 and GPK4, both wells being initially non-productive, were very successful and improved the productivity of the wells by a factor of 20. This observation is in agreement with the characteristics of the rather flat or even decreasing pressure curves recorded during the stimulations: for GPK2 and at least the first stimulation of GPK4, they indicate an effective stimulation where the pressure is clipped by the fracturing process.
Nevertheless, the flow regimes of the two wells are different: a formation linear flow regime at GPK2 indicates that a conductive fracture is connected to this well. For GPK4, the bilinear flow regime means that pressure losses do not only occur in the formation but also in the fracture itself. The high pressure level during the stimulation supports this observation. The decrease of pressure at constant flow rate during the stimulation is typical for the creation of tensional fractures which would require a higher pressure to open and which, in general, would have a lower conductivity than shear fractures.

In contrast to GPK2 and GPK4, the well GPK3 could not be significantly improved, although the highest volume has been injected and the largest number of seismic events and also the strongest events were recorded. The post-stimulation tests showed that this well is characterized by formation linear flow regime, but with an infinitely high conductive fracture connected. The surface area and storage of this structure have been calculated from post-stimulation tests and are up to 47000 m² and 2 – 5 m³/bar. Due to the initially high productivity of the well, flow rates up to 30 l/s could be injected at the beginning without significant stimulation. An effective stimulation could only be performed in the last days of the operation and it seems that probably a great amount of the injected water penetrated into the formation without a significant stimulation effect.

A comparison of flow logs from GPK3 (left in Fig. 8) and GPK4 (right in Fig. 8) shows the difference between the two wells which are responsible for the different flow regime. GPK3 shows a distinct outlet of about 70 % at 4760 m measured depth where UBI (Ultrasonic Borehole imager) and geological analysis identified an intersecting open fracture zone which was also initially highly productive. This structure connects the wells GPK3 and GPK2 (Dezayes et. al., 2005) and runs below GPK4 in 5100 m. The connection is also hydraulically visible in the reaction of GPK2 to drilling in GPK3 and vice versa. In contrast, GPK4 shows a zone of continuous fluid loss over a well length of 100 m (dashed line in Fig. 8, right). The hydraulic indications of a tensile fracturing process during stimulation suggest that there is an axial fracture in GPK4 which would also explain the low hydraulic conductivity. Such a tensile fracture could be operative only in the vicinity and therefore does not mean a contradiction to the general knowledge that shearing is the main permeability creating process.

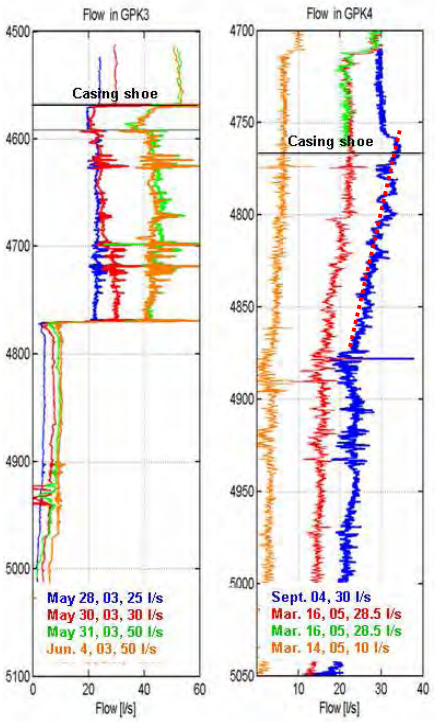

Figure 8: *Flow logs in GPK3 (left) and GPK4 (right) in measured depth along the well. While GPK3 shows a distinct flow outlet at 4760 m, GPK4 is characterized by continuous flow loss between the casing shoe at 4756 m and about 4870 m (red dashed line).*

The different efficiency of the stimulations is explained by Tischner et al. (2007) who found that the pressure reached during a stimulation is mainly controlled and clipped by rock stress and the means to influence the productivity is then to adjust the flow rate. The higher the flow rate (for the given extrinsic rock stress), the higher the productivity will be. For GPK3 the flow rate was not high enough to raise its productivity above 0.3.

The summary in table 1 also lists microseismic parameters in order to establish a correlation between the seismic and the hydraulic behaviour. One striking feature is that the volume of the stimulated area (determined by the distribution of microseismic events in space and listed in the last column) seems to be correlated to the strength of microseismic events. The stimulation of GPK3 created the strongest events of M=2.9 during the shut-in and the seismic cloud reached the highest volume. The injection into GPK2 created a smaller stimulated volume and yielded smaller events, and the stimulation of GPK4 was the 'softest' with regards to stimulated volume and events size. This observation is again in agreement with the hypothesis by Baisch et al. (2006) suggesting the event size depends on the size of the activated area (compare paragraph 'Discussion/Seismics' herein).

Moreover, table 1 suggests that neither the injected volume nor the number of the arising microseismic events are the key parameters for the efficiency of a stimulation. GPK3 was stimulated with highest flow rate therefore highest event rate and accordingly the most seismic events. Also a high volume of the stimulated area (as a consequence of a high injected volume) is not a meaningful parameter. Therefore the success of a stimulation is not reflected in the seismic parameters directly, but the spatial seismic intensity correlates with the stimulation success, as shown below.
Moreover, the

Correlation Of Hydraulics And Spatial Seismic Intensity

The region where most seismic events were recorded is in the depth section from 4800 to 5100 m. Fig. 13 shows slices of 100 m thickness plotting the seismic intensity, that means the number of events in boxes of 50x50x100 m, in a colour coded contour plot. Regions with lowest seismic intensity are blue, with highest red.
In all three depths, the intensity of seismicity around GPK2 and GPK4 is more focused and concentrated then around GPK3. Around GPK3, the seismicity is less dense and spatially more dispersed. This correlates with the only minor impact of the injections into GPK3 due to the high permeable fault zone intersecting the well which might have delivered the water far into the formation without considerable stimulation effect. In contrast, the high intensity of events around GPK2 and GPK4 correlate with a highly successful stimulation and an improvement in productivity of a factor of 20.
Therefore we correlate this systematic pattern with the characteristics of the stimulations and conclude that an efficient stimulation is characterised by a narrow spatial extend of the seismicty and a high seismic intensity.

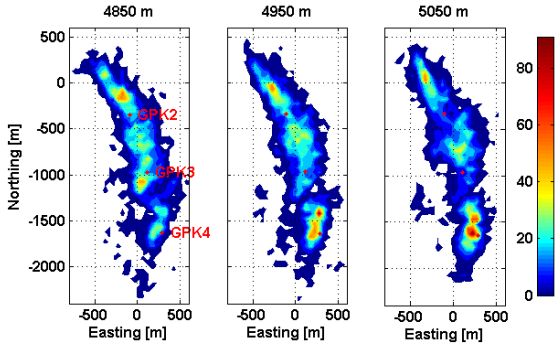

Figure 15: *Seismic event density in the depth 4800 – 5100 m.*

Correlation between Seismicity And Injected Volume

For a fast evaluation of the stimulation success, a measure of energy release by the seismicity is desirable. McGarr (1976) suggested that a measure of deformation during water injections is the total volume of injected water. Furthermore, he found a linear relation between the total seismic moment and the injected volume. Michelet (2002) proved that this relation holds for the stimulation of GPK2, as is shown in Fig. 9. The conclusion was that the injection flow rate could be a means to control the earthquake strength and therefore to control the effectiveness of the stimulation.

Since the seismic moment cannot be inferred from the locations of the microseismic events without using the recorded waveforms, we were looking for another way to correlate a measure of energy/deformation to the injected volume. For this purpose, at each moment, we calculated the total number of events which happened until this time, the cumulative amplitude from the sensor 4550, and also the cumulative volume. Then we made a crossplot of cumulative number of events, respectively cumulative amplitude, versus injected volume. We show examples from the stimulations of GPK3 and GPK4 to demonstrate differences between them.

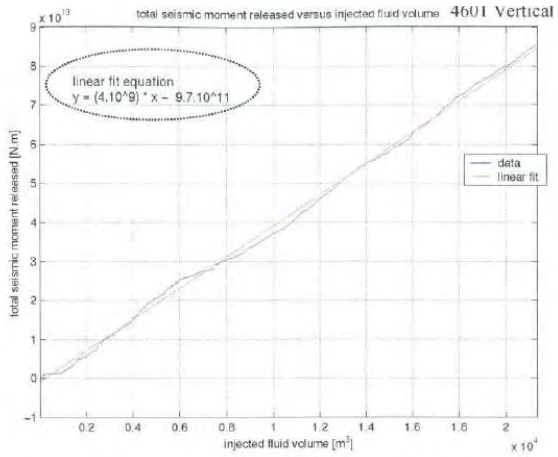

Figure 9: *Cumulative seismic moment vs. injected volume. (Figure taken from Michelet, 2002)*

GPK3 stimulation is illustrated in Fig. 10. The cumulative amplitude is the pink line, the cumulated events are the green, blue and yellow lines which were multiplied by factors to have the same slope like the cumulated amplitude line.

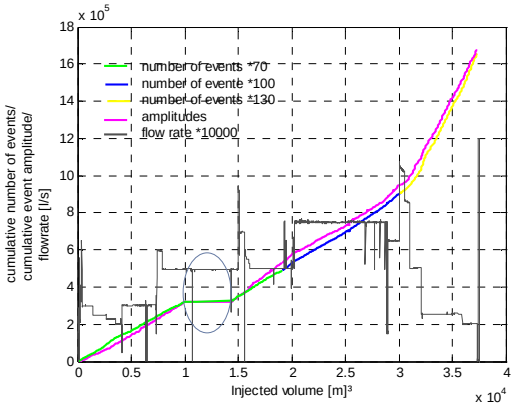

Figure 10: *Cumulative events and amplitude versus volume for GPK3. The colors of the cumulative event number indicate, as in Figure 4, the phase of injection. Blue is dual injection, also visible from the high flow rate of almost 80 l/s. The ellipse indicates a data gap.*

The onset of seismicity is rather direct with the start of the injection. The correlation between the event number and the injected volume is linear, which suggests that a constant number of events is released per injected volume – that means a constant event rate per time for a fixed flow rate, which was already observed earlier and demonstrated in Fig. 4. The correlation between cumulative amplitude and cumulative volume is also linear. This also implies that cumulative amplitude and event quantity are proportional. This might be due to the high number of events with relatively little fraction of big events – or by the averaging effect of the calculation of the sum. At least, these proportionalities should be regarded closer in the future.

The whole characteristic changes only after the dual stimulation and more events or a higher amplitude release per volume are observed (compare Fig. 4, red arrow). The cumulative amplitude clearly becomes steeper in the stepwise shut-in phase of the stimulation reflecting the occurrence of stronger events. The fact that the cumulative event number had to be multiplied by a higher factor than before (to match the amplitude curve) indicates that not more events have occurred but that events have in average a higher amplitude.
For the two GPK4 stimulations, the same linearity is illustrated in Fig. 11 and 12. It is obvious again that the second stimulation of GPK4 was not effective at the beginning, since the seismicity starts only after the injection of 5000 m³.

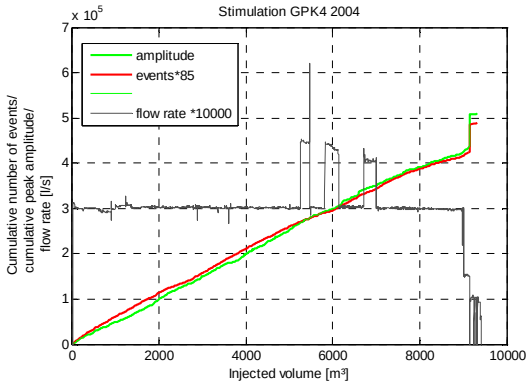

Figure 11: *Cumulative events and amplitude vs. injected volume for the first stimulation of GPK4.*

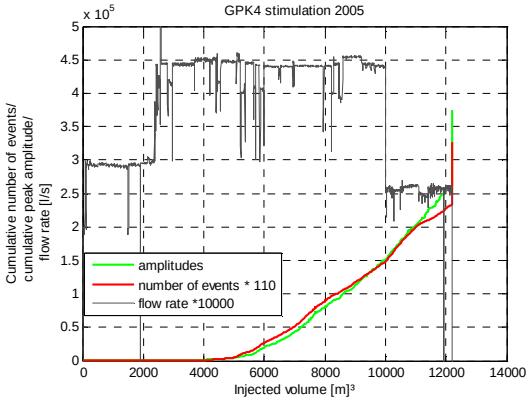

Figure 12: *Cumulative events and amplitude vs. injected volume for the second stimulation of GPK4.*

As a summary we can say that, for all stimulations, both the cumulated event number and cumulated sensor amplitude correlate linearly with the injected volume. Despite from the factor, this correlation is similar to the correlation of total released seismic moment per injected volume and might therefore be used as a fast measure of release energy during a stimulation. Nevertheless, during shut-in, like in GPK3, the amplitude per volume, a proxy for the energy release, increases. Therefore we conclude that not the flow rate, but rather the volume injected, determines the energy release.

CONCLUSION

The stimulations of the three deep wells in 4 steps activated a rock volume of about 3 km³ of the formation. It is systematically observed that the strongest microseismic events occur in the shut-in following the stimulation and that they occur at the outer boundary of the already stimulated area. These observations confirm the theory of Baisch et al. (2006) concerning the origin of those larger events. The temporal development of the distance of the seismic events from the well reflects a kind of diffusive behaviour and can be matched with the permeability obtained from hydraulic tests.

The GPK2 stimulation improved the productivity of the well by a factor of 20 and was an efficient stimulation. GPK3, the dual stimulation, improved only little the productivity due to a permeable fracture zone which probably led the water too far to the outer zones. GPK4 was stimulated twice, and at least the first stimulation had a comparable success to GPK2. It has been shown in an earlier paper by Tischner et. al., (2007), that the productivity reached during the stimulation is completely retained afterwards. For each stimulation, the total number of events released during the injection as well as the cumulative sensor amplitude correlate linearly with the injected volume. This correlation is similar to the correlation of total released seismic moment per injected volume (McGarr, 1976).

The microseismic event distribution observed during the stimulations of GPK2, GPK3, and GPK4 differs for each stimulation and seems to be related to the degree of productivity improvement: the occurence of high seismic activity correlates with a noticeable productivity improvement like for GPK2 and GPK4 while a more diffuse structure and lower number of events per volume correlates with a minor improvement of productivity, as observed in GPK3.

ACKNOWLEDGEMENT

The study was performed within the framework of the European “Hot Dry Rock” project Soultz. The project is funded by the European Commission, the French Ministère délégué à la Recherche et aux Nouvelles Technologies, the French Agence de l’Environnement et de la Maîtrise de l’Energie, the German Bundesministerium für Umwelt, Naturschutz und Reaktorsicherheit, the Projektträger of the Forschungszentrum Jülich in Germany and by the Members of the EEIG “Exploitation Minière de la Chaleur”. The authors also thank Ben Dyer who kindly provided all the seismic data.

REFERENCES

Baisch, S., Weidler, R., Vörös, R. and Jung, R. (2006), „ A conceptual model for post-injection seismicity at Soultz-sous-Fôrets”, Geothermal Resources Council, Trans., Vol. 30, 601-606.

Baria, R., Jung, R., Tischner, T., Nicholls, J., Michelet, S., Sanjuan, B., Soma, N., Asanuma, H., Dyer, B. and Garnish, J. (2006), “Creation of an HDR reservoir at 5000 m depth at the European HDR project”, *Proceedings thirty-first Workshop on Geothermal Reservoir Engineering*, Standford University, Standford, California, January 30-February 1, 2006.

Dezayes, C., Genter, A. and Hooijkaas, G.R. (2005), “Deep-Seated Geology and Fracture System of the EGS Soultz Reservoir (France) based on Recent 5 km Depth Boreholes”,

Proceedings, World Geothermal Congress 2005, Antalya, Turkey, April 24-29, 2005.

Dyer, B. C., (2001), "Soultz GPK2 Stimulation June/July 2000.", *Seismic Monitoring report*, prepared for GEIE "Exploitation Minière de la Chaleur", BP38, F-67250 Kutzenhausen.

Dyer, B. C., (2004), "Soultz GPK3 Stimulation and GPK3-GPK2 circulation May to July 2003", *Seismic Monitoring report*, prepared for GEIE "Exploitation Minière de la Chaleur", BP38, F-67250 Kutzenhausen.

Dyer, B. C., (2005), "Soultz GPK4 Stimulation September 2004 to April 2005", *Seismic Monitoring report*, prepared for GEIE "Exploitation Minière de la Chaleur", BP38, F-67250 Kutzenhausen.

Hettkamp, T., Baumgärtner, J., Baria, R., Gérard, A., Gandy, T., Michelet, S. and Teza, D. (2004), "Electricity production from hot rocks", *Proceedings Twenty-Ninth Workshop on Geothermal Reservoir Engineering*, Stanford University, Stanford, California, January 26-28, 2004.

McGarr, A., (1976), "Seismic moments and volume changes", *Journal of geophysical research*, 81, no8, 1487-1494.

Michelet, S., (2002), "Source parameter analysis and interpretation for microseismic data from the Soultz-sous-Forêts Hot Dry Rock site", Memoire pour l'obtention du Diplôme d'Ingénieur de l'Ecole de Physique du Globe, Strasbourg.

Streltsova, T., S. (1988). Well testing in heterogeneous formations. Wiley&Sons, New York.

Tischner, T., Pfender, M. and Teza, D. (2006), "Hot Dry Rock Projekt Soultz: Erste Phase der Erstellung einer wissenschaftlichen Pilotanlage", *Abschlussbericht zum Vorhaben 0327097,* Tgb. Nr. (BGR): B1.15-10125/06, Januar 2006.

Tischner, T., Schindler, M., Jung, R. and Nami, P. (2007), "HDR Project Soultz: hydraulic and seismic observations during stimulation of the 3 deep wells by massive water injections", *Proceedings, Thirty-Second Workshop on Geothermal Reservoir Engineering*, Stanford University, California, January 22-24, 2007.

Valley, B., Evans, K.F. (2006), "Stress state at Soultz to 5 km depth from wellbore failure and hydraulic observations", Synthetic 2nd year report of the Soultz project (2004-2008), ETH Zürich, presented at the EHDRA scientific meeting held in Soultz, June 15 – 16, 2006.

Weidler, R., Gérard, A., Baria, R., Baumgärtner, J. and Jung, R. (2002), "Hydraulic and micro-seismic results of a massive stimulation at 5 km depth at the European Hot-Dry-Rock test site Soultz, France", *Proceedings, Twenty-seven Workshop on Geothermal Reservoir Engineering,* Stanford University, Stanford, California, January 28-30, 2002

APPENDIX 3 – chemical stimulation

APPENDIX 3(a)

Sandrine Portier, Laurent André and François-D. Vuataz, 2007, Review on chemical stimulation techniques in oil industry and applications to geothermal systems, a technical report prepared for the EC-financed co-ordination project ENGINE (Enhanced Geothermal Innovative Network for Europe), Work Package 4: Drilling, stimulation and reservoir assessment, CREGE-Centre for Geothermal Research, Neuchâtel, Switzerland, November 2007.

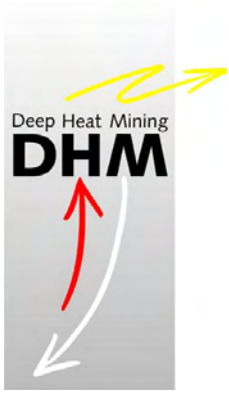

DHMA
Deep Heat Mining Association

ENhanced Geothermal Innovative Network for Europe
Work Package 4 :
Drilling, stimulation and reservoir assessment
Participant No 28:
Deep Heat Mining Association – DHMA, Switzerland

Technical report

Review on chemical stimulation techniques in oil industry and applications to geothermal systems

by Sandrine Portier, Laurent André & François-D. Vuataz

CREGE – Centre for Geothermal Research, Neuchâtel, Switzerland

May 2007

CENTRE DE RECHERCHE EN GEOTHERMIE
c/o CHYN
CH-2009 Neuchâtel, Suisse
www.crege.ch

Table of contents

Review on chemical stimulation techniques in oil industry and applications to geothermal systems

Sandrine Portier, Laurent André [2] & François-D. Vuataz

CREGE – Centre for Geothermal Research, c/o CHYN, CH-2009 Neuchâtel, Switzerland

e-mail : sandrine.portier@crege.ch; francois.vuataz@crege.ch

[2] Present address : BRGM, Bureau de Recherches Géologiques et Minières, EAU/M2H, F-45060 Orléans Cedex, France

e-mail: l.andre@brgm.fr

1 Introduction

The Enhanced Geothermal Systems (EGS) are dedicated to the exploitation of the heat present in deep hot rocks of limited permeability. But this extraction is only feasible if the reservoir permeability is sufficient to ensure a fluid circulation between injection and production wells. Economic exploitation of enhanced geothermal systems is dependant on natural or induced mineral precipitation and associated decrease in permeability of the system. This may inhibit fluid flow in well casings or in rock fractures and therefore decrease the heat extraction from the system. One solution to this problem consists in injecting a reacting fluid into the wells, in order to dissolve the secondary minerals scaled on the casing or partially sealing the fractures, to increase the permeability and hence to develop the reservoir.

A study of the literature on acidification of geothermal reservoirs has been attempted mainly based on the Proceedings of the annual Stanford Workshop on Geothermal Reservoir Engineering, the annual Transactions of the Geothermal Resources Council and the last three World Geothermal Congress. Surprisingly, the number of references is very limited, with few recent papers and most of the studies were carried out by a team from the Philippines. Apparently, experiments in geothermal fields are not all published. On the other hand, a wealth of research and publications is mainly available on these topics in the oil industry literature.

Chemical stimulation techniques were originally developed to increase or to recover oil and gas wells production rates to commercial levels. This technology, developed for more than one century by oil industry for the stimulation of oil and gas wells, has also been used in geothermal wells for the last 20 years.

Acid stimulation jobs intend to clean (pre-existing) fractures by dissolving filling materials (secondary minerals or drilling mud) and mobilizing them for an efficient removal by flow transport. Acid treatments have been applied to wells in oil and gas bearing rock formations for many years. Acidizing is probably the most widely used work-over and stimulation practice in the oil industry. By dissolving acid soluble components within underground rock formations, or removing material at the wellbore face, the rate of flow of oil or gas out of production wells or the rate of flow of oil-displacing fluids into injection wells may be increased.

The role and the impact of the different reactants used for the chemical treatments (hydrochloric acid (HCl), hydrofluoric acid (HF), chelatants and mixed compounds) will be explained and some examples of acidizing treatments in geothermal wells will be described. First, various methods used to prevent scaling in oil, gas and geothermal wells or to improve the reservoir fracturation will be presented in this note. The second part of this note will be focused on the chemical stimulation of sandstone reservoirs. Acidizing geothermal wells can be related to sandstone acidizing techniques, because most geothermal reservoirs produce from silicated magmatic or volcanic rocks. Finally, the third part of this technical note is more focused on the cleaning of geothermal wells.

2 Brief history and experience acquired with acidizing

The main objective of a stimulation treatment is to increase the rate at which the formation delivers hydrocarbons naturally. Acid treatments have been applied to wells in oil and gas bearing rock formations for many years. Acidizing is a widely used work-over and stimulation practice in the oil industry. By dissolving acid soluble components within underground rock formations or removing material at the wellbore face, the flow rate of oil or gas out of production wells or the flow rate of oil-displacing fluids into injection wells may be increased.

Acidizing predates just about all well stimulation techniques. Other techniques, such as hydraulic fracturing, were developed much more recently. Acidizing may, in fact, be the oldest stimulation technique still in modern use. The earliest acid treatments of oil wells are believed to have occurred as far back as 1895. The Standard Oil Company used concentrated hydrochloric acid (HCl) to stimulate oil wells producing from carbonate formations in Lima, Ohio, at their Solar Refinery. The acidizing process was applied with great success in the Lima, Ohio wells. Many wells were acidized with remarkable results in the short term. However, the first acid treatment in 1895 was probably considered a novel idea that would not last very long, and acidizing was used very infrequently during the next 30 years probably due to the lack of an effective method for limiting acid corrosion. However, throughout its history, acidizing has a repeating record of quickly and inexplicably losing popularity, seemingly independent of results at times.

Because of the growing interest surrounding acid treatments of limestone formations, new treatments for sandstone formations began to appear. In 1933, Halliburton conducted the first sandstone acidizing treatment using a mixture of hydrochloric and hydrofluoric acid (HF), in a test well belonging to the King Royalty Co., near Archer City, Texas. Unfortunately, the results of first attempt were very discouraging. Dowell did introduce a mixture of 12% HCl – 3% HF, called “Mud acid”, in 1939. Successful wellbore treatments were pumped in the Gulf Coast area. This acid mixture is still quite common and is now known as “regular strength” mud acid.

In 1947, the first hydraulic fracturing treatment was completed in the Hugoton Field (Kansas) and fraccing has also become a standard treatment to improve production. Since that time, hydraulic fracturing has increased recoverable reserves more than any other technique. Historically, carbonate fracture acidizing has experienced limited success in geologic reservoirs characterized by high-closure stress or temperatures above 120° C. Although many formations in North America are sandstone and require the use of granular propping agents, acid fracturing is more commonly used in Europe and the Middle East, especially in Bahrain and Saudi Arabia.

Numerous matrix acidizing treatments of sandstone formations have been conducted since the mid-1960s. In the 1970s and early 1980s there was a proliferation of “novel” sandstone acidizing systems, in order to provide certain benefits such as retarding HF spending, stabilizing fine particles, preventing precipitation of HF-rock reaction products. In the 1980s and into the 1990s, developments in sandstone acidizing addressed treatment execution more than fluid chemistry. More recently, fluid chemistry has again stepped to the forefront (twists on old systems are developed).

Recent years have seen a marked increase in well stimulation activity (acid and frac jobs) with the number of treatments performed more than doubling through the 1990s. In 1994, 79% of the jobs were acid jobs, but since they are lower cost than hydraulic fracturing treatments, they only consumed 20% of the money spent for well stimulation. For acid jobs, the observed failure rate was 32%. Failure rate for the less frequent but more expensive hydraulic fracturing treatments was much lower, only 5%. In analyzing the reasons for job failure, one-third were due to incorrect field procedures, while two-thirds were attributed to incorrect design or improperly identifying well damage.

The acidification of geothermal wells is not frequently used but the operations were borrowed from the treatments performed on oil or gas wells.

3 Technology overview

Advances in oil and gas well stimulation—matrix acidizing, fracture acidizing, hydraulic fracturing, extreme overbalance operations—enable operators to optimally increase well/reservoir productive capacity. Two basic types of acidizing operations can be conducted:

(1) **Matrix acidizing** is performed below fracturing rate and pressure. Acid flows through the matrix with reactions taking place in existing pores and natural fractures.

(2) **Fracture acidizing** is performed above fracturing rates and pressures. Etching of the created fractures provides well stimulation, not just damage removal.

Acid fracturing treatments can be a solution for wells with impaired production. Not only would acid fracturing increase well productivity, but it also would help retain the generated hydraulic conductivity for a longer time period.

The design of any acid-stimulation treatment should begin with a thorough evaluation of the characteristics of the targeted formation. The composition, structure, permeability, porosity, and strength of the rock must be determined, along with formation temperature and pressure and the properties of reservoir fluids.

Furthermore, understanding reservoir mineralogy is essential to designing truly effective acidizing treatments. For most of the 20th century, acidizing oil and gas wells to optimize production gave unacceptably erratic results in primary and remedial applications. The reliability and effectiveness of acid-stimulation technology began to change for the better in the mid-1990s, driven by improved understanding of the complex chemical and physical reactions of minerals with acidizing fluids. Both fundamental and applied research, and results of field work all have confirmed that—whether in a sandstone or carbonate reservoir, a mature field, deepwater environment, or high-temperature reservoir—reliably achieving long-term production increases from acidizing requires a thorough understanding of the formation mineralogy.

Essentially, the productivity of a given well may be impaired either by the natural characteristics of the reservoir rock and fluids or by damage resulting from drilling, completion or production operations. Fracture acidizing treatments can be designed that penetrate deep into lower permeability rock.

3.1 Matrix acidizing

This process is performed below fracturing flow rate and pressure and is normally used for the removal of skin damage associated with work-over, well killing or injection fluids and to increase formation permeability in undamaged wells.

3.1.1 Protocol

It is in the removal of near-wellbore formation damage that acidizing find its primary application. With respect to acidizing, especially sandstone acidizing, assessment of formation damage is perhaps the single most important factor in treatment design. To assess formation damage, it is first necessary to know the skin term in the Darcy's law equation defining well production rate, and its effect on production rate. The production rate is directly proportional to permeability and inversely proportional to skin. Skin damage is a mathematical representation of the degree of damage present. Permeability and skin can be measured with a pressure transient well test. Formation damage can occur during any well operation, including:

- drilling;
- cementing;
- perforating;
- production;
- workover;
- stimulation.

Therefore, in assessing formation damage, all aspects of a well and its history should be investigated, including:

- reservoir geology and mineralogy;
- reservoir fluids;
- offset well production;
- production history;
- drilling history (including fluids used);
- cementing program (including cement bond logs);
- completion and perforation reports (including fluids used);
- workover history;
- stimulation history.

In order to make the most of acidizing, acid treatment design must be approached as a process. The general approach is as follows:

1- select an appropriate stimulation candidate well;
2- design an effective treatment;
3- monitor the treatment for subsequent improvement.

Treatment volumes for matrix acidizing range from 120 to 6,000 liters per meter (L/m) of targeted interval, pumped at the highest rate possible without fracturing the formation.

3.1.2 Conventional acid systems

A number of different acids are used in conventional acidizing treatments. The most common are:

- Hydrochloric, HCl
- Hydrofluoric, HF
- Acetic, CH_3COOH
- Formic, HCOOH
- Sulfamic, H_2NSO_3H
- Chloroacetic, $ClCH_2COOH$.

These acids differ in their characteristics. Choice of the acid and any additives for a given situation depends on the underground reservoir characteristics and the specific intention of the treatment, for example near well bore damage removal, dissolution of scale in fractures, etc.

Factors controlling the reaction rate of acid are: area of contact per unit volume of acid; formation temperature; pressure; acid concentration; acid type; physical and chemical properties of formation rock and flow velocity of acid. These factors are strongly interrelated.

Reaction time of a given acid is indirectly proportional to the surface area of carbonates in contact with a given volume of acid. Extremely high area-volume ratios are the general rule in matrix acidizing. Therefore it is very difficult to obtain a significant acid penetration before spending during matrix treatments.

As temperature increases, acid spends faster on carbonates. It is often necessary to increase pumping rate during acid fracturing to place acid effectively before it is spent. Pre-cooling the formation, or alternating stages of acid and water is another approach.

An increase in pressure up to 500 psi will increase spending time for HCl. Above this pressure, only a very small increase in spending time can be expected with increases in pressure.

As concentration of HCl increases, acid spending time increases because the higher strength acid dissolves a greater volume of carbonate rocks. This reaction releases greater volumes of $CaCl_2$ and CO_2, which further retards HCl.

Physical and chemical composition of the formation rock is a major factor in determining spending time. Generally, the reaction rate of limestone is more than twice that of dolomite; however, at high temperatures reaction rates tend to be nearly equal.

Velocity has a large effect on reaction rate. Retarded acids should be evaluated under flowing conditions since static tests often yield misleading results. In fracture acidizing, an increase in pumping rate increases fracture width. This decreases area-volume ratio, thereby increasing acid reaction time.

The majority of acidizing treatments carried out utilize hydrochloric acid (HCl). However, the very fast reaction rate of hydrochloric acid, and other acids listed above, can limit their effectiveness in a number of applications. All conventional acids including HCl and organic acids react very rapidly on contact with acid sensitive material in the wellbore or formation. Wormholing is a common phenomenon. The rapid reaction means the acid does not penetrate very far into the formation before it is spent. Conventional acid systems are therefore of limited effectiveness in treatments where deep acid penetration is needed. There was an early recognition that it was desirable to delay the rate of reaction of the acid and a variety of techniques have been developed to achieve this. Patents relating to several of these techniques have been issued. Further information on these retarded acid systems is given below.

3.1.3 Retarded Acid Systems

HCl and HF are two acids reacting quickly with carbonates and silicates. However, the objectives of acid treatment are to increase porosity and permeability of the medium, deeply in the formation. Methods, which have been developed to slow the acidizing process, include:

- Emulsifying the aqueous acid solutions in oil (or solvents such as kerosene or diesel fuel) to produce an emulsion, which is reacting slower.
- Dissolving the acids in a non-aqueous solvent (alcohol, gel,...).
- The use of non-aqueous solutions of organic chemicals which release acids only on contact with water.
- The injection of solutions of methyl acetate, which hydrolyses slowly at very high temperatures to produce acetic acid.

In addition to these methods, of which emulsifying the acid is probably the most important, some retardation of the reaction rate can be achieved by gelling the acid or oil wetting the formation solids. Gelled acids are used to retard acid reaction rate in treatments such as acid fracturing. Retardation results from the increased fluid viscosity reducing the rate of acid transfer to the fracture wall. However, use of the gelling agents (normally water soluble polymers) is limited to lower temperature formations as most gelling agents degrade rapidly in acid solution at temperatures above 55°C.

Some retardants can be added to the mud acid (HCl-HF mixture) to slow the reaction rate of acid with the minerals. A key is to inject a solution not containing HF explicitly but a compound able to generate HF at greater depth of penetration and longer reaction time for maximum dissolution of fines (Crowe et al., 1992). This retardant hydrolyzes in water when it enters in the reservoir to form HF according to the reaction:

$HBF_4 + H_2O \rightarrow HBF_3OH + HF$

Other retardant systems can be used as the emulsifying of the aqueous acid solutions in oil, the dissolving of the acids in a solvent (alcohol, gel…) or the injection of solutions of methyl acetate, which hydrolyses slowly at very high temperatures to produce acetic acid.

Malate et al. (1998) also proposed an acid system applicable for moderate to deep penetrations. They used a phosphonic acid complex (HEDP) to hydrolyse NH_4HF_2 instead of HCl. HEDP has 5 hydrogens available that dissociate at different stochiometric conditions. Mixture of HEDP acid with NH_4HF_2 produces an ammonium phosphonate salt and HF.

3.1.4 Other compounds: Chelatants

Besides acids, the chelatants are solutions used as formation cleanup and for stimulating wells especially in formations that may be damaged by strong acids (Frenier et al., 2001). If these compounds are applied in gas and oil wells, this is not yet the case in a routine mode for the development of geothermal reservoirs. They act as a solvent, increasing the water-wetting operations and dissolving (entirely or partially) some minerals containing Fe, Ca, Mg and Al.

The chelatants are mainly used in oil and gas wells and they present as advantage to have very low corrosion rates, much lower than the one observed with HCl solutions, in the same conditions. As a consequence, the use of chelatants needs small amounts of inhibitor to protect the casings.

Among the chelatants, the most used are compounds of the EDTA family (EDTA: Ethylenediaminetetraacetic acid; HEDTA: Hydroxyethylenediaminetriacetic acid; HEIDA: Hydroxyethyliminodiacetic acid; NTA: Nitrilotriacetic acid). The disadvantages of using chelatants are their high cost compared to acids and for some of them, their impact on the environment.

3.2 Fracture acidizing

Fracturing treatments are defined as treatments in which the injection rate of the fluid is larger than the fluid leakoff into the matrix of the formation. Pressure in the wellbore will therefore buildup and eventually lead to tensile failure of the rock, creating a conductive channel. Because of the reactive nature of the fluid, the addition of acid in treatments can dissolve and remove primary and secondary minerals (scales) sealing the fractures. The aim is to change the future flow pattern of the reservoir from radial to linear to effectively stimulate the reservoir and increase production.

In fracture acidizing, the ideal, but rarely achieved outcome is a fracture plane that is continuously conductive from the wellbore all the way to the tip to provide maximum production enhancement from the

surrounding rock. To be effective, etched fracture surfaces must retain sufficient conductivity for production enhancement after fracture closure.

Although a large mass of rock may be dissolved, if the resultant fracture face dissolution does not render the surfaces with sufficient differential relief, the fracture conductivity under closure stress will be low at least for sedimentary rocks. If the acid spends too quickly, excessive spending and acid leakoff near the wellbore will result in little or no conductivity toward the fracture tip. Lack of active acid penetration deep along the fracture plane will result in very short conductive fractures.

Sometimes, acid fracturing was preferred to hydraulic fracturing because proppant cleanout in a well with coiled tubing required operational and safety resources. Additionally, the high conductivity of an acid-etched fracture made acid fracturing a more attractive technique if comparable fracture lengths could be achieved. After several acid fracturing treatments were experienced, it became clear that a normal response of the treated wells was a sharp production increase followed by a slight gain in average production.

Also called acid fraccing, this technique is widely used for stimulating limestone, dolomite formations or formations presenting above 85 % acid solubility. It consists to inject first a viscous fluid at a rate higher than the reservoir matrix could accept leading to the cracking of the rock. Continued fluid injection increases the fracture's length and width and injected HCl acid reacts all along the fracture to create a flow channel that extends deep into the formation. The key to success is the penetration of reactive acid along the fracture. However, the treatment volumes for fracture acidizing are much larger than the matrix acidizing treatment, being as high as 12 000 - 25 000 L/m of open hole.

Three geometric quantities are needed for proper treatment design:

- Acid penetration: distance travelled by acid at end of pumping.
- Live acid penetration: farthest point reached by live acid at end of given pumping stage (live HCl strength > 0.10%).
- Etching distance: maximum distance that etching has occurred. For a one acid stage treatment this is the same as live acid penetration.

3.2.1 Techniques

Acid fracturing is a stimulation technique where acid, usually HCl, is injected into the reservoir at fracturing pressures. Fracture acidizing is also called acid fracturing, acid-fraccing or acid-fracture treatment.

Acid (normally 15% HCl) is then injected into the fracture to react with the formation and create a flow channel (by etching of the fracture surface) that extends deep into the formation. This allows more reservoir fluid to be drained into the wellbore along the new fractures once the well is put back to production.

As the acid flows along the fracture, the fracture face is dissolved in a nonuniform manner, creating conductive or etched channels that remain open when the fracture closes. The effective fracture length is a function of the type of acid used, the acid reaction rate, and the fluid loss from the fracture into the formation. The length of the etched fracture limits the effectiveness of an acid-fracture treatment. The fracture length depends on acid leakoff and acid spending. If acid fluid-loss characteristics are poor, excessive leakoff will terminate fracture extension. Similarly, if the acid spends too rapidly, the etched portion of the fracture will be too short. The major problem in fracture acidizing is the development of wormholes in the fracture face; these wormholes increase the reactive surface area and cause excessive leakoff and rapid spending of the acid. To some extent, this problem can be overcome by using inert fluid-loss additives to bridge wormholes or by using viscosified acids.

The effective length of an acidized fracture is limited by the distance that acid travels along the fracture before it is spent. This is controlled by the acid fluid loss, the reaction rate and the fracture flow rate. This problem is more difficult to solve when the acid reaction rate is high, owing to high formation temperature.

The acid fluid-loss mechanism is more complex than that of non-reactive fluids. In addition to diffusive leak off into the formation, flowing acid leaks off dynamically by dissolving the rock and producing wormholes. Wormholes are very detrimental in fracture acidizing. They greatly increase the effective surface area from which leak off occurs and are believed to affect acid fluid loss adversely. Acid leaks off predominantly from wormhole tips rather than the fracture face. As wormholing and excessive leak-off occur, the leak-off rate exceeds the pump rate, and a positive net fracturing pressure cannot be

maintained to keep the fracture open. At this point in the treatment, this may be as soon as 6 minutes after starting to pump acid, the fracture extension slows or stops.

Acid fluid loss control has long been a problem in fracture acidizing. The most common techniques involve use of viscous pads. The principle behind these is to lay an impermeable filter cake on the fracture face and minimize wormholing. In practice these filter cakes are relatively ineffective in controlling acid fluid loss because of the quick penetration in wormholes and the constant erosion of fracture faces during treatment.

The key to success is penetration of reactive acid along the fracture. This is more difficult to achieve in acid fraccing than in propped fractures (the other main form of frac treatment). Acid penetration is particularly important in low permeability formations which are frequently subject to scaling where small fractures meet larger fractures. Acid fracturing methods, which can achieve deep acid penetration, offer large potential to solve scaling problems.

3.2.2 Fluids used

To achieve deeper penetration in fracture acidizing, it is often desirable to retard acid reaction rate. This can be done by gelling (polymers and surfactants), emulsifying, or chemically-retarding the acid, in effect, making it more difficult for the H^+ ions to contact a reactive surface. Also HCl can be retarded by adding $CaCl_2$ or CO_2. Another approach is to use naturally retarded acetic or formic acid.

An ideal fracture acidizing fluid is able to penetrate long distances, etch fracture faces, increase the permeability of the matrix where the fluid enters the formation by diffusion, and remove any existing formation damage (Table 1). In addition the low viscosity of the fluid means that maximum production rate should be attained quickly following the treatment. The pad fluid used in conventional treatments would probably be needed.

Table 1: Fluid properties required from an acid fracturing fluid are shown in Table below.

Acid fracturing fluid properties required	Low viscosity
	Etches fracture face by dissolution
	Leaks off into formation mainly by diffusion
	Causes minimal formation damage
	No wormholing

Fluids used in the fracture acidizing process (pad fluid, acid or additives) can be detrimental to well performance following the job. This can be due to clean up problems or a reduction in the formation permeability adjacent to the fracture.

A particular problem is the removal of high viscosity fluids. The time required to achieve cleanup increases significantly as fluid viscosity increases. Similar increases in cleanup time are seen as fracture length increases.

Ideally the best acid system for fracturing is one that only etches the fracture face by dissolution and leaks off into the formation mainly by diffusion. It is also very desirable to be able to obtain deep penetration along fractures without resorting to the use of high viscosity components.

3.2.3 Typical treatment modes

Acid solubility of the formation is a key factor influencing whether fracture acidizing or proppant treatments should be employed. If the formation is less than 75% acid soluble, proppant treatments should be used. For acid solubilities between 75 and 85%, special lab work can help define which approach should be used. Above 85% acid solubility, fracture acidizing would be the most effective approach.

There are four primary fracture acidizing processes:

- Fluid-loss control strives to contain the acid in natural/ created fractures.
- Conductivity enhancement pumps a viscous fluid padpumped ahead of the acid to generate a fracture geometry. Subsequent acid injection then fingers through the viscous pad. The process

results in longer acid penetration distances and more effective conductivity at a greater distance along the induced fracture.

- Etched height control uses fluid density differences to control fluid placements, such as avoiding water-producing zones or gas caps.

- Tailored treatments may include foamed acids, heated acids, zonal coverage acid, and closed-fracturing acid.

Fluid-loss control is critical for achieving a good fracture acidizing treatment. Acid leakoff can be controlled by viscosifying the acid, adding solid particulates or using alternate stages of acid and nonacid fluids. Methods for thickening acid include emulsified acid, foamed acid, polymer gelled acid, and surfactant gelled acid. Silica flour and 100-mesh sand are common solid particulates.

In larger open hole, acid diversion is important, otherwise only the interval, which breaks down or fractures first will be treated. Diversion can be achieved with packers.

The following techniques have been developed:

- Viscous preflush in fracture acidizing.
- Chemically retarded acid for selective etching.
- Combination of density and viscosity controlled fracture acidizing.

Various acid combinations are employed. However, a frequent mixture is 15% HCl and 10% acetic acid.

A typical treatment consists of pumping the acid mixture at pressures of 0.1 to 0.3 bar per metre. When acid is pumped at high rates, over 1000 liters per minute, it is called fracture acidizing. Several services companies offer some or the whole series of chemical treatments for oil, gas or geothermal wells as shown on figure 1.

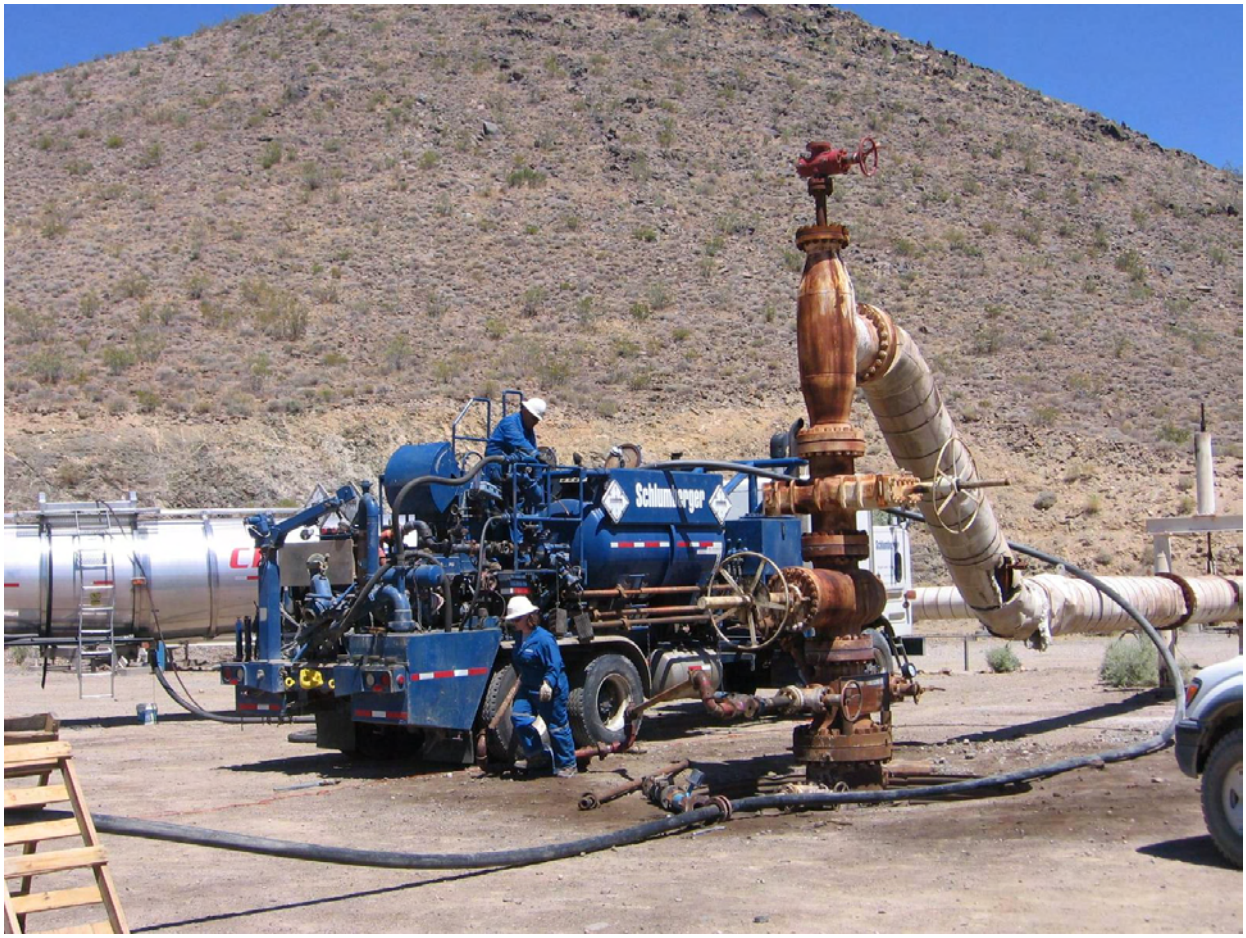

Figure 1: Installation of a pumping unit for injection of chemical compounds at Coso geothermal field (photo P. Rose, EGI, Univ. of Utah)

4 Chemical stimulation in sandstone reservoirs

The objective of acidizing sandstone wells is to increase permeability by dissolving clays and other pore plugging materials near the wellbore. Clays may be naturally occurring formation clays or those introduced from drilling, completion or workover fluids.

Treatment fluid selection in sandstone formations is highly dependent on the mineralogy of the rock as well as the damage mechanism. Hydrofluoric (HF) acid is typically used to dissolve the damaging silicate particles. Nonacid systems are sometimes used to disperse whole mud and allow it to be produced with the treating fluid. The criteria for selecting the treating fluid are mineralogy, formation damage mechanism, petrophysics and well conditions.

The treating fluid, therefore, must remove existing damage without creating additional damage through interactions with the formation rock or fluids. A formation is sensitive if the reaction between the rock minerals and a given fluid induces damage to the formation. The sensitivity of a formation to a given fluid includes all the detrimental reactions that can take place when this fluid contacts the rock. These detrimental reactions include the deconsolidation and collapse of the matrix, the release of fines or the formation of precipitates. The precipitation of some damaging compounds cannot be avoided. Treating and overflush fluid stages are sized; so, there is sufficient volume to push potential precipitates deep enough into the reservoir to minimize their effects because of the logarithmic relationships between pressure drop and distance from the wellbore.

Sandstones can be sensitive to acid depending on temperature and mineralogy. Ions of silicon, aluminum, potassium, sodium, magnesium and calcium react with acid and can form precipitates at downhole temperatures, once their solubility product is exceeded. If these precipitates occur in the near wellbore area, they can damage the formation. Sensitivity depends on the overall reactivity of the formation minerals with the acid. Reactivity depends on the structure of the rock and the distribution of minerals within the rock, i.e., the probability of the acid reaching the soluble minerals.

The sensitivity of sandstone will also depend on the permeability of the formation. Low permeability sandstones are more sensitive than high-permeability sandstones for a given mineralogy. Acid formulations should be optimized on the basis of a detailed formation evaluation (Davies *et al.*, 1992, Nitters and Hagelaars, 1990).

4.1 Sandstone acidizing process (treatment design)

There are a limited number of reasons why sandstone acidizing treatments do not succeed.

The six-step process to successful sandstone acidizing is as follows:

1. determine the presence of acid-removal skin damage;
2. determine appropriate fluids, acid types, concentrations, and treatment volumes;
3. determine proper treatment additive program;
4. determine treatment placement method;
5. ensure proper treatment execution and quality control;
6. evaluate the treatment.

All sandstone acid treatments are variations of the following maximum step procedure:

1. formation water displacement;
2. acetic acid stage;
3. HCl preflush stage;
4. main acid (HF) stage;
5. overflush stage;
6. diverter stage;
7. repeat steps 2-7 (as necessary);
8. final displacement stage.

Sandstone acidizing reactions occur where the fluids meet minerals. As fluid is injected, the position of the zone where reactions take place moves radially outward from the wellbore. As the acid moves through the near wellbore region where all acid soluble minerals have been dissolved, it retains its full strength. Acid spending takes place in the reaction front. The radial width of this zone depends on the

minerals present and the temperature of the reservoir at the point of contact, which is affected by any residual cool down effects due to difference between fluid and rock temperature. When the injected fluid is totally spent, it moves through the unreacted minerals.

The primary reactions occur when fresh acid contacts fresh reservoir. This typically happens in the near wellbore region. As spent acid moves through this same matrix, the secondary and tertiary reactions occur with the reaction products precipitating further away from the wellbore. It is important to keep the injected fluid moving to carry reaction products past the critical matrix region of the well.

Proper treatment design can be very effective in decreasing the negative effects of pumping acids into sandstone through the use of multiple injection stages and correct fluid selection. A typical matrix treatment in a sandstone will include a preflush, a main fluid and an overflush. When long intervals are treated, diversion stages are pumped after the overflush and before the next stage of preflush.

4.1.1 Preflush

The sequence of fluids used in a sandstone treatment is largely dependent on the damage type(s) being addressed.

A preflush is a fluid stage pumped ahead of the main treating fluid. Multiple preflush stages are sometimes used to address multiple damage mechanisms and prepare the surface for the main treatment fluids. In sandstone reservoirs, the acid preflush, performed most often with a HCl solution, serves two purposes:

- To displace the formation brines, usually containing K, Na, or Ca ions, away from the wellbore so there will be no mixing with HF acids. This decreases the probability of forming alkali-fluosilicates such as potassium hexafluorosilicate.

- To dissolve as much of the calcareous material as possible, prior to injection of the HF acid to minimize calcium fluoride precipitation.

Due to reservoir heterogenities, it is unlikely that the acid preflush will remove all of the calcite. However, it has been shown that reducing calcite below 6% is sufficient to avoid precipitation (Figure 2). This has been investigated and confirmed by fieldwork done by McLeod (1984) and others. Strength and volume guidelines are based on this criterium (Economides and Nolte, 1987).

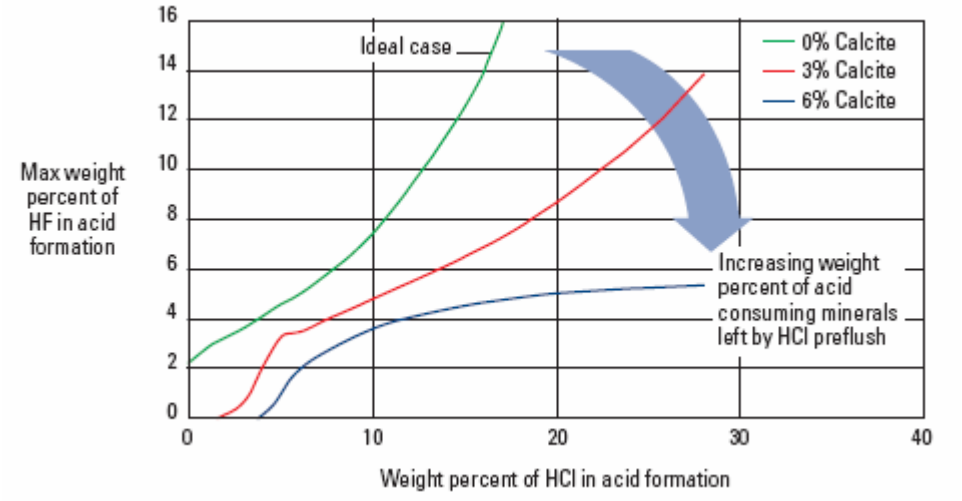

Figure 2: HCl/HF ratio to avoid precipitation, based on AlF_3 and CaF_2 precipitation (Schlumberger, 2003)

HCl can shrink hydrated clays, however, most clays have very little solubility in HCl. One possible exception is chlorite, an iron-rich, three-layer clay. Strong HCl can leach Fe^{2+} iron (and possibly aluminium and magnesium) from chlorite, leaving an amorphous silica residue. HCl does not dissolve sand. However, HCl can dissolve carbonates present in sandstone formations.

Using an additional ammonium chloride (NH4Cl) brine preflush for sandstone acid treatments is an emerging practice. This preflush conditions the formation clays as it moves formation water away from

the near wellbore area. The $NH4^+$ ions in the brine exchange with the alkali (Na, K, or Ca) ions on the clay particles; so, they will be displaced from contact with the mud acid. The effectiveness of this procedure appears to be controlled by the brine concentration at a radial distance of 0.75 m from the wellbore. This preflush is pumped at the start of the job to establish injectivity before the regular mud acid treatment is pumped. It is only pumped once and is not a part of the regular treating sequence.

4.1.2 Main flush

The main fluid in a sandstone acid treatment is the fluid used to remove the damage. It is typically a mixture of hydrofluoric (HF) and hydrochloric (HCl) or organic acids. HF acid is used because it is the only common, inexpensive mineral acid able to dissolve siliceous minerals. It is mixed with HCl or organic acid to keep the pH low when it spends to aid in prevention of detrimental precipitates. These mixtures are called mud acids because they were originally developed to treat siliceous drilling mud damage. HF acid should not be used in sandstone formations with high carbonate content. The risk of forming calcium fluoride precipitates is too great, since it is unlikely that a sufficient amount of HCl acid preflush can be pumped. The accepted cutoff point for the use of hydrofluoric acid is 20% calcite + dolomite based on the guidelines developed by McLeod in 1984.

Hydrofluoric acid (HF) can dissolve carbonates, clays felspars, micas, chert and quartz. However, the primary reason to use HF acid is to remove clay. If any carbonates are present in a sandstone, these should be removed with a preflush of HCl. If a sandstone formation contains more than 20% carbonate, the well should be acidizied with HCl only. Table 2 shows the chemical composition of minerals that are typically present in sandstones and generalizes the solubility of these minerals in HCl and HCl-HF.

Table 2: Solubility of sandstone minerals

Minerals	**Solubility**	
	HCl	**HCl-HF**
Quartz	No	Very low
Felspars	No	Low to moderate
Micas	No	Low to moderate
Kaolinite	No	High
Illite	No	High
Smectite	No	High
Chlorite	Low to moderate	High
Calcite	High	High, but CaF_2 precipitation
Dolomite	High	High
Ankerite	High	High
Siderite	High	High

During the mainflush, the HF acid reacts mainly with the associated minerals of sandstones (clays, feldspars and micas), rather than with quartz. The reaction rates of HF with clays or feldspars are 100 to 200 times faster than the one with quartz. It results from these reactions an enlargement and interconnections of the pores in the matrix, facilitating fluid flow. The risk of using HF acid is the strong affinity of Si and Al with F, which can cause the precipitation of silicium or aluminum complexes (SiF_6^{2-}, AlF^{2+}, AlF_2^+, AlF_3, AlF_4^-), then damaging the formation by plugging. This is why HCl is added to HF: hydrochloric acid keeps a low pH and prevents the formation of fluorosilicates, fluoroaluminates, and fluoride salts.

The trend in HF acid concentration is away from the previous standard 3% HF + 12% HCl.

1.5% HF + 13.5% HCl is becoming the normal choice and Table 3 shows general recommandations for specific well conditions.

Table 3: Alternate sandstone acid procedures for specific formation conditions

Well and formation conditions	Treatment fluid recommandation
Bottomhole treating temperatures > 100°C	1.5% HF + 13.5% HCl
Permeability < 5 md	1.5% HF + 13.5% HCl
Quartz content: Over 90% 50 to 90%	 3% HF + 12% HCl 3% HF + 12% HCl or retarded HF
Feldspar, 15 to 30%	1.5% HF + 13.5% HCl
Chlorite clay: 1 to 5% > 5%	 3% HF + 10% Acetic 1.5% HF + 10% Acetic or Formic

4.1.3 Overflush

The overflush is an important part of a successful sandstone acid treatment. It performs the following functions:

- Displacement of the nonreacted mud acid into the formation.
- Displacement of the mud acid reaction products away from the wellbore.
- Removal of potential oil-wet relative permeability problems caused by some corrosion inhibitors.

The overflush fluid must be miscible with the acid in order to displace it. Therefore, aqueous base liquids should be considered as the first displacing and flushing fluid. This may be followed by other fluid systems depending on the concerns and well conditions. Studies of displacement fronts indicate that the reactivity and fluid character of the overflush have a major influence on the volume required to displace the spent mud acid. Recent experience indicates the advantage of including HCl or acetic acid in the first part of the overflush to maintain a low-pH environment for the displaced spent mud acid stage. The minimum total overflush volume should provide at least 0.9 m of radial penetration into the formation to move potential problems past the critical matrix where the greatest pressure drop occurs. Damage effects are minimized beyond the critical matrix because of the logarithmic relationship between pressure drop and distance from the wellbore. Volumes that are less than twice the mud acid stage volume should be considered inappropriate. Formation permeability anisotropy may require doubling or even tripling this volume, if the reservoir pressure is sufficient to unload the injected fluid.

Large overflushes help prevent the near wellbore precipitation of amorphous silica. At formation temperatures of 93°C or greater, amorphous silica precipitation occurs while the mud acid is being pumped into the formation. The precipitate is somewhat mobile at first, but it can set up as a gel after flow stops. If this potentially damaging material is kept moving by the overflush fluid, it will be diluted and moved beyond the critical matrix.

4.2 Acid strength versus composition of the formation

The acid used as a preflush or an overflush to a main treatment containing hydrofluoric acid depends on the silt and clay content of the formation, its permeability and the presence of HCl sensitive minerals, like chlorite, glauconite and zeolites. For operational simplicity, the same acid is used for both pre- and overflush. Organic acids are recommended for use in conjunction with, or instead of, HCl in sensitive formations. Although they will dissolve the carbonate, they work more slowly. When pumping organic acids as stand-alone fluids, they should be mixed in ammonium chloride rather than fresh water. Organic acids also act as a low-pH buffer and complexing agent that helps minimize the tendency of iron compounds to precipitate as the acid spends. However, they do not dissolve iron scale or prevent clay swelling.

Determining the proper blend of HCl and HF to use in a mud acid mixture, and whether HCl or organic acid is used, is a complex process. The selection depends on the silt and clay content of the formation, its permeability and the presence of HCl sensitive clays. The criteria are similar to those for choosing the acid preflush or overflush concentration.

For the preflush operation in acidizing treatments, a solution of hydrochloric acid at a concentration of 10 to 15 % is most often used. For the mainflush, the mud acids generally range from 10 % HCl – 5 % HF to 12 % HCl – 3 % HF. Some examples of mud acids are given in Table 4 for the treatment of sandstones.

Table 4: Acid guidelines for the chemical treatment of sandstones according to the composition of the formation (after Crowe et al., 1992)

Temp. (°C)	Rock mineralogy (%)	Rock permeability (milliDarcy [md])					
		> 100 md		20 to 100 md		< 20 md	
		HCl (%)	HF (%)	HCl (%)	HF (%)	HCl (%)	HF (%)
< 100	High quartz (> 80), low clay (< 10)	12	3	10	2	6	1.5
	High clay (> 10), low silt (< 10)	7.5	3	6	1	4	0.5
	High clay (> 10), high silt (> 10)	10	1.5	8	1	6	0.5
	Low clay (< 10), high silt (> 10)	12	1.5	10	1	8	0.5
> 100	High quartz (> 80), low clay (< 10)	10	2	6	1.5	6	1
	High clay (> 10), low silt (< 10)	6	1	4	0.5	4	0.5
	High clay (> 10), high silt (> 10)	8	1	6	0.5	6	0.5
	Low clay (< 10), high silt (> 10)	10	1	8	0.5	8	0.5

The cleaner the sandstone (lower silt and clay content) and the higher the permeability, the lower the HCl/HF ratio, and the more aggressive the treatment can be. Typically, the HCl/HF ratio is either 4/1, 6/1, or 9/1. A higher volume of weak acid must be pumped to attain the same results as a smaller volume of a stronger acid. This is an important consideration when designing treatments for environmentally sensitive areas, where disposing spent acids can create problems. The ratio of HCl/HF should be increased if the formation contains clay rather than calcite cementing materials. If the HCl/HF ratio is less than 9/1, change the recommendation to the 9/1 ratio that contains a lower HF content. For example, if a 6% HCl + 1% HF fluid is normally used, change to a 4.5% HCl + 0.5% HF mixture. Mud acids should only be used in formations with less than 20% carbonate (calcite + dolomite) because of the increased risk of forming damaging calcium fluoride precipitates at higher carbonate content. HCl or acetic acids are used for these formations. The specific acid used is dependent upon reservoir temperature and the presence of HCl sensitive clays as shown in Table 4.

4.3 Review of current practices to successful sandstone acidizing

The rate of acid injection is dictated by allowable injection pressure. Selection of acid concentrations must be based on the formation characteristics. Knowledge of permeability, porosity and mineralogy is imperative. Amounts and types of clays and felspars are especially important to ascertain. This information can be obtained trough X-ray diffraction analysis. However, the location of minerals is of greatest importance. SEM (scanning electron microscopy) and thin-section analysis are additionally useful in identifying locations of quartz, clays, feldspars, carbonates, and other minerals.

For HCl-HF mixtures, a small amount of acetic acid (e.g., 3%) may be added to reduce precipitation of aluminium fluoride compounds, as the pH of the HCl-HF mixture rises with acid spending, by buffering the acid mixture and by complexing with aluminium, chelating effect.

Corrosion inhibitor is always necessary. It must be added to all acid stages (acid preflush, main acid, and acid overflushes). It is the “dilute” acid mixtures, like 15% HCl, that have a lot of water present that are corrosive. If concentrated HCl (37% solution) is pumped, corrosion inhibitor is not necessary. That is water present (more than 63% by weight) in acid mixture that causes corrosion.

Iron control is required in any acidizing treatment. Therefore, an iron-control agent is almost always needed. Products exist in two general categories: iron-complexing or iron-sequestering agents, and iron-reducing agents. One or more of these can be used in an acid mixture. Combinations can be effective, especially at higher temperatures, where dissolved iron contents may be high. Iron-control agents react with dissolved iron and other dissolved metal ions to inhibit solids precipitation by maintaining iron cations in solution, as acid spends and pH increases.

A clay stabilizer is often recommended but not necessary for the purpose of preventing migration and/or swelling of clays following an acid treatment. Common clay stabilizers are either polyquaternary amines (PQA) or polyamines (PA), at 0.1-0.4%. Clay stabilizer seems to be most effective when added to the overflush only.

It may be advisable to include a calcium sulphate ($CaSO_4$) scale inhibitor in the acid stages or the overflush if treating a well containing high sulphate concentration (>1000 ppm) in the formation water. $CaSO_4$ scale inhibitors are typically phosphoric acid or polyacrylate polymers.

Coiled tubing (CT) is a very useful tool for improving acid placement. Coiled tubing utility is versatile. However, when applied properly, it is an excellent tool. Coiled tubing is of less use in fracturing acidizing because of rate limitations. It is still best to pump fracturing treatments through larger strings, such as production tubing. Coiled tubing is most useful in matrix and wellbore treatment. It offers some major advantages in acidizing, including:

- Ease with which an acid injection can be terminated, if it appears that continuing injection is not doing any further good, and switch to flush.
- Ease with which treatment displacement with nitrogen can be achieved quickly to push reactive fluids away from the wellbore, energizing the near-wellbore fluid zone, thereby enhancing flowback.

Disadvantages include:

- Pump rate limitations.
- Depth limitations in openhole sections of very deep deviated wells. But some experiments report coil tubing applications up to a depth of 4000 m.
- If solids are needed (perhaps for diversion), there may be problems pumping them through smaller diameter CT strings.
- Acid mixtures must be very thoroughly mixed and must remain that way prior to and during injection. Corrosion in a CT string is especially disastrous.

Overall, coiled tubing is very effective in placing acid, especially in smaller treatments, and treatments for damage very near the wellbore. Treatment evaluation involves the following:

- Pressure monitoring during injection will indicate diverter effectiveness and possibly evolution of skin removal. These methods for evaluating pressure responses are based on interpreting recorded wellhead pressure values and corresponding injection rates as treatment progresses.
- Flowback sample analysis is important for observation of sludge, emulsion, solids production, and related problems.
- Production rate comparison and analysis (before and after) is the most obvious and simple measure of success. Rate comparison should only be made seriously after all spent acid has been returned and well production has returned to formation fluids only.
- Well test analysis (skin removal). Post-stimulation well testing is the truest indicator of success or failure.
- Payout and ROI (return on investment) are among the bottom-line factors to the operator. Relative low-cost formation damage removal treatments, such as acidizing, are unrivaled in their potential financial significance.

Recently, there have been advancements with unconventional methods introduced to the industry by creative, reasonable risk-taking, stimulation design engineers. Some examples of such interesting methods are:

- Maximum rate/maximum pressure HF acidizing.
- High-concentration HF acidizing.
- CO_2-enhanced HF acidizing.
- On-the-fly minimum volume HF acidizing.

4.4 Acidizing damage

Acidizing damage mechanisms include:

- Inadvertent injection of solids.
- Use of incompatible additives or improper mixing procedures.
- Reprecipitation of acid reaction products.

- Loss of near-wellbore formation compressive strength.
- Formation of emulsions.
- Formation of sludge.
- Water blocking.
- Wettability alteration.
- Post-treatment fines migration.

The reprecipitation of reaction products is a serious concern in sandstone acidizing containing alumino-silicates. Many reactions take place in the formation as HF injection proceeds.

The chemical reactions between sandstone minerals and HF acids have been extensively described in the literature. There are three classes of HF reactions: primary, secondary and tertiary.

Primary reactions describe the action of the unspent acid with the various minerals. The presence of calcium (Ca^{2+}) will cause calcium fluoride (CaF_2^{+}) to precipitate. Sodium (Na^{+}) and potassium (K^{+}) can create alkali-fluosilicates and alkali-fluoaluminates when formation minerals, or sodium or potassium brines, react with the hexafluorosilicic acid produced by this reaction. The fluosilicate and fluoaluminate compounds are more likely to form during the initial phases of the dissolution, since a high concentration of HF relative to the clay enhances the reaction. Precipitation of these compounds will occur when the amount present increases above the solubility limit.

Secondary reactions result from the action of the hexafluorosilicic acid with remaining acid and the rock. The driving force for this reaction is the greater affinity of fluorine for aluminum than for silicon. Silica gel precipitation is well documented. This precipitation occurs when the initial HF is nearly consumed. An exchange reaction occurs on the surface of the clays and fines to generate fluoaluminates and silica gel. The silica is deposited on the surface of the mineral particles, and the fluoaluminates remain in solution. This precipitate is more like to occur when fast-reacting aluminosilicates, such as clays, are present. The damaging effect of silica gel precipitates is still a point of debate; however, it does appear that they are more damaging at higher than lower temperatures.

Tertiary reactions are the reactions of the aluminum fluorides and aluminosilicates. The reaction is insignificant at temperatures below 90°C. At higher temperature, the reaction can be considerable depending on the stability of the formation clays with HCl. As the reaction drives on, and HF is spent, complex aluminofluorides may be precipitated out deep in the matrix. Kalfayan (2001) recommendations of 9% HCl + 1% HF are based on these observations.

Post-treatment fines migration is quite common in sandstone acidizing. It may be difficult to avoid in many cases. The reaction of HF with clays and other aluminosilicates minerals, and quartz, can release undissolved fines. Also, new fines may be generated as a result of partial reaction with high-surface-area minerals, particularly the clays. Postacidizing fines migration problems can be reduced by bringing a well on slowly after acidizing, and increasing rate step-wise over time (e.g., one to two weeks), rather than maximizing return production right away.

Besides that, dissolved iron precipitate as iron compounds when acid spends. Iron is another potential source of precipitation during sandstone acidizing. Precipitation is due to the formation of colloidal ferric hydroxide as the acid spends (pH > 2). Sources of ferric iron (Fe^{3+}) include some minerals (chlorite and glauconite clays) and tubing rust (iron oxide). These reactions begin to precipitate gelatinous ferric hydroxide at a pH of 2.2. The nature of the precipitate (crystalline or amorphous) varies as a function of the anions present (Smith *et al.*, 1969). Precipitation of ferric hydroxide during acid injection is normally not a problem, if an adequate HCl tubing wash was used to remove most of the soluble FeO_2. All acids used for matrix treatments should also contain iron control additives, either sequestering or reducing agents or both. Ferrous iron (Fe^{2+}) is typically not problematic, since ferrous hydroxide precipitates at a pH between 7.7 and 9.

The main sources and causes of precipitates formed during sandstone matrix acidizing are summarized in Table 5. The formation of these potentially damaging precipitates is affected by the complex mineralogy of many sandstones.

Damage can be caused during hydraulic fracturing operations too.

Table 5: Possible precipitates in sandstone acidizing (Schlumberger, 2003)

Precipitate	Origin
Calcium fluoride (CaF_2)	Carbonate-HF reaction CaF_2 can be caused by an inadequate HCl preflush to remove calcium ions from calcite cementing materials or to flush calcium chloride completion fluids away from the near wellbore.
Amorphous silica	Clay and silicate dissolution in HF. Amorphous silica results from both secondary and tertiary HF acidizing reactions.
Sodium and potassium fluosilicates	Feldspar and illite clay dissolution in HF produce these primary reaction products. They can also form if seawater or sodium or potassium brines are mixed with spent HF.
Sodium and potassium fluoaluminates	Silico-aluminate dissolution in HF. Fluoaluminates, like fluosilicates, occur when spent mud acid (H_2SiF_6) reacts with the formation. They can also form if seawater or sodium or potassium brines are mixed with spent HF.
Aluminium hydroxides and fluorides	Clay and feldspar dissolution in HF can cause these precipitates.
Iron compounds	Iron minerals or iron oxides (rust) can react with HCl-HF to produce these compounds.

4.5 Completions versus composition

To help improve completions for reservoirs rich in one or more of the minerals listed in Table 6 special consideration should be given to drilling procedures and to treatments/stimulants with the aim of minimizing damage or considering remedial treatments.

Table 6: Mineral – related procedures for completions

Mineral	Potential Effect	Maximizes Damage	Minimizes Damage	Remedy
Smectite	swelling	fresh water, HF	air, KCl, oil-based mud drilling	HCl; re-perforate. & fracturing
Mixed Layer Clay	swelling; mobile fines	fresh water, HF	air, KCl, oil-based mud drilling	HCl; re-perforate. & fracturing
Kaolinite	mobile fines	HF	air, foam drilling	clay stabilized; low flow rates
Chlorite	iron gel precipitate	high pH muds; O_2 rich	air, foam; HCl sequestered	HCl sequestered, low strength
Carbonate minerals	complex CaF precipitates	HF	salt muds; oil-based mud	HCl
Quartz, Feldspar Glass (silt)	mobile fines; gel precipitate	high pH muds	air, foam; bland fluids	clay stabilized; foam fracturing

5 Geothermal wells acidizing procedures

Acidizing geothermal wells is related to sandstone acidizing in that most geothermal reservoirs produce from volcanic rocks (andesite). Formation conditions are often conducive to large-volume, high-rate acid treatments. In geothermal wells, the strongest indication of acid-removable formation damage is a sharp drop in production rate. Nearly all geothermal wells that are acidizing candidates have been damaged by:

- Drilling mud solids and drill cuttings lost to the formation fractures.
- Scale (calcium carbonate, silica, calcium sulphate, and mixtures).

Various methods have been tried to prevent scaling in geothermal wells, including varying pressure, temperature or pH changes and scale inhibitors. If scale inhibitors have solved many problems, one promising alternative method is the acidizing.

One thing geothermal wells have in their favour is that complete damage removal is not necessary. Partial removal of damage with acid treatment may eventually result in complete damage removal when the treated well produces back. The high-rate and high-energy backflow from geothermal wells can blow out damage that was not dissolved by acid. Damage that was softened, broken up, or detached from downhole tubulars and fracture channels can be produced back through a large diameter casing completion. Erosion of production lines may occur if drill cuttings are produced back during blow down of a well after stimulation. Care must be taken in this regard. A temporary flow line may be required until solids production has stopped.

A very successful method of acidizing geothermal wells has been a basic, high-rate, brute-force method. High acid concentrations have been shown to be effective in geothermal wells producing from natural fractures not containing separate, large carbonate zones.

Hydrochloric acid (HCl), hydrofluoric acid (HF) or both have been used since the 1980's in hydrothermal wells. Strawn (1980) listed yet these two acids as the most effective ones. HCl was selected to treat limestone, dolomite and calcareous zones whereas HF was used to dissolve clay minerals and silica.

The only acid additives necessary in a geothermal acid job are:

- Corrosion inhibitor and inhibitor intensifier (often required).
- High-temperature iron-control (reducing) agent.

Water-wetting surfactants, necessary in oil well stimulation, are not needed in geothermal wells because of the absence of hydrocarbons. Suspending agents (nonemulsifier surfactants) are also not needed, although they seem to be included often in geothermal well stimulation job proposals. Clay stabilizer is not needed.

Conventional acid placement techniques are less effective for the long, open-hole or liner-completed intervals typically encountered in geothermal wells. High-temperature foam systems may improve zone coverage. Gelling agents for thickening acid have been shown to be ineffective in geothermal liner completions. The best way to maximize acid coverage in geothermal wells is by pumping at maximum injection rates.

During the 1990's, the acidification technique has been used more often, principally for the reservoir development or to treat formation damage caused by drilling mud and scaling (mineral deposits) in geothermal wells (Buning et al, 1995; Buning et al, 1997; Malate et al., 1997; Yglopaz et al., 1998; Malate et al., 1999, Barrios et al., 2002, Jaime-Maldonado and Sánchez-Velasco, 2003). This protocol has not really evolved since these years. In each of the experiments proposed by the authors, the same technique is used. The acidification occurred in three main steps:

1. A preflush, usually with hydrochloric acid (10%). The objective of this preflush is to displace the formation brine and to remove calcium and carbonate materials in the formation. The preflush acid minimizes the possibility of insoluble precipitates.
2. A main flush with hydrochloric – hydrofluoric acid mixture. A mixture of 10% HCl – 5% HF (called Mud acid) is generally prepared by dissolving ammonium bifluoride (NH_4HF_2) in HCl. A mixture of 1% of HCl and 56 kilos of NH_4HF_2 will generate 1% HF solution. Regular mud acid (12% HC l-3% HF) is made from 15% HCl, where 3% HCl is used to hydrolyse the fluoride salts.
3. A postflush/overflush usually by either HCl, KCl, NH_4Cl or freshwater.

Concerning the injected amounts for the cleaning out of the geothermal wells, the mainflush volume was based on a dosing rate of 900 litres per metre of target payzone. The preflush volume was based on a dosing rate of 600 litres per metre of target zone (Malate et al., 1997; Barrios et al., 2002).

In geothermal well acidizing, more acid often is better. Naturally fractured volcanic formations can withstand high HF concentration. The HCl-HF stage can be 10% HCl - 5% HF, or 10% HCl - 7% HF, for example. These acid mixtures have been used successfully in stimulating geothermal wells in Southeast Asia (the Philippines), where a large number of acid treatments have taken place. Acid volumes can vary quite a bit. These acidizing treatments have also employed an acid formulation containing 3% HCl - 5% HF and an organophosphonic acid. The mixture is less corrosive and may help slow scale reprecipitation, as the phosphonic acid complexes with certain cations in spent acid.

HCl-HF mixture dissolves clays originating from drilling mud and reacts with most constituents of the sandstone formation. It results from these reactions an enlargement and interconnections of the pores in the matrix, facilitating the fluid flow. But, it seems that rapid acid consumption with clays and silicates, matrix disintegration in near wellbore and subsequent precipitation of various reaction byproducts (i.e. complex fluosilicates, fluoaluminates, and fluoride salts) have somewhat restricted the usefulness of mud acid for matrix stimulation treatment. A new acid treatment system (called sandstone acid) is used in treating sandstone formations at some geothermal wells in the Philippines. The new HF acid compared with the usual mud acid systems has a lower reaction rate and a limited solubility action on clays but higher reaction rate and dissolving power with quartz (Malate et al., 1998).

Some retarded or slow reacting HF acid such as fluoroboric, fluoroaluminic and hexa-fluoro-phosphonic were developed to improve rock permeability. Most of these acid systems rely on the use of weak organic acids and their secondary reactions to slowly generate HF acid. Malate et al. (1998) proposed a new acid system applicable for moderate to deep penetrations. They used a phosphonic acid complex (HEDP) to hydrolyse NH_4HF_2 instead of HCl. HEDP has 5 hydrogens available that dissociate at different stochiometric conditions. Mixture of HEDP acid with NH_4HF_2 produces an ammonium phosphonate salt and HF. 76 liters of HEDP acid per 3785 liters of water are required to react with approximately 56 kilos of NH_4HF_2 to produce a 1% HF solution.

The advantages of sandstones acid are:

- Limiting clays dissolution and preventing disintegration of pore matrix by coating them with a film blocking reactions.
- Sandstone acid has better dispersing properties and is an excellent antiscalant inhibiting precipitates formation in the vicinity of the well.
- Excess HCl are not needed to avoid the fluoride salt precipitates. As a consequence, sandstone acid aids in reduction of corrosion.

All these protocols are listed in Schlumberger (2003). However, these properties of acid mixtures should be investigated if one wishes to influence the fractures properties beyond a radius of 5 meters around the wells.

Treatment volumes, injection rates, acid placement techniques, acid system selection and evaluation of the results when stimulating geothermal wells, all follow the same criteria as for oil wells. The important difference is the formation temperature. High temperature reduces the efficiency of corrosion inhibitors (and increase their cost) as well as increasing the acid/rock reaction rate. The high acid rock reaction rate requires the use of a retarded acid system to ensure acid will not all be spent immediately next to the wellbore, but will penetrate deeper into the formation. Protecting the tubulars against corrosion is another serious challenge. This requires careful selection of acid fluids and inhibitors (Buijse et al., 2000), while cooling the well by injecting a large volume of water preflush may reduce the severity of the problem.

6 Review of the chemical treatments in geothermal reservoirs

A study of the literature on acidification of geothermal reservoirs has been attempted. The majority of the papers concern the cleaning out of geothermal wells.

The cleaning out of geothermal wells to increase their productivity after scaling deposits constitutes the main application of the acid treatments. This technique has been used extensively in some geothermal fields in the Philippines (Buning et al, 1995; Buning et al, 1997; Malate et al., 1997; Yglopaz et al., 1998; Malate et al., 1999, Jaime-Maldonado and Sánchez-Velasco, 2003, Amistoso et al., 2005), in El Salvador (Barrios et al., 2002) and in USA (Morris et al., 1984; Entingh, 1999). It presents interesting results, such as the well injectivity increasing by 2 to 10-folds according to the studied reservoirs.

At the Larderello geothermal field (Italy), several stimulation methodologies have been used successfully by ENEL (Capetti, 2006). Among them, chemical stimulation operations were carried out by injection of acid mixtures. First, various laboratory tests were realised on reservoir rock samples to optimize the HCl/HF ratios and the effect on mineral dissolution. Field tests have shown impressive results on five deep wells for reservoir rocks composed of phyllites, hornfels and granites: the improvement of injectivity, respectively productivity ranged from a factor 4 to 10.

In the field of EGS, few chemical treatments have been applied to stimulate fractured reservoirs. Since 1976, some experiments have been tried with more or less of success at Fenton Hill (USA) and Fjällbacka (Sweden). At Coso geothermal field however, 24 wells were successfully treated.

A summary of the chemical stimulation experiments carried out on geothermal fields and EGS reservoirs are presented in Table 7.

Table 7: Results of HCl-HF treatments for scaling removal and connectivity development

Geothermal Field	Number of treated wells	Variation of the injectivity index before and after acid treatment (kg/s/bar)	Improvement factor
Bacman (Philippines)	2	0.68 → 3.01 0.99 → 1.4	4.4 1.4
Leyte (Philippines)	3	3.01 → 5.84 0.68 → 1.77 1.52 → 10.8	1.9 2.6 7.1
Tiwi (Philippines)	1	2.52 → 11.34	2.6
Mindanao (Philippines)	1		2.8
Salak (Indonesia)	1	4.7 → 12.1	2.6
Berlín (El Salvador)	5	1.6 → 7.6 1.4 → 8.6 0.2 → 1.98 0.9 → 3.4 1.65 → 4.67	4.8 6.1 9.9 3.8 2.8
Las Tres Virgenes (Mexico)	2	0.8 → 2.0 1.2 → 3.7	2.5 3.1
Los Azufres (Mexico)	1	3.3 → 9.1	2.8
Beowawe (USA)	1	-	2.2
Coso (USA)	30	24 wells	sucessful
Larderello (Italy)	5	11 → 54 4 → 25 1.5 → 18 - 11 → 54	4.9 6.3 12 4 4.9

6.1 Salak geothermal field (Indonesia)

An acid treatment was carried out to improve the production characteristics of a geothermal well in the Salak geothermal field following an accurate analysis of the possible causes for the initial poor performance of the well. Despite promising indications, the initial steam flow rate from the Awi 8-7 well, drilled during 2004, was below expectations (Pasikki, R. G. and Gilmore, T. G., 2006). An acid stimulation treatment was designed and carried out to improve well performance. The treatment used a hydrofluoric acid system known as Sandstone Acid. The acid was placed to the target interval zone with a two-inch coiled tubing unit to maximize control over the treatment. Well test results before and after stimulation demonstrate that the acid stimulation has successfully produced improvements in overall well

characteristics such as reduction of skin, increase of injectivity and permeability-thickness product, and production output. Based on the positive results obtained in this case, further application of this method is envisaged for other poor-performing wells with similar characteristics.

6.2 Las Tres Virgenes and Los Azufres geothermal fields (Mexico)

In Las Tres Virgenes geothermal field, the steam is supplied by four wells located near the power plants, but LV-11 and LV-13 recorded low wellhead pressure and marginal steam production. LV-11 is a deviated well and was drilled in September 2000 to a total depth of 2081 m. LV-13 was drilled to a total depth of 2200 m. An acidizing job was performed in order to improve the production characteristics of these wells. Acid treatment included a pre, post and over flush using chloride acid (HCl) and a chloride acid-fluoride acid (10% HCl- 5% HF). The acid was injected using a coiled tubing unit. Matrix acid stimulation job for production well LV-11 and LV-13 was successfully conducted without major problems. Post-acid completion tests results indicated major improvements in the injectivity index where a considerable drop in wellbore pressures of the two wells (~30 bars) were recorded that indicated a reduction in the pressure resistance inside the wellbore. The post-acid pressure falloff data also confirmed the improvement in the well where a negative skin (-5.8) was obtained in LV-13 and similar for LV-11. The post-acidizing discharge tests also showed substantial improvement compared with the previous well production characteristics to the acid job. As a result, within less than a month the field steam production increased from 3.2 MW_e to 7.3 MW_e.

The Los Azufres geothermal field is located in the northern portion of the transmexican volcanic belt, 250 km of Mexico city. Currently, 78 wells have been drilled at depths ranging between 700 and 3500 meters. Well Az-9AD is located in the northern zone of Los Azufres geothermal field and it was drilled from January 7 to April 22 on 2003, to a total depth of 1500 m. Early testing and survey analysis indicated that the low output of Az-9AD was caused by considerable drilling induced wellbore damage in its open hole section, where 1326 m^3 of mud were lost. Skin factor of 16 was causing additional pressure drop equivalent to 41 bars, reducing its optimal flow rate. The success of earlier acid treatment jobs in Mexico and the analysis of the available information encouraged the company to apply the same technique for this well during 2005. Acid treatment of well Az-9AD introduced very significant improvement in the wellbore showing 174% increase in production capacity. The results of this job have been used for encouraging new stimulation programs, such as those in wells Az-56R and Az-9A located in the north zone of Los Azufres geothermal field.

6.3 Beowawe geothermal field (Nevada, USA)

The Beowawe geothermal field is composed of a production zone within a volcanic and sedimentary rocks sequence. The geothermal fluid contained in the formation is of $NaHCO_3$ type with a very low salinity (1000-1200 ppm of total dissolved solids).

A first acid stimulation was performed in November 1982 on the Batz well (Epperson, 1983). The acid amounts consisted of about 18.9 m^3 of 15 % HCl acid for the preflush followed by a mainflush composed of 37.8 m^3 of 12% HCl - 3% HF. Then, a Beowawe fluid injection of 35 m^3 was performed to displace the acid farther in the formation. As a consequence, the acidification impact modified the acid displacement pressure from 27.5 bars to about 13.8 bars.

In August 1983, a second acidification test was performed on another well, Rossi 21-19 (Morris et al., 1984). Firstly, 79.5 m^3 of a 14.5% HCl solution was pumped at rates of 40-42 $L.s^{-1}$ and was displaced deeper in the formation by injecting 389 m^3 of water. A water injection test followed this first acidification but no significant change was noted in the injectivity of the well. Secondly, a new reservoir acidification was performed, using 156 m^3 of a 12% HCl - 3% HF acid solution. A total of 480 m^3 of water were injected to displace the acid solution in the formation. The following water injection test then showed a 2.2 fold increase of the injectivity.

6.4 The Geysers geothermal field (California, USA)

An acid stimulation was performed in January 1981 on the OS-22 well (Entingh, 1999). An amount of 75.7 m^3 of 5 % HCl and 10% HF were pumped and 70 m^3 of fresh water were injected to displace the acid mixture deeper into the formation. But, no effect on the well productivity was recorded.

6.5 Coso geothermal field (California, USA)

The Coso Geothermal Field, located in east central California, hosts a world-class power-generating project that has been in continuous operation for the past 15 years. A field experiment was designed for dissolving calcite in a wellbore at the Coso field. The most promising mineral dissolution agent to emerge from the laboratory studies was the chelating agent nitrilotriacetate (NTA) (Rose et al., 2007). The well that was selected was producer 32A-20, which had recently failed due to calcite deposition. A total of 57 m^3 of a 10 wt% solution of NTA was injected into the well in a series of three injections. The solutions were each injected at 13.5-16 $L.s^{-1}$. The total volume of fluid injected (57 m^3) was calculated to be approximately the volume of the open-hole section of the well. Upon completion of the injection of the NTA solution, the well was shut in for approximately four hours, giving the chelating agent time to dissolve the calcite scale.

Once the well was opened, at first the brine was clear, but soon turned to milky white, indicating the presence of the calcium-NTA complex. The concentration of the unreacted NTA dropped from about 34'000 ppm to approximately 2'000 ppm during the experiment. The final value of 2'000 ppm indicated that the milky white NTA solution being produced was nearly completely complexed with calcium. These experiments indicate that NTA can be an effective dissolution agent for the dissolution of wellbore calcite. The production of unreacted NTA early in the production cycle indicated that a longer shut-in period may have resulted in a more complete reaction of the NTA solution and more wellbore calcite dissolution.

A total of 30 wells were treated with HCl and 24 gave successful results (Evanoff et al., 1995).

6.6 Baca geothermal field (New Mexico, USA)

For the development of the fracture network in the Baca Union Project, different methods of reservoir stimulation were compared. Acid stimulation had not been selected because of the filling of the natural fractures. Composed of authigenic material such as quartz, feldspar and pyrite (Pye and Allen, 1982). Therefore the acid stimulation should require substancial amounts of hydrochloric acid with uncertain results. A hydraulic fracturation was selected and performed on Baca-20 well in October 1981 utilizing a cooling water followed by a high viscosity frac fluid (Morris and Bunyak, 1981). Different compounds were used to do this hydraulic stimulation as proppant (sintered bauxite), hydroxypropyl polymer gel (stable at high temperature) and calcium carbonate added to act as a fluid-loss additive.

Nevertheless, all these treatments have not allowed a significant increase of the injectivity. It was also thought that the calcium carbonate has plugged the natural fractures and flow paths in the formation. As a consequence, an acid treatment was performed. A volume of 166 m^3 of hydrochloric acid at a concentration of 11.9% was used but this acidizing treatment has not allowed the development of the well productivity (Entingh, 1999).

6.7 Fenton Hill HDR project (New Mexico, USA)

This HDR reservoir, located in north-central New Mexico, is composed at a depth of 3-4 km of a highly jointed Precambrian plutonic and metamorphic complex, basically of granitic composition. This HDR project was operated by Los Alamos National Laboratory. Many experiments, in the laboratory and on the field, were performed to study the impact of a chemical treatment on this rock.

Different works were performed on cuttings and granite cores at the laboratory scale to study the impact of chemical treatments on permeability increases. Aqueous solutions of Na_2CO_3, NaOH and HCl were investigated on well-known crystalline rocks. Sarda (1977) reported the results (Table 8).

Table 8: Impact of three chemical treatment at 100 °C and 100 bars during 144 h (Sarda, 1977)

Chemical Treatment	Weight Loss	Permeability increase
Na_2CO_3	-0.3 %	2-fold
HCl	- 6 %	negligible
NaOH	- 6 %	20-fold

Those laboratory experiments have demonstrated that Na_2CO_3 dissolves SiO_2 primarily by attacking the quartz component of the granite. Holley et al. (1977) showed that the amount of dissolved silica increased with increasing sodium carbonate concentration and with increasing time.

Field experiments were attempted in November 1976 to reduce the impedance of the deep enhanced reservoir by a chemical leaching treatment. Na_2CO_3 was used to dissolve quartz from the formation. A total of 190 m^3 of 1 N Na_2CO_3 solution was injected. About 1000 kg of quartz were dissolved and removed from the reservoir but no impedance reduction resulted.

6.8 Fjällbacka HDR project (Sweden)

The experimental HDR reservoir of Fjällbacka is made of a granite composed of two main facies, the predominant variety being a greyish-red, biotite monzogranite. This granite contains abundant fractures and minor fractures zones, which showed an evidence of being hydraulically conductive and which were filled with calcite, chlorite and clay minerals (Sundquist et al., 1988; Wallroth et al., 1999). Most of the stimulation experiments were hydraulic fracturing but an acid treatment was performed in 1988. An amount of 2 m^3 of HCl-HF acid was injected in Fjb3 to leach fracture filling. The results have shown the efficiency of acid injection in returning rock particles.

6.9 Experiments at EGS reservoir of Soultz-sous-Forêts (Alsace, France)

The Soultz-sous-Forêts Enhanced Geothermal System (EGS), established in the Rhine Graben, North of Strasbourg (France), has been investigated since the mid 1980's. The final goal of this project is to extract energy for power production from a regional randomly permeable natural geothermal reservoir with the complementary resource coming from a forced fluid circulation between injection and production boreholes within a granitic basement.

Recently chemical treatments were performed at Soultz-sous-Forêts (France). This deep granitic reservoir contains fractures partially filled with a mixture of secondary carbonates (calcite and dolomite), various kinds of clay minerals (Illite, chlorite….) and silica. In order to dissolve these carbonates and to enhance productivity around the wells, each of the three 5-Km deep boreholes (GPK2, 3 and 4) were treated with different amounts of hydrochloric acid. If GPK3 has shown weak variations of its injectivity, GPK4 presented a real increase of its injectivity and productivity after the treatments and GPK2 presented also a very sensible improvement despite the fact that the treatment was only a very little test.

6.9.1 Preliminary tests on cores

In order to define the most effective acid mixture to be used in the stimulation of the deep reservoir, laboratory test were performed both in batch and in the continuous flowing conditions (Erga, 2000). The batch experiments consisted to test the reactivity of acid mixtures (HCl/HF) on core samples of granite formed by micas, phylites, hydrothermal veins, quartz and feldspars at 50°C and 150°C. Batch results indicated the mixtures 12/3 and 12/6 (in weight %) as the best one to attack these rocks and minerals. These 12/3 (wt%) and 12/6 (wt%) mixtures were then used in a series of tests in flowing conditions at 30, 50, 70 and 90°C. The evolution of the weight losses were followed by electronic scanning microscope analyses to determine the mineralogical phases influenced by acidification treatment. On a core coming from a depth of 1996 m in EPS1, weight losses of about 80-100 $mg.cm^{-2}$ were measured and the most effective acid mixture was the ratio 12/3 percent by weight.

6.9.2 GPK2 well

The first injection tests performed on GPK2 on January 23 and February 12, 2003, with water injection volumes of 9214 m3 and 5814 m3 respectively, showed an injectivity in GPK2 estimated to about 0.3 $L.s^{1}.bar^{-1}$. It was then decided to improve the well injectivity by a soft acidizing. During this test, only 1.5 tons of HCl were injected. First, 500 kg of HCl were injected at a concentration of 1.8 $g.L^{-1}$ and with a flow of 30 $L.s^{-1}$.

It showed an immediate and strong impact (see "A" on Figure 3), demonstrating that part of the injection pressure required to inject the total flow was due to very near well bore scaling. The second part of the test, performed at concentrations of 1.8 $g.L^{-1}$ and 0.9 $g.L^{-1}$ for flows of about 15 and 30 $L.s^{-1}$ respectively, showed less immediate impacts but nevertheless the global result was impressive (see differences between "D" and "E" on Figure 3) for such a little quantity of acid injected, the injectivity has increased up to approximately 0.5 $L.s^{-1}.bar^{-1}$.

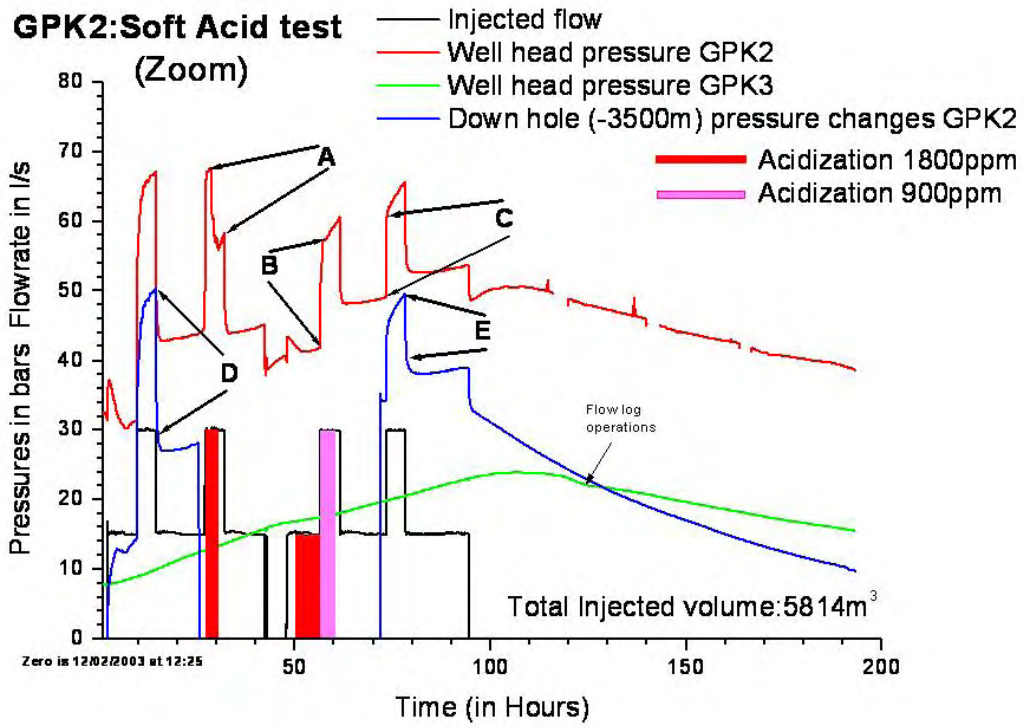

Figure 3: Impact of soft acidification test on GPK2 (Gérard et al, 2005).

6.9.3 GPK3 well

The second acidification test was run in GPK3 in June 2003 during a circulation test between GPK3, the injection well, and GPK2, the producer. A total of 950 m^3 of an acid solution, with a concentration of about 3.2 $g.L^{-1}$, were injected at a flow of 21.3 $L.s^{-1}$. Up to 3 tons of HCl were used in GPK3. The results are shown on Figure 4. Figure 4 shows a sudden drop of the wellhead pressure of GPK3 (slope break at 240 h) after the injection of about 4000 m^3 of acid and fresh water. This break could be caused by acidic water and its action in the reservoir, in particular in the large fault identified at 4750 m and able to absorb more than 75 % of the injected fluid (Gérard et al, 2005). Nevertheless, it is difficult to estimate the real improvement of the GPK3 injectivity due to acid treatment, because no water injection test was performed in the same conditions before and after acid injection, unlike for GPK4 well.

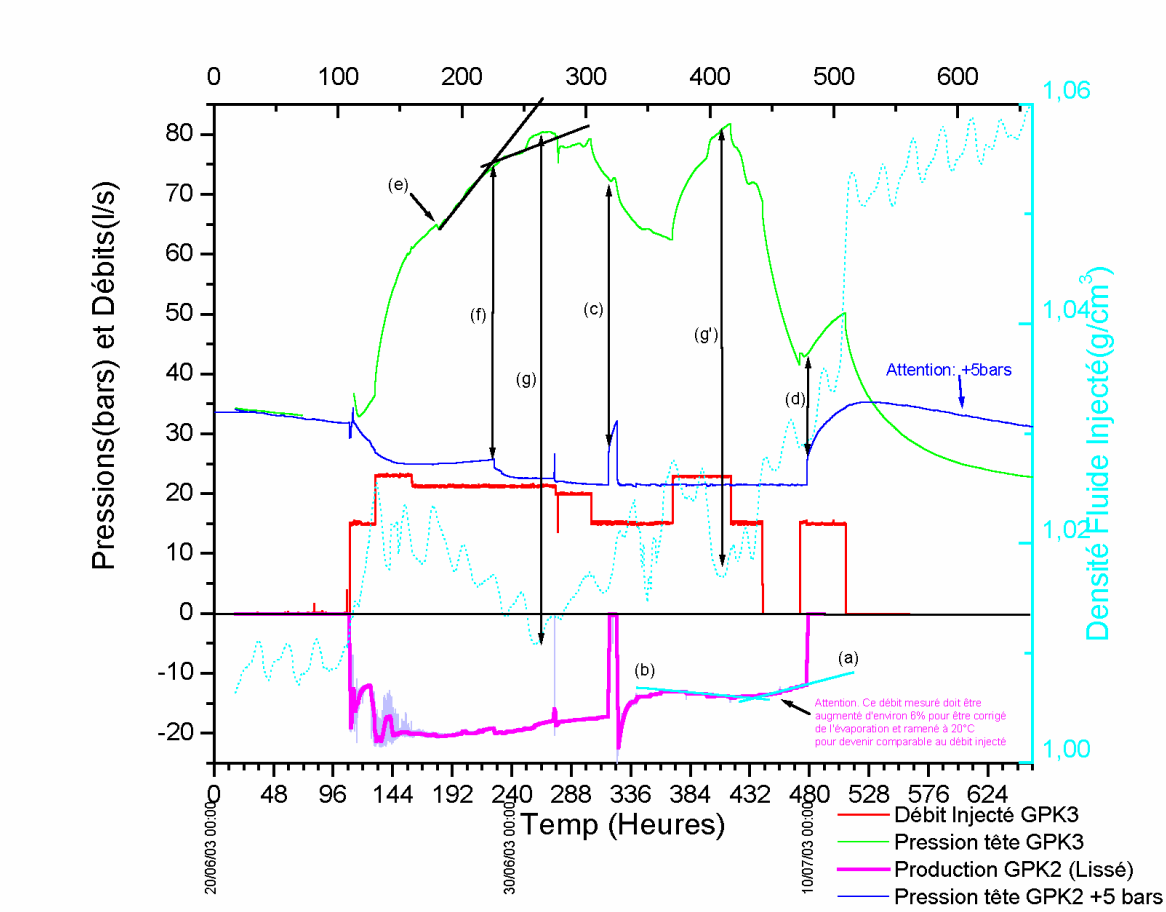

Figure 4: Impact of acidification test on GPK3 (Gérard et al, 2005).

6.9.4 GPK4 well

In February 2005, an acidified (HCl) water injection was tested to improve the injectivity around GPK4 well. The experiment began on 22 February 2005 with an injectivity test of the well before soft acidification. It consisted of the injection of 4'500 m^3 of water at increasing flow rates (9 $L.s^{-1}$, 18 $L.s^{-1}$, 25 $L.s^{-1}$) in 24-hour steps. The injection of water acidified by the addition of approximately 2 $g.L^{-1}$ of hydrochloric acid started on 2 March 2005 at a flow rate of 27 $L.s^{-1}$. It lasted 2 days, followed by one day of injecting fresh water at much lower rates in decreasing steps. A total volume of 5'200 m^3 was injected; with a total weight of acid (HCl) of 11 tons. When the wellhead pressure was back to the value observed during the previous injectivity test, an identical test was repeated on 13 March 2005, that is injection of 4'500 m^3 of water in flow rate steps of 24 hours at 9 $L.s^{-1}$, 18 $L.s^{-1}$ and 25 $L.s^{-1}$.

The impact of the acidified water on the wellhead pressure during the first acid injection in GPK4 well is shown on Figure 5. Despite the fact that the injection was performed in an over-pressurised reservoir, the injection pressure was decreasing during the last hours of the acidification test. Moreover, it is interesting to compare the data from two tests of water injection performed in the same conditions before (February 22, 2005) and after (March 13, 2005) the acid injection. Results (Gérard et al., 2005) show that after some 72 hours of water injection in the second test (24 hours at 9 $L.s^{-1}$, 24 hours at 18 $L.s^{-1}$ and 24 hours at 26 $L.s^{-1}$), the GPK4 wellhead pressure was about 40 bars below the value observed in the same conditions before acidification. This represents a decrease of the apparent reservoir impedance seen from the wellhead by a factor ~1.5 (0.20 to 0.30 $L.s^{-1}.bar^{-1}$).

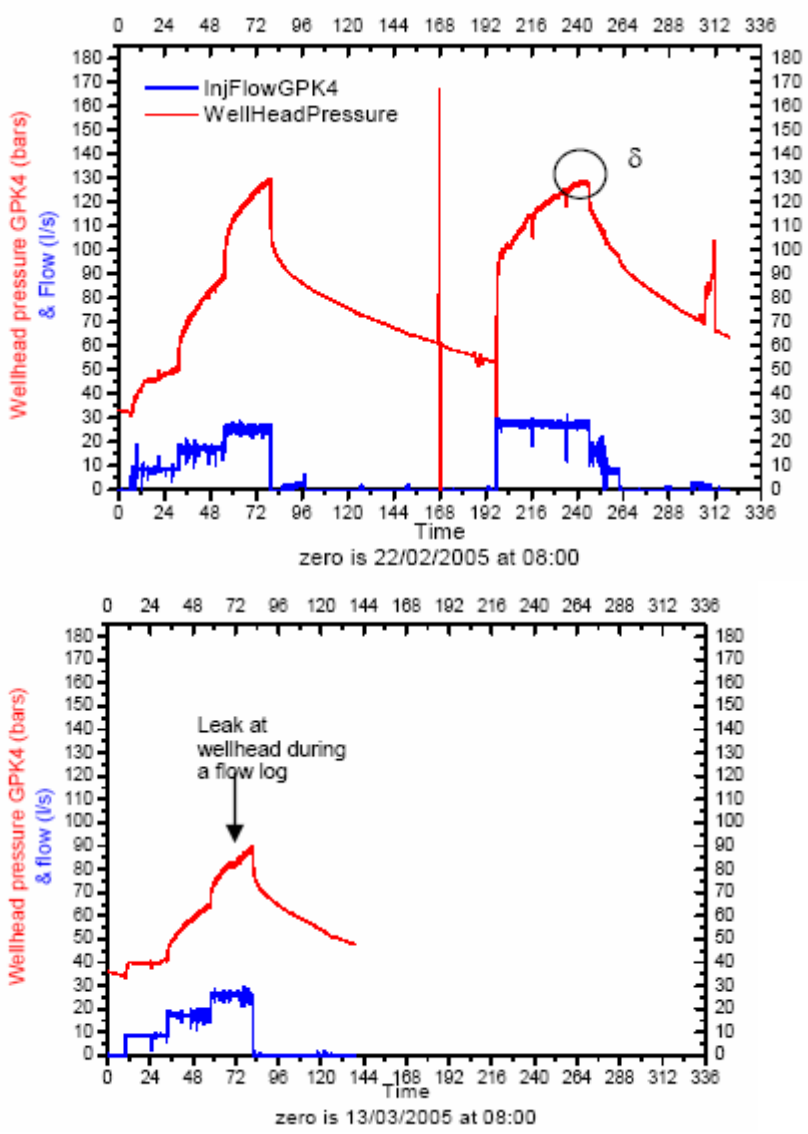

Figure 5: Impact of acidification test on GPK4; above, before and during acidification injection, below, after acidification (Gérard et al, 2005).

In May 2006, new tests began with a test of the well injectivity before acidification. The acid treatment was performed in four stages:

- Injection of 2000 m^3 of cold water deoxygenized at 12 $L.s^{-1}$, 22 $L.s^{-1}$ then finally at 28 $L.s^{-1}$.
- A preflush of 25 m^3 HCl diluted at 15% (3 tons) (with deoxygenized water) was pumped ahead of the HCl-HF acid mixture during 15 minutes at 22 $L.s^{-1}$.
- A main flush consisted of the injection of 200 m^3 of Regular Mud Acid (RMA), (12% hydrochloric (HCl) - 3% Hydrofluoric (HF) acid mixture treatment), with addition of a corrosion inhibitor, at a flow rate of 22 $L.s^{-1}$ during 2,5 hours.
- A postflush by injection of 2'000 m^3 cold water deoxygenized without inhibitor at a flow rate of 22 $L.s^{-1}$ then 28 $L.s^{-1}$ during 1 day.

When the wellhead pressure was back to a value identical to that observed in the previous injectivity test, a 3-day test identical to that of March 13, 2005 was repeated. Figure 6 shows the impact of RMA acid job on the wellhead pressure by comparison before and after the second acid injection in GPK4 well. The repetition of the injectivity test showed that the difference in the over pressure values at the wellhead between the beginning of the test and the end were 16 bars. This represents a 35% reduction of the wellhead pressure due to the acidification treatment. After some preliminary evaluation of downhole pressure changes, performed by GEOWATT, this leads to a provisional estimate of GPK4 injectivity after chemical treatment slightly lower than 0.40 $L.s^{-1}.bar^{-1}$.

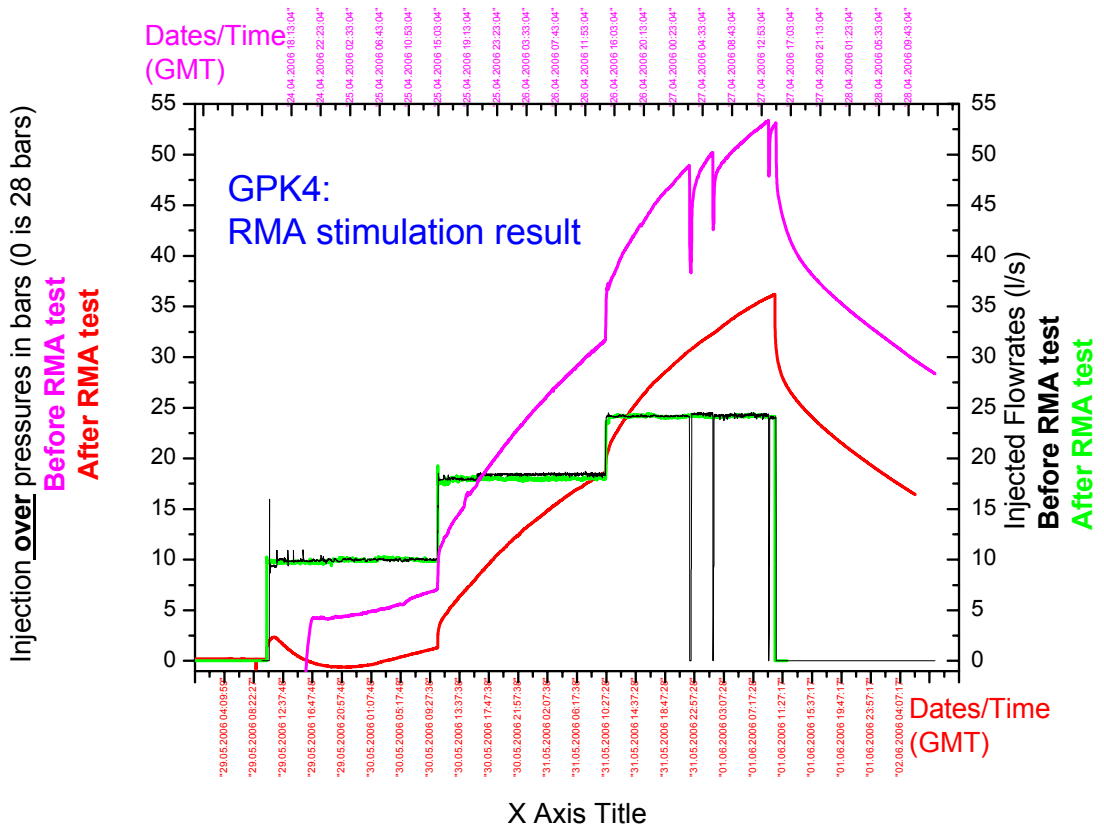

Figure 6: Impact of the RMA acidification test on the wellhead measured by comparison before and after the acidification test on GPK4 well (May 2006) (GEIE, 2006).

6.9.5 Chemical stimulation with chelating agents

An alternative to acid treatment is the use of chelating agents such as ethylenediaminetetraacetic acid (EDTA) or nitrilotriacetic acid (NTA). Such chelating agents have the ability to chelate, or bind, metals such as calcium. Through the process of chelation, a calcium ion would be solvated by the chelating agent, allowing the calcite to be transported either to the surface by flowing the well or further into the formation by injecting into the well. The rate of calcite dissolution using chelating agents is not as fast as is the rate of calcite dissolution using strong mineral acids. The lower dissolution rate means that the chelating agent will be able to take a more balanced path and more evenly dissolve calcite along the wellbore and in all available fractures, rather than following the first fluid entry zone and leaving the rest of the wellbore relatively untouched.

The current state-of-the-art method for chemically removing wellbore silica scale is through HF treatments, which are expensive and hazardous. Laboratory data indicate, however, that aqueous solutions at high pH can dissolve wellbore silica and near-wellbore formation silica and quartz reasonably well and at much lower cost than HF treatments. What has prevented geothermal operators from using caustic solutions in the past is the fear of calcite deposition, which is strongly favored at high pH. Laboratory studies have indicated that calcite is dissolved rather than precipitated at high pH in the presence of chelating agents. This suggests that thermally stable chelating agents at high pH can provide the basis for an affordable and effective mineral dissolution approach.

Although thermal stability studies have not been completed, the literature suggested that NTA could be used at temperatures as high as 290°C, whereas the other two chelating agents, EDTA and HEDTA, were significantly less thermally stable with maximum use temperatures in the range of 200°C. The calcite dissolution experiments in the high temperature flow reactor confirmed the superior performance of NTA above 200°C. Therefore, a field experiment was designed for dissolving calcite and other minerals with a high pH solution of NTA in GPK4 well.

In October 2006, the chelatants stimulation was performed (Figure 7). About 38 tons of NTA were injected with 200 m^3 of cold water at a flow rate of 35 $L.s^{-1}$. A total of 850 m^3 of water were injected to displace the chelating agent in the formation. Figures 7 and 8 show the impact of the chelatants stimulation after the production test on the wellhead pressure and flow rate.

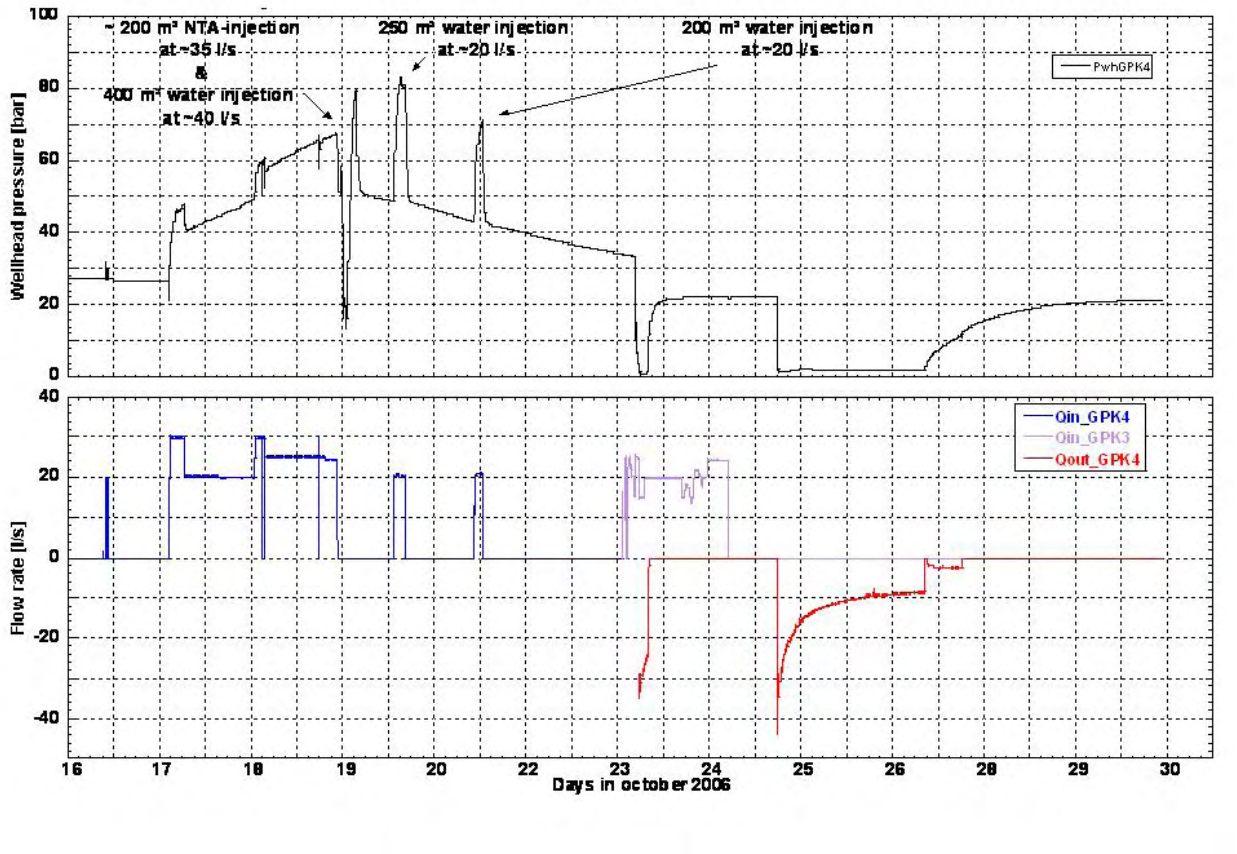

Figure 7: History plot of the chelatants stimulation 06OCT16 and production test 06OCT23 in GPK4 well (GEIE, 2006).

6.9.6 Chemical stimulation of the farfield of the wells GPK4 and GPK3

Although conventional stimulation fluids, such as hydrochloric (HCl) or mud acid, can clean up the wellbore and stimulate the matrix, they do not penetrate deep into the formation nor stabilize fines. Conventional acids can also have adverse effects in formations with certain types of clays, or alumino-silicates like zeolite and chlorite, that are unstable in HCl acid. Consequently it was decided to develop the expected result of the NTA treatment in GPK4 by using Organic Clay Acid for High Temperature (OCA-HT). This stimulation fluid penetrates deep into the sensitive formation and stabilizes clays and fines without the adverse effects of conventional acid systems. OCA fluid is a high-performance acid system designed for sensitive sandstone matrix formations that can present the biggest challenge to conventional acidizing treatments. Because of the damaging precipitation of secondary and tertiary reaction products, conventional mud acid has the highest chance of failure in formations with very high temperature or a high clay content that is sensitive to HCl. OCA fluid combines a retardation effect and advanced chelation technology for stimulation deep into the reservoir with minimal precipitation. It reduces the risk of diminished production as well as secondary and tertiary mineral precipitation that can block pores. Its retarded properties allow a reduced corrosivity. OCA fluid also combats sludging problems that plague conventional acid systems and stabilizes formation fines while maintaining the integrity of the sandstone structures to promote long-term production.

New tests were run in February 2007. The operation consisted in cooling the GPK4 well and only stimulating it with 200 m³ of "Organic Clay Acid HT". The operation was also performed on well GPK3. Organic Clay Acid is a delayed acid proposed in its high temperature version (OCA HT). Its maximum

temperature of use is slightly higher than 200°C, while the inhibition of corrosion can be efficiently ensured until 177°C. In fact, it was considered as being safe enough to use a corrosion inhibitor to guarantee a protection during 4 hours with 80°C for steels.

Figure 8 illustrates the impact of the successive chemical treatments on the productivity of GPK4 well. One can remark that now (March 2007) the productivity of GPK4 after few days only reached a stable value of 5l/s/MPa despite the fact that the produced fluid was stored in a lined lagoon and not reinjected in the well GPK3 during that test. One can also observe on figure 8 that during that production test of March 2007 the pressure in the reservoir at the impact of GPK3 dropped at a rate of around 1 bar/day. That implies a possible higher productivity of GPK4 when some reinjection in GPK3 will be performed.

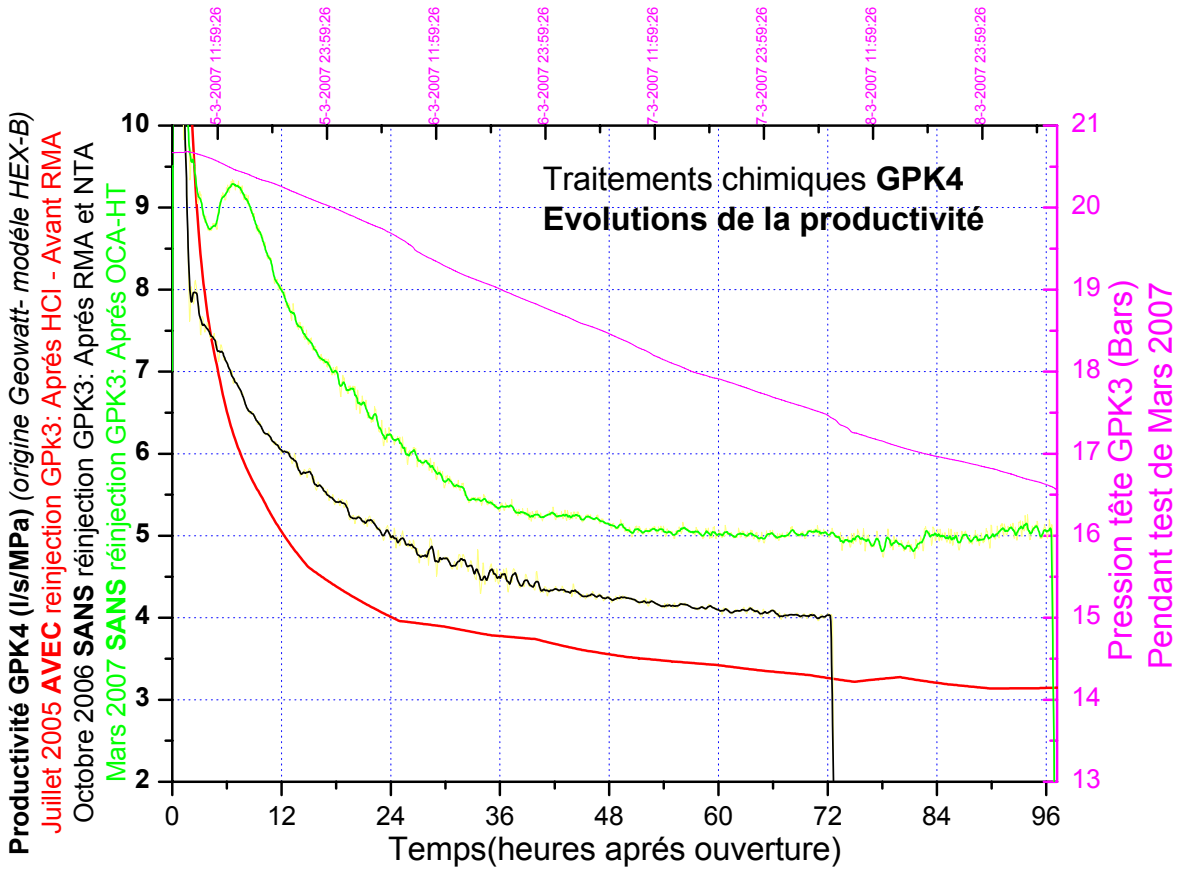

Figure 8: GPK4 productivity evolution with time during chemical treatments (GEIE, 2007).

7 Conclusions

Current economic conditions dictate that oil field operators maximize well/reservoir productivity or injectivity. Achieving the goal of long-term, low-cost sources of hydrocarbons will require significant technology advances in the area of well stimulation. From this papers review, it is apparent that these technological advances will affect many different portions of this industry, from old, mature fields, where significant reserves have previously been economically unattractive, to the new, major ultradeepwater projects that are being evaluated today. The challenge will be to increase productivity, and then to maintain that increased productivity throughout the life of the field to provide improved ultimate recovery.

New and innovative stimulation technologies are emerging that will modify some of previous tried and more or less proven methods. Still, in other cases, we see enhancements to improve the performance of existing technologies. It appears that the future challenge will be for the petroleum industry to find more-cost-effective ways to improve well productivity. It appears that well stimulation will remain a dynamic part of the petroleum industry.

Challenges in sandstone acidizing still exist, although great improvements have been made in the last decade. Factors that contribute to these challenges include: multiple types of co-existing formation damage; uncertain rock mineralogy; multiple fluids and pumping stages; complex chemical reactions between fluids and formation minerals; and fast reaction kinetics at elevated temperatures. Others are: inadequate zonal coverage; limited active acid penetration; rock deconsolidation due to acid-rock interactions; acid emulsion and sludge tendencies; corrosion; and health, safety and environmental (HSE) concerns. These factors contribute to the low success rate of sandstone acidizing treatments especially in acid-sensitive, and clay- and carbonate-rich sandstone formations at high temperatures.

Deleterious side-effects of acidizing in sandstone formations—such as clay swelling, fines migration, gel formation or particle precipitation—may be minimized or avoided altogether by designing hydrofluoric acid (HF) stimulation treatments with compatible chemical and physical properties. Smectite and mixed illite-smectite clays are among the most water-sensitive clays, while illites and chlorites are less prone to ion exchange. Also of concern when acidizing sandstone in the presence of illite, potassium feldspars, sodium feldspars, and zeolites, because these compounds can contribute to the formation of matrix-blocking precipitates.

Clay swelling can occur when acidizing fluids exchange ions with formation minerals, choking off production by obstructing the matrix, unless care is taken to sustain the salinity of the injected fluid after ion exchange. Many water-sensitive clays contain potassium chloride (KCl) and sodium chloride (NaCl) ions that can be exchanged with ions in injected fluids to lower the salinity of the fluid. For example, when a 3% ammonium chloride (NH_4Cl) acidizing fluid flows across a typical ion-exchanging clay, the fluid becomes 3.3% NaCl, a brine too weak to prevent clay swelling, thus requiring a 5% NH_4Cl or equivalent solution.

The acid treatments were developed by oil industry for improving the productivity of oil and gas wells. This technology was partially adapted to the geothermal wells, most often to remove the mineral scaling deposited in the wells after several years of exploitation. Nevertheless, acid treatments also allow the enhancement of the fractures network. They have been successfully performed in geothermal granitic reservoirs like Fjällbacka or Beowawe. In recent years, the reliability of acidizing sandstone intervals has been significantly improved. In the USA, about 90 percent of wells treated have responded with two- to four-fold production increases.

Recently, this technology has been applied to the Soultz reservoir. The three 5-Km deep wells (GPK2, GPK3 and GPK4) were treated with different amounts of chemicals and the injectivity of each well was differently affected. If encouraging results were obtained with GPK2 and GPK4, the injectivity improvement of GPK3 well is apparently less marked but the diagnostic for this well was not really performed[1].

Nevertheless, the high reactivity and a weak flow prevent the penetration of acid in the far field between the wells. This high reactivity also involves the risk of creating wormholes, able to increase the porosity but not always the permeability of the medium.

The increase of acid concentration augments the reactivity in the vicinity of the injection well and creates a new porosity. But the high acidity of the solution has also the disadvantage to decrease the solution pH and to augment the risk of damaging the casing.

The answer could be an increase of the flow to force the acid transport farther in the formation or the use of another acid (e.g. HF), which will dissolve silicates minerals. The result will be an enhancement of the fractures network and of the fractures connectivity.

Finally, simulators have been developed to track the propagation of reaction fronts and to gain insight into the effectiveness of acid injection as a well stimulation techniques. Reactive transport modelling was used to simulate injectivity recovery by acid injection (Xu et al., 2004; André et al., 2006). The predicted amount of scaling minerals dissolved by acid was consistent with the estimal amount.

[1] It can be also noted that the likely origins of the very limited efficiency of all the methods (including hydraulic stimulation) used for trying to improve the injectivity of GPK3 well seem rather specific and are still a subject of discussion.

8 References

Allen, T.O. and Roberts A.P. (1989). Production Operations Vol 1 & 2. Well Compilations, Workover and Stimulation. OGCI Inc. Technical Publications, Tulsa, Oklahoma.

Almond, S.W., Harris, R.E. and Penny, G.S.(1995). Utilization of biologically generated acid for drilling fluid damage removal and uniform acid placement across long formation intervals. Proc. European Formation Damage Control Conference, 15-16 May, 1995, The Hague, the Netherlands, SPE 30123, pp.465-478.

André, L., Rabemanana, V. and Vuataz, F.-D., 2006. Influence of water-rock interactions on fracture permeability of the deep reservoir at Soultz-sous-Forêts, France. Geothermics 35, 507-531.

André, L., Rabemanana, V. and Vuataz, F.-D. (2005). Geochemical modelling of water-rock interactions and implications on the properties of the Soultz fractured reservoir. Proc. EHDRA Scientific Conference, March 17-18, 2005, Soultz-sous-Forêts, France.

Amistoso, A.E., Aqui, A.R., Yglopaz, D.M. and Malate, R.C.M. (2005). Sustaining steam supply in Palinpinon 1 production field, Southern Negros Geothermal Project, Philippines. World Geothermal Congress, Antalya, Turkey, 24-29 April, 2005.

Barrelli, A., Cappetti, G., Manetti, G. and Peano, A. (1985). Well stimulation in Latera Field. Geothermal resources Council Transactions, vol. 9(2), pp. 213-219.

Barrios, L.A., Quijano, J.E., Romero, R.E., Mayorga, H., Castro, M. and Caldera, J. (2002). Enhanced permeability by chemical stimulation at the Berlin Geothermal Field, El Salvador. Geothermal Resources Council Transactions, vol. 26, September 22-25, 2002.

Buning, B.C., Malate, R.C.M., Lacanilao, A.M., Sta Ana, F.X.M. and Sarmiento, Z.F. (1995). Recent experiments in acid stimulation technology by PNOC-Energy development corporation, Philippines. Proc. World Geothermal Congress, vol. 3, pp. 1807-1812.

Buning, B.C., Malate, R.C.M., Austria, J.J.C., Noriega, M.T. and Sarmiento, Z.F. (1997). Casing perforation and acid treatment of well SK-2D Mindanao 1 Geothermal project, Philippines. Proc. 22nd Workshop on Geothermal Reservoir Engineering, January 27-29, 1997, Stanford, California, USA.

Burgos, B., Buijse, M., Fonseca, E., Milne, A., Brady, M., and Olvera, R. (2005). Acid Fracturing in Lake Maracaibo: How Continuous Improvements Kept on Raising the Expectation Bar. Schlumberger and Shell Venezuela S.A, 2005 SPE Annual Technical Conference and Exhibition, 9-12 October, Dallas,Texas, USA, SPE 96531.

Crowe, C., Masmonteil, J. and Thomas, R. (1992). Trends in Matrix Acidizing. Oilfield Review, pp. 24-40.

Erga, F. (2000). Esperimenti di acidificazione in flusso continuo di soluzione acida. Erga, Gruppo Enel, 20 p.

Entingh, D.J. (1999). A review of geothermal well stimulation experiments in the United States. Geothermal Resources Council Transactions, October 17-20, 1999, vol. 23, pp. 175-180.

Evanoff, J., Yeager, V. and Spielman, P. (1995). Stimulation and damage removal of calcium carbonate scaling in geothermal wells: a case study. World Geothermal Congress, Florence, Italy, pp. 2481-2485.

Epperson, I.J. (1983). Beowawe acid stimulation. Geothermal Resources Council Transactions, pp. 409-411.

Flores, M., Barajas, E.N. and Rodriguez, M.A. (2006). Productivity analysis and acid treatment of well AZ-9AD at the Los Azufres Geothermal field, Mexico. Geothermal Resources Council Transactions, vol. 30.

Flores, M., Davies, D., Couples, G. and Palsson, B. (2005). Stimulation of geothermal wells, can we afford it? World Geothermal Congress, Antalya, Turkey, 24-29 April, 2005.

Frenier, W.W., Fredd, C.N. and Chang, F. (2001). Hydroxyaminocarboxylic Acids produce superior formulations for matrix stimulation of carbonates at high temperatures. SPE 71696.

Gérard, A., Fritz, B. and Vuataz, F.-D. (2005). Results of soft acid injection tests performed at Soultz in wells GPK2, GPK3 and GPK4 – Extended summary: revised status on 14 March 2005. Proc. EHDRA Scientific Conference, March 17-18, 2005, Soultz-sous-Forêts, France.

Holley, C.E., Blatz, L.A., Tester, J.W. and Grigsby, C.O. (1977). The interaction of granite with aqueous sodium carbonate. Geothermal Resources Council Transactions, vol. 1, pp. 147-148.

Jacquot, E. (2000). Modélisation thermodynamique et cinétique des réactions géochimiques entre fluides de bassin et socle cristallin: application au site expérimental du programme européen de recherche en géothermie profonde (Soultz-sous-Forêts, Bas-Rhin, France). PhD thesis, Université Louis Pasteur, Strasbourg, France.

Jaimes-Maldonado, J.G. and Sánchez-Velasco, R. (2003). Acid stimulation of production wells in Las Tres Vírgenes Geothermal field, BCS, México. Geothermal Resources Council Transactions, vol. 27, October 12-15, 2003.

Kalfayan, L. (2001). Production Enhancement With Acid Stimulation. Pennwell Books.

Leschi, P., Demarthon, G., Davidson, E., and Clinch, D. (2006). Delayed-Release Acid System for Cleanup of Al Khalij Horizontal Openhole Drains. Total E&P and Halliburton, 2006 SPE International Symposium and Exhibition on Formation Damage Control, 15-17 February, Lafayette, Louisiana, USA, SPE 98164.

Malate, R.C.M., Yglopaz, D.M., Austria, J.J.C., Lacanilao, A.M., and Sarmiento, Z.F. (1997). Acid stimulation of injection wells in the Leyte Geothermal power project, Philippines. Proc. 22nd Workshop on Geothermal Reservoir Engineering, January 27-29, 1997, Stanford, California, USA.

Malate, R.C.M., Austria, J.J.C., Sarmiento, Z.F., DiLullo, G., Sookprasong, A. and Francia, E.S. (1998). Matrix Stimulation Treatment of Geothermal Wells Using Sandstone Acid. Proc. 23rd Workshop on Geothermal Reservoir Engineering, January 26-28, 1998, Stanford, California, USA.

Malate, R.C.M., Sookprasong, P.A., Austria, J.J.C., Sarmiento, Z.F. and Francia, E.S. (1999). Wellbore Soaking: a Novel Acid Treatment of Geothermal Injection Wells. Proc. 24th Workshop on Geothermal Reservoir Engineering, January 25-27, 1999, Stanford, California, USA.

Mendez, A., Neumann, L.F., de Almeida Pinto, E., Torres, R., Farias, R., and Acosta, M. (2005). Achieving True Sandstone-Reservoir Stimulation in Deepwater Horizontal Wells. BJ Services Co. and Petrobras, 2005 SPE Annual Technical Conference and Exhibition, 9-12 October, Dallas, Texas, USA, SPE 95826.

Molina, P.O., Malate, R.C.M., Buning, B.C., Yglopaz, D.M., Austria, J.J.C. and Lacanilao, A.M. (1998). Productivity Analysis and Optimization of Well SK-2D, Mindanao I Geothermal Project Philippines. Proc. 23rd Workshop on Geothermal Reservoir Engineering, January 26-28, 1998, Stanford, California, USA.

Morris, C.W. and Bunyak, M.J. (1981). Fracture stimulation experiments at the Baca Project Area. Proc. 7th Workshop on Geothermal Reservoir Engineering, Stanford, California, USA, pp. 53-60.

Morris, C.W., Verity, R.V. and Dasie, W. (1984). Chemical stimulation treatment of a well in the Beowawe Geothermal Field. Geothermal Resources Council Transactions, pp. 269-274.

Mukherjee, H. and Cudney, G. (1993). Extension of acid fracture penetration by drastic fluid loss control. Journal of Petroleum Technology, pp 102-105.

Nguyen, P.D. (2006). Controlling Formation Fines at Their Sources To Maintain Well Productivity. Halliburton. SPE 97659.

Pasikki, R.G. and Gilmore, T.G. (2006). Coiled Tubing Acid Stimulation: The Case of AWI 8-7 Production Well in Salak Geothermal Field, Indonesia. Proc. 31st Workshop on Geothermal Reservoir Engineering, January 30-February 1, 2006, Stanford, California, USA.

Pauwels, H., Fouillac, C. and Fouillac, A.M. (1993). Chemistry and isotopes of deep geothermal saline fluids in the Upper Rhine Graben: origin of compounds and water-rock interactions. Geochim. Cosmochim. Acta, 57, pp. 2737-2749.

Pournik, M. (2004). Evaluation of sandstone acidizing with high strength HF solutions. Master of Science in Engineering, University of Texas, Austin, USA.

PTTC (2000). Well stimulation advances. Workshop co-sponsored by PTTC's North Midcontinent Region and the Wichita Chapter of Society of Petroleum Engineers, February 9, 2000, Wichita, KS, 3 p.

Pye, D.S. and Allen, W.C. (1982). Hydraulic fracturing at the Baca Project New Mexico. Geothermal Resources Council, Special Reports, pp. 127-136.

Rose, P., Xu, T., Kovac, K., Mella, M. and Pruess, K. (2007). Chemical Stimulation in near-wellbore geothermal formations: silica dissolution in the presence of calcite at high temperature and high pH. Proc. 32st Workshop on Geothermal Reservoir Engineering, January 22-24, 2007, Stanford, California, USA.

Sarda, J.P. (1977). Chemical leaching. Proc. 2nd NATA-CCMS Information Meeting on Hot Dry Rock Geothermal Energy, June 28-30, 1977, Los Alamos, New Mexico, USA.

Schlumberger (2003). Sand Control Pumping Services. pp. 37-70.

Serpen, U. and Türeyen, O.I. (2000). Acidizing geothermal wells. Geothermal Resources Council Transactions, vol. 24, September 24-27, 2000.

Strawn, J.A. (1980). Results of acid treatment in hydrothermal direct heat experiment wells. Geothermal Resources Council Transactions, vol. 4, September 1980.

Sullivan, R.B. (2006). Evaluation of Nonlinear Fracture Relative Permeabilities and Their Impact on Waterfrac Performance in Tight Gas Sands. Anadarko Petroleum Corp. SPE 98329.

Sundquist, U., Wallroth, T. and Eliasson, T. (1988). The Fjällbacka HDR Geothermal Energy project: reservoir characterisation and injection well stimulation. Chalmers University of Technology, Report Number Fj-9.

Tuedor, F.E. (2006). A Breakthrough Fluid Technology in Stimulation of Sandstone Reservoirs. Schlumberger. SPE 98314.

Ventre, A-V. and Ungemach, P. (1998). Soft Acidizing of Damaged Geothermal Injection Wells. Discussion of Results Achieved in the Paris Basin, Proc. 23rd Workshop on Geothermal Reservoir Engineering, January 26-28, 1998, Stanford, California, USA.

Wallroth, T., Eliasson, T. and Sundquist, U. (1999). Hot Dry Rock research experiments at Fjällbacka, Sweden. Geothermics, 28(4), pp. 617-625.

Williams, B.B. et al,. (1979). Acidizing Fundamentals. New York and Dallas Society of Petroleum Engineers, European Formation Damage Control Conference, 15-16 May, The Hague, the Netherlands. SPE Monograph No. 6.

Xie, T. (2004). A parametric study of sandstone acidizing using a fine-scale simulator. Master of Science in Engineering, University of Texas, Austin, USA.

Xu, T., Ontoy, Y., Molling, P., Spycher, N., Parini, M. and Pruess, K. (2004). Reactive transport modeling of injection well scaling and acidizing at Tiwi field, Philippines. Geothermics, 33 (4), pp. 477–491.

Yglopaz, D.M., Buning, B.C., Malate, R.C.M., Sta Ana, F.X.M., Austria, J.J.C., Salera, J.R.M., Lacanilao, A.M. and Sarmiento, Z.F. (1998). Proving the Mahanagdong B Resource: A Case of a Large-Scale Well Stimulation Strategy, Leyte Geothermal Power Project, Philippines. Proc. 23rd Workshop on Geothermal Reservoir Engineering, January 26-28, 1998, Stanford, California, USA.

Selected websites

Guides to acid stimulation for improving productivity in oil, gas, injection, and disposal wells: outlines the purposes and benefits of acidizing, and shows how to design and execute successful acid treatments.

http://www.bjservices.com/

http://www.cleansorb.com/

http://www.corelab.com/

http://www.halliburton.com/

http://www.slb.com/content/services/stimulation/

NB: This list is not exhaustive and does not represent any recommendation for specific services companies.

APPENDIX 3(b)

Patrick Nami, Rüdiger Schellschmidt, Marion Schindler and Torsten Tischner, 2008, Chemical stimulation operations for reservoir development of the deep crystalline HDR/EGS system at Soultz-sous-Forêts (France), *Proc. 32nd Workshop on Geothermal Reservoir Engineering*, Stanford University, Stanford, Cal., Jan 28-30, 2008, SGP-TR-185.

PROCEEDINGS, Thirty-Second Workshop on Geothermal Reservoir Engineering
Stanford University, Stanford, California, January 28-30, 2008
SGP-TR-185

CHEMICAL STIMULATION OPERATIONS FOR RESERVOIR DEVELOPMENT OF THE DEEP CRYSTALLINE HDR/EGS SYSTEM AT SOULTZ-SOUS-FORÊTS (FRANCE)

P. Nami[1], R. Schellschmidt[1], M. Schindler[2], T. Tischner[2]

[1]Leibniz Institute for Applied Geosciences (GGA-Institute)
Stilleweg 2, D-30655, Hannover, Germany
e-mail: nami@soultz.net
[2]Federal Institute for Geosciences and Natural Resources (BGR)
Stilleweg 2, D-30655, Hannover, Germany

ABSTRACT

The main objective of the European HDR/EGS-project at Soultz is the installation of a geothermal pilot plant for power production by the end of 2008.
After drilling of the three 5000 m deep wells to form a triplet with two producers (GPK2 and GPK3) and a central injector (GPK3), the wells were hydraulically stimulated through massive water injection. In addition to hydraulic stimulation, a series of chemical stimulation operations were undertaken to achieve increasing the performance of the wells and the near-wellbore permeability of the geothermal reservoir. Several acid systems such as hydrochloric acid (HCl), Regular Mud Acid (HCl-HF) and Organic Clay Acid ($C_6H_8O_7$-HF-HBF_4-NH_4Cl) were injected to dissolve minerals deposits in the wellbore as well as filling materials of fractures in the vicinity of the wells. Also a high-pH chelating agent (NTA) was tested as alternative to the more usual acid treatments.
Whereas acid treatments have resulted in a productivity improvement of the production wells (GPK2 and GPK4) up to 50%, almost no amelioration was obtained in the injection well GPK3. The use of chelating agents resulted in some productivity deterioration of GPK4.
The results of stimulation experiments were evaluated using short-term hydraulic tests, conventional pressure transient analysis, interference pressure data, microseismic monitoring, temperature and flow logs. This combination of evaluation techniques helped in getting insight into the origin of the productivity enhancement.

INTRODUCTION

The European HDR/EGS test site is located in the Rhine Graben near Soultz-sous-Forêts, around 50 km north of Strasbourg in France. The aim is the electricity production by extracting geothermal energy from hot deep crystalline rocks. The first implementation phase envisages the construction of a 1.5 MW geothermal power plant.
In the second phase the production of 100 l/s with at a wellhead temperature of 180°C is targeted. The power plant can then be expanded up to 6 MW. For this purpose an underground heat exchanger has been created through hydraulic and chemical stimulation techniques.
Three wells (GPK3 as central injection well and both GPK2 and GPK4 as production wells) were drilled to 5000 m depth in the crystalline basement to build the HDR/EGS system. The wells were first subjected to hydraulic stimulations. Their productivities were thus enhanced by factors of up to 20. However, some of the induced seismic events during hydraulic stimulation were large enough to be felt by the local population. The potential public concern about seismic events was one important reason for undertaking chemical treatments as additional or even alternative method to hydraulic stimulations. The second and most important argument for chemical stimulation was the evidence of fracture-filling carbonates and other soluble minerals, based on drill cutting and core analysis, as well as on geophysical logs.
Chemical stimulation consists of acid injection into the formation at a pressure below the fracturing pressure to remove near-wellbore permeability damage and material deposited in fractures through dissolution process. This method to enhance the well performance is widely used in oil and gas wells (Economides and Nolte, 2000). Although matrix stimulation has been extensively established as a common workover and stimulation of oil and gas wells, mostly in sandstone and carbonate formations, their application to geothermal wells is recent and leads back to the 1980's (Strawn, 1980; Epperson, 1983; Barelli et al., 1985; Portier et al., 2007). Various chemical treatments have been performed mostly in volcanic and metamorphic formations, principally to reduce near-wellbore damage caused by drilling activities and scaling (Buning et al., 1997; Malate et al., 1997; Malate et al., 1998; Yglopaz et al., 2000, Jaimes-Maldonado and Sánchez-Velasco, 2003; Axelsson et al., 2006).
This paper presents an overview of all the chemical stimulations tested in Soultz and their impact on

injectivity/productivity enhancement. The integration of results from seismic, temperature and flow logging helps in detecting the productive zones of the wells and their changes due to chemical stimulations.
It is to note that the injectivity/productivity of the Soultz wells is time dependant in general. Therefore, values for the injectivity/productivity have to be referred to a specific duration of injection/production. Throughout this paper, the injectivity/productivity is determined after a test duration of three days and is rounded to the next 0.05 l/(s*bar). The experience in Soultz shows that there is no significant difference between injectivity and productivity at moderate pressure changes. The terms injectivity and productivity can be considered therefore as synonymous.

SITE DESCRIPTION

The European HDR/EGS is located near Soultz-sous-Forêts/France in the western edge of the Rhine Graben; about 50 km north of Strasbourg (see Figure 1).

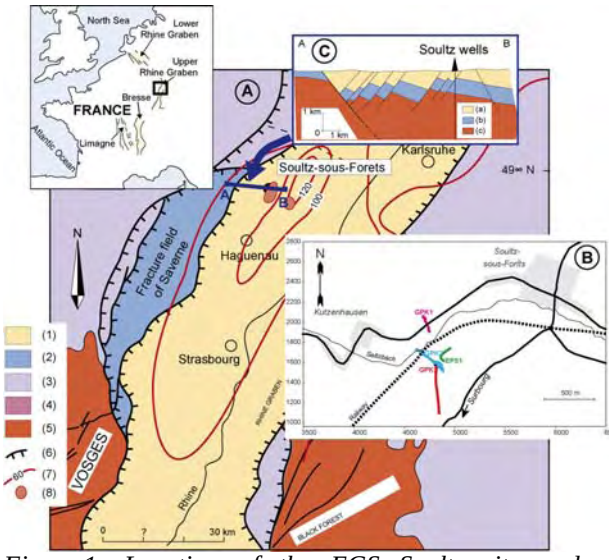

Figure 1: Location of the EGS Soultz site and geology of the Upper Rhine Graben (Hooijkass et al., 2007). A: (1) Cenozoic sediments; (2) Cenozoic volcanics; (3) Jurassic; (4) Triassic; (5) Hercynian basement; (6) boundary faults; (7) other faults; (8) isotherms (in °C) at 1500m depth (Haenel et al., 1979); (9) local thermal anomalies (Haenel et al., 1979); B: local map of the Soultz wellfield showing well trajectories; C: W–E cross-section through the Rhine Graben border and the Soultz site. (a) Cenozoic; (b) Mesozoic; (c) Hercynian basement.

Various authors (Garnish et al., 1994; Baumgärtner et al., 1998; Hettkamp et al., 2004; Baria et al., 2005; Gérard et al., 2006) provided summaries of the project's history since its creation.
The HDR/EGS target is a Paleozoic altered and fractured granite overlain by 1400 m thick sedimentary cover. The fracture network ranges from micro-cracks to high-permeability large normal faults filled with minerals from hydrothermal alteration (illite, quartz, calcite…), which are naturally permeable (Genter et al., 1995; Sausse et al., 2006; Hooijkass et al., 2007). The abnormal high temperature gradient of about 100°C/km within the sedimentary cover and the overall non-linear trend results from deep hydrothermal convection loops occurring within the fractured basement.

CHEMICAL STIMULATION OPERATIONS

The chemical stimulation operations were made by injecting acid from the wellhead through the inner casing string (91/2" for GPK3 and GPK4 and 7" for GPK2). Corrosion inhibitors were used to protect the inner casing string. With exception to chemical treatments with HCl, the other operations were conducted by specialised service companies. The equipments were configured to assure the mixing and acid injection in a row.
Table 1 shows the various chemical treatments conducted in the deep Soultz wells (Portier et al., 2007). All the wells were subjected to chemical stimulation with injection of low-concentrated hydrochloric acid. Due to its poor connectivity with the injection well GPK3 after successive hydraulic and chemical stimulations, the production well GPK4 was mostly chemically stimulated.

Table 1: Overview of chemical stimulations of the three deep Soultz wells.

		GPK2	GPK3	GPK4
Conventional acid systems	Hydrochloric Acid (0.09-0.45%HCl)	●	●	●
	Regular Mud Acid (12%HCl-3%HF)			●
Chelatants	Nitrilotriacetic Acid (19% Na_3NTA-NaOH)			●
Retarded acid system	Organic Clay Acid (5-10% $C_6H_8O_7$, 0.1-1% HF, 0.5-1.5% HBF_4, 1-5% NH_4Cl)		●	●

Conventional acid systems

Stimulation with hydrochloric acid (HCl)

Chemical treatments with low-concentrated HCl were performed in the three wells after the hydraulic stimulation (Table 2).
The objective of this low-concentrated but long-extended stimulation was to dissolve secondary carbonates (calcite and dolomite) existing in the fractures.

Table 2: Overview of the stimulations with low HCl-concentration in the three deep wells.

Well	Date	Dura-tion [hours]	Total mass of HCl [t]	HCl-concen-tration [%]	Diluted HCl injected [m³]	Flow rate [l/s]
GPK2	13.02.2003	6	1.4	0.18	650	30
	14.02.2003	10		0.18	810	15
				0.09		30
GPK3	27.06.2003	12	3	0.45	865	20
GPK4	02.02.2005	48	11	0.2	4700	27.2

In 2003, the first deep well (GPK2) was stimulated by injection of hydrochloric acid. A significant reduction of near wellbore friction losses was observed immediately after the acid front reached the openhole section (Figure 2). Nevertheless, the improvement was most important only at high flow rate above 30 l/s. It is likely that turbulent friction losses inside the wellbore, where a fish is stuck, were reduced due to the acid injection. No clear indications were found for an improvement in the formation around the well GPK2.

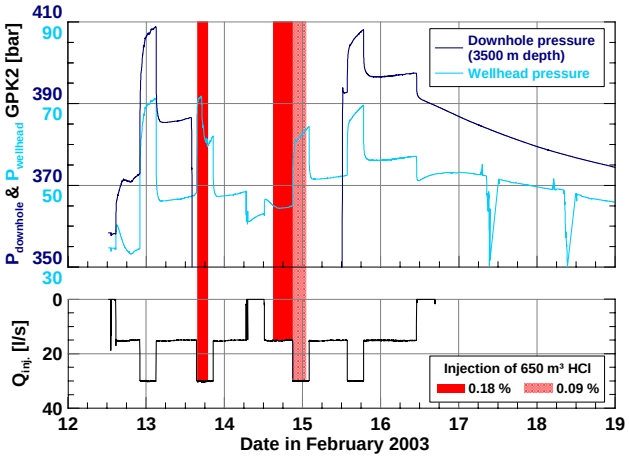

Figure 2: History plot of the chemical stimulation with HCl in GPK2. A significant drop of the pressure difference after HCl-injection was observed.

During a circulation test between GPK2 and GPK3 in 2003, hydrochloric acid was injected in GPK3 over a time period of 12 hours. No reduction of the injection pressure was observed during or after the acid injection meaning that this acid stimulation failed.
The injection of hydrochloric acid in GPK4 in 2005 improved the well injectivity/productivity by 50%, but it is questionable whether this improvement was achieved in the openhole or through leakages in the casing. This point will be discussed later.

Stimulation with Regular Mud Acid (RMA)

RMA was exclusively injected in GPK4. RMA is a mixture of hydrochloric acid (HCl) and hydrofluoric acid (HF) widely used in oil and gas wells. The dissolution of minerals like clay, feldspars and micas (Portier et al., 2006) was intended by applying this acid mixture. A HCl-preflush was first injected to avoid calcium fluoride (CaF_2) precipitation that can lead to well damage. The treatment was carried out in four steps:

- Injection of 2000 m³ of fresh water deoxygenized at 18 l/s, 22 l/s and 28 l/s for more than 24 hours
- A preflush of 25 m³ HCl at 15% (with deoxygenized water) with a flow rate of ~22 l/s
- A main flush of 200 m³ RMA with concentration of 12% HCl and 3% HF and with addition of corrosion inhibitor, at flow rate of ~22 l/s
- A postflush of 2000 m³ fresh water at flow rates of 22 l/s and 28 l/s during 22 hours.

Figure 3 shows the history plot of the stimulation in GPK4. A less pronounced slope is observed after the injection of the treatment mixture than before, indicating an enhancement of the reservoir (blue dash lines in Figure 3).

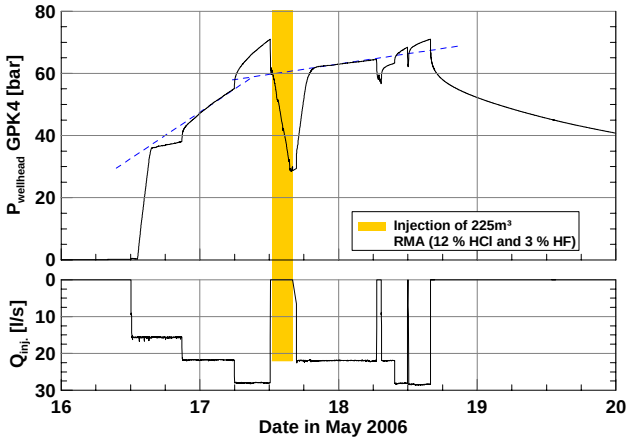

Figure 3: History plot of the chemical stimulation with RMA in GPK4. The slope change of the pressure (blue dash line) for the same flow rate before and after the RMA-injection indicates a gain in productivity.

Stimulation with Chelatants

After the stimulation with RMA, the well GPK4 was subjected to a chemical treatment with chelatants in October 2006. The purpose of this reactant ($C_6H_9NO_6$, nitrilotriacetic acid) is to form complexes with cations like Fe, Ca, Mg, and Al, and thereby to reduce the activity of these cations, leading to an enhanced dissolution of the corresponding minerals (calcite...). Chelatants are less corrosive in comparison to acids like HCl.
The stimulation design was made as follows:

- Injection of ~4500 m³ fresh water to pressurize the reservoir at average flow rate of ~24 l/s for a period of 53 hours
- main flush of 200 m³ (pH 12) constituted of caustic soda (NaOH) and 19% diluted Na_3NTA, at flow rate of ~35 l/s during 1.6 hours
- Postflush of 400 m³ fresh water at 40 l/s
- Two short injections of fresh water at 20 l/s (volume 200 m³ and 250 m³)

Figure 4 shows the history plot of the stimulation with NTA. The analysis of the pressure behaviour after the injection of NTA shows an abnormal increase of the wellhead pressure. During the succeeding short water injections, the wellhead pressure was even higher than shortly before the injection of the reactant, suspecting a plugging of the productive zones. A production test was therefore carried out on October 25, 2006 to remove residuals of the NTA-solution.

At the beginning of the production test, large quantities of magnetite-rich grey sands were produced, followed by a yellow-coloured fluid, probably containing chelatants. A geochemical analysis of water samples showed a neutral pH (7.1-7.4) of the produced fluid, and thus the almost complete removal of the chelating agents from the well. The test had to be stopped after ~ 2000 m³ production due to storage limitations and other planned technical operations.

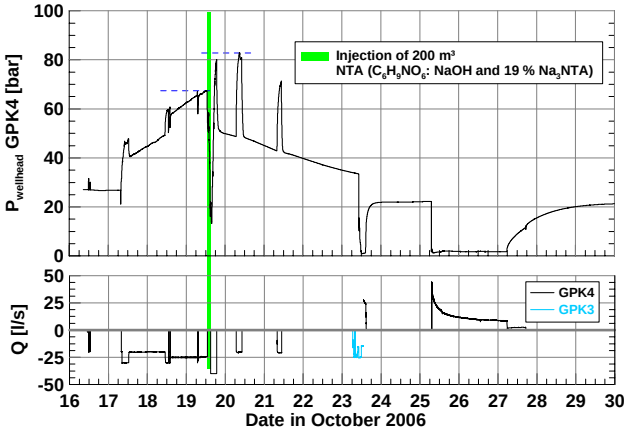

Figure 4: History plot of the chemical stimulation with NTA in GPK4. The wellhead pressure during the injection of 250 m³ water is higher than before the NTA injection, indicating loss in productivity.

Retarded acid systems

The chemical stimulation of GPK3 and GPK4 with Organic Clay Acid (OCA) completed a series of hydraulic and chemical stimulations for productivity enhancement of all deep Soultz wells, which started in 2000. The OCA-stimulation fluid is designed for formations with very high temperature or/and with high clay content that are sensitive to conventional stimulation fluids (HCl). The retardation effect of OCA fluid allows a stimulation going deep into the reservoirs. The OCA-fluid injected was composed of 5-10% citric acid ($C_6H_8O_7$), 0.1-1% HF, 0.5-1.5% HBF_4, and 1-5% NH_4Cl (Schlumberger catalogue).

GPK3

The well was treated on February 15, 2007 by proceeding as follows:

- Injection of 1200 m³ of fresh water at flow rate of 35 l/s
- main flush of 250 m³ of OCA at flow rate of ~55 l/s
- First postflush of 250 m³ fresh water at flow rate of 45 l/s
- Second postflush of ~1070 m³ fresh water at average flow rate of 30 l/s

Figure 5 shows the history plot of the chemical treatment in GPK3. The pressure increase after the first 250 m³ water injection, pumped at the same flow rate as before the chemical treatment, has a slope similar to the one shortly before the end of the preflush (see blue dash line in Figure 5). This preliminary analysis shows almost no gain in productivity.

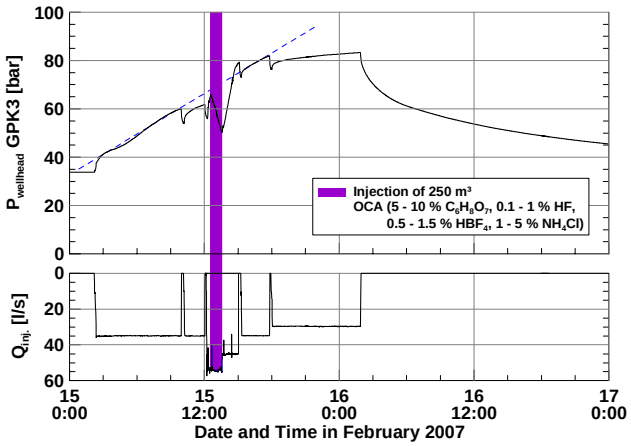

Figure 5: History plot of the stimulation with OCA in GPK3. A nearly similar pressure trend is observed before and after the OCA-injection at the same flow rate. No gain in productivity was achieved.

GPK4

The well GPK4 was stimulated on March 21, 2007 with Organic Clay Acid according to the following steps:

- Preflush of fresh water at average flow rate of ~30 l/s
- main flush of 200 m³ OCA-fluid at ~55 l/s (density: 1.04 g/cm^3)
- Posflush of fresh water at 40 l/s and 35 l/s

The wellhead pressure and the flow rate during the chemical treatment with OCA are shown in Figure 6.
During the preflush-phase, a fast increase of the wellhead pressure, immediately followed by a stronger trend of the pressure buildup was observed, although the injection flow rate at the time was constant by ~30 l/s (dotted red circle in Figure 6). This abrupt increase of pressure slope suggests some plugging of the well.
After the displacement of OCA-fluid into the formation the pressure was almost constant although a constant injection rate usually leads to a pressure increase under Soultz conditions.
The wellhead pressure reached a value of ~120 bar just before the injection of OCA and rose up to a maximum of 130 bar during the postflush phase until the shut-in.

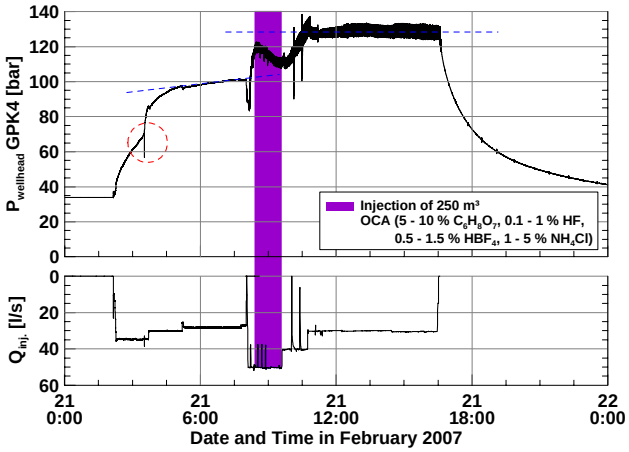

Figure 6: History plot of the stimulation with OCA in GPK4. Steady-state behaviour of the pressure is observed during the postflush phase.

A flat pressure trend at a very high level is typical for a fracturing process. Consequently fracturing effect has to be considered additionally to acid effect. If some outlets of the well were plugged during injection, as it is indicated by the pressure curve, the fracturing pressure might be exceeded even for a "low" flow rate of 30 l/s. In that case the pressure is controlled by the rock stress.

HYDRAULIC TESTS FOR THE EVALUATION OF CHEMICAL STIMULATIONS

GPK2

Hydraulic tests were carried out in this well to evaluate the impact of the hydraulic stimulation. No relevant test was performed in this well after the chemical stimulation with HCl. However the injectivity index after this chemical treatment could be evaluated from the circulation tests in 2003 (between GPK2 and GPK3) and 2005 (between GPK3 and the two production wells GPK2 and GPK4). The injectivity after this HCl-treatment was estimated at ~0.45°l/(s*bar).

GPK3

At GPK3 an injection test was carried out in August 2004 (04AUG17) after the hydraulic and chemical stimulation with HCl. This test served as reference for the evaluation of the succeeding chemical stimulations (Figure 7).

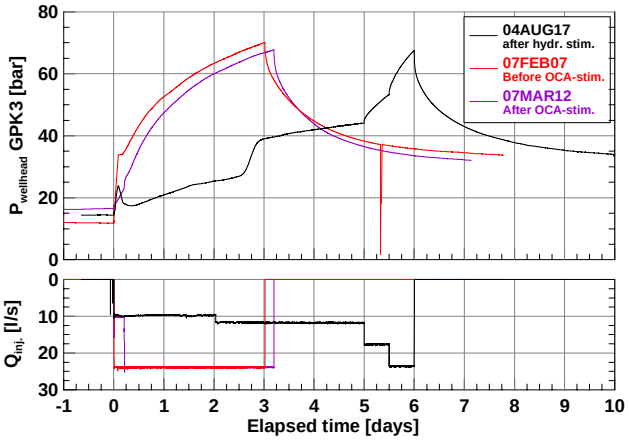

Figure 7: Injection tests performed in GPK3. The maximum wellhead pressure during the injection test after the stimulation with OCA is almost the same as during the injection test after the hydraulic stimulation in 2004.

A total of 7000 m³ fresh water was injected at flow rates of 12, 18 and 24 l/s for a period of 6 days. The injectivity derived from this test was about 0.35 l/(s*bar).
The second injection test in GPK3 was conducted after the RMA and before the OCA-stimulation, on February 07, 2007. In this constant rate test, a total volume of 6230 m³ was pumped during 3 days at a flow rate of 24 l/s. The injectivity calculated from this test was again estimated at about 0.35 l/(s*bar).
The impact of the OCA-stimulation was evaluated by a third injection test. It consisted of a short step of 10 l/s to slowly cool the well, followed by an injection of 24 l/s for more than 3 days (07MAR12). No significant pressure reduction, compared to the previous tests, was observed after the OCA-stimulation in GPK3 and consequently, a significant improvement of the productivity was not achieved. The injectivity index after 3 days is about 0.40 l/(s*bar), very close to the one calculated before this chemical treatment (0.35 l/(s*bar)).

GPK4

The impact of the stimulation operations at GPK4 was evaluated before and after each stimulation by performing a unique step rate injection test. About 4500 m³ of fresh water were injected at increasing

flow rates (9 l/s, 18 l/s and 24 l/s) in one-day step. The characteristics of the wellhead pressure at the beginning of the tests is highly influenced by both temperature and density effects. The density effect disappears rapidly, after injection of one borehole volume, whereas the temperature effect vanishes slowly. Former tests showed that the additional temperature drop induced by an increase of the flow rate from 9 l/s to 18 l/s after one day of injection is small. Therefore, it is possible to evaluate the wellhead pressure from the beginning of the second injection phase on. In particular, changes of productivity can be evaluated by comparing the wellhead overpressure, from the beginning of the second injection step on (see Figure 8).

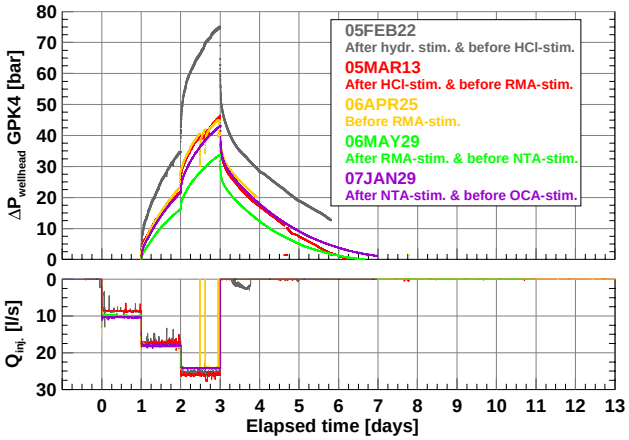

Figure 8: Comparison of the wellhead overpressure (from the second step on) during the step rate tests in GPK4.

After the second hydraulic stimulation of GPK4 in 2005, the first step rate injection test was carried out in GPK4 (grey-coloured curve in Figure 8). The analysis of this tests gave a productivity index, after three days of injection, of ~0.20 (l/s*bar).
The chemical treatment with HCl yielded a gain in productivity of GPK4 (red curve in Figure 8). The productivity index after this stimulation was evaluated at 0.30 l(s*bar).
The step rate test 06MAY29 (green-coloured curve in Figure 8) performed after the RMA-stimulation shows that after three days of injection the wellhead overpressure from the second step is about 35 bar, that means ~11 bar less than before the stimulation (step rate test 06APR25 (yellow and red-coloured curves in Figure 8). The RMA-stimulation has therefore resulted to an enhancement of the productivity index from 0.30 to 0.40 l/(s*bar).
Similar to the previous stimulation of GPK4 with RMA, a step rate test was performed in January 2007 to assess the stimulation effect with NTA (purple-coloured curve in Figure 8). The wellhead overpressure in GPK4 after the NTA-injection was ~9 bar higher than before the chemical treatment, and led to a productivity index of ~0.30 l/(s*bar). The use of chelants has however led to a negative impact on productivity, although conclusive results from labor experiments on calcite dissolution with chelating agent were recorded (Mella et al., 2006; Rose et al., 2007). It is likely, that during the injection of chelatants, which are also used as cleaning agents, scales from the casing were detached and transported into the reservoir, plugging its access to some extent.
No injection test has been performed after the OCA-stimulation. An assessment of the well was however possible, by analysing the production tests carried out before and after this stimulation.
The average production rate in the test after the OCA-stimulation was ~ 1.4 times higher than before, concluding a gain in productivity (see Figure 9). The productivity index was ~0.40 l/(s*bar) before and ~0.50 l/(s*bar) after the OCA-stimulation.
Unlike the previous production tests, the temperature curve of the production test performed after the OCA-stimulation showed a decreasing trend even after 4 days of production and despite the highest production rate. Obviously a part of the production came from the upper part of the well (see discussion).

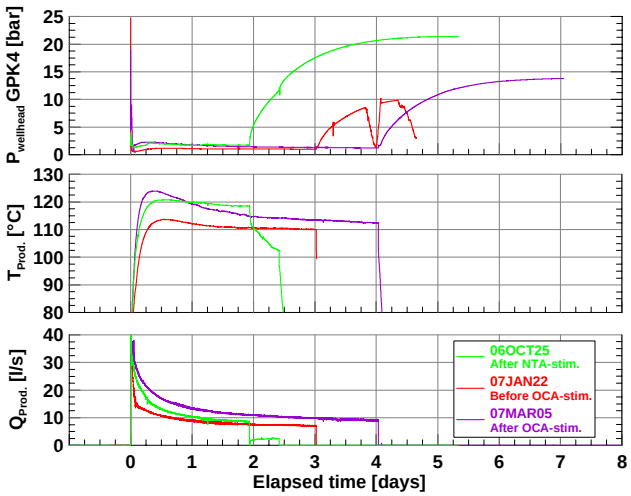

Figure 9: Compilation of all production tests performed in GPK4.

The results obtained both from tracer tests (Sanjuan et al., 2007) and from the analysis of the microseismic activity triggered by the hydraulic stimulations (Baria et al., 2004; Baria et al., 2006) have clearly identified a good connection between GPK2 and GPK3. However, a high impedance barrier between GPK3 and GPK4 was observed. The main issue of the reservoir development was therefore to ameliorate the weak link between GPK3 and GPK4. From the step rate test performed in GPK4, the pressure response in GPK3 and GPK2 was observed throughout the stimulation operations to follow the connection to GPK4 as illustrated in Figure 10.
Almost no pressure response was observed in GPK3 and in GPK2 during the first two stimulations. However, a sensitive pressure response was measured

in the two wells after the stimulation with RMA. The difference pressure in GPK3 is higher than in GPK2 because of its proximity to GPK4. For the same reason, the reaction time is in GPK3 shorter.
It is likely that due to the chemical treatments of GPK4 different geological structures were stimulated than due to the first hydraulic stimulations in 2004/2005. The pressure propagation to GPK2 might be explained by the improvement of a structure between GPK3 and GPK4, reaching an already connected structure between GPK2 and GPK3.

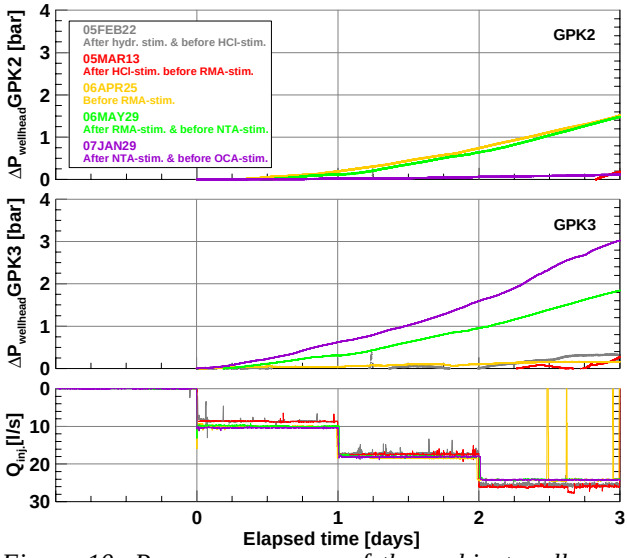

Figure 10: Pressure response of the ambient wells (up: in GPK2, middle: in GPK3) during the step rate injection tests in GPK4. The well GPK3 was deactivated during the test 06APR25 prior to the RMA-stimulation, while GPK2 was deactivated during and after the OCA-stimulation.

DISCUSSION

Overview of the productivity of the deep Soultz wells

Figure 11 summarizes the development of the calculated productivity of GPK3 and productivity of GPK2 and GPK4 with time, starting in 2000.
The values shown here are injectivities/productivities obtained from post-stimulation hydraulic tests, as described in this paper. All hydraulic and chemical stimulations are evaluated as well as the performance of the wells during circulation.
While GPK3 did not change much its productivity with all applied stimulations, the productivity of GPK4, in contrast, was improved by the chemical treatments. These trends are discussed in more detail later in this section.

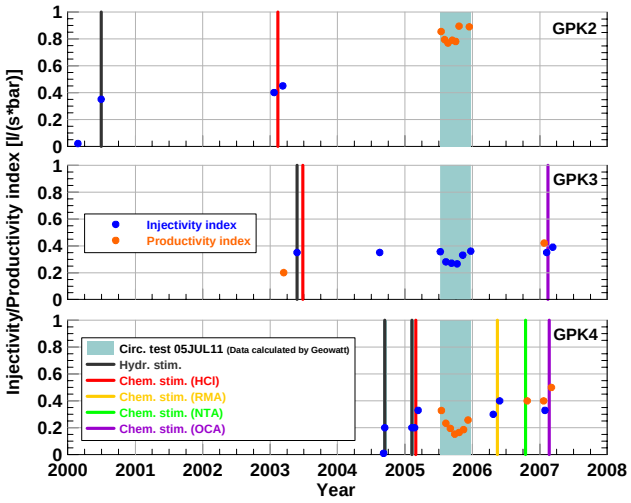

Figure 11: Compilation of the productivity of the deep Soultz wells before and after each stimulation. The dots in the shaded area were derived from the circulation test 2005 and calculated by Geowatt, 2006.

Marginal productivity enhancement after OCA-stimulation in GPK3

The weak impact of the acid stimulations in GPK3 coincides with the existence of a large infinite conductive fracture as the dominant outlet. GPK3 is connected to a natural fracture zone which takes 60-70% of the total flow (Figure 12, left). This status was already the initial state of the well directly after drilling and could not be improved much.

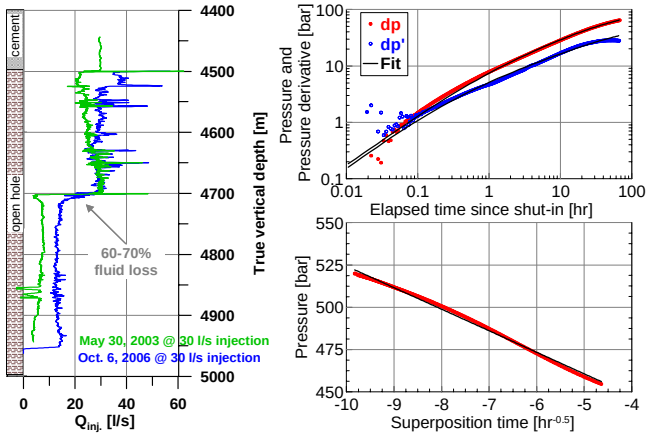

Figure 12: Left: Caliper-corrected flow profiles in GPK3 from 2003 (cyan) and 2006 (blue). Depth is given in true vertical depth (TVD). Right: Pressure transient analysis of the injection test (07JUN04) performed in GPK3 in June 2007. Up: Log-Log diagnosis of the shut-in phase Down: Downhole pressure as function of the square root of the superposition time.

Figure 12, right shows the diagnosis plots of the shut-in phase after an injection test performed in GPK3. The flow is characterised by a pressure change

proportional to the root of time (1/2-unit slope in both the pressure and pressure derivative curves as well as linear trend of the pressure as function of the root of the superposition time, Bourdet, 2002). Thus, the hydraulic behaviour of GPK3 is dominated by a formation linear flow, a typical flow regime for large, infinite conductive fractures intersecting the formation.
The effective fracture area was estimated between 25000 and 50000 m² and the formation transmissibility was about 0.05 to 0.2 Dm (Tischner et al., 2006). There is no potential to improve the well by dissolving minerals from these fracture faces and therefore, a substantial productivity enhancement by using chemical stimulation can not be expected.

Improvement of GPK4 productivity by chemical treatments

As described in this paper in detail, the productivity of GPK4 was improved by the chemical treatments with RMA and OCA, whereas the NTA operation diminished the productivity. The question of where in the well or reservoir the acid improves the permeability is discussed here in more detail.
Figure 13 shows a compilation of data available after the HCl-acidizing in 2005 but before any of the chemical treatments were applied in 2006.

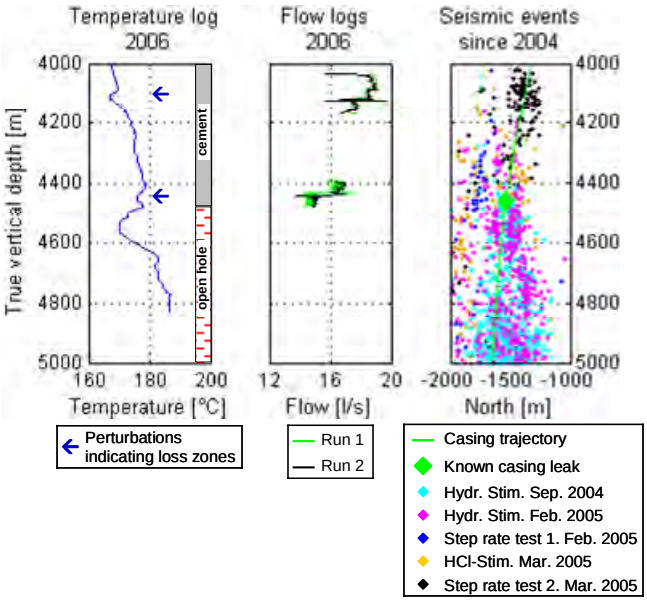

Figure 13: Compilation of measured temperature and flow (left and middle) in April 2006 prior to any further chemical stimulation, together with microseismic events recorded during the hydraulic and chemical stimulation in 2004 and 2005.

Already after the HCl-acidizing in February 2005, a correlation between seismicity during this operation and the leakages in the casing (at 4110 and 4440 m TVD respectively) on the one hand and the productivity improvement on the other hand were discussed.
While the lower leak was already known since 2005, the upper one became only obvious after the temperature anomalies were recorded in 2006. The correlation with the accumulation of seismic events at 4110 m TVD is striking, and also the improvement of productivity by 50% indicates that the main part of permeability creation has been done here.
This scheme of productivity enhancement by chemical stimulation correlating with seismicity during chemical treatments with RMA and OCA is also found. The flow log and the seismicity recorded in between those operations are illustrated in Figure 14.
The events which are clearly located at the level of the upper leakage (~4110 m TVD), trending south- and upward, carry forward the development of the seismic cloud observed during the step rate test in March 2005. These observations led to address the issue whether the acid injections had impact, as intended, only in the openhole.

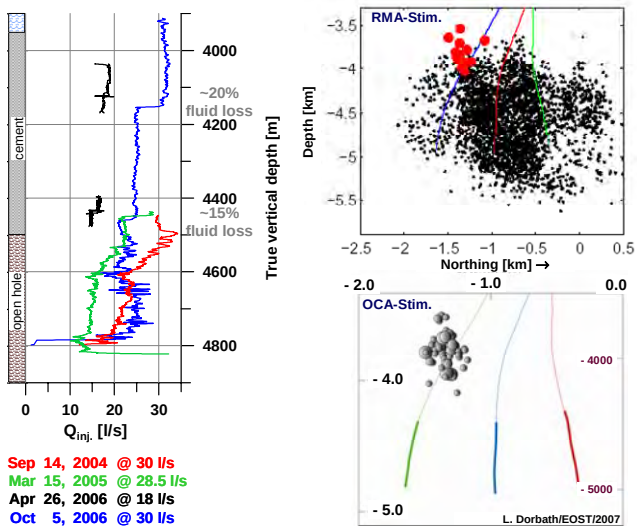

Figure 14: Seismic events during chemical treatments with RMA (left, red circles) and OCA (right) in GPK4, illustrated in side view. No seismicity was observed during the intermediate stimulation with NTA. Source of figure: Louis Dorbath, EOST.

A conclusion from flow logs alone is difficult and a direct evidence for a productivity enhancement could not be found, especially since the well is not fully accessible (Figure 13). Therefore, and because of the high and almost constant pressure during the stimulation with OCA, we take into account the hydraulic stimulation of fluid pathways in the cemented casing section.
For this purpose, we analyzed the stress conditions at the leakage levels. Valley & Evans, 2007 proposed

an estimation of the stress state below 3500 m by following the assumption that the maximum pressure attained during the stimulation provides a direct estimation of the minimum horizontal stress (Cornet & Bérard, 2003; Cornet et al., 2007). The following estimation of the minimum horizontal stress function of the true vertical depth was derived by Valley & Evans, 2007:

$$\sigma_{h\,min}\,[\mathrm{MPa}] = -1.78 + 14.06\,z\,[\mathrm{km}] \quad (1)$$

The estimation of downhole pressure during the stimulations is presented in Figure 15.
The maximum pressure during the hydraulic stimulations (gray-coloured symbols) almost matches the estimation of the minimum horizontal stress. During the stimulation with the OCA-fluid, the wellhead pressure in GPK4 reached ~130 bar. An estimation of the pressure gradient in the reservoir by assuming an average reservoir temperature of 70°C, gives a value of ~13.6 MPa/km, very close to the estimation of Valley & Evans, 2007.

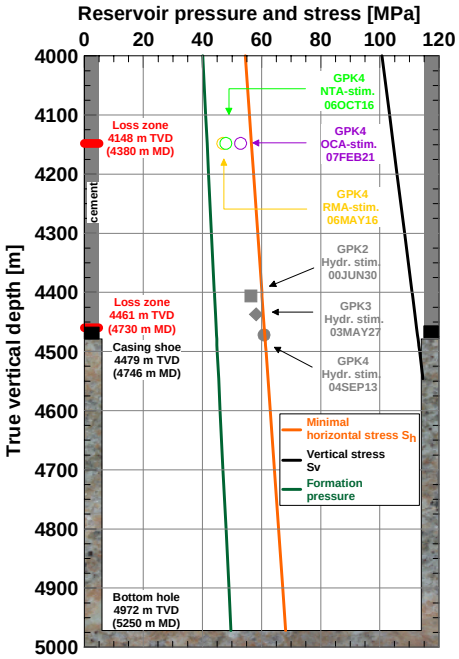

Figure 15: Estimation of the minimal horizontal stress at the HDR/EGS test site in Soultz (Valley & Evans, 2007) and maximum downhole pressure recorded during the stimulations in GPK4. The downhole pressure at the first outlet during the OCA-stimulation (purple circle) is close to the fracture reopening pressure.

As already mentioned in the OCA description, we have to take into account some plugging of the lower part of the well during the preflush and postflush of this operation. Therefore, a high flow rate up to 30 l/s may have entered the formation through the casing leakages. Thus, hydraulic fracturing around the casing leakages corresponds very likely to the observed seismicity.
Regarding the fact that we reached pressure conditions which enable a hydraulic fracturing process during the OCA-stimulation, it is questionable whether the acid itself had any impact on the productivity. The mechanical stimulation alone is able to explain the productivity improvement, the seismicity and also the improved hydraulic communication (Figure 10) between GPK3 and GPK4 after this injection of OCA.
In a future circulation, the improved hydraulic connection between GPK3 and GPK4 will lead to a higher production from GPK4. On the other hand the production temperature from GPK4 should be lower due to the production from upper recharge zones.

CONCLUSION

The deep Soultz wells have been stimulated hydraulically and chemically, in order to develop the underground reservoir prior to electricity production. The results of the stimulation operations are summarized as follows:

GPK2

The well has a productivity of ~0.50 l/(s*bar) in single well tests. Due to a good hydraulic communication with GPK3, the well GPK2 has a productivity of ~0.80 l/(s*bar) under circulation conditions, caused by the increasing reservoir pressure. This difference shows the importance of a reinjection into the same reservoir during a future circulation.
The chemical stimulation with HCl mainly reduced flow resistance in the borehole itself which might consist of the restriction and the lost tool and cable. Nevertheless, a significant turbulent flow regime occurs in the well.

GPK3

The productivity index of GPK3 is about 0.40 l/(s*bar) and remained almost unchanged after successive stimulation operations with HCl and OCA. An infinitive conductive fracture with a large fracture area between 25000 and 50000 m² intersects the open borehole at 4700 m MD and hampers a further improvement by chemical stimulations.

GPK4

The productivity of the well was 0.20 l/(s*bar) after hydraulic stimulations and has improved to ~0.50 l/(s*bar). In comparison to GPK2, the hydraulic communication with GPK3 was weaker prior to the chemical stimulations and therefore GPK4 was less productive than GPK2 during the circulation in 2005.

The chemical stimulations with RMA and OCA improved the productivity of the wells by 30 and 25% respectively, but we attribute at least a part of this gain to a simultaneous hydraulic stimulation of two loss zones in the cemented part of the casing. Stress conditions during the OCA stimulation were favourable for a hydraulic stimulation and were probably caused by a plugging of the well during the pre- and postflush. Moreover, we found a correlation of the upper leak (4110 m TVD) with an accumulation of seismic events. Therefore, a gain of productivity only from the openhole section and the reservoir at 5000 m depth is not likely.
The chemical stimulations with RMA and NTA additionally improved the hydraulic communication between GPK3 and GPK4.

The chemical stimulation campaign, performed at Soultz generated an improvement factor of 1.12 to 2 of the injectivity/productivity. The effectiveness of chemical stimulation can be further improved by using techniques to divert the treatment fluid toward selected zones in the reservoirs (drill pipe, coiled tubing...). As already mentioned, chemical stimulations were performed by injecting acid from the wellhead through the casing string. The stimulation zone was therefore the whole openhole section of the wells (500 to 650 m length). Particularly in fractured crystalline formations, where the reservoir permeability is strongly controlled by the pre-existing natural fracture network, a "focussed" acidizing of this high-permeable joints and fracture zones is essential.

ACKNOWLEDGEMENT

The study was performed within the framework of the European "Hot Dry Rock" project Soultz. The project is funded by the European Commission, the French Ministère de l'Enseignement supérieur et de la Recherche, the German Bundesministerium für Umwelt, Naturschutz und Reaktorsicherheit, the Projektträger Jülich in Germany and by the members of the EEIG "Heat mining".

REFERENCES

Axelsson, G., Thóhallsson, S., Björnsson, G. (2006), "Stimulation of geothermal wells in basaltic rock in Iceland", *ENGINE Workshop 3: Stimulation, of reservoir and microseismicity*, Kartausen Ittingen, Zürich, Switzerland.

Barrelli, A., Cappetti, G., Manetti, G. and Peano, A. (1985), "Well stimulation in Latera Field", *Geothermal Resources Council Transactions*, **9**, 213-219.

Baria, R., Michelet, S., Baumgärtner, J., Dyer, B., Gerard, A., Nicolls, J., Hettkamp, T., Teza, D., Soma, N., Asanuma, H., Garnish, J., Megel, T. (2004), "Microseismic monitoring of the world's largest potential HDR reservoir", *Proceedings, Twenty-Ninth Workshop on Geothermal Reservoir Engineering*, Stanford University, Stanford, California, USA.

Baria, R., Jung, R., Tischner, T., Nicholls, J., Michelet, S., Sanjuan, B., Soma, N., Asanuma, H., Dyer, B., Garnish, J. (2006), "Creation of an HDR reservoir at 5000 m depth at the European HDR project", *Proceedings Thirty-First Workshop on Geothermal Reservoir Engineering*, Standford University, Stanford, California, USA.

Baumgärtner, J., Gérard, A., Baria, R., Jung, R., Tran-Viet, T., Gandy, T., Aquilina, L., Garnish, J., (1998), "Circulating the HDR reservoir at Soultz; maintaining production and injection flow in complete balance", *Proceedings, Twenty-Third Workshop on Geothermal Reservoir Engineering*, Stanford University, Stanford, California, USA.

Bourdet, D. (2002), "Well Test Analysis: The Use of Advanced Interpretation Models", *Elsevier*, Amsterdam.

Buning, B.C., Malate, R.C.M., Austria, J.J.C., Noriega, M.T. and Sarmiento, Z.F. (1997), "Casing perforation and acid treatment of well SK-2D Mindanao 1 Geothermal project, Philippines", *Proceedings, Twenty-Second Workshop on Geothermal Reservoir Engineering*, Stanford University, Stanford, California, USA.

Cornet, F.H., Bérard, Th., Bourouis, S. (2007), "How close to failure is a granite rock mass at a 5km depth?", *International Journal of Rock Mechanics & Mining Sciences*, **44**, 47-66.

Economides, M.J. and Nolte, K.G. (2000), "Reservoir Stimulation", Third Edition, Wiley, NY and Chichester.

Epperson, I.J. (1983), "Beowawe acid stimulation", *Geothermal Resources Council Transactions*, **7**, 409-411.

Garnish, J., Baria, R., Baumgärtner, J., Gérard, A., (1994), "The European Hot Dry Rock Programme 1994–1995", *Geothermal. Resources. Council. Transaction*s, **18**, 431-438.

Genter, A., Traineau, H., Dezayes, C., Elsass, P., Ledésert, B., Meunier, A., Villemin, T. (1995), "Fracture analysis and reservoir characterization of the granitic basement in the HDR Soultz project (France)", *Geothermal Science and Technology*, **4**, 189-214.

GEOWATT (2006), “Circulation test GPK2 / GPK3 / GPK4-Test 05Jul11-Interpretation with HEX-B”, *Technical note*, Ref. TN17.16/CB/Tm/TK.

Gérard, A., Genter, A., Kohl, T., Lutz, P., Rose, P., Rummel, F. (2006), “The deep EGS (Enhanced Geothermal System) project at Soultz-sous-Forêts (Alsace, France)”, *Geothermics*, **35**, 473-484.

Hettkamp, T., Baumgärtner, J., Baria, R., Gérard, A., Gandy, T., Michelet, S., Teza, D. (2004), “Electricity production from hot rocks”, *Proceedings, Twenty-Ninth Workshop on Geothermal Reservoir Engineering*, Stanford University, Stanford, California, USA.

Hooijkaas, G.R., Genter, A., Dezayes, C. (2007), “Deep seated geology of the granite intrusions at the Soultz EGS site based on 5 km depth boreholes”, *Geothermics*, **35**, 484-506.

Jaimes-Maldonado, J.G. and Sánchez-Velasco, R. (2003), “Acid stimulation of production wells in Las Tres Vírgenes Geothermal field, BCS, México”, *Geothermal Resources Council Transactions*, **27**, 699-705.

Malate, R.C.M., Yglopaz, D.M., Austria, J.J.C., Lacanilao, A.M., Sarmiento, Z.F. (1997), “Acid Stimulation of injection wells in the Leyte geothermal power project, Philippines”, *Proceedings, Twenty-Second Workshop on Geothermal Reservoir Engineering*, Stanford University, Stanford, California, USA.

Malate, R.C.M., Austria, J.J.C., Sarmiento, Z.F., DiLullo, G., Sookprasong, A. and Francia, E.S. (1998), “Matrix Stimulation Treatment of Geothermal Wells Using Sandstone Acid”, *Proceedings, Twenty-Third Workshop on Geothermal Reservoir Engineering*, Stanford University, Stanford, California, USA.

Mella, M., Rose, P., Kovac, K., Xu, T., Pruess, K. (2006), “Calcite Dissolution in geothermal reservoirs using chelants”, *Geothermal Resources Council Transactions*, San Diego, California, USA.

Portier, S., André, L., Vuataz, F-D. (2006), “Review of chemical stimulation techniques and results of acid experiments at Soultz-sous-Forêts”, *Proceedings, EHDRA Scientific Conference*, Soultz-sous-Forêts, France.

Portier, S., André, L., Vuataz, F-D. (2007), “Review of chemical stimulation techniques in oil industry and applications to geothermal systems”, *Technical Report, ENGINE work package 4: Drilling, stimulation and reservoir assessment*, Neuchâtel, Switzerland.

Rose, P., Xu, T., Kovac, K., Mella, M., Pruess, K. (2007), “Chemical stimulation in near-wellbore geothermal formations: silica dissolution in the presence of calcite at high temperature and high pH”, *Proceedings, Thirty-Second Workshop on Geothermal Reservoir Engineering*, Stanford University, Stanford, California, USA.

Sanjuan B., Pinault J.-L., Rose P., Gérard A., Brach M., Braibant G., Crouzet C., Foucher J.-C, Gautier A., Touzelet S. (2007), “Tracer testing of the geothermal heat exchanger at Soultz-sous-Forêts (France) between 2000 and 2005”, *Geothermics*, **35**, 622-653.

Sausse, J., Fourar, M., Genter, A. (2006), “Permeability and alteration within Soultz granite inferred from geophysical and flow log analysis”, *Geothermics*, **35**, 544-560.

Strawn, J.A. (1980), “Results of acid treatment in hydrothermal direct heat experiment wells”, *Geothermal Resources Council Transactions*, **4**, 427-430.

Tischner, T., Pfender, M., Teza, D. (2006), “Hot Dry Rock Projekt Soultz: Erste Phase der Erstellung einer wissenschaftlichen Pilotanlage”, *Abschlußbericht zum Vorhaben 0327097*, Tgb. Nr. (BGR): B1.15-10125/06.

Valley, B., Evans, K.F. (2007), “Stress state at Soultz-sous-Forêts to 5km depth from wellbore failure and hydraulic observations”, *Proceedings, Thirty-Second Workshop on Geothermal Reservoir Engineering*, Stanford University, Stanford, California, USA.

Yglopaz, D., Austria, J.J., Malate, R.C., Buning, B., Sta. Ana, F.X., Salera, J.R., Sarmiento, Z. (2000), “A large-scale well stimulation campaign at Mahanagdong geothermal field (Tongonan), Philipines”, *Proceedings World Geothermal Congress 2000*, 2303-2307.

APPENDIX 3 (c)

Patrick Nami, Marion Schindler, Torsten Tischner and Rüdiger Schellschmidt, 2008, Chemical stimulation results at Soultz and overview of the flow performance of the wells, *paper presented at the EHDRA Scientific Conference, Soultz-sous-Forêts*, September 24-25, 2008.

EC Contract SES6-CT-2003-502706

PARTICIPANT ORGANIZATION NAME: GGA Institute

Related with Work Package……

Related with Working Group……

CHEMICAL STIMULATION RESULTS AT SOULTZ AND OVERVIEW OF THE FLOW PERFORMANCE OF THE WELLS

P. Nami [1], M. Schindler [2], T. Tischner [2], R. Schellschmidt [1]

[1]*Leibniz Institute for Applied Geosciences (GGA), Stilleweg 2, D-30655 Hannover, Germany*

[2]*Federal Institute for Geosciences and Natural Resources (BGR), Stilleweg 2, D-30655 Hannover, Germany*

e-mail: nami@soultz.net

ABSTRACT

The "Enhanced" or "Engineered Geothermal Systems" (EGS) and sometime called "Hot Dry Rock" (HDR) is a technology which has been developed in Soultz-sous-Forêts (France) for more than 20 years, aiming at exploiting the heat contained within the crystalline and fractured rocks. The concept consists of drilling two or more boreholes to depths where temperatures are of commercial interests and extracting the heat from the rock mass between them by circulating fluid around the geothermal loop.

After the drilling operations the wells were subjected to hydraulic stimulations through large volume fluid injection into the rock mass at high flow rate as to enhance the very low natural permeability of the deep crystalline rocks. In addition to this stimulation method, a series of chemical stimulations was carried out for increasing the performance of the wells and near-wellbore permeability of the geothermal reservoir. Several acid systems such as hydrochloric acid (HCl), Regular Mud Acid (HCl-HF) and Organic Clay Acid ($C_6H_8O_7$-HF-HBF_4-NH_4Cl) were injected to dissolve minerals deposits in the wellbore as well as filling materials of fractures in the vicinity of the wells. Also a high-pH chelating agent (NTA) was tested as alternative to the more usual acid treatments.

The stimulation operations were accompanied by hydraulic tests, microseismic monitoring, temperature and flow logs, as to evaluate the flow performance of the wells and estimated the permeability enhancement of the rock mass.

Whereas acid treatments have resulted in a productivity improvement of the production wells (GPK2 and GPK4) up to 50%, almost no amelioration was obtained in the injection well GPK3. The use of chelating agents resulted in some productivity deterioration of GPK4.

INTRODUCTION

The geothermal pilot site is located in the Rhine Graben some 50 km north of Strasbourg and close to the French-German border. The system in Soultz consists of three wells - two production wells (GPK2 and GPK4) and one central injection well GPK3 - drilled to 5000 m depth. To reduce the risk of hydraulic short-circuiting between the wells, the boreholes were directionally drilled from one platform as to achieve a distance of 600 to 700 m apart at 5000 m (see Figure 1).

After the drilling operations the wells were subjected to hydraulic stimulations through large volume fluid injection into the rock mass at high flow rate as to enhance the very low natural permeability of the deep crystalline rocks. In addition to this stimulation method, a series of chemical stimulations was carried out for increasing the performance of the wells and near-wellbore permeability of the geothermal reservoir. Several acid systems were injected to dissolve mineral deposits in the wellbore as well as filling materials of fractures in the vicinity of the wells (Portier et al., 2007). The potential public concern about induced seismic events from hydraulic stimulation was also one important reason for undertaking chemical treatments as additional or even alternative method to hydraulic stimulations.

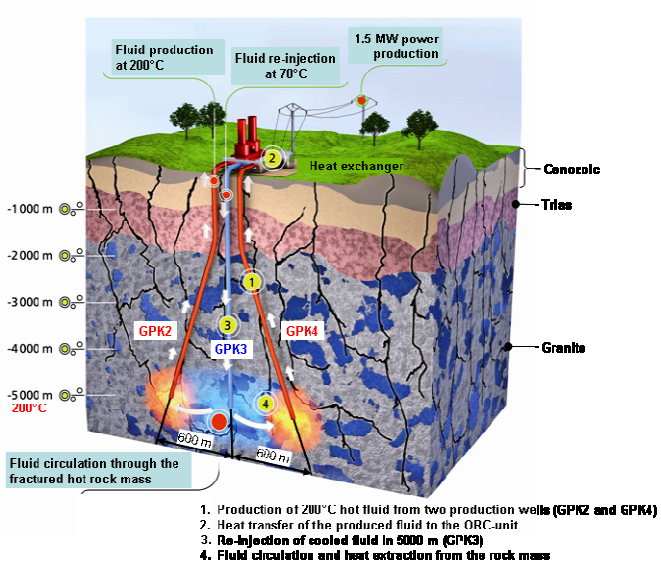

Figure 1: The HDR/EGS-system at Soultz-sous-Forêts

The stimulation operations were followed by the construction of a 1.5 MWel Organic Ranking Cycle (ORC) power unit. A long shaft pump (LSP) was installed in GPK2 at 350 m depth as to boost the production flow rate and an electrical submersible pump (ESP) is to be installed in the second production well GPK4 for increasing the production flow rate and testing the under high temperature conditions. Since summer 2008, the power plant has been in a testing phase for a while and we started to produce electricity with a flow rate of 90 m³/h.

This paper presents an overview of all the chemical stimulations tested in Soultz and their impact on injectivity/productivity enhancement. Furthermore, an estimation of the permeability and transmissibility enhancement of the rock mass is shown.

CHEMICAL STIMULATION OPERATIONS

The chemical stimulation operations were made by injecting acid from the wellhead through the inner casing string (95/8" for GPK3 and GPK4 and 7" for GPK2). Corrosion inhibitors were used to protect the inner casing string. With exception to chemical treatments with HCl, the other operations were conducted by specialised service companies. The equipments were configured to assure the mixing and acid injection in a row. Nami et al., (2007) made a detailed description of the chemical stimulation operations at Soultz.

Table 1 shows the various chemical treatments conducted in the deep Soultz wells. All the wells were subjected to chemical stimulation with injection of low-concentrated hydrochloric acid. Due to its poor connectivity with the injection well GPK3 after successive hydraulic and chemical stimulations, the production well GPK4 was mostly chemically stimulated.

Table 1: Overview of chemical stimulations of the three deep Soultz wells.

		GPK2	GPK3	GPK4
Conventional acid systems	Hydrochloric Acid (0.09-0.45%HCl)	●	●	●
	Regular Mud Acid (12%HCl-3%HF)			●
Chelatants	Nitrilotriacetic Acid (19% Na_3NTA-NaOH)			●
Retarded acid system	Organic Clay Acid (5-10% $C_6H_8O_7$, 0.1-1% HF, 0.5-1.5% HBF_4, 1-5% NH_4Cl)		●	●

OVERVIEW OF THE FLOW PERFORMANCE AFTER CHEMICAL STIMULATIONS

Determination of hydraulic parameters

The following parameters were estimated from hydraulic tests before and after each stimulation operation to characterize the hydraulic properties of the wells and the rock mass as well:

- Injectivity index or productivity index, II or PI
- Impedance, Z
- Equivalent Porous Media Permeability (EPM), k_{eq}
- Transmissibility, T

The **Injectivity index or productivity index II or PI** of the well is defined as:

$$II \text{ or } PI = \frac{q}{\Delta p} \qquad (1)$$

q flow rate [l/s]
Δp differential pressure [bar]
II or PI injectivity index [l/s/bar)]

The **impedance Z** of the well is:

$$Z = \frac{\Delta p}{q} = \frac{1}{II}$$

q flow rate [l/s]
Δp differential pressure [bar]
Z impedance [bar/l/s]

The equivalent porous media permeability k_{eq} is:

$$k_{eq} = -\frac{\mu}{2\pi h} \cdot \frac{q}{\Delta p} \cdot \ln\left(\frac{r_w}{r_i}\right)$$

r_w radius of well [m]
r_i radius of influence [m]
q flow rate [m³/s] (production positive)
Δp differential pressure [Pa] (values higher than formation pressure are positive)
q/Δp injectivity index [m³/(s·Pa)]
μ dynamic viscosity [Pa·s]
h open hole length [m]

A transformation of the equation gives:

$$k_{eq} = -\frac{1}{2\pi h} \cdot \ln\left(\frac{r_w}{r_i}\right)\mu \cdot \frac{q}{\Delta p} = m. \cdot \mu \cdot \frac{1}{h} \cdot \frac{q}{\Delta p} = m.\mu \cdot II \cdot \frac{1}{h}$$

with

$$m = -\frac{1}{2\pi} \cdot \ln\left(\frac{r_w}{r_i}\right)$$

The **transmissibity T** is defined as:

$$T = k \cdot h = -\frac{1}{2\pi h} \cdot \ln\left(\frac{r_w}{r_i}\right)\mu \cdot \frac{q}{\Delta p} \cdot h = m.\mu \cdot \frac{q}{\Delta p} = m.\mu \cdot II$$

The following parameters were used to calculate the flow parameters:

	GPK2	GPK3	GPK4
r_i [m] =	500		
μ [mPa·s]	2×10^{-4}		
r_w [m] =	0.108	0.121	0.118
m [-] =	1.34	1.33	1.33
h [m] =	620	544	498

Comparison between injectivity index estimated from downhole and from wellhead data

For comparing the hydraulic parameters determined from downhole data and from wellhead data, the step rate test 05FEB22 carried out in GPK4 was used (see Figure 2, up und middle). During this test, a downhole pressure sensor was deployed in the well at 4700 m MD.
The calculated injectivity index for each step was made by considering the superposition of the preceding step (Figure 2, up and middle).
A discrepancy between the injectivity index from downhole data and from wellhead data is observed during the first step, due to temperature effect. This effect diminishes with time during the injection in the second step and almost disappears in the third step. During the shut-in period, the temperature effect is visible (Figure 2, down).
From this observation one can conclude that the injectivity index derived from downhole data is the same as the one derive from wellhead data, as long as the temperature effect disappears. Hence, the calculation of the injectivity index is also reliable by using wellhead data and by considering the third step of injection. The calculation beyond the period of

injection was made by extrapolating the measured data with a logarithmic function.
All single-well injection tests carried out in Soultz are characterized by a transient pressure trend, with the longest injection duration of 7 days (Injection test 03JAN23 in GPK2). Therefore the estimated hydraulic parameters are time-dependent and a consistent comparison of the estimated parameters has to be refereed to a specific duration of injection/production.

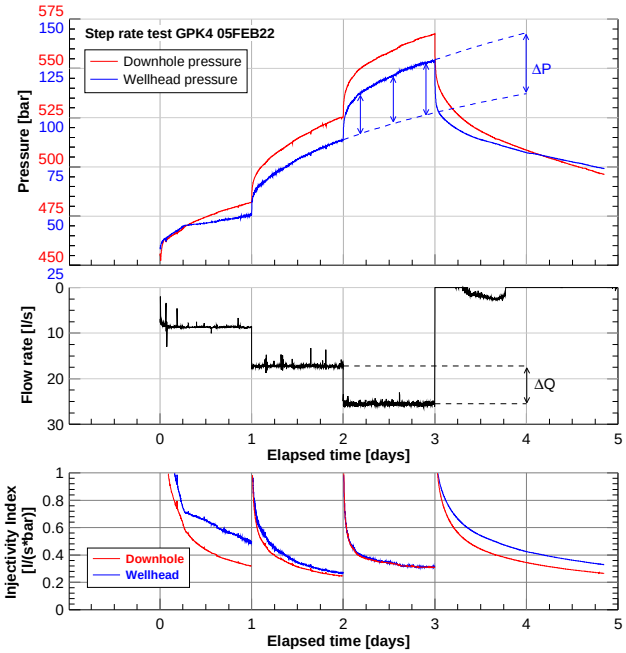

Figure 2: Up and middle: Pressure and flow rate recorded during the step rate test 05FEB22 in GPK4. The test was carried out after the hydraulic stimulation. Down: Injectivity index calculated from wellhead and downhole data. The values are identical during the third step.

Comparison between injectivity index and productivity index

The well injection/production rate is related to the injectivity/productivity index by the differential injection/production pressure. The flow reversibility of the Soultz wells was analyzed by comparing the flow performance derived from injection and a production test. Both the production test (06OCT23) and a step rate test (07JAN29), carried out after the NTA-stimulation and before the OCA-stimulation was used for this purpose.

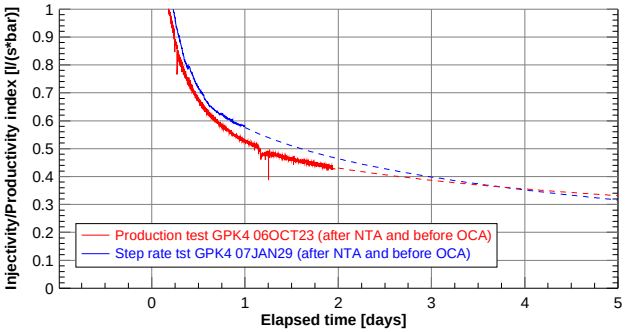

Figure 3: Comparison between injectivity index and productivity index in GPK4. The two test were carried out after the NTA-stimulation and before the OCA-stimulation

The calculated flow performance from both tests shows the difference between injectivity index and productivity index at the beginning of the tests. After a period of five days, the estimated productivity index nearly equals the injectivity index. Figure 3 shows that there is no significant difference between injectivity and productivity at moderate pressure changes. The terms injectivity and productivity can be considered therefore as synonymous.

Overview of the pre- and post-stimulation flow performance

Figure 4 summarizes the development of the flow performance of the Soultz wells before and after each stimulation operation. The values shown here are injectivities/productivities obtained from pre- and post-stimulation hydraulic tests. All hydraulic and chemical stimulations are evaluated as well as the performance of the wells during circulation.
It is to note that the injectivity/productivity of the Soultz wells is time-dependent in general. Therefore, values for the injectivity/productivity have to be referred to a specific duration of injection/production. Throughout this paper, the injectivity/productivity is determined after a test duration of five days and is rounded to the next 0.05 l/(s*bar).

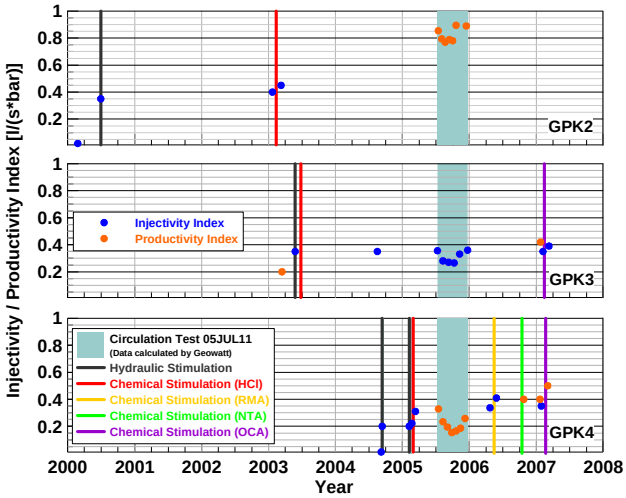

Figure 4: Compilation of the productivity of the deep Soultz wells before and after each stimulation. The dots in the shaded area were derived from the circulation test 2005 and calculated by Geowatt, 2006.

The results of the stimulation operations are summarized as follow:

GPK2

The natural permeability of the rock mass estimated from pre-stimulation hydraulic tests in GPK2 gives a value of ~9 x 10^{-17} m². GPK2 has been stimulated hydraulically with very good results. It has a productivity of 0.5 l/(s*bar) in single well tests, implying an equivalent porous medium permeability of ~2 x 10^{-15} m² (transmissibility at ~10^{-12} m³). Due to a good hydraulic communication with GPK3, the well GPK2 has a productivity of ~0.8 l/(s*bar) under circulation conditions, caused by the increasing reservoir pressure. This difference shows the importance of a reinjection into the same reservoir during a future circulation.
The chemical stimulation with HCl mainly reduced flow resistance in the borehole itself which might consist of the restriction and the lost tool and cable. Nevertheless, a significant turbulent flow regime occurs in the well.

A leak at ~3900 m TVD, very close to the casing restriction, contributes to a loss of ~30% of the initial flow rate. In the current state, this leak does not form a connection of the well to the upper reservoir (Pfender et al., 2006).

GPK3

The estimated initial productivity index in GPK3 was 100 times higher than the productivity index of GPK4 (0.1 l/(s·bar)), implying an equivalent porous medium permeability of ~5 x 10^{-16} m². The present productivity index of GPK3 is about 0.4 l/(s*bar) and remained almost unchanged after successive stimulation operations with HCl and OCA. The estimated equivalent porous medium permeability after the stimulation operations is estimated from pre- and post-stimulation tests at ~2 x 10^{-15} m² (transmissibity at ~3 x 10^{-13} m³). An infinitive conductive fracture with a large fracture area between 25000 and 50000 m² intersects the open borehole at 4700 m MD and hampers a further improvement by chemical stimulations (Tischner et al, 2006).

GPK4

The low-pressure hydraulic test conducted in GPK4 to characterize the natural permeability of the granite indicated an injectivity index of 0.01 l/(s·bar), implying an equivalent porous medium permeability (EPM) of the rock mass of ~5 x 10^{-17} m² and a transmissibity of ~5 x 10^{-14} m³.
The hydraulic stimulations carried out in GPK4 have improved the flow performance by a factor of 20. The estimated injectivity index was 0.2 l/(s·bar), enhancing the permeability to the millidarcy-range (10^{-15} m²) and the transmissibility to ~5 x 10^{-13} m³.
The RMA and OCA chemical stimulations improved the productivity of the wells by 30 and 25% respectively, but at least a part of this gain is attributed to two loss zones in the cemented part of the casing. Stress conditions during the OCA stimulation were favourable for a hydraulic stimulation and were probably caused by a plugging of the well during the pre- and postflush (Nami et al., 2007). Moreover, we found a correlation of the upper leak (4110 m TVD) with an accumulation of seismic events. Therefore, a gain of productivity only from the openhole section and the reservoir at 5000 m depth is not likely.
The estimated equivalent porous medium permeability (EPM) after the chemical stimulations remained in the millidary-range at around 2 x 10^{-15} m².
The RMA and NTA stimulations additionally improved the hydraulic communication between GPK3 and GPK4.

Figure 5 shows the impact of each stimulation method in the wells. It can be retrieved that the hydraulic stimulation is the technique which mostly brought an enhancement of the wells. In addition, this technique is accompanied by the triggering of microseismic events, helping to follow in real time the impact of the stimulation during the whole operation. However, some of the induced seismic events during hydraulic stimulation can be large enough to raise public concern. A better understanding of the generation of these events is therefore essential.
In addition to short-term hydraulic tests before and after each stimulation, logs (flow logs, temperature logs, UBI logs) may be systematically run for a better characterisation of the impact of each stimulation.

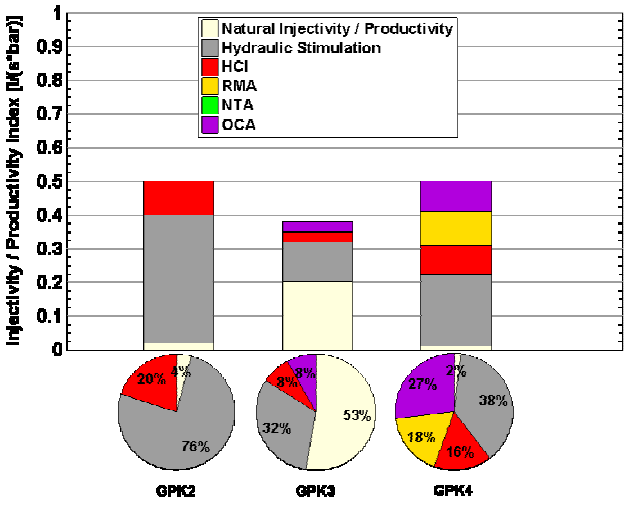

Figure 5: Contribution of each stimulation method to the current performance of the Soultz wells.

CONCLUSION

The deep Soultz wells have been stimulated hydraulically and chemically, in order to develop the underground reservoir prior to electricity production. The results of the stimulation operations are summarized as follows:

GPK2

The well has a productivity of ~0.50 l/(s*bar) in single well tests. Due to a good hydraulic communication with GPK3, the well GPK2 has a productivity of ~0.80 l/(s*bar) under circulation conditions, caused by the increasing reservoir pressure. This difference shows the importance of a reinjection into the same reservoir during a future circulation.
The chemical stimulation with HCl mainly reduced flow resistance in the borehole itself which might consist of the restriction and the lost tool and cable. Nevertheless, a significant turbulent flow regime occurs in the well.

GPK3

The productivity index of GPK3 is about 0.40 l/(s*bar) and remained almost unchanged after successive stimulation operations with HCl and OCA. An infinitive conductive fracture with a large fracture area between 25000 and 50000 m² intersects the open borehole at 4700 m MD and hampers a further improvement by chemical stimulations.

GPK4

The productivity of the well was 0.20 l/(s*bar) after hydraulic stimulations and has improved to ~0.50 l/(s*bar). In comparison to GPK2, the hydraulic communication with GPK3 was weaker prior to the chemical stimulations and therefore GPK4 was less productive than GPK2 during the circulation in 2005.
The chemical stimulations with RMA and OCA improved the productivity of the wells by 30 and 25% respectively, but we attribute at least a part of this gain to a simultaneous hydraulic stimulation of two loss zones in the cemented part of the casing. Stress conditions during the OCA stimulation were favourable for a hydraulic stimulation and were probably caused by a plugging of the well during the pre- and postflush. Moreover, we found a correlation of the upper leak (4110 m TVD) with an accumulation of seismic events. Therefore, a gain of productivity only from the openhole section and the reservoir at 5000 m depth is not likely.

The chemical stimulations with RMA and NTA additionally improved the hydraulic communication between GPK3 and GPK4.

The pre-stimulation hydraulic tests performed in the production wells (GPK2 and GPK4) give a natural permeability of the rock mass of ~5-9 x 10^{-17} m², which is in the range of the effective permeability of granite. The succeeding hydraulic stimulation operations have enhanced the permeability in the range of millidarcy (10^{-15}m²). The higher initial flow performance of GPK3 remained nearly unchanged after the stimulation operations. The equivalent porous medium permeability (EPM) was also estimated in the range of millidarcy. A significant permeability creation after chemical stimulations was therefore not achieved.

The effectiveness of stimulation operations can be further improved by hydraulically stimulating selected zones (packer…) or by using techniques to divert the treatment fluid toward selected zones in the reservoirs (drill pipe, coiled tubing...). All the stimulation operations in Soultz were performed by injecting water (for hydraulic stimulation) or acid (for chemical stimulation) from the wellhead through the casing string. The stimulation zone was therefore the whole openhole section of the wells (500 to 650 m length). Particularly in fractured crystalline formations, where the reservoir permeability is strongly controlled by the pre-existing natural fracture network, a “focussed” stimulation of this high-permeable joints and fracture zones is essential.

REFERENCES

Nami, P., Schellschmidt, R., Schindler M., Tischner, T. (2008), Chemical stimulation operations for reservoir development of the deep crystalline HDR/EGS at Soultz-sous-Forêts (France). *Proceedings thirty-Third Workshop on Geothermal Reservoir Engineering*, Stanford University, Stanford, California, USA.

Pfender, M., Nami, P., Tischner, T., Jung, R. (2006), Status of the Soultz deep wells based on low rate hydraulic tests and temperature logs. *Proceedings, EHDRA Scientific Conference,* Soultz-sous-Forêts, France, June 15-16, 2006.

Portier, S., André, L., Vuataz, F-D. (2007), Review of chemical stimulation techniques in oil industry and applications to geothermal systems, *Technical Report, ENGINE work package 4: Drilling, stimulation and reservoir assessment*, Neuchâtel, Switzerland.

Tischner, T., Pfender, M., Teza, D. (2006), Hot Dry Rock Projekt Soultz: Erste Phase der Erstellung einer wissenschaftlichen Pilotanlage, *Abschlußbericht zum Vorhaben 0327097*, Tgb. Nr. (BGR): B1.15-10125/06.

APPENDIX 4 – geology, stresses and flow paths

APPENDIX 4(a)

Albert Genter, Ch. Dezayes, B. Ledesert, Judith Sausse and Benoît Valley, 2008, Geological reconnaissance of deep fractured geothermal reservoirs: what have we learnt at Soultz in 20 years? *paper presented at the EHDRA Scientific Conference, Soultz-sous-Forêts,* September 24-25, 2008.

EC Contract SES6-CT-2003-502706

PARTICIPANT ORGANIZATION NAME: GEIE

Related with Work Package 5

Related with Working Groups 6/7

GEOLOGICAL RECONNAISSANCE OF DEEP FRACTURED GEOTHERMAL RESERVOIRS: WHAT WE HAVE LEARNT AT SOULTZ IN 20 YEARS?

Genter A.*, Dezayes Ch.**, Ledesert B.,***, Sausse J.****, Valley B.*****

**GEIE EMC, Kutzenhausen, France*

***BRGM, Orléans, France*

****Cergy University, France*

*****Nancy University, France*

******ETH-Zurich, Switzerland*

e-mail: genter@soultz.net

ABSTRACT

The Soultz geothermal project has been running for 20 years by taking into account both the nature and the structure of the deep crystalline basement penetrated by several deep exploration and geothermal wells. A lot of geological works have been done for exploring the crystalline rocks based on drilling data (cuttings, cores, well logging, borehole image logs) in the top basement (2km), in the upper reservoir (3,5km) and in the lower reservoir (5km). Fractures are nearly vertical and the major orientation in the granite is mainly NNW-SSE. Natural fractures and faults show a multi-scale organization in the deep granite from micro-cracks to large-scale normal faults. The geothermal target is a fractured granite reservoir characterized by hydrothermally altered and fractured zones showing low naturally permeability during drilling operations prior to any stimulations. The mineralogical composition of the fracture zones is made of some typical alteration mineral assemblages such as illite, secondary quartz, carbonates and locally sulfurs. This paper summarizes the main milestones and knowledge about Geology obtained in the Soultz wells over 20 years.

INTRODUCTION

The EGS technology has been under development over 20 years in the northern part of Alsace (France). This area was primarily selected due to the occurrence of one of highest large-scale geothermal anomaly well known from deep temperature measurements collected in a former petroleum field (Gérard et al., 1984). The geothermal area is located within the Upper Rhine graben which forms a part of the European Cenozoic rift system that extends in the foreland of the Alps from the Mediterranean to the North Sea coast (Dézes et Ziegler, 2001). The Moho which is the boundary between the Earth's crust and the mantle shows a topography of its depth thickness with a doming structure below the Rhine graben (Figure 1).

PRE-DRILLING PHASE

Previous data: the old Péchelbronn-oil field

At concessional scale, the Soultz area was well known before any geothermal drilling activity due to the large amount of geological data collected before the 70s' during the oil exploration of the Péchelbronn-Merkwiller oil field. More than 3000 oil wells were done giving a quite good overview of the geology within the post-Palaeozoic sediments. For example, in 1905, 1164 wells had been drilled representing a cumulative length of 290 km, the deeper well reached 600 m depth. In 1927, the first geophysical resistivity logging operation has been performed by the Schlumberger brothers. During oil exploration, numerous temperature measurements have been made in the Péchelbronn oil-bearing region (Haas et Hoffmann, 1929). Based on approximately 500 measurements, this old study shown that isotherms are influenced primarily by the tectonic structure of the Rhine graben (Figure 2). Indeed, there is a strong horizontal and vertical increase of temperature which is especially marked in the vicinity of fault zones. For example, the hottest zone at 400 m depth is located along the western part of the Soultz horst and is characterized by NE-SW elongation (Hass et Hoffmann, 1929). On the top of this area, the GPK1 well was drilled in 1987-1988 at 2000m.

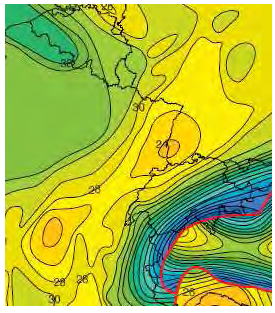

FIGURE 1. Map of the Moho depth expressed in km in Europe (Dézes et Ziegler, 2001). The Rhine graben is characterized by a minimum Moho depth of 24 km.

From a geological point of view, a structural compilation was done by Schnaebele et al. (1948) which illustrated the compartmenting of this area by normal faults inducing a horst and graben structure (Figure 3). In the 80s', several oil companies did seismic exploration in order to image the structure of the fault system inside the sedimentary cover of the Rhine graben. Therefore, before the GPK1 drilling, the top of the crystalline basement was known from both seismic reflection profiles and from a former oil well 4616 drilled to 1403m close to the site which reached the basement at 1380m. During oil exploration, a core was taken in this well and the petrography shown a typical granite rock composition. All these data were available and partly reinterpreted when the Soultz project started with the drilling of GPK1 (Figure 4).

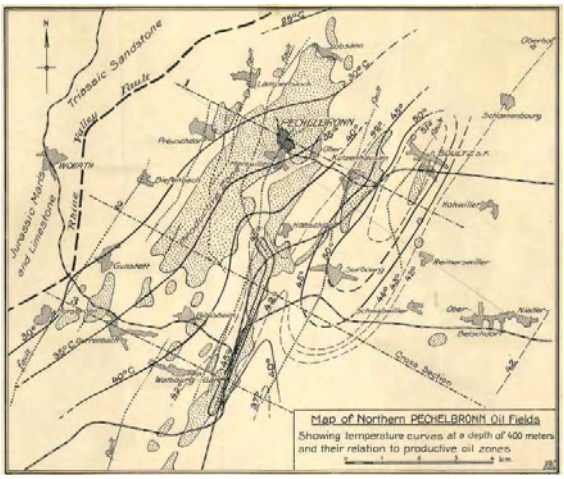

FIGURE 2. Temperature map done at 400 m depth based on data collected in oil wells between Merkwiller and Soultz (Haas et Hoffmann, 1929).

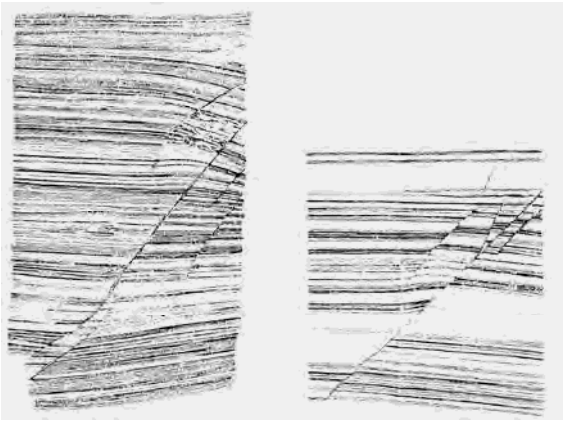

FIGURE 3. Example of normal faults observed at outcrop scale in the Péchelbronn oild field (Schnaebele et al., 1948).

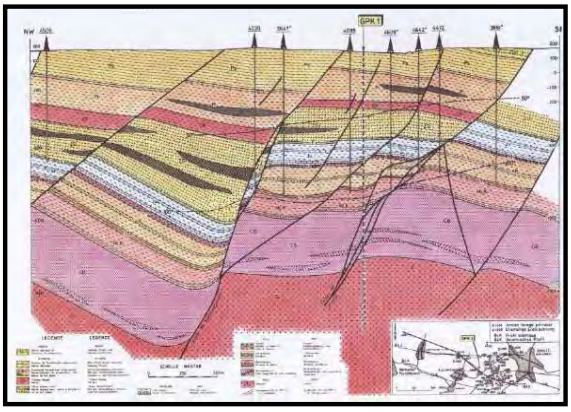

FIGURE 4. Geological W-E cross-section showing the Soultz Horst structure based on seismic line interpretation and old petroleum borehole data (Cautru, 1988).

Main geological studies before GPK1 drilling

Before any drilling operation, two different kinds of fracture studies were done by BRGM: a satellite image analysis and a structural study on relevant crystalline outcrops. At regional scale, a satellite image, called SPOT, was taken on November 1986 in order to investigate the large-scale fracture network visible on an area of 4500km². Large-scale fracture sets were outlined and are characterized by N-S, NE-SW, ENE-WSW and NW-SE orientations (Genter, 1989). On a field, a structural study was conducted in old quarries at Windstein located on the closest crystalline outcrops lying about 15 km westward of the geothermal site in the Vosges mountains. This structural analysis gave the first overview of the main nearly vertical pre-existing fracture sets which are oriented NW-SE, NNE-SSW and NE-SW (Genter and Martin, 1988).

EXPLORATION PHASE TO 2 KM DEPTH

After a pre-drilling phase leading to the site selection of the Péchelbronn-Soultz area (Gérard and Kappelmeyer, 1986), the first exploration vertical well GPK1 (Géothermie Puits Kutzenhausen 1) was drilled in 1987-1988 to 2 km depth by conventional drilling system (Herbrich, 1988). The bottom hole temperature was 140°C whereas 200°C was expect ed.
In 1987, the first exploration well, GPK1, reached 2 000 m, drilled in destructive mode. Originally, GPK1 was planned for a full coring of the basement (1400-2000m). Due to technical issues, the coring failed and only spot coring representing about a cumulative length of about 50 m of Triassic sediments and granitic cores was collected. Temperature at the bottom depth was 140°C. Based on well logging d ata, borehole image, cuttings analysis and spot coring calibrated on outcropping analogues, a first conceptual model of hydrothermally altered and fractured zone was defined at Soultz (Genter, 1989). The top of the basement was reached as expected at 1375 m. It corresponds to a Visean grey biotite-rich granite made of Feldspar megacrysts (Figure 5). This Visean granite is characterized by a heat production derived from radioactive logs of about 5 $\mu W/m^3$ (Rummel, 1991).

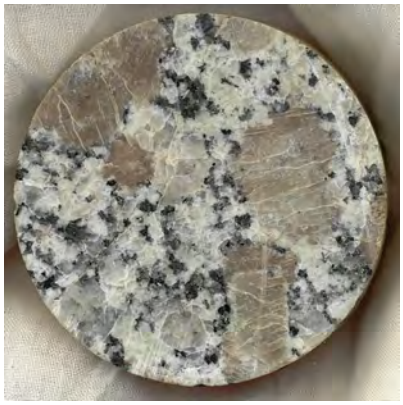

FIGURE 5. Granite core section from GPK1 well (3510m).

Surprisingly, a major permeable fracture zone having low natural permeability was evidenced at 1817m depth in GPK1 well based on total mud losses, gas and brines outflow (Vuataz et al., 1990) and specific hydrothermal alteration minerals such as clay mineral (Genter, 1989). The main secondary deposits related fracture zones are calcite, secondary quartz, illite and hematite mainly. Strong hydrothermal alteration halo was evidenced around this major permeable fault zone from cuttings, borehole image and well logging analysis (Genter et al., 1989, Traineau et al., 1991). The main hydrothermal alteration effect corresponds to the precipitation of illite (K-rich dioctaedric phyllosilicate) which results from the transformation of the primary biotite and Ca-plagioclase mainly (Figure 6b).

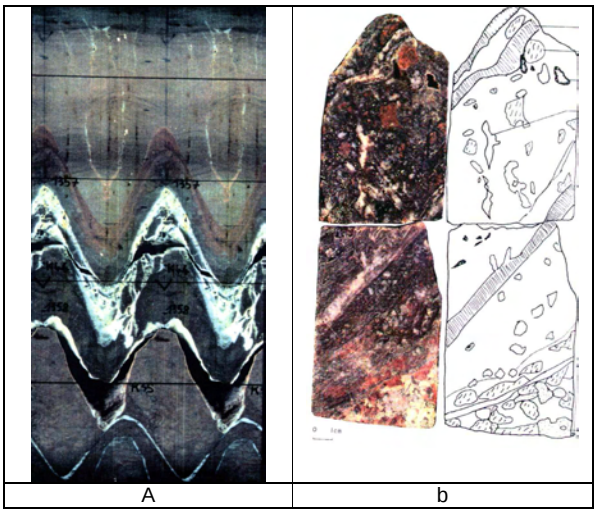

A | b

FIGURE 6. Examples of cores collected at Soultz. a) Fracture zone filled with barite and galena in the Triassic sandstone (EPS1, 1205 m, vertical scale 1m). b) Core K19 collected in a permeable fracture zone in GPK1 at 1809 m showing crushed granite and secondary quartz vein (vertical scale 30 cm).

Fracture geometry was deduced from electrical borehole imagery technique, called FMS (Formation MicroScanner) (Genter at al., 1991) and by acoustic borehole televiewer called BHTV (Figure 7, Tenzer et al., 1991). The main fracture orientation was N170°with high dipping va lues.

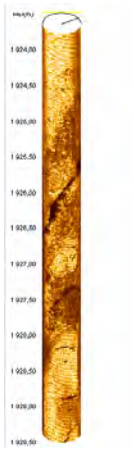

FIGURE 7. Example of 3D view of natural fractures visible on borehole image logs at Soultz.

In 1991, the reference well EPS1 which is an old oil well deepened to 2227 m, was deepened and fully cored with mining system to TD. Samples come from the lower Triassic sandstones formation (Buntsandstein) and from the same porphyritic granite penetrated previously by GPK1 (Genter and Traineau, 92). This well was originally planned to do the geological reconnaissance to 3,5km but from 2 km, as the deviation from horizontal was higher than 20°, the well was stopped. The high quality and the high recovery of the coring permit to characterize the granite petrography and its mineralogy, the hydrothermal alteration minerals as well as the fracture systems. A high quality structural and petrographic database was collected and used in various geological studies.

A major fractured zone filled with barite and sulphides was cross-cut at 1200 m in Triassic sandstones (Figure 6a). About 10 m thick of Permian clastic formations overlie the granite. The top of the basement was confirmed at 1417 m depth, i.e., deeper than in the northern well GPK1 confirming that this major interface is dipping southward with a low angle. The well penetrated the same granite massive (Stussi et al., 2002). A major permeable fracture zone was penetrated at 2160 m depth characterized by an outflow of geothermal brine (Figure 8). In this zone, organic matter is intimately associated with hydrothermal alteration like tosudite, a clay mineral bearing lithium (Ledesert et al., 1993). High mercury porosity values up to 25% were measured within this hydrothermally altered zone. Primary quartz was fully dissolved (Ledesert et al., 1999). The concept of HAFZ was refined based on core results by taking into account minerals dissolution and fracture organization (Genter et al., 1998, 2000). Pre-existing nearly-vertical fractures are mainly oriented N10°E and N170°E on core and BHTV (Genter et al., 1995; Genter et Traineau, 1996).

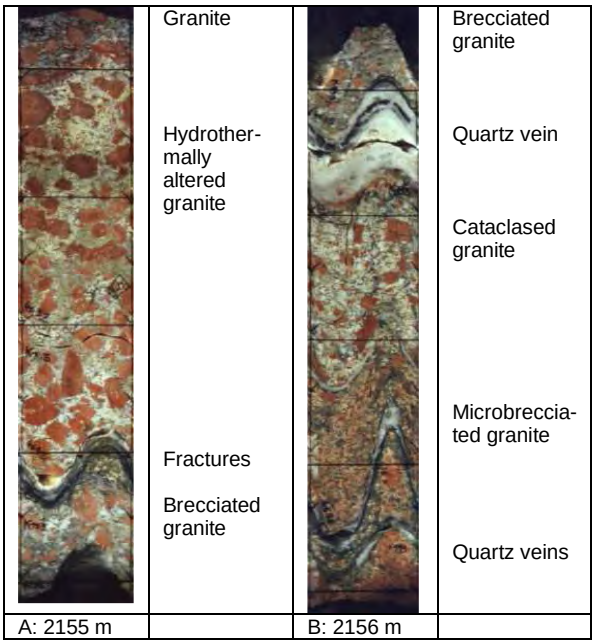

FIGURE 8. Example of Hydrothermally altered and fracture zone observed on core section in EPS1 well between 2155 and 2156 Measured Depth.

The fracture network was also investigated at very fine resolution scale with micro-crack studies done on cores in primary quartz crystals (Dezayes et al., 2000; Schild et al., 1998). In order to reconstruct the Tertiary palaeostress field and compare it with the structural Rhine graben evolution, palaeostress studies were carried out based of striated planes observed on cores (Dezayes et al., 1995) and on Vosges granite analogues (Dezayes, 1995). The cluster organization of fractures was validated based on core study by investigating fracture spacing, fracture thickness and fracture filling distribution with depth (Genter et al., 1997, Sausse et al., 1998).
Petrophysical characterization was mainly based on core samples taken in EPS1 (Rummel, 1991; Ledesert, 1993, Surma, 2003; Surma et Géraud, 2003, Sausse et al., 2006). Matrix porosity (Mercury, water) and thermal conductivities were evaluated. Altered samples show a large variation of porosity and thermal conductivity with an overall decrease of the thermal conductivity with the increase of porosity (Surma et Geraud, 2003).

Based on petro-structural studies on cores sample, the fabric of the granite was investigated. Sub-horizontal magmatic primary foliations were evidenced from petrofabric measurements (Schulmann et al., 1997). Sub-horizontal magnetic foliations indicate a magma emplacement in the centre of the batholith (Just et al., 2004). The dating of hydrothermal events on alteration minerals like illite give scattered ages between Permian, Jurassic and Cretaceous (Schleicher et al, 2006). Fluid inclusion studies showed that one of several fluid inclusion types has similar temperature to present thermal state (Dubois et al., 1996, Ledesert, 1993).

In the meantime, the reinterpretation of 5 seismic lines calibrated with oil well data permitted to build a 3D image of the Soultz Horst (Figure 9) in the sediments with the goCad geomodeller (Renard and Courrioux, 1994).

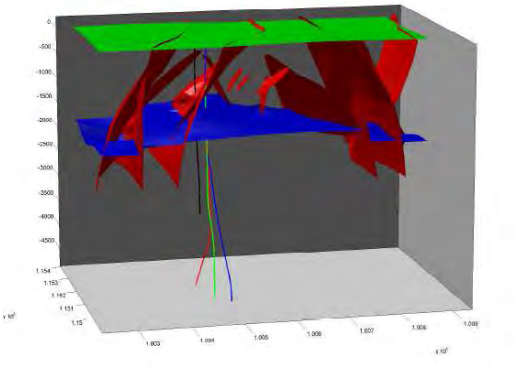

FIGURE 9. 3D model in the sediments derived from seismic line interpretation (goCad software).

EXPLORATION PHASE TO 3,5 KM DEPTH

The exploration phase to 3,5 km depth started by the deepening of GPK1 in destructive mode to 3,6km depth. The bottom hole temperature was 160°C. A core was taken at 3,510 m. The well penetrated the same granite massive (Genter et Traineau, 1991). The major permeable fracture zones characterized by outflow, mud losses, gas, and geodic quartz are located at 2815 m and 3490 m depth (Figure 10).

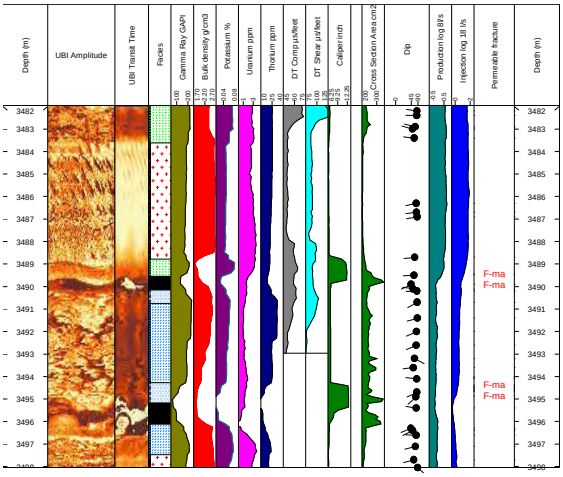

FIGURE 10. Relationship between permeable fracture, well logging data and flow log in a permeable fracture zone in GPK1 at 3,5 km.

The main nearly-vertical fracture orientation is N10°E, N20°E and N175°E. Fracture zone orientations are N140°E a nd N160°E in GPK1 and GPK2 (Genter et al., 1998). Frac ture apertures were evaluated from electrical borehole image ARI (Sausse et Genter, 2005). In GPK1, relationship between fracture zones and connected permeable paths were outlined (Evans et al., 2005).

The exploration of GPK2 showed a major permeable fracture zone penetrated at 2120 m provoking total mud and cutting losses from that depth to TD (Genter et Tenzer, 1995). Major faulted zones are located at 3240m and 3510 m and suspected at TD (3900 m). Fractures observed on UBI are nearly vertical and oriented N170°E±15° (Genter et al., 1997).

EXPLORATION PHASE TO 5 KM DEPTH

The deepening of GPK2 in 1999 to 5000 m showed the occurrence of a new fine grained two mica granite unit from 4860 m depth and confirmed by core examination (Genter et al., 1999). Rock dating of MFK rich granite and two mica fined grained granite gives 330 ±7 My and 327 ±3 My respectively (Alexandrov et al., 2001; Cocherie et al., 2004). Fractures are nearly vertical and oriented N170°E (Dezayes et al., 2004). Based on cuttings, fracture zones are located at 4580 m, 4780 and 4880 m (Genter et al., 1999). Calcimetry measurements in the cuttings samples showed some degree of matching of carbonate concentration and fracture zones (Grall et al., 2007). Compilation of geological data allows to propose a two granite body conceptual model (Dezayes et al., 2003; Hooijkaas et al., 2006).

The drilling of GPK3 and GPK4 gave similar geological results. A new fine grained two mica granite unit was evidenced from 4730 m depth in GPK3 (Dezayes et al., 2003). Fractures observed on UBI are nearly vertical and oriented N170°E (Dezayes et al., 2004; Valley, 2007). In GPK3, a natural large permeable fracture zone is located at 4770 m depth (Dezayes et al., 2003). There is not enough data for proposing a relevant fracture zone concept definition in the 2 mica granite. In the deepest part of GPK4, there is no natural large permeable fracture zone (Dezayes et al., 2005).

FRACTURE SCALES

The fracturing of the basement of the Upper Rhine Graben permitted to define structures at various scales and allowed to quantify their characteristic size (Valley, 2007; Figure 11).

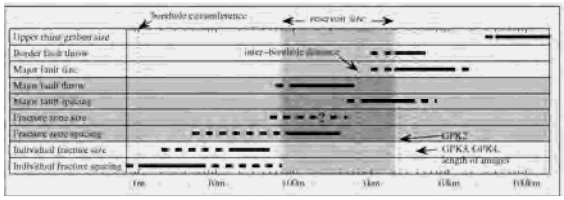

FIGURE 11. Synthesis of the size of the various structures crossing the Upper Rhine Graben basement. In grey are highlighted the relevant size for the reservoir development and the relevant structure which correspond to that size (Valley, 2007).

A general overview at fracture zone scale was done by Dezayes and Genter (2008). 39 fracture zones have been determined in the five deep wells of Soultz, GPK1, EPS1, GPK2, GPK3 and GPK4, and in the seismic monitoring well, named 4550. These zones have been plotted in 3D and compared with VSP and microseismicity results (Sausse et al., 2008)

CONCLUSIONS

As the Soultz geothermal target is a hidden granite batholith made of two superimposed granite units overlain by a thick post-Paleozoic sedimentary cover, the reconnaissance by drilling of this granitic body is much more difficult to explore than conventional high enthalpy fields. There are no surface hydrothermal manifestations of a deep resource such as fumaroles, hot springs, altered zone or geysers. The main indirect traces indicating a potential geothermal resource is the occurrence of high temperature at shallow depth (50°C at 400m depth) well-known from old-petroleum wells. Before drilling, a lot of sub-surface information was available in the sediments: seismic profiles, thousands of wells of various depth, and temperature measurements. The geothermal target is a Paleozoic altered and fractured granite overlain by a thick sedimentary cover made of Permian, Triassic, Jurassic and Tertiary sedimentary formations.

Based on 20 years of activities, geothermal exploration was mainly driven by high quality dataset acquisition, evaluation of rock composition of the pre-fractured crystalline rocks (petrography/mineralogy) and fracture network characterisation. Conceptual model of Hydrothermally Altered Fractured Zones (HAFZ) has been proposed at least for the MFK rich granite. 2 mains type of hydrothermal alterations were evidenced: pervasive and vein alterations. Occurrences of Hydrothermally Altered and Fractured Zones with illite, calcite and secondary quartz and low natural flow (brines) were found at various depths in the different Soultz wells. The fracture system is not homogenously distributed in space but some concentrations of fractures occur which alternate with poorly fractured sections. Highest fracture densities are mainly localized in the upper part of the geothermal site within 1400 and 2200 m depth. Fracture geometry is strongly influenced by the graben tectonics and shows nearly vertical fractures striking close to N170°E orientation.

CURRENT LIMITATIONS AND PERSPECTIVES

Despite of an exhaustive research work about geological characterisation, one must admit that there are still many open questions about deep-seated geology of the geothermal system. In sediments, there was not so many works. However, the vertical evolution of faults orientation with depth is debatable. Are faults striking with the same azimuth and dip with depth in sediment and in basement? Is there any variation in terms of orientation between N20°-N40°E fault geometry in sediments and N140°-N170° faults in the granite and in the Buntsandstein? Then, some new and innovative methods for imaging the top of the basement will be very helpful for evaluating the vertical persistence of faults as well as to check the occurrence of transverse faults oriented E-W. In granite, the HAFZ concept was proposed between core and well scales in the MKF-rich granite but no HAFZ model is available for the 2 mica granite. Fracture organisation and fracture extension beyond the borehole wall still remain open questions even VSP survey brings new inputs about large-scale fault zone. Fracture filling (composition, thickness) is always difficult to characterize based on cutting samples and well logging data.
Some research works for improving fracture zone concept based on various information (core, wells, analogues) are recommended. We need innovative geophysical tools/methods for better characterise the fault extension within the inter-well domain and in the reservoir and also 3D tool for taking into account the 3D complexity of fault geometry in hard rocks. Finally, relationships between channelling, permeability, hydrothermal alteration, and fault geometry have to be clarified.

REFERENCES

Alexandrov, P., Royer, J.J., Deloule, E., (2001). 331 ± 9 Ma emplacement age of the Soultz monzogranite (Rhine Graben basement) by U/Pb ion-probe zircon dating of samples from 5 km depth. *C.R.A.S.,* **332**, 747-754.

Cautru, J.P., (1988). Coupe géologique passant par le forage GPK1 calée sur la sismique réflexion, document BRGM IMRG, unpublished.

Chèvremont, Ph., Thiéblemont, D., Laforêt, C., Genter, A., Traineau, H., (1992). Etude pétrologique du massif granitique recoupé par le forage EPS-1 (Soultz-sous-Forêts, France). Rapport BRGM RCS 92 T15 SGN/IRG.

Cocherie, A., Guerrot, C., Fanning, C.M., Genter, A., (2004). Datation U-Pb des deux faciès du granite de Soultz (Fossé Rhénan, France). *Comptes Rendus Geoscience*, **336**, 775-787.

Dezayes Ch., Villemin Th., Pecher A., (2000). Microfracture pattern compared to core-scale fractures in the borehole of Soultz-sous-Forêts Granite, Rhine Graben, France, *Journal of Structural Geology*, vol. **22**, 723-733.

Dezayes, C., Genter, A., (2008). Large-scale fracture zone network based on Soultz borehole data. *Proceedings of the EHDRA scientific conference* 24-25 September 2008, Soultz-sous-Forêts, France.

Dezayes, Ch. (1995). Caractérisation et interprétation d'un volume rocheux fracturé à partir des données de forage. PhD thesis, Université de Savoie, France, 246 pp.

Dezayes, Ch., Chèvremont, Ph., Tourlière, B., Homeier, G., Genter, A., (2005). Geological study of the GPK4 HFR borehole and correlation with the GPK3 borehole (Soultz-sous-Forêts, France). Open file report BRGM/RP-53697-FR, 94 pp.

Dezayes, Ch., Genter, A. Gentier, S., (2004). Fracture network of the EGS Geothermal Reservoir at Soultz-sous-Forêts (Rhine Graben, France). Geothermal Resources Council Transactions, Palm Springs, California, USA, Vol. 28, 213-218.

Dezayes, Ch., Genter, A., Homeier, G., Degouy, M., Stein, G., (2003). Geological study of GPK3 HFR borehole (Soultz-sous-Forêts, France), Open file report BRGM/RP-52311-FR, 128 pp.

Dezayes, Ch., Villemin, Th., Genter A., Traineau, H., Angelier, J., (1995). Analysis of fractures in boreholes of the Hot Dry Rock project at Soultz-sous-Forêts (Rhine Graben, France), *Scientific Drilling*, vol. **5**, 31-41.

Dèzes, P., Ziegler, P. A., (2001). European Map of the Mohorovicic discontinuity. 2nd EUCOR-URGENT Workshop (Upper Rhine Graben Evolution and Neotectonics), Mt. St. Odile, France.

Dubois, M., Ayt Ougougdal, M., Meere, P., Royer, J.-J., Boiron, M.-Ch., Cathelineau, M., (1996). Temperature of paleo- to modern self-sealing within a continental rift basin: The fluid inclusion data (Soultz-sous-Forêts, Rhine Graben, France). *Eur. J. Mineral.*, vol. **8**, 1065-1080.

Evans, K.F., Genter, A., Sausse, J., (2005). Permeability creation and damage due to massive fluid injections into

granite at 3.5 km at Soultz: Part 1 - Borehole observations, *Journal of Geophysical Research*, **110**, B04203.

Genter, A., (1989). Géothermie Roches Chaudes Sèches : le granite de Soultz-sous-Forêts (Bas Rhin, France). Fracturation naturelle, altérations hydrothermales et interaction eau - roche. *PhD thesis*, **Université d'Orléans**, France, 201 pp.

Genter, A., Castaing, C., Dezayes, Ch., Tenzer, H., Traineau, H., & Villemin, T., (1997), Comparative analysis of direct (core) and indirect (borehole imaging tools) collection of fracture data in the Hot Dry Rock Soultz reservoir (France), *Journal of Geophysical Research*, **vol. 102**, B7, 15419-15431.

Genter, A., Cautru, J.-P., Montaggioni, P., Traineau, H., (1989), Geological interpretation of well logging data from the granitic section of the Soultz-sous-Forêts GPK1 well. *SPWLA*, 12th International Well Logging Symposium, SAID, **paper EE**, 25-27 Oct. 1989, Paris, 12 pp.

Genter, A., Dezayes, Ch., Gentier, S., Ledésert, B., Sausse, J., (1998). Conceptual fracture model at Soultz based on geological data. Geologisches Jahrbuch: Sondehefte: Reihe E. Geophysik ; H. SE 1, 4th International Hot Dry Rock (HDR) Forum, Strasbourg, France, Sept. 28-30 1998, 93-102.

Genter, A., Homeier, G., Chèvremont, Ph., Tenzer, H., (1999). Deepening of GPK-2 HDR borehole, 3880-5090 m (Soultz-sous-Forêts, France). Geological monitoring. Open file report BRGM/RR-40685-FR, 81 pp.

Genter, A., Martin, P., (1988). Analyse de la fracturation relevée sur les carottes de granite du forage GPK1 (Soultz-sous-Forêts, Bas-Rhin). *BRGM Open file report,* **RR-26086-FR**, 37 pp.

Genter, A., Martin, P., Montaggioni, P., (1991), Application of FMS and BHTV tools for evaluation of natural fractures in the Soultz geothermal borehole GPK1. *Geothermal Science & Technology*, **vol. 3**, 69-82.

Genter, A., Tenzer, H., (1995). Geological monitoring of GPK-2 HDR borehole, 1420-3880 m (Soultz-sous-Forêts, France). Soultz-sous-Forêts, Open file report BRGM/RR-38629-FR, 46 pp.

Genter, A., Traineau, H., (1991). Geological survey of the HDR borehole EPS1, Soultz-sous-Forêts, Bas-Rhin. Open file report BRGM/RR-32433-FR, SGN, IRG.

Genter, A., Traineau, H., (1996). Analysis of macroscopic fractures in granite in the HDR geothermal well EPS1, Soultz-sous-Forêts, France, *Journal of Volcanology and Geothermal Research*, **72**, 121-141.

Genter, A., Traineau, H., Bourgine, B., Ledésert, B., Gentier, S., (2000). Over 10 years of geological investigations within the European Soultz HDR project, France. Proceedings of the World Geothermal Congress 2000, Kyushu-Tohoku, Japan, May 28 - June 10, 2000, Editors E. Iglesias, D. Blackwell, T. Hunt, J. Lund, S. Tamanyu, 3707-3712.

Genter, A., Traineau, H., Dezayes, Ch., Elsass, P., Ledésert, B., Meunier, A., Villemin, T., (1995). Fracture analysis and reservoir characterization of the granitic basement in the HDR Soultz project (France). *Geothermal Science & Technology*, vol. **4** (3), 189-214.

Gérard, A., Kappelmeyer, O., (1986). The Soultz-sous-Forêts project and its specific characteristics with respect to the present state of experiments with Hot Dry Rocks, Proceedings EEC/US workshop on Hot Dry Rocks – Brussels, Belgium, 28-30 May 1986.

Gérard, A., Menjoz, A., Schwoerer, P., (1984), L'anomalie thermique de Soultz-sous-Forêts, *Géothermie Actualités*, **n°3** , 35-42.

Grall, C., Ledésert, B., Hébert, R., Genter, A., Bartier, D., Dezayes, Ch. Gérard, A., (2007). How calcimetry can help for a better knowledge of flow pathways in the Soultz-sous-Forêts Enhanced Geothermal System. Proceedings EHDRA Scientific Conference, 28 & 29 June 2007, Soultz-sous-Forêts, France, 6 p.

Haas, J.-O., Hoffmann, C.R., (1929), Temperature gradient in Pechelbronn ol bearing region, lower Alsace: its determination and relation to oil reserves. *Bull. Amer. Assoc. Petr. Geol.*, **XIII, n°10** , 1257-1273.

Herbrich, B., (1988), Le forage géothermique de Soultz-sous-Forêts (GPK1). Rapport de fin de sondage, *Rapport Compagnie Française de Géothermie*, 88 CFG 03, 118 pp.

Hooijkaas, G.R., Genter A., Dezayes C., (2006) Deep-seated geology of the granite intrusions at the Soultz EGS site based on data from 5 km-deep boreholes. *Geothermics*, **35**, n°5-6, p. 484-506.

Just, J., Kontny, A., de Wall, H., Hirt, A.M., Martín-Hernández, F., (2004). Development of magnetic fabrics during hydrothermal alteration in the Soultz-sous-Forêts granite from the EPS-1 borehole, Upper Rhine Graben. In: Martin-Hernandez F, Lüneburg CM, Aubourg C, Jackson M (eds), Magnetic fabric: Methods and applications, *Geological Society*, special publication **238**: 509-526.

Ledésert, B. (1993). Fracturation et paléocirculations hydrothermales. Application au granite de Soultz-sous-Forêts, PhD thesis, Université de Poitiers, France, 220 pp.

Ledésert, B., Berger, G., Meunier, A., Genter, A., Bouchet, A., (1999). Diagenetic-type reactions related to hydrothermal alteration in the Soultz-sous-Forêts granite, France, *Eur. J. Miner.*, vol. **11**, 731-741.

Ledésert, B., Joffre, J., Amblès, A., Sardini, P., Genter, A., Meunier, A., (1996). Organic matter in the Soultz HDR granitic thermal exchanger (France): natural tracer of fluid circulations between the basement and its sedimentary cover. *J. Volcan. & Geotherm. Research*, vol. **70**, 235-253.

Renard, Ph., Courrioux, G., (1994). Three-dimensional geometric modelling of faulted domain: The Soultz horst example (Alsace, France). *Computers & Geosciences*, **Vol. 20 (No. 9)**, 1379-1390.

Rummel, F., (1991). Physical properties of the rock in the granitic section of borehole GPK1, Soultz-sous-Forêts, *Geothermal Science & Technology*, **vol. 3**, 199-216.

Sausse J., (1998). Caractérisation et modélisation des écoulements fluides en milieu fissuré. Relation avec les altérations hydrothermales et quantification des paléocontraintes. PhD thesis, Université Henri Poincaré, Nancy I, France, 336 pp.

Sausse J., Fourar M., Genter A., (2006). Permeability and alteration within the Soultz granite inferred from geophysical and flow log analysis, *Geothermics*, Vol. **35**, No. 5-6, 544-560.

Sausse, J., Dezayes, Ch., Dorbath, L., Genter, A., Place, J., (2008). 3D fracture zone network at Soultz based on geological data, Image logs, microseismic events and VSP results, Proceedings of the EHDRA scientific conference 24-25 September 2008, Soultz-sous-Forêts, France.

Sausse, J., Genter, A., (2005). Types of permeable fractures in granite, P. K. Harvey, T.S. Brewer, P. A. Pezard & V. A. Petrov (eds)., Petrophysical Properties of Crystalline Rocks, *Geological Society of London*, special publication, **240**, 1-14.

Sausse, J., Genter, A., Leroy, J.L., Lespinasse, M., (1998). Altération filonienne et pervasive: Quantification des perméabilités fissurales dans le granite de Soultz sous Forêts (Bas-Rhin, France). *Bulletin de la Société Géologique de France*, **169** (5): 655-664.

Schild, M., Vollbrecht, A., Siegesmund, S., Reutel, Ch., (1998). Microcracks in granite cores frm EPS1 geothermal drill hole, Soultz-sous-Forêts (France): paleostress directions, paleofluids and crack-related Vp-anisotropies, *Geol Rundsch***, 86**, 775-785.

Schleicher, A.M., Warr, L.N., Kober, B., Laverret, E., Clauer, N., (2006). Episodic mineralization of hydrothermal illite in the Soultz-sous-Forêts granite (Upper Rhine Graben, France), *Contribution Mineralogy Petrology*, **152**, 349-364.

Schnaebele, R., Haas, J.-O., Hoffmann, C.R., (1948). Monographie géologique du champ pétrolifère de Pechelbronn. *Mémoire Service Carte Géologique Alsace*, **vol. 7**, Strasbourg, France, 254 pp.

Schulmann, K., Jezek, J., Venera, Z., (1997). Perpendicular linear fabrics in granite: Markers of combined simple shear and pure shear flows? In: Granite: From segregation of melt to emplacement fabrics (edited by Bouchez, J. L., Hutton, D. H. W. & Stephens, W. E.). Kluwer Acedemic Publishers, Dordrecht, 159-176.

Stussi, J.-M., Cheilletz, J.M., Royer, J.J., Chèvremont, P., Féraud, G., (2002). The hidden monzogranite of Soultz-sous-Forêts (Rhine Graben, France). Mineralogy, petrology and genesis, *Géologie de la France*, **1**, 45-64.

Surma, F., Géraud, Y., (2003). Porosity and thermal conductivity of the Soultz-sous-Forêts granite. Pure and *Applied Geophysics*, **160** (2003) 1125-1136.

Tenzer, H., Mastin, L., Heinemann, B., (1991). Determination of planar discontinuities and borehole geometry in the crystalline rock of borehole GPK1 at Soultz-sous-Forêts, *Geothermal Science & Technology*, **vol. 3**, 31-67.

Traineau, H., Genter, A., Cautru, J.-P., Fabriol, H., Chèvremont, Ph., (1991), Petrography of the granite massif from drill cutting analysis and well log interpretation in the geothermal HDR borehole GPK1 (Soultz, Alsace, France); European HDR Project at Soultz-sous-Forêts. *Geothermal Science & Technology*, **vol. 3**, 1-29.

Valley, B., (2007). The relation between natural fracturing and stress heterogeneities in deep-seated crystalline rocks at Soultz-sous-Forêts (France), PhD thesis, ETH-Zürich, Switzerland, 260 pp.

Vuataz, F.-D., Brach, M., Criaud, A., Fouillac, C., (1990). Geochemical monitoring of drilling fluids: a powerful tool to forecast and detect formation waters. *SPE*, Formation Evaluation, June 1990, 177-184.

APPENDIX 4(b)

Keith Evans, Albert Genter, Judith Sausse, 2005, Permeability creation and damage due to massive fluid injections into granite at 3.5km at Soultz: 1. borehole observations, *J. Geophys. Res.*, 110, B04203, doi:10.1029/2004JB003168, 2005.

Permeability creation and damage due to massive fluid injections into granite at 3.5 km at Soultz: 1. Borehole observations

Keith F. Evans
Engineering Geology, Department of Earth Science, Swiss Federal Institute of Technology, Zürich, Switzerland

Albert Genter
Bureau de Recherches Géologiques et Minières, Orléans, France

Judith Sausse
UMR CNRS 7566 G2R, University of Nancy 1, Vandoeuvre, France

Received 10 May 2004; revised 23 December 2004; accepted 10 January 2005; published 22 April 2005.

[1] The process of porosity and permeability creation in rock masses through increased pore pressure is important in many areas of geoscience, particularly for engineered geothermal sysytems. In this paper, we analyze an unusually complete data set to determine the hydraulic and mechanical changes that occurred about a 3.6 km deep borehole in previously undisturbed granite because of massive fluid injections. The hole is open for 750 m and intersects a relatively transmissive fault near the bottom at 3.5 km. The equivalent porous medium permeability of the rock mass in the 650 m above the fault was very low ($\sim 10^{-17}$ m^2), and focused at 17 naturally permeable fractures that lay within hydrothermally altered zones. During injection, some 95% of the flow entered the rock mass at just 10 "major flowing fractures," most of which were naturally permeable. Following the injections, the transmissivity of the section above the fault increased 200-fold, and the number of permeable fractures increased to $\sim$100, the distribution being clearly organized, with major flowing fractures each surrounded by clusters of weakly-flowing, newly permeable fractures. These zones of permeability creation/enhancement correlate with the presence of hydrothermal alteration, which in turn reflects the intersection of the borehole with extensive, hydrothermally altered, cataclastic shear structures. Thus permeability creation/enhancement occurred primarily within these structures, the major flowing fractures representing the core of the structures and the clusters of newlypermeable fractures denoting the damage zone. Comparison of sonic televiewer logs run before and after the injections showed that all permeable fractures had suffered damage and major flowing fractures had suffered dislocations of millimeters to centimeters.

Citation: Evans, K. F., A. Genter, and J. Sausse (2005), Permeability creation and damage due to massive fluid injections into granite at 3.5 km at Soultz: 1. Borehole observations, *J. Geophys. Res.*, *110*, B04203, doi:10.1029/2004JB003168.

1. Introduction

[2] Hot Dry Rock (HDR) systems (also known as Enhanced Geothermal Systems) offer the attractive prospect of producing large quantities of CO_2-emission-free energy from deep, low-porosity, crystalline rocks that can be found at drillable depths in many parts of the world. The HDR concept is to drill two or more boreholes to depths where temperatures are of commercial interest, and extract the heat from the rock mass between them by circulating fluid around the loop. The natural permeability of deep, crystalline rocks is generally too low to permit the requisite flow to pass between the holes and thus must be enhanced. This is accomplished by an operation referred to as reservoir stimulation in which a large volume of fluid is injected into the rock mass at high flow rates. The objective is to produce a network of connected, permeable fractures within the target rock volume between the wells. Injections conducted at seven HDR test sites around the world have demonstrated that the technique is effective in producing large, permanent increases in rock mass permeability [*Murphy et al.*, 1999]. However, the mechanisms underlying the increases are still debated [*Evans et al.*, 2005; *Jung and Weidler*, 2000]. The early view that the high-pressure injections serve to drive extensive mode I hydrofractures through the crystalline rock is not supported by the data. Rather, it appears that shearing of fractures and faults within the rock mass in response to

0148-0227/05/2004JB003168$09.00

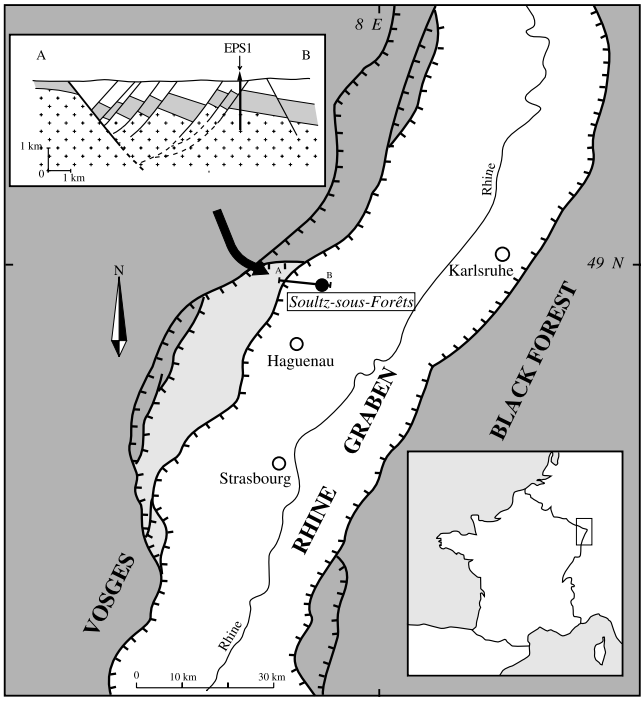

Figure 1. Location of the Soultz Hot Dry Rock test site near the center of the Upper Rhine Graben. The 3.6 km deep borehole GPK1 penetrates the basement at a depth of approximately 1400 m within a Horst structure. From *Dezayes et al.* [1995] (with permission from Springer).

the elevated pore pressure is the primary permeability creating mechanism [*Pine and Batchelor*, 1984; *Tezuka and Niitsuma*, 2000]. Laboratory experiments [*Esaki et al.*, 1992; *Gentier et al.*, 2000; *Yeo et al.*, 1998] and theoretical considerations [*Wang et al.*, 1988] provide a firm basis to expect that shearing of naturally rough fractures produces irreversible increases in fracture permeability. However, the essential details of the process as it occurs within reservoirs, such as the scale of coherent slip, and its relation to structure, are rarely directly constrained. Such information is crucial for predictive modeling of long-term reservoir performance, an important step in commercialization. That geologic structures exert a strong influence on the stimulation process is suggested by the pattern of microseismic events whose locations, after appropriate processing, commonly define discrete structures that are either planes or lines [*Niitsuma et al.*, 1999]. While there has been progress in using microseismic data to obtain quantitative insight into permeability creation and flow within the rock mass, it is only at the borehole that changes in fracture transmissivity and the flow field can be quantitatively determined with some certainty, and the relation to geological structures established. In this paper we analyze borehole logs run in a 3.6 km deep well in granite at the European Union's HDR test site at Soultz-sous-Forêt in France to determine the mechanical and hydraulic changes that took place within the rock mass about the hole as a consequence of massive fluid injections. The data are particularly suitable for study because the injections were made into previously undisturbed basement, and the data set is exceptionally complete. We show that permeability creation or enhancement is largely limited to weak natural fractures, which are elements of hydrothermally altered, cataclastic shear zones that intersect the borehole. These structures contain the natural conduits through which fluid moves through the rock mass under natural conditions. Almost all fractures that undergo permeability enhancement show evidence of dislocation, largely in shear. These changes are evaluated within the context of the stress prevailing at the site in the companion paper by *Evans* [2005] (hereinafter referred to as paper 2). The results also provide key background for the interpretation of microseismicity that accompanied the injections, although that aspect of the work is presented elsewhere [*Evans et al.*, 2005].

2. Background

[3] The European Union's HDR test site is located near Soultz-sous-Forêts in the Rhine Graben some 50 km north of Strasbourg, France (Figure 1). At the site, the block-faulted, Hercynian age, monzogranite graben basement lies at a depth of 1.4 km, below a cover of Permian and Mesozoic sediments. In 1992, an existing, 2000 m deep well, GPK1, was extended vertically to 3600 m and the casing shoe set at 2850 m, leaving 750 m of $6\frac{1}{4}$ inch of open hole [*Garnish et al.*, 1994]. The bottom hole temperature was 160°C. A suite of conventional wire line logs were run by Schlumberger together with the fracture imaging logs of Formation Micro-Imager (FMI), Azimuthal Resistivity Imager (ARI), and Ultrasonic Borehole Imager (UBI). Low-pressure hydraulic tests showed the permeability of the rock mass was low except for a fracture zone intersected at 3490 m. In 1993 the well was subjected to a stimulation program designed to enhance this permeability [*Jung et al.*, 1995]. Four high-pressure injections of fresh water were conducted on various open hole intervals (Table 1). The first test (designated 93AUG19) was a minor injection below the fault at 3490 m, whereas the third test (93OCT01) targeted the fault. Both tests used a mechanical packer for isolation and are of minor importance to this paper save to note that the packer failed on both occasions, although not before a twofold decrease in fault impedance had been accomplished in the 93OCT01 injection, as discussed later. The second test (93SEP01) was a massive injection of 25,000 m^3 of fresh water into the 550 m borehole section above 3400 m, the lower hole section, which included the fault, having been filled with sand. The records of this test are shown in Figure 2a. Injection rate was increased stepwise from 0.15 to 36 L s^{-1} over a period of 16 days, and the well then shut in for 1 day before being vented. Spinner and temperature logs were run daily, including during the shut-in and venting periods. The fourth test (93OCT11) was a large water injection (19,000 m^3) into the entire open hole section. The records of this test are shown in Figure 2b. Injection rate was maintained at 40 L s^{-1} for 5 days before being increased to 50 L s^{-1} for the final day. The injectivity of the well increased by a factor of 15 as a consequence of the injections. Some 19,000 microearthquakes were detected during the test series with an array of deep borehole accelerometers. The event locations largely fell within an ellipse, centered on the well, that was 1200 m high, 1000 m long in a NW-SE direction, and 400 m wide [*Jones et al.*, 1995]. Since the events are believed to be

Table 1. Key Parameters of the Four Stimulation Injections Conducted on Various Sections of the 750 m Open Hole Section of GPK1

Test	Interval, m	Flow Rate, L s^{-1}	Maximum Differential Pressure, MPa	Volume Injected, m^3	Reference
93AUG19	3560–3590	1.6/6	12.1/16.2	30	*Jung* [1993]
93SEP01	2850–3400	0.15–36	3.8–9.2	25,000	*Jung et al.* [1995]
93OCT01	3457–3507	3.3/5.3	>4.9/>5.9	176	*Jung* [1993]
93OCT11	2850–3590	41/53	8.4/8.9	19,000	*Jung et al.* [1995]

generated by the shear slippage of natural fractures whose strength has been reduced by the high pore pressure, they suggest that permeability enhancement of natural fractures extended some considerable distance from the well bore [*Audigane et al.*, 2002; *Fabriol et al.*, 1994]. In November 1993, a month after the last injection, a further Schlumberger UBI log was run. Comparison of this with the prestimulation UBI log run in April revealed changes in the state of natural fractures imaged in the well. This paper is largely concerned with relating these changes to the development or enhancement of fracture permeability, and identifying the processes responsible for the permeability enhancement or "stimulation."

[4] Since the majority of data are derived from logs of one sort or another, precise depth matching is crucial. The depth scales of all surveys and logs were adjusted to match a reference depth-along-hole scale, defined on the basis of a collection of spinner logs that had been run with a casing collar locator [*Evans*, 2001]. The reference scale is thus tied to "drillers depth" at the top of the open hole section, i.e., 2850 m. All depths in this paper are referred to this scale unless otherwise stated and are written as value in meters reference depth (XXX mRD). The error in matching depths to this reference is estimated as ±0.5 m for geophysical logs and ±2 m for tube wave surveys. *Henriksen* [2001] also produced a depth scale for GPK1 using the log from a Schlumberger GPIT (General Position and Inclination Tool) survey sonde, but assumed the casing shoe was at 2849 m. This scale is one meter shallower than the reference scale at the casing shoe, and 0.2 m deeper at hole bottom, with a linearly decreasing discrepancy in between (within ±0.2 m).

[5] The site has since been developed further. In 1995, a second borehole was drilled to 3.8 km and linked to GPK1 through stimulation injections to form a circulation loop at 3 km [*Baumgärtner et al.*, 1998, 1996]. More recently, the 3.8 km hole was extended to 5 km and two further holes drilled to 5 km to develop a deeper circulation system [*Hettkamp et al.*, 2004; *Weidler et al.*, 2002]. However, in this paper we will focus exclusively on the effect on the rock mass of the major injections conducted on GPK1 in 1993.

3. Characterization of the Natural State of the Granite Rock Mass

3.1. Natural Fracture Characteristics

[6] Some 500 natural fractures were identified on the prestimulation UBI images [*Evans*, 2000]. *Genter et al.* [1997] correlated fractures seen on a BHTV log from the neighboring hole EPS1 with those present in the core. They concluded that the BHTV log detected only the widest 25% of fractures, which had acoustic apertures greater than approximately 1–2 mm. However, these are likely to be the more hydraulically significant. The orientation distribution of the fractures is shown in Figure 3a. The vast majority are high-angle and strike within ±45° of N-S.

[7] Detailed information about the nature and history of the granite and its natural fractures was obtained from a nearby borehole EPS1, which was drilled and fully cored to 2227 m in 1991 [*Genter and Traineau*, 1992]. Petrological studies of the core suggest that the fractures can be grouped into two classes that have a different history and characteristics, and are distinguished by the presence or otherwise of

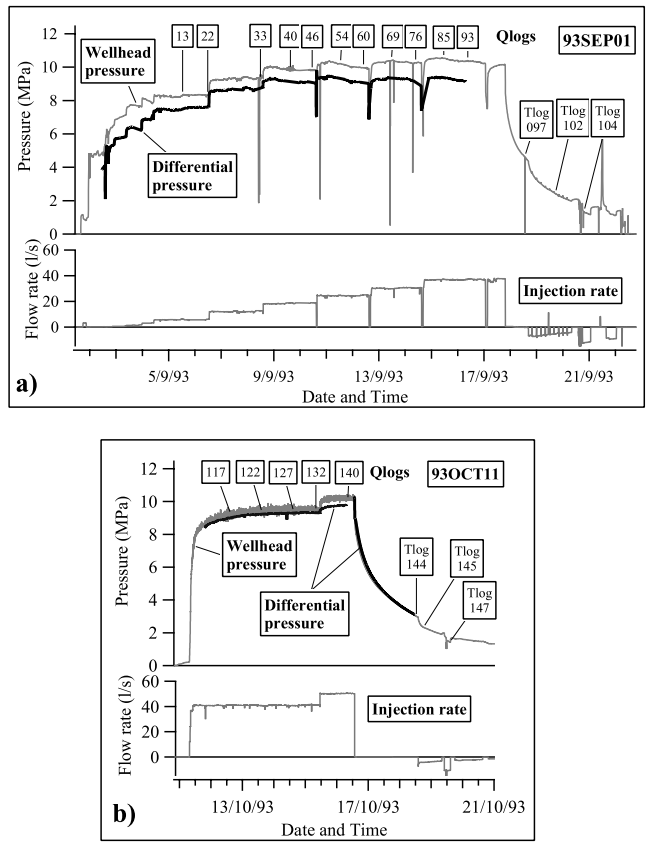

Figure 2. (a) Pressure and flow rate records for the first stimulation injection of the GPK1 open hole section 2850–3350 m. Differential pressure is the excess of downhole well bore pressure above the natural formation pressure and is largely uniform over the open hole sections during the injections. This is because the densities of the cold water in the well bore and the hot formation fluid are essentially the same and the pressure drop along the open hole section is negligible at even the highest flow rates [*Evans et al.*, 1996]. The times of spinner and shut-in/venting temperature logs are indicated. (b) Records for the 93OCT11 injection of the entire open hole section to 3590 m measured depth (MD).

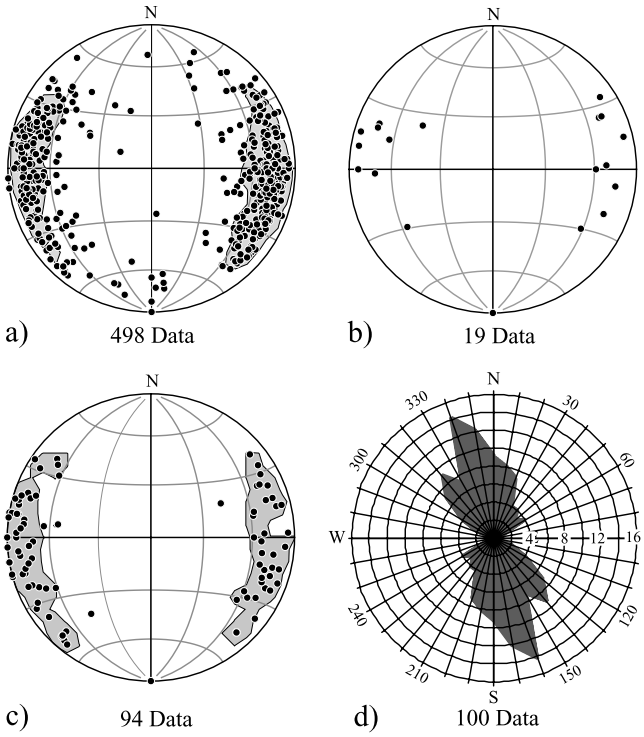

Figure 3. (a) Orientation distributions of poles to natural fractures identified on the UBI log run in the open hole section of GPK1 (lower hemisphere, equal-area projection); (b) poles to fractures recognized as permeable prior to stimulation; (c) poles to fractures recognized as permeable following the stimulation (high confidence); and (d) distribution of strikes of hydrothermally altered shear structures in the granite (see Figure 8a of *Genter et al.* [1998] for corresponding plot of poles).

hydrothermal alteration. Three alteration events are recognized as having affected the granite [*Genter and Traineau*, 1996]. The first is an early, pervasive alteration that slightly affected the entire granite and is possibly related to the cooling of the pluton. The event is associated with the development of mode I tension fractures that tend to be relatively narrow and filled with chlorite and calcite. The second is a later event that produced localized hydrothermal alteration of fractures. The nature and clustered organization of these altered fractures suggests they are the expression of fracturing within extensive shear structures through which much fluid flowed. Most large-scale structures within the basement rock mass probably belong to this type. Collectively they define an old structural trend that was reactivated during the Tertiary (Eocene compression, Oligocene extension) and in the present-day stress field [*Dezayes et al.*, 1995; *Genter et al.*, 1995; *Larroque and Laurent*, 1988]. The third alteration event involved haemetite deposition in fractures near the top of the granite and is unimportant to this paper [*Genter*, 1989; *Sausse*, 2000].

3.2. Natural Rock Mass Permeability Characteristics

[8] A series of low-pressure hydraulic tests was conducted on the entire open hole section to characterize the natural permeability of the granite. These indicated an open hole transmissivity for a 1 MPa perturbation of 0.6 L s^{-1} MPa^{-1}, implying an EPM (equivalent porous medium) permeability of the rock mass of 3×10^{-16} m^2. Spinner logs indicated that almost all flow in/out of the rock mass occurred at a prominent brittle shear zone (referred to sometimes as a fault) at 3490 m, which was the dominant permeable and geological structure in the open hole section (see Figure 13 of paper 2) [*Jung et al.*, 1995]. Much lower permeabilities are obtained if this fault is excluded from the test interval. For example, at the start of 93SEP01 injection, when the well was sanded back to 3400 m, the downhole pressure excess over the formation pressure, hereafter referred to as the differential pressure (see Figure 2 caption for details), rose to 3.9 MPa for an injection rate of 0.15 L s^{-1}. This implies an EPM permeability for the 550 m section of 1.5×10^{-17} m^2, which is within the range of values measured on intact core samples of 1×10^{-16} to 1×10^{-18} m^2 [*Rummel*, 1991]. Despite this low permeability, a further 17 permeable fractures, whose locations are indicated in Figure 4, were present in the well. These were identified from perturbations in a thermal log run after a low-pressure injection, and as the sources of tube waves in the following investigations: a VSP (vertical seismic profile) survey, a Schlumberger DSI (Dipole Source Imager) sonic log, and a CSMA (Camborne School of Mines) long-spaced sonic log that used a large sparker source (Figure 4). The analysis of these data is described elsewhere [*Evans*, 2001] so only key results will be presented here. In deciding which of the indicators was real, greater weight was given to the thermal log and least weight to the DSI log. The tube waves generated by the sparker source generally corroborated the permeable fracture locations identified from the thermal log. However, the Schlumberger DSI log was less successful and gave numerous spurious permeability indications below 3300 m due to tube wave generation at borehole irregularities, despite processing to remove this effect [*Tezuka et al.*, 1997]. The sparker source was not prone to this problem, probably because of its lower center frequency (400 Hz as opposed to 700 Hz for the DSI source). All 18 of the flow points identified coincided with prominent fractures on the UBI reflectivity log. The orientation distribution of these fractures is shown in Figure 3b, and is similar to that of the population as a whole (Figure 3a).

3.3. State of Stress

[9] The stress state at the site is described in paper 2 [*Evans*, 2005]. Here, it suffices to note that the stress regime is consistent with an active graben setting. The minimum principal stress is horizontal with orientation N80°E ± 15°, and has a magnitude that is approximately 50% of the vertical stress. The magnitude of the maximum horizontal principal stress, S_{Hmax}, is uncertain, although it cannot significantly exceed the vertical stress without requiring the rock mass to be unusually strong [*Evans*, 2005]. Since microseismic events with both strike-slip and normal faulting mechanisms are observed, S_{Hmax} magnitude is taken as approximately equal to the vertical stress. Pressure-limiting behavior was observed during the injections suggesting that jacking occurred, although this was probably limited to the uppermost 50–100 m of the open hole. Below this depth, the fluid pressure in the borehole during the major injections remained largely below the

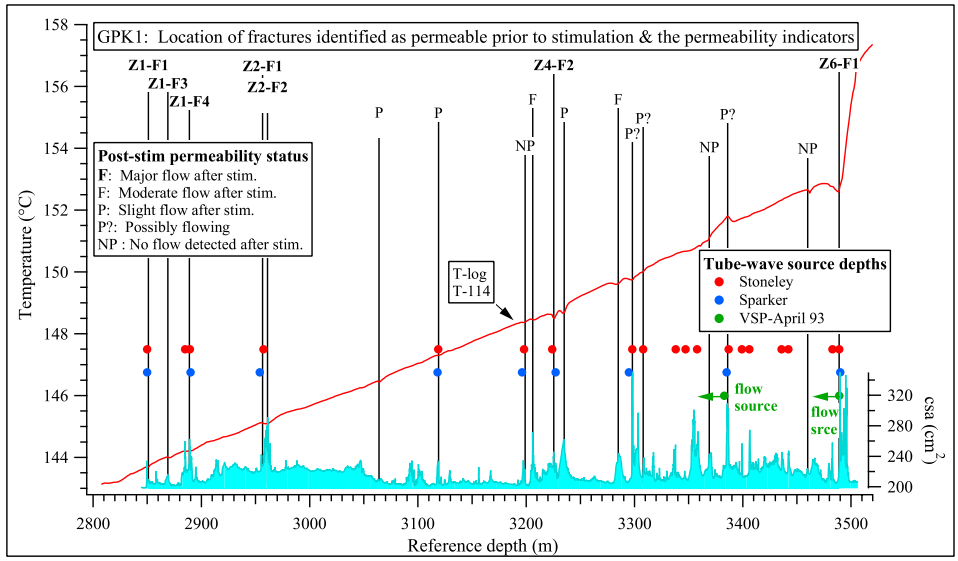

Figure 4. Locations of natural (i.e., prestimulation) permeable fractures identified largely on the basis of temperature log perturbations (considered the most reliable permeability indicator). The colored solid circles denote the locations of permeable fractures indicated by various tube/Stoneley wave methods. The arrows indicate the source and sinks of cross flow occurring in the well under ambient conditions, as inferred from the noise level of the VSP surveys. The labels at the top denote the eventual permeability rank of the fracture after the stimulation. NP denotes that the fracture was identified as permeable prior to stimulation but showed no evidence of supporting flow during or following stimulations. The positive temperature perturbation at 3386 m represents an outflow of relatively warm fluid that travels up the hole.

level of the minimum horizontal principal stress and thus shearing rather than jacking is the favored damage mechanism.

4. Stimulation Injection Tests

[10] The 1993 injections have been described extensively elsewhere [e.g., *Jung et al.*, 1995], so only the key points relevant to stimulation will be mentioned. The first major injection, 93SEP01, was conducted with the borehole below 3400 m filled with sand, leaving 550 m of open hole. The evolution of transmissivity during the injection is best seen in the cross plots of wellhead flow versus differential pressure (i.e., a Q-P plot) shown in Figures 5a and 5b. Rock mass permeability was initially very low (i.e., 1.5×10^{-17} m^2 for the 0.15 L s^{-1} stage) but rapidly increased with injection, notably after differential pressure rose above 5 MPa and the first microseismic events were observed [*Evans et al.*, 2005]. By the end of the 6 L s^{-1} stage, the differential pressure had risen to a stable 7.6 MPa, implying a twentyfold increase in EPM permeability. Subsequent step increases in flow rate of 6 L s^{-1} produced pressure responses that were progressively smaller, converging on a pressure limit at about 9.0 MPa above ambient (Figure 5a). In later stages, small pressure increases accompanied the flow rate steps, but these were transient, the pressure gradually declining back to the 9.0 MPa differential pressure level. This pressure-limiting behavior most likely

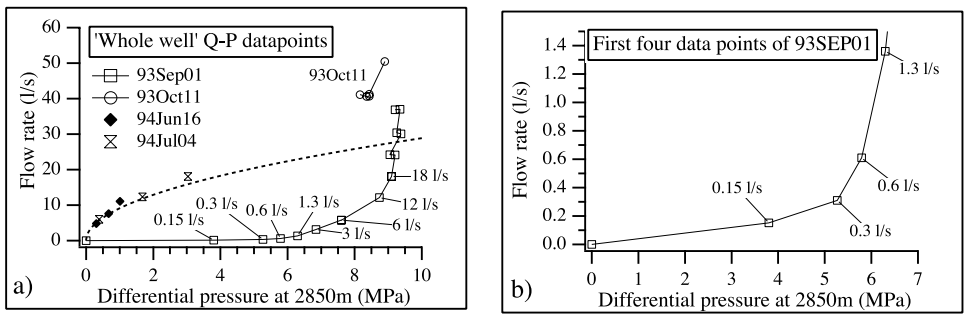

Figure 5. (a) Cross plot of wellhead flow versus differential pressure prevailing at the end of each of the stages of the two major stimulation injections of 1993 and also two relatively low-pressure production (94JUN16) and injection (94JUL04) tests conducted in 1994. The pressure-limiting behavior at 9.0 MPa is evident. The 1994 test data points define a parabola, indicating that the impedance governing flow is turbulent-like [*Evans et al.*, 1996; *Kohl et al.*, 1997]. (b) Expanded view of the first stages of 93SEP01 showing that major transmissivity increases accelerate when differential pressure exceeds 5 MPa.

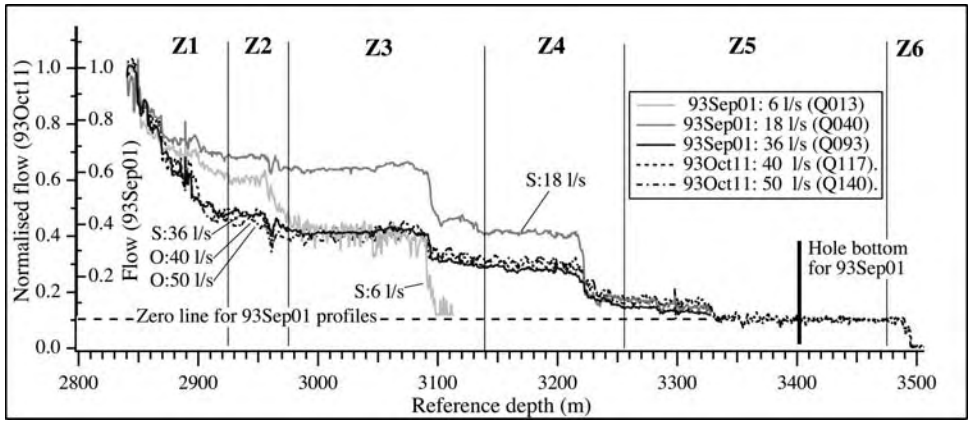

Figure 6. Selection of flow profiles from spinner logs run during the 93SEP01 and 93OCT11 injections. Steps indicate points where significant flow enters the rock mass. The scale of the 93SEP01 profiles has been chosen so that the zero flow at 3350 m (hole bottom of most logs) matches the flow fraction that prevailed at that depth in the 93OCT11 tests (10%). This shows that the flow distribution along the common depth section is the same during 93OCT11 as at the end of 93SEP01. However, significant changes in the profile occurred during 93SEP01, the fraction of flow entering below 3050 m increasing up to the 18 L s^{-1} stage and decreasing thereafter. The boundaries of the six zones used in the flow zone impedance analysis (Figure 7) are indicated. Each of the zones contains a single, highly localized flow point near its center, with the exception of zone 1 which contains five flow points.

reflects jacking limited to near the casing shoe [*Cornet and Jones*, 1994; *Evans*, 2005].

[11] A selection of flow profiles (Q logs) derived from spinner logs run during both injections at the times indicated in Figures 2a and 2b is shown in Figure 6. Steps in the profile indicate points where significant flow enters the rock mass. The uppermost 50 m of the open hole section includes five discrete flow points, all of which can be associated with distinct fractures. However, the underlying 700 m contains only a further five clear steps, which are localized and isolated at 100–150 m intervals. On the basis of this distribution, the hole was divided into six sections, denoted zones 1–6, whose boundaries are indicated in Figure 6. Each zone except zone 1 contains an isolated flow point near its center, usually composed of one or two neighboring, occasionally complex fractures [*Evans*, 2000]. The flow profile changed significantly during the 93SEP01 injection. During the first half of the injection, transmissivity increased most rapidly in the lower part of the open hole so that during the 18 L s^{-1} stage, the majority of the injected water entered the rock mass below 3050 m (Figure 6). Thereafter, the trend reversed so that by the end of the injection, some 60% of the injected fluid entered the rock mass at zone 1 [*Jones et al.*, 1995]. This change in stimulation trend at 18 L s^{-1} coincided with accelerated upward growth of microseismic activity [*Jones et al.*, 1995], and is seen most clearly in the Q-P plots of the zonal flow contributions presented in Figure 7. These show that once the limiting differential pressure of 9.0 MPa was reached at 18 L s^{-1}, subsequent increases in flow rate were taken almost entirely by zone 1; that is, the transmissivity of the lower hole section largely ceased to increase. The differential pressures for jacking at the center of each zone as predicted from the standard stress state described by *Evans* [2005] are also shown in Figure 7. These indicate that jacking could, in principle, occur down to 3150 m. However, for the reasons discussed by *Evans* [2005], jacking was most likely limited to the zone 1 and possibly zone 2. It should be noted that localized jacking at zone 1 would serve to limit pressure in the entire open hole interval. Thus the apparent pressure-limiting behavior seen in the Q-P plots of the deeper zones in Figure 7 should not be taken to indicate that jacking occurred at those depths. At the end of the test, the well was shut in for 12 hours before being vented.

[12] After the sand was cleaned out, and an injection performed on the fault at 3490 m (93OCT01), the second major injection was conducted (93OCT11), this time on the entire hole. Flow rate was kept constant at 40 L s^{-1} for 4 days before being increased to 50 L s^{-1} for the final day (Figure 2b). At the end of the 40 and 50 L s^{-1} stages the downhole pressures exceeded ambient by 8.4 and 8.9 MPa, respectively, somewhat less that the 9.1 MPa prevailing at the end of the 36 L s^{-1} stage of 93SEP01 (Figure 5). Thus some changes had taken place within the rock mass during the shut-in period that served to increase transmissivity. Since microseismic activity was low during this period, the underlying processes were aseismic [*Evans*, 1998]. Importantly, the flow profile throughout the injection was largely the same as prevailed at the end of the 93SEP01 injection, except for the addition of a further outlet at the fault at 3490 m (Figure 6). Furthermore, a similar flow profile was also seen in later low-pressure tests conducted on the entire hole in 1994. Thus the fracture aperture changes underlying the transmissivity increases were permanent, and not significantly pressure-dependent, implying that the fractures were propped open [*Jung et al.*, 1995]. The 1994 low-pressure tests also showed that the impedance governing flow along the flow paths that connected the borehole to the far field was turbulent-like, resulting in the parabolic whole

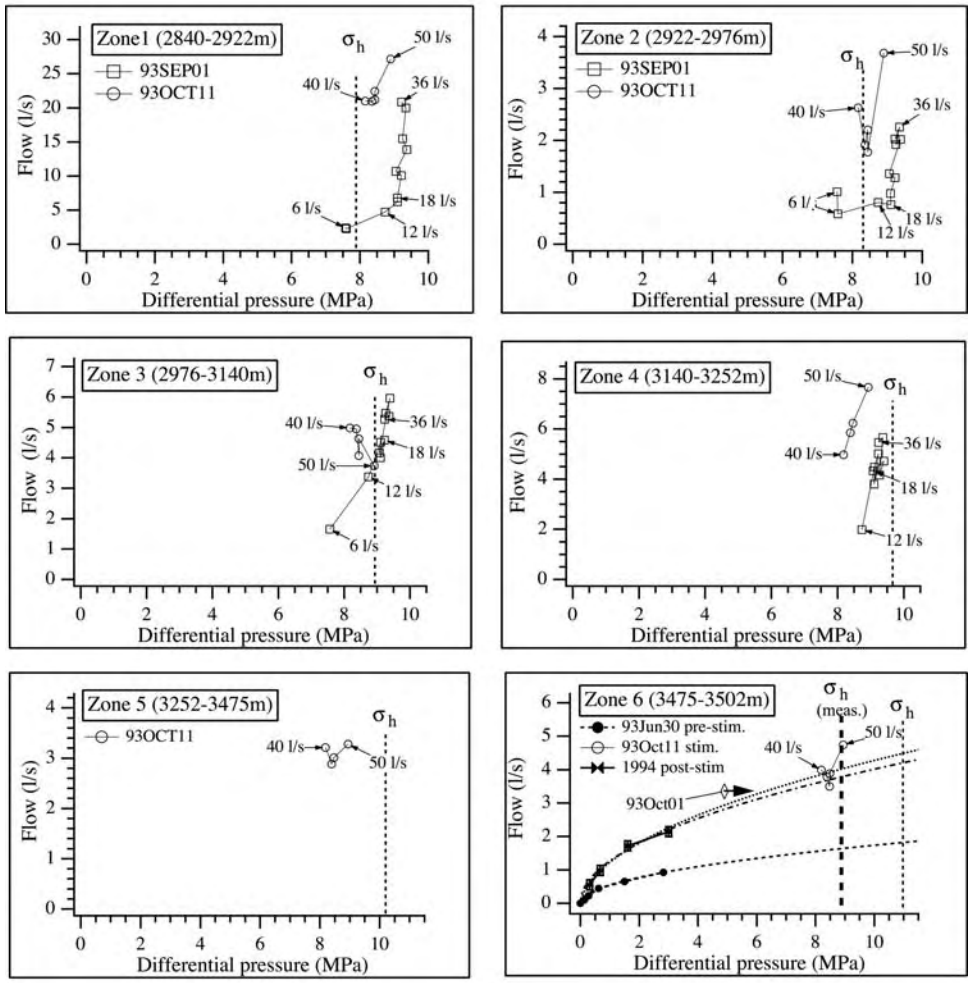

Figure 7. Q-P plots of the flow entering the rock mass over each of the six zones (Figure 6) at the time of the spinner logs during the 93SEP01 and 93OCT11 injections. Note that zones 5 and 6 were sanded off during the former. The vertical dotted lines indicate the jacking pressure at the center of each zone predicted from the stress characterization and are 1-2 MPa lower than predicted from the preferred characterization (paper 2). These suggest jacking is most likely at zone 1. It should be noted that jacking at one zone will serve to limit pressure at all zones. Under pressure-limiting conditions, transmissivity changes show as flow rate changes. Thus the transmissivity of zones 3 and 4 increases up to the 18 L s^{-1} stage but only slightly thereafter. The plot for zone 6 includes data from a low-pressure, prestimulation test (93JUN30), a single data point from the attempt to stimulate the fault with a packer (93OCT01), and the low-pressure production and injection tests conducted in 1994. The low-pressure prestimulation and poststimulation data both define parabolas, indicating that the impedance to flow is governed by turbulent-like losses. It is also noteworthy that the single data point from 93OCT01 lies on the poststimulation parabola. This suggest the twofold reduction in impedance was accomplished during this test rather than the later 93OCT11 (see *Evans et al.* [1996] for details).

well impedance curve shown in Figure 5 [*Kohl et al.*, 1997]. Parabolic impedance curves were also obtained for the fault in zone 6, both before and after the stimulation injections, the impedance of the former being twice the latter (Figure 7). This impedance reduction appears to have occurred during the 93OCT01 packer injection rather than the 93OCT11 stimulation injection, as discussed later.

[13] Low-pressure injection and production tests conducted in 1994 indicated the injectivity of the entire well for a 1 MPa differential pressure was 9.0 L s^{-1} MPa^{-1}, compared with 0.6 L s^{-1} MPa^{-1} before the injections. Thus the stimulations produced a fifteenfold increase in transmissivity of the whole well. For the 550 m section of hole that was open during the 93SEP01 injection, the increased was approximately 200-fold.

5. Identification of Poststimulation Permeable Fractures From Spinner and Temperature Logs

[14] Spinner logs are adequate for quantifying flow at the major flow points but are unable to detect small inflows or outflows owing to bearing friction and noise arising from a

variety of sources including variations in cross-sectional area (CSA). While the effect of CSA-variations can be corrected for in principle, in practice, significant CSA-correlated energy is usually present in the residual profile. The problem is often particularly severe near zones of inflow/outflow because it is here that spalling tends to occur and turbulence is greatest. The effect is to smooth the profile in the vicinity of major inflow or outflow, resulting in ambiguity in identifying the fractures responsible for the flow. Temperature logs (T logs) run under appropriate conditions can overcome these problems and precisely identify the flow point [*Drury and Jessop*, 1982; *Keys*, 1990]. For the situation in question, temperature logs run during production and especially venting following the injections proved most useful. This is because the up-moving borehole fluid at a given depth tends to be hotter than the rock, since it is sourced from greater depth: Hence fluid flowing out of the cooler rock produces a step in the temperature profile. Cooling of the rock prior to production through injection of cold fluid, such as during the stimulation injections, serves to enhance the temperature contrast.

[15] An example of permeable fracture identification for a 35 m section of hole that included the flowing fractures in zone 4 is shown in Figure 8. The section contains two fractures that were identified as naturally permeable prior to stimulation (marked ''Orig Perm''). These are the most prominent features in the prestimulation UBI reflectivity log of the section. Spinner logs indicated that neither supported major flow during the two stimulation injections, the active fracture lying several meters higher (Z4-F1). However, in all subsequent tests, the major flow occurred at the uppermost of the naturally permeable fractures. This behavior of flow activity switching between neighboring fractures within a flow zone is seen elsewhere in the well, and suggests they are both outlets of the same penetrative flow channel. No other distinct flowing fractures in this section can be identified from the flow logs. An inflow is suggested somewhere between 3230 and 3235 mRD, but the precise flow point is obscured by the remnant CSA-correlated noise. The situation is clarified by the temperature logs; most show two steps that are consistent with the flow of relatively cool fluid into the well bore near two fractures, one of which is naturally permeable. These identifications are particularly clear because the signals are large. However, the temperature signatures of in-flowing fluid were usually smaller and varied in magnitude from log to log, as is evident from the perturbations near the fracture at 3235 mRD. Thus a flow recognition criterion was established to help discriminate between temperature perturbations and noise for small signals. Specifically, a fracture was recognized as flowing if two T logs showed an offset of at least 0.08°C within ±1 m of the location of the fracture. Using this criterion, the following semiquantitative ranking of flow was defined:

[16] F is major flow (>5% of net well flow) detected by spinner log. The fractures transmitting the flow were assigned a unique identification number of the form Zn-Fm, where ''n'' is the zone number and ''m'' is the fracture number in the zone.

[17] F is minor flow that able was detect on spinner logs.

[18] P indicates that no clear signal was resolved on the spinner logs but the criterion for flow recognition from the T logs was met.

[19] P? indicates that a clear signal was evident on one T log and an inconclusive signal on another (such as one significant bit in the correct sense), both signals occurring within ±1 m of a fracture trace on the UBI log. In this case the fracture was judged to be possibly permeable.

[20] It is important to note that fractures identified as permeable through the T logs were actually flowing at the time of the logs, and that these were all run more than a day after venting or production commenced. Thus such fractures are not merely permeable, but must also be connected to a permeable network of substantial capacity. Fractures recognized as permeable in the zone 4 section of Figure 8 are indicated by the arrows to the right of the T logs. The rank of the flow is denoted by a letter to the right of the poststimulation UBI log. The P that appears to the left of this log indicates that the adjacent fracture is a candidate flowing fracture, and the P to the right indicates ''high-confidence'' recognition. Some validation of the flow recognition criterion is provided by the observation that candidate inflow points almost always coincided with the location of a natural fracture whose sonic reflectivity image was enhanced in the poststimulation UBI log, as described shortly.

[21] Some limitations of the procedure used to identify permeable fractures should be mentioned. One common problem arose when a flow point identified from the T logs coincided with two or more distinct fractures; that is, two or more fractures lay within ±1 m of the point. In such cases, the fracture whose trace showed the greatest enhancement on the poststimulation UBI reflectivity log was selected as the more probable source of flow (the estimation of trace enhancement will be described shortly). Both fractures were selected as permeable if their traces were equally enhanced. Flow points with ranking ''P?'' were excluded. We shall refer to the data set thus formed as the ''high-confidence'' data set. To assess the impact of the selection procedure on the results, a ''lower-confidence'' data set was formed that included all fractures which lay within ±1 m of the flow points. This data set also included fractures with ranking P?. The high-confidence and lower-confidence data sets had 93 and 115 entries, respectively. These values are not greatly different given that 520 fractures were identified in the poststimulation UBI log. However, both data sets might be incomplete inasmuch as there may be flowing fractures that do not produce a significant perturbation on the temperature logs, either because the flow is too small or because the temperature of the out-flowing fracture fluid does not differ significantly from that of the local borehole fluid. Thus the 93 members of the high-confidence, flowing fracture data set should be considered a lower bound to the true number of flowing fractures. A listing of the fracture data sets is given in Appendix 1 of *Evans* [2001].

[22] The location and flow rank of fractures identified as flowing following the stimulations are shown in Figure 9. The inclusion of temperature logs in the analysis greatly increased the number of fractures recognized as permeable to at least 93. Thus, out of the ~500 fractures identified from the UBI images in the open hole section, at least 20% supported flow to some degree. For the section stimulated in

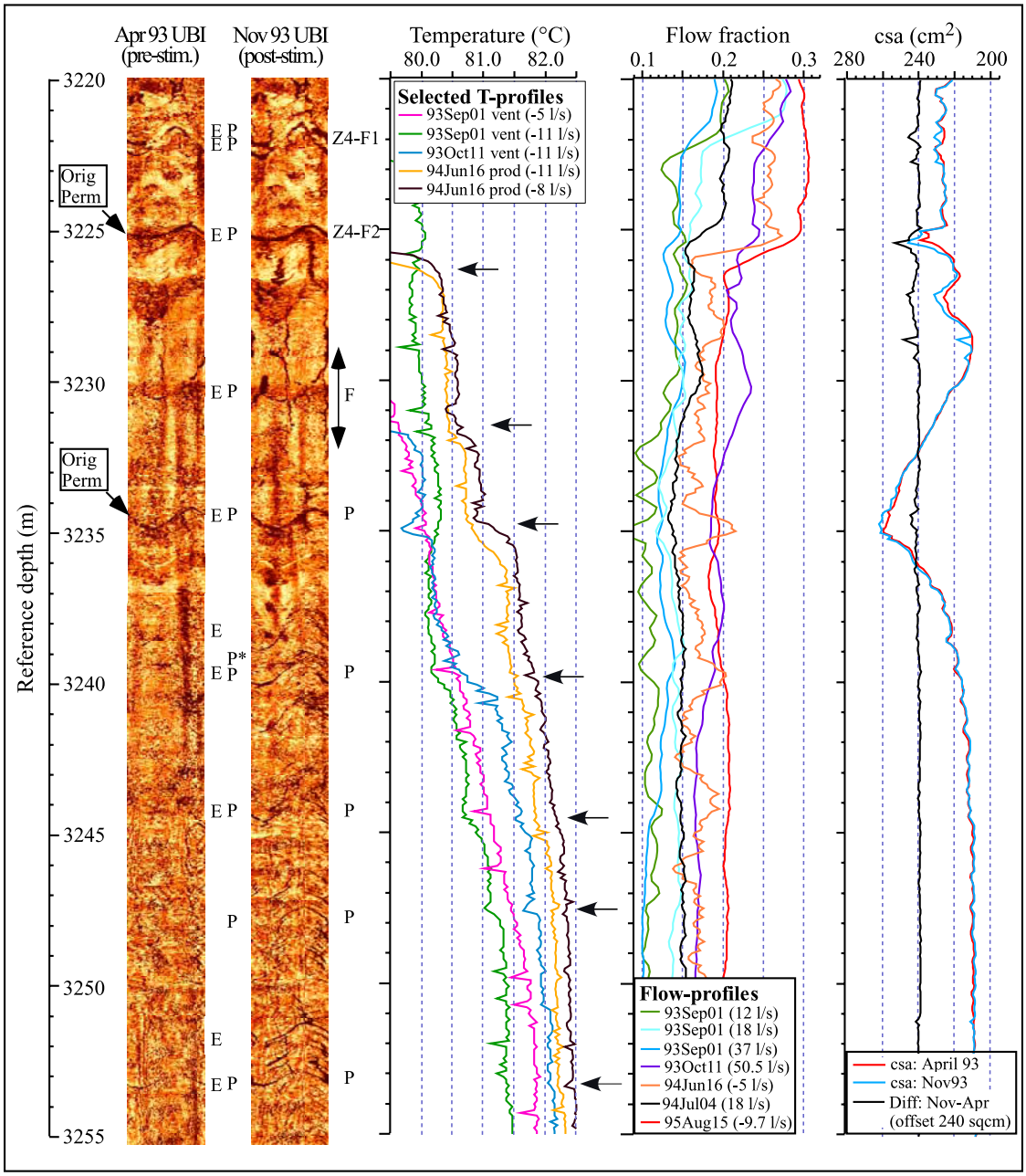

Figure 8. Collection of depth-adjusted logs for a 35 m section of GPK1 that includes the active flow points of zone 4. The logs from left to right are the prestimulation and poststimulation sonic reflectivity (UBI) logs, a collection of temperature logs run during venting and production tests, a collection of flow logs that show the evolution of flow during and following stimulation, and the prestimulation and poststimulation CSA profiles. The arrows denote features in the temperature log that indicate a flow of cooler fluid into the well bore. These points correlate with the location of fractures. Moreover, the trace of these fractures is seen to be more enhanced following the stimulation, suggesting that they have suffered damage.

93SEP01, which contains ~400 fractures, the flowing fraction is 25%. The vast majority of these have ranking P, and most are newly permeable. Hence they indicate where the rock mass has been effectively stimulated in the vicinity of the borehole wall. No newly permeable fractures are present in the section below 3400 m, which was pressurized only during the 93OCT11 injection. Above this, the distribution of permeable fractures is strongly organized with swarms of newly permeable, minor flowing fractures clustered about the major flowing fractures. These observations are discussed more fully later. Figure 9 also shows the distribution of drilling-induced tension fractures (including en echelon type) along the well. Most were evident in the prestimulation FMI log, the stimulation merely serving to enhance their definition on the UBI reflectivity log [*Bérard and Cornet*, 2003]. Importantly, they show no evidence of supporting flow. The few exceptions to this (e.g., 3328 mRD) invariably involve the intersection of the

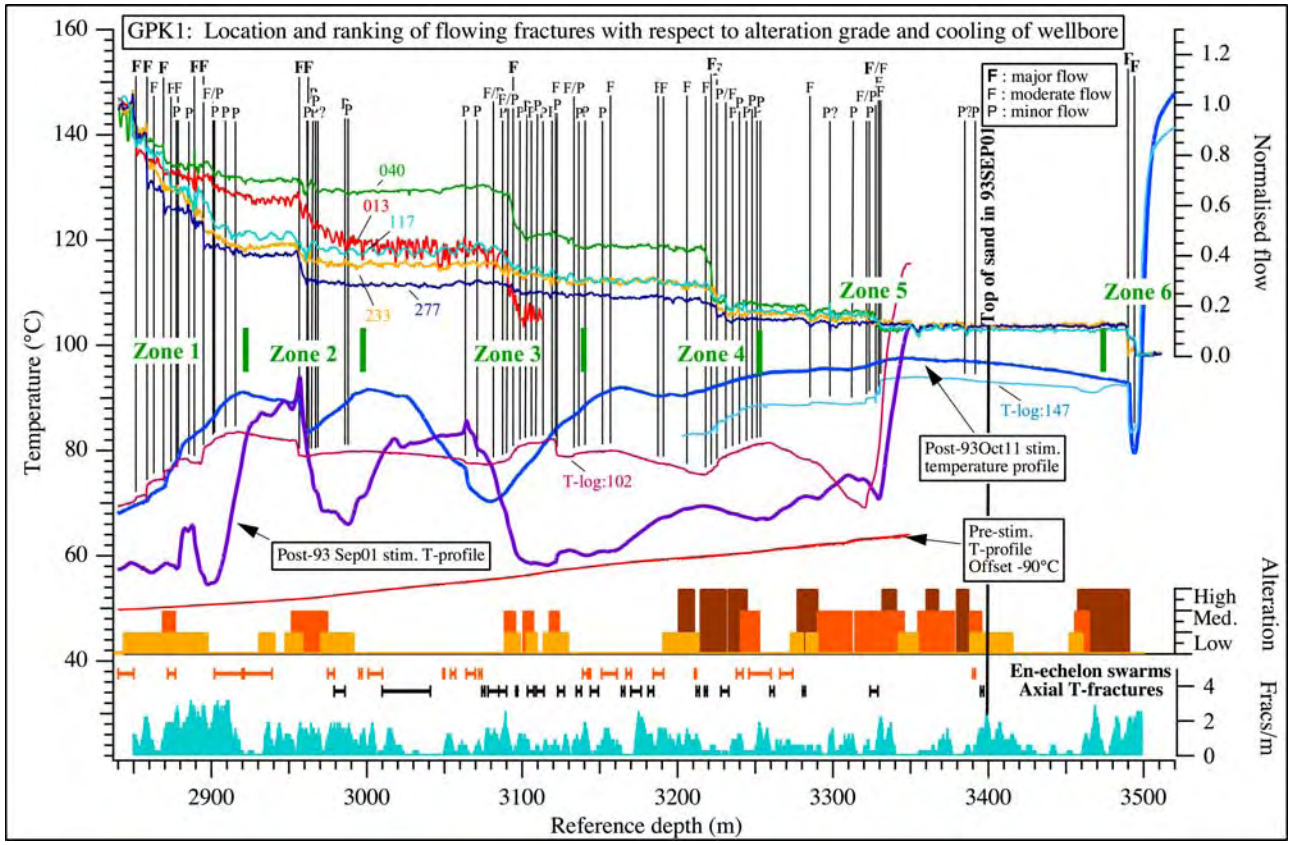

Figure 9. Location of fractures identified as permeable following the stimulations. The labels above the vertical lines denote the degree of flow they support. The label lines are hung from temperature logs run during the vent periods that followed shut-in after the two injections. T logs run prior to stimulation and during the two shut-in periods following the injections are also shown. No newly permeable fractures are present below 3350 m, indicating that the 93OCT11 stimulation was not effective. Above this, the distribution of permeable fractures is strongly organized with clusters of minor flowing fractures, most of which are newly permeable, clustered about the major flowing fractures. The two zones that suffered less cooling centered at 2940 and 3040 m correlate with sections with no permeable fractures. Profiles of fracture density and alteration are shown at the bottom. The flowing fractures tend to occur in zones of altered rock rather than zones of high fracture density. The location and extent of axial and en echelon tension fractures are indicated below the alteration index.

tension fracture with a natural fracture whose image on the poststimulation UBI reflectivity log is markedly enhanced. In such cases, it is possible that the penetrative flow occurs through the natural fractures, and that the tension fracture is a shallow feature that merely spreads the flow emergent at the borehole, similar to the situation described by *Jung* [1991] for a fracture at 1812 m. The absence of flow at the tension fractures indicates shallow penetration, which is consistent with a thermal origin, as proposed by *Brudy and Zoback* [1999] and *Bérard and Cornet* [2003]. An important corollary is that the well bore pressure in sections with nonpermeable axial tension fractures must have remained less than the minimum principal stress during stimulation; otherwise, the fractures would have extended.

6. Correlation of Newly Permeable Fractures With Indications of Damage or Shearing

[23] A close correspondence was found between the development of permeability of a fracture during stimulation and the enhancement of its trace in the poststimulation UBI reflectivity log. This can be seen in Figure 8 where fractures recognized as enhanced are marked with an E. Almost all newly permeable fractures are enhanced, a result that holds for the complete data set. To promote consistency in recognizing a fracture trace as enhanced, the following rules were adopted: (1) Enhancement must be fairly obvious. (2) Almost all of the trace must be visible on the poststimulation log (this excluded many stacks of en echelon fractures that probably represent tension fractures formed where the borehole axis is not aligned with a principal stress [*Brudy and Zoback*, 1999]). (3) It was not necessary for the entire trace to be enhanced, but the greater part.

[24] The trace enhancement study was conducted twice using different versions of the prestimulation and poststimulation UBI sonic reflectivity images that were available. Image comparison was only possible to 3451 mRD, the limit of the April 93 UBI log. However, no newly permeable fractures lay below this depth. The first study, reported by *Evans* [2001], used images prepared by Karlsruhe

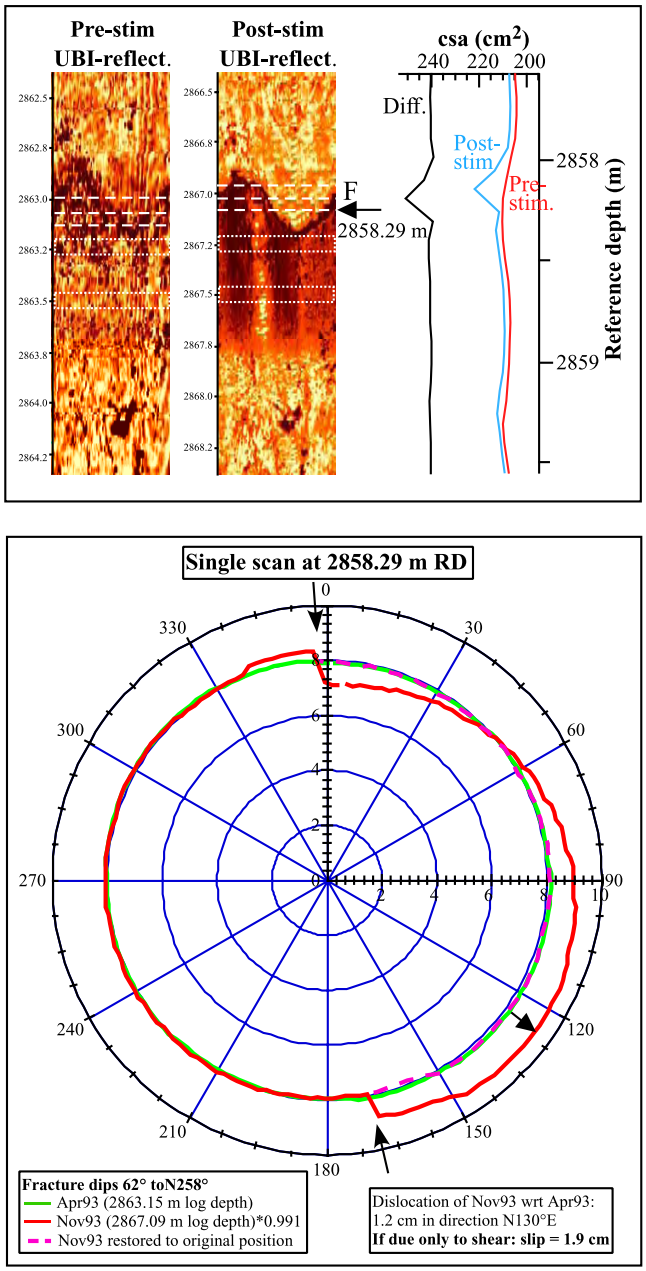

Figure 10. Example of the estimation of fracture dislocation at fracture Z1-F2 (2858.20 mRD). (top) UBI reflectivity images and derived cross-sectional area of the fracture before and after the 1993 injections. (bottom) Prestimulation (green) and poststimulation (red) plots of the borehole derived from scan lines taken at the midpoint of the fracture marked by the arrow in Figure 10 (top). The paired arrows at 12 o' clock and 5 o' clock indicate the locations where the scan lines cross the fracture. A large dislocation is evident. The horizontal component of its Burgers vector is 1.2 cm toward N130°E (indicated by the arrow). The dotted line is the poststimulation figure after removal of the dislocation. The fracture was initially impermeable but accepted progressively more flow during the injections.

University that had not been processed with the same equalization color scale. Axial tension fractures were excluded from the analysis. Of 102 fractures above 3451 mRD identified as permeable after the stimulation, 89 (or 87%) were found to have enhanced UBI reflectivity traces. This compared with 38 (or 11%) enhanced traces of the 350 fractures in the complementary nonpermeable data set (listed in Appendix 1 of *Evans* [2001]). The study was repeated using dynamically equalized images supplied by the BRGM, in which the color equalization had been optimized over a 2 m moving window to enhance detail [*Henriksen*, 2001] (see Figure 8 for an example). The superior resolution of these images justified a different approach. Specifically, of 45 new flow points that were recognized following the stimulation, in 43 cases at least one enhanced natural fracture trace was found to lie within ±1 m of the flow point depth. Conversely, a total of 33 enhanced traces were identified that did not correspond to any recognized flow point. Thus, despite the elements of subjectivity in the recognition of enhanced traces, there is little doubt that fractures which became permeable during the stimulation injections also tended to have enhanced traces on the UBI reflectivity log.

[25] Enhancement is taken to indicate an increase in the intrinsic ultrasonic reflectivity of the fracture expression at the borehole wall. The influence of such factors as sonde parameters, centralization, and log processing is considered to be minor since the same sonde operating at the same frequency was used in both surveys and both logs were processed in the same way, at least for the BRGM images. Moreover, most traces that showed enhancement in reflectivity also had a discernable signature on the poststimulation travel time log. These observations might be explained by either washing out of fracture filling or the effects of damage due to dislocation. Later it will be shown that permeable fractures tend to be hydrothermally altered, and often contain illite, a mineral that is friable and relatively easily mobilized. However, if washing out consistently occurred, it might also be expected to occur during drilling, and thus leave a signature on the prestimulation travel time log, contrary to observation for most fractures. A more consistent explanation is that the enhancement reflects damage through dislocation. Given the stress conditions prevailing during injection (i.e., pressure less than the minimum principal stress at least where nonpermeable tension fractures are observed) and the range of orientations of the fractures involved, dislocation in shear is strongly favored (paper 2). Shearing would tend to damage the fracture filling as well as the fracture walls, rendering it more prone to washing out. Thus these data imply a link between shearing and permeability creation.

[26] Direct measurements of changes in the geometry of the borehole wall at the major flowing fractures revealed that all but two had suffered dislocations of millimeters to centimeters, mostly in shear. The changes were resolved by comparing scans of the prestimulation and poststimulation UBI travel time logs taken at the same depth across the fracture. An example is shown in Figure 10. Millimeter resolution of the horizontal component of the dislocation vector was obtained by adjusting the radial distance scales of the scans so that the borehole curvatures matched [*Evans*, 2001]. The scans were then superposed to resolve

Table 2. Horizontal Component of Dislocations Measured at All Major Flowing and Four Lesser Flowing Fractures and Their Interpretation[a]

Reference Depth, m	Flow Ranking	Horizontal Distance		Inferred Slip, mm	Comments
		Magnitude, mm	Orientation, °E of North		
2858.1	Z1-F2	12	130	19	single fracture dipping 62° to N258°E (Figure 10)
2888.0	Z1-F4	4	90		3.5 m axial fracture pair with 3 mm opening mode and 6 mm dip-slip dislocation
2894.9	Z1-F5	3	49		single fracture dipping 76° to N317°E
2916.0	P	2.5	71	14	single fracture dipping 83° to N42°E
2956.8	Z2-F1/F2	6	72		9 m complex vertical fracture with predominant opening mode dislocation (Figure 11)
2963.8	P	3.5	35	6.5	top member of double fracture (dip 74° to N278°E) at base of axial fracture (Figure 11)
2964.27	P	2	35 ± 20	7	bottom member of double fracture at base of axial fracture (Figure 11)
2966.8	P	3.5	40	5.5	single fracture dipping 60° to N270°E (Figure 11)
3093.2	Z3	2.5 ± 1	35 ± 25	2	single vertical natural fracture dipping 88° to N150°E (Figure 11)
3221.8	Z4-F1	2.5	63	13	double fracture dipping 80° to N40°E
3225.3	Z4-F2	5	80 ± 15		single fracture dipping 68° to N93°E intersected by vertical fracture
3386.65	P?	2.5 ± 10	140 ± 20	5.0 ± 2.0	double fracture dipping 68° to N269°E (Figure 15)

[a]Inferred slip refers to the slip magnitude obtained for simple planar fractures by assuming the measured dislocation reflects dilation-free shear displacement. The estimates are from *Evans* [2001] and K. F. Evans (Quantitative assessment of slip occurring on fractures during the 1993 stimulation of GPK1 at Soultz-sous-Forêts, France from BHTV travel time data, unpublished final report to New Energy Development Organisation (NEDO), Japan for the Project Universal Understanding and Design of Engineered Geothermal Systems, 2001). The error in estimating the horizontal dislocation is typically ±1 mm unless otherwise stated.

changes in Figure 10 of the borehole wall around the scan line. The method provides a direct measure of the magnitude and direction of the horizontal component of the dislocation (Burgers) vector, but not the true vector itself. The latter can be derived by making an assumption about the nature of the dislocation; for example, that it reflects shear displacement on the fracture without dilation. The analysis is reported by *Evans* [2001, also K. F. Evans, Quantitative assessment of slip occurring on fractures during the 1993 stimulation of GPK1 at Soultz-sous-Forêts, France from BHTV travel time data, unpublished final report to New Energy Development Organisation (NEDO), Japan for the Project Universal Understanding and Design of Engineered Geothermal Systems, 2001], and the results are summarized in Table 2. The estimates of the horizontal dislocation in most cases agree with those obtained in an earlier, more limited study of the same data by *Poitrenaud* [1994] whose results are reported by *Cornet et al.* [1997]. However, total dislocation magnitudes differ significantly in some cases due largely to differing interpretations: *Poitrenaud* [1994] assumed all horizontal dislocation vectors reflected shearing without dilation, whereas *Evans* [2001] found evidence of a significant opening mode component at some fractures. An example is shown in Figure 11 for the flowing fractures at zone 2. The complex fracture zone extends over some 10 m and is accompanied by spalling, reflecting the presence of alteration. *Poitrenaud* [1994] examined a scan line at 2956.8 m RD (2966 m in his depth scale) and found 0.5 cm of horizontal dislocation. He ascribed this to shear slip without dilation on the high-angle fracture and obtained a slip estimate of 4.7 cm. However, analysis of many scan lines taken across the fracture zone suggests that the horizontal deformation reflects predominantly mode I dislocation of an axial fracture pair that step irregularly between natural fractures, essentially splitting the borehole along a 9 m section. The sense of the dislocation is such that the east wall moves coherently toward the northeast with respect to the west wall by 0.5 mm. It is possible that a component of vertical dislocation is also present, since the data do not allow dip-slip movement on vertical fractures to be resolved. The nature of this dislocation will be discussed later. The largest dislocation magnitude found by Evans was 19 mm shear for Z1-F2 (Figure 10), in accord with the value found by Poitrenaud for that fracture. All but two of the major flowing fractures and four minor flowing fractures in the section stimulated during the 93SEP01 injection suffered measurable dislocations (Table 2). The study only included fractures that displayed a strong signature in the poststimulation UBI sonic reflectivity log. Hence it is possible that other fractures also suffered millimeter-size dislocations.

7. Discussion

[27] The analysis indicates that almost all fractures that were stimulated (i.e., were either newly permeable, or had their permeability enhanced) showed evidence of damage or dislocation. It is shown in paper 2 that these fractures, indeed, most natural fractures in the reservoir, are ''critically stressed'' inasmuch as they support shear stress levels that would be verging on failure if their strength were governed by a friction criterion. It is also shown that conditions for jacking were probably met only at depths above 2950 m. Thus the observations below 2950 m represent a relatively clear example of shear-induced permeability creation/enhancement.

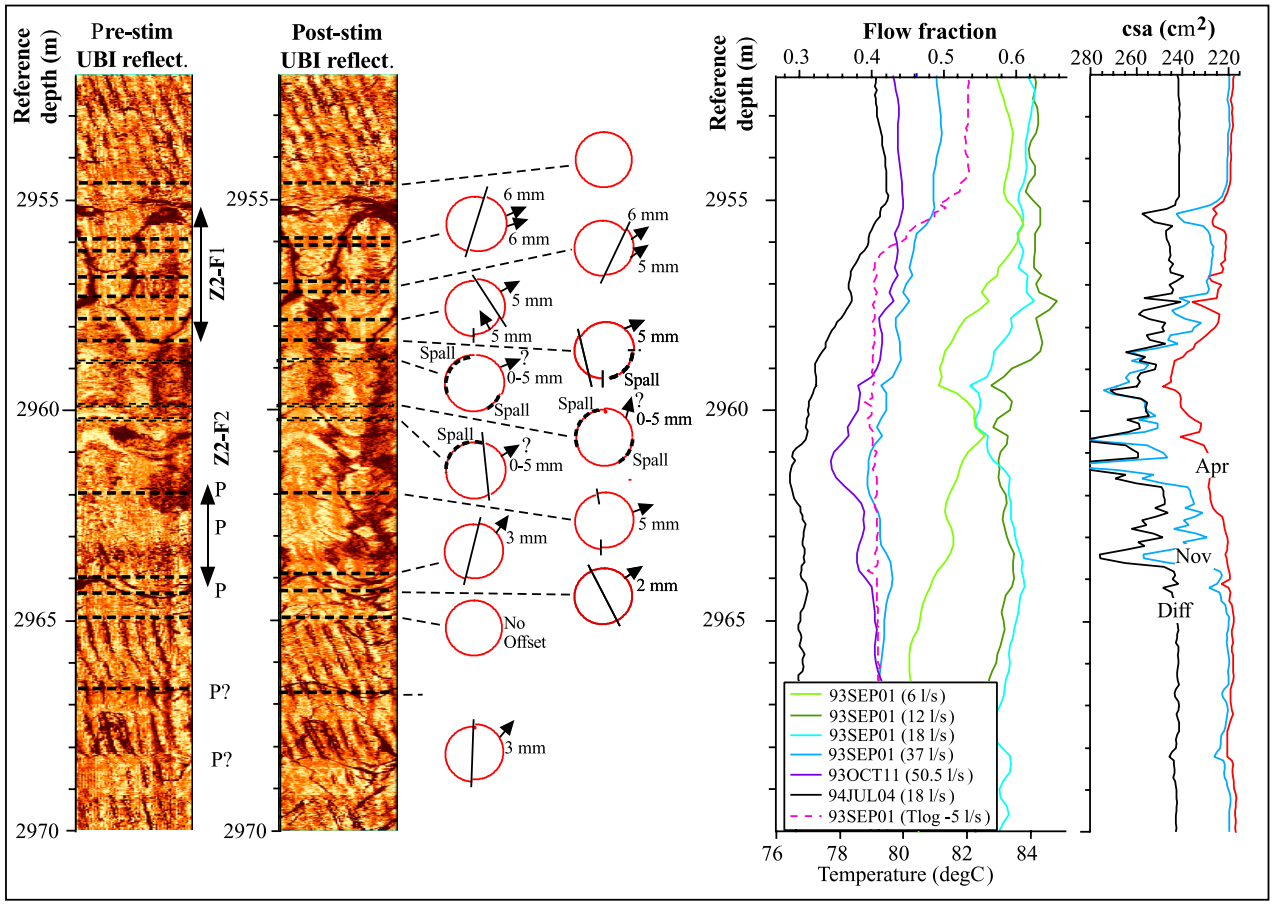

Figure 11. (left) Prestimulation and poststimulation UBI reflectivity images of the borehole in the vicinity of flow zone 2. The poststimulation figure of the borehole around the scan lines indicated on the logs is shown by the circles. If a dislocation was inferred to have developed between logs, the fracture across which it occurred is denoted by a line, and the sense of horizontal displacement of the east wall with respect to the west is indicated by an arrow. Sections of borehole wall where spalling occurred are shown by the dashed sectors of circle. The presence of spalling greatly reduced the resolution of the analysis and rendered the dislocation estimates indicated by question mark as uncertain. Collectively, the scans suggest the borehole was split by a pair of axial fractures that extend continuously between 2955 and 2964.5 m and which suffered a dislocation whose opening mode component is about 5 mm. The selection of flow profiles obtained from Q and T logs run during the stimulation program and a low-pressure injection test conducted in 1994, shown at center, indicates that the location of flow activity varied during the stimulations. (right) The noise in the flow logs is largely due to variations in the cross-sectional area of the borehole across the zone.

[28] Stress, hydraulic, and microseismic data all suggest that jacking occurred within the reservoir in the vicinity of the uppermost 50–100 m of the open hole. However, the borehole fracture images at these depths show little evidence of classical hydrofracturing. For the most part, flow entered the rock mass through natural fractures, and most of those that took significant flow showed evidence of shear. The exceptions are two flow zones, Z1-F4 and Z2-F1 (Figure 11), where features suggestive of hydrofractures were evident on the poststimulation UBI log. The features took the form of a pair of irregular, axial fractures of lengths 4 m and 9 m, respectively, that developed by linking adjacent segments of natural fracture to produce through-going features. These terminated above and below against lower-angle natural fractures. Scans across the features showed that they accommodated a significant component of opening mode dislocation in the direction of S_{hmin} and that the magnitude of the offset was fairly constant along their length. Although the analysis is not sensitive to any vertical component to the dislocation, the manner in which the fractures step back and forth at the intersection of natural fractures suggests some vertical shear displacement may also have occurred [*Evans*, 2001]. The relatively constancy of the dislocation magnitude along the length of the fractures suggests they are "Khristianivich and Zheltov"-type hydrofractures whose vertical growth is contained above and below by the two subparallel natural fractures or weakness interfaces that slip and thus arrest vertical crack growth [*Keer and Chen*, 1981]. *Jung and Weidler* [2000] note that such fractures will be held open after stimulation pressures have dissipated by the irreversible slip on the bounding interfaces, and that they can explain several other

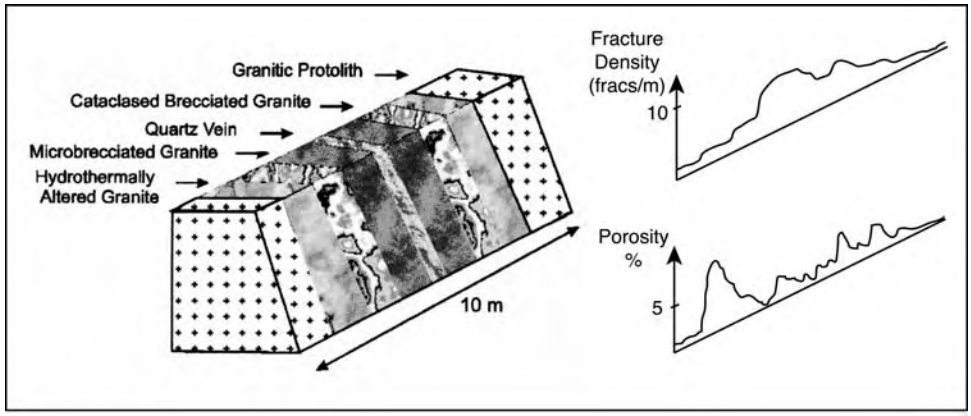

Figure 12. Cross section through an hydrothermally altered (second event) structure. The fracture density is a maximum at the center, whereas the porosity is greatest at the margins where extensive leaching has taken place. The internal structure and type of alteration identify it as a shear structure through which significant quantities of fluid have passed. After *Genter et al.* [2000].

aspects of the hydraulic response of the rock mass to the stimulation injections in the reservoir. While the axial features may indeed constitute examples of this type of hydrofracture, it is not clear whether they formed before or after slip on the bounding fractures. In the former case they would be a hydrofracture, whereas in the latter case, they could represent a linking fracture that opens as a consequence of slip on the bounding fractures in a "pull-apart" geometry [*Evans et al.*, 2005]. There is evidence of the latter for the fracture Z1–F4 where a large, 6 cm wide offset in the vertical trace of one limb between two parallel, 60° dipping natural fractures suggests the slip vector lies in the plane of the natural fractures (for otherwise the promontory formed by the step could not remain intact). Some 7 mm of downdip shear is required on the natural fractures to account for the measured 3 mm of opening-mode dislocation [*Evans*, 2001]. However, the nature of the dislocation at flow zone 2 (Figure 10) is uncertain.

[29] Stimulation was much more effective in the 550 m section of hole that was open during the 93SEP01 injection, with some 25% of the 400 natural fractures present showing evidence of flow after the stimulation, many of them newly permeable. It is clear from Figure 9 that the distribution of permeable fractures in this section is not random. Rather, it is organized into a pattern of a series of clusters of newly permeable fractures, each containing a major flowing fracture near its center, separated by zones devoid of permeable fractures. Thus the clusters form stimulated zones. A key question is what controls the location of the stimulation zones? The profile of fracture density derived from the poststimulation UBI log is shown at the foot of Figure 9. While there are some sections of hole with no resolved fractures, these are very short. In general, natural fractures are present in the borehole sections that are without stimulated fractures. Thus the absence of stimulation cannot be ascribed to the absence of fractures. Also shown at the foot of Figure 9 is the profile of "second-event" hydrothermal alteration derived from cuttings, augmented by several core samples. The depths of origin of the cuttings were estimated by correcting for the transit time in the drilling mud, although smoothing of the profile due to mixing is unavoidable. Three levels of alteration were distinguished based essentially on the degree of development of clay minerals, notably illite, and the removal of primary minerals, such as biotite and plagioclase. For the low alteration grade, biotite is mainly altered and transformed into illite; for the moderate alteration grade, biotite and plagioclase are in the process of illite transformation; and for the high alteration grade, the biotite and plagioclase are removed and in places geodic secondary quartz deposited [*Genter and Traineau*, 1996]. It is evident that the gaps in the distribution of permeable fractures correlate well with the absence of hydrothermal alteration. This observation suggests that the generation and enhancement of permeability (i.e., stimulation) occurred primarily in altered rock.

[30] The localized zones of hydrothermal alteration are interpreted as representing the intersection of the borehole with the major, hydrothermally altered, cataclastic shear structures described by *Genter and Traineau* [1996] on the basis of observations from the EPS1 core. A typical cross section across one of these structures is illustrated in Figure 12. These high-angle structures trend on average to the NNW (Figure 3d), and are composed of smaller-scale, hydrothermally altered, slickensided fractures in diverse orientations [*Genter et al.*, 2000]. The density of fractures is greatest at the core where fillings of illite and quartz, occasionally geodic, are prevalent. In contrast, the porosity is a maximum near the peripheral contact with the protolith, reflecting leaching of plagioclase feldspars [*Genter et al.*, 1998]. Alteration zone widths, which are a measure of the local width of the structures, range from centimeters to tens of meters in the EPS1 core [*Genter and Traineau*, 1996]. Thus the swarms of newly permeable fractures that cluster around the major flowing fractures, and appear as enhanced on the poststimulation sonic reflectivity log, are interpreted as representing the shear failure of preexisting, small-scale fractures that define the internal architecture of the shear structures. The location and waveforms of microseismic events suggest they are the seismic expression of the shear failure of these fractures [*Evans et al.*, 2005, also K. F. Evans et al., Source parameters of induced microseismicity at Soultz: Large stress drops and low b-values, manuscript in preparation, 2005].

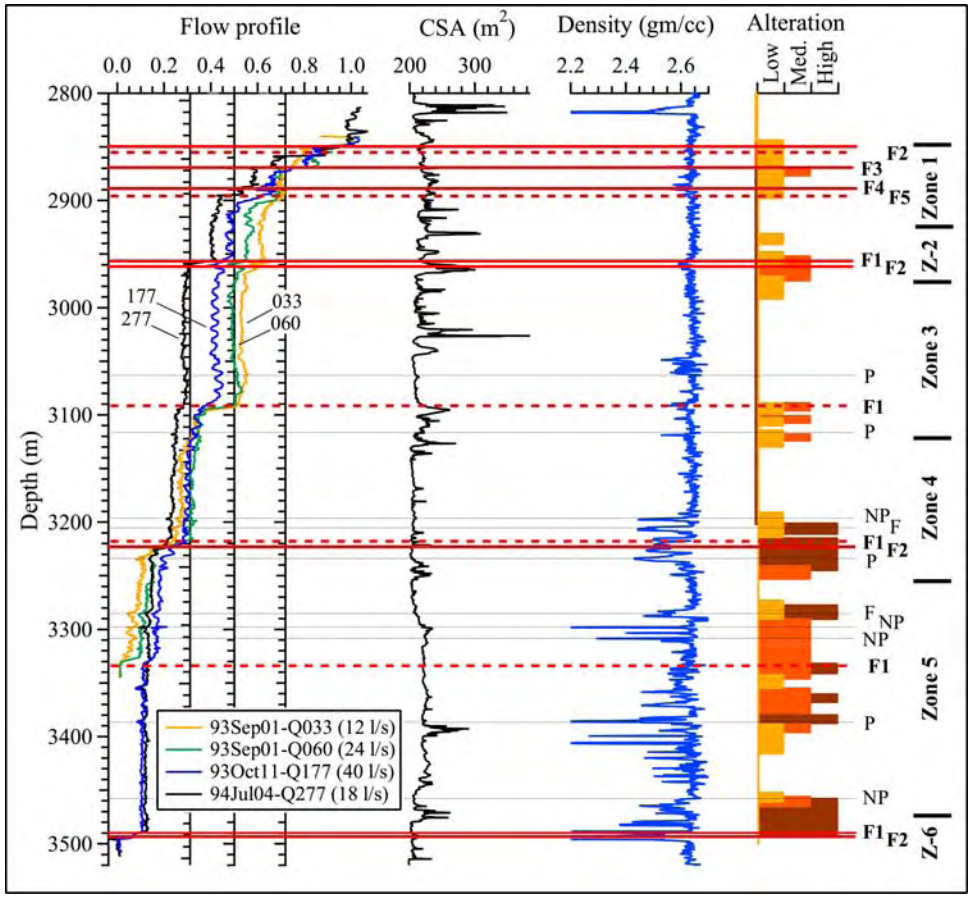

Figure 13. Correlation between the location of naturally permeable fractures (all solid lines), major flowing fractures (bold lines in red, both solid and dotted) with alteration determined from cuttings. The density and cross-sectional area (CSA) logs are also shown together with a collection of flow profiles from spinner logs. Almost all naturally permeable and major flowing fractures lie in zones of altered rock. Indeed, eight of the 13 discrete fractures that supported major flow at some time or other were identified as naturally permeable (i.e., prior to stimulation). The five exceptions are shown by the red dashed lines. The poststimulation flow ranking of the fractures is shown to the right (see Figure 4 legend).

[31] The major flowing fractures, and the prestimulation, permeable fractures represent the outlets of flow conduits defined within the core zone of the cataclastic shear structures. The spatial relationships between the major flowing fractures, the prestimulation permeable fractures and the zones of alteration are shown in Figure 13. Of the 18 prestimulation permeable fractures (denoted by solid lines, both regular and bold), all except one lie in altered zones. This indicates that the conduits through which fluid moves through the rock mass under ambient conditions are contained within the major shear structures. The bold lines (both solid and dashed) denote the locations of 13 fractures that supported major flow at some time during the injections. All except 4, in the uppermost highly stimulated zone, coincide with medium-to-high alteration, implying that the major flowing conduits established by the stimulation injections are also confined within the major shear structures. Indeed, all but the five major flowing fractures shown in Figure 13 by the red dashed lines were recognized as permeable prior to stimulation. Thus the major flow conduits under forced fluid flow conditions tend to develop along the connected paths within the shear structures that are the conduits through which fluid moves under natural conditions. It is also noteworthy that of the seven bands of medium-to-high alteration seen along the well, all but one, centered at 3380 m, contained a major flow zone, suggesting such structures readily admit the creation and enhancement of connected, high-permeability conduits within them. There are two important exceptions to this, which are discussed below.

[32] An important question is why the stimulation was so ineffective below 3350 m. This section includes two distinct alteration zones, each of which contains a large, naturally permeable, fracture complex with a high-grade alteration halo. One is a double fracture at 3386 mRD that was exposed to both stimulation injections, and the other is the fault at 3490 mRD that was sanded off for the 93SEP01 injection (Figure 13 of paper 2). These are the most prominent hydrogeological features in the entire well, yet they suffered no measurable transmissivity enhancement during the major injections, and have no surrounding clusters of newly permeable minor fractures. Their hydrological prominence is evident in Figure 14 which shows a seismic section from a VSP survey conducted along the

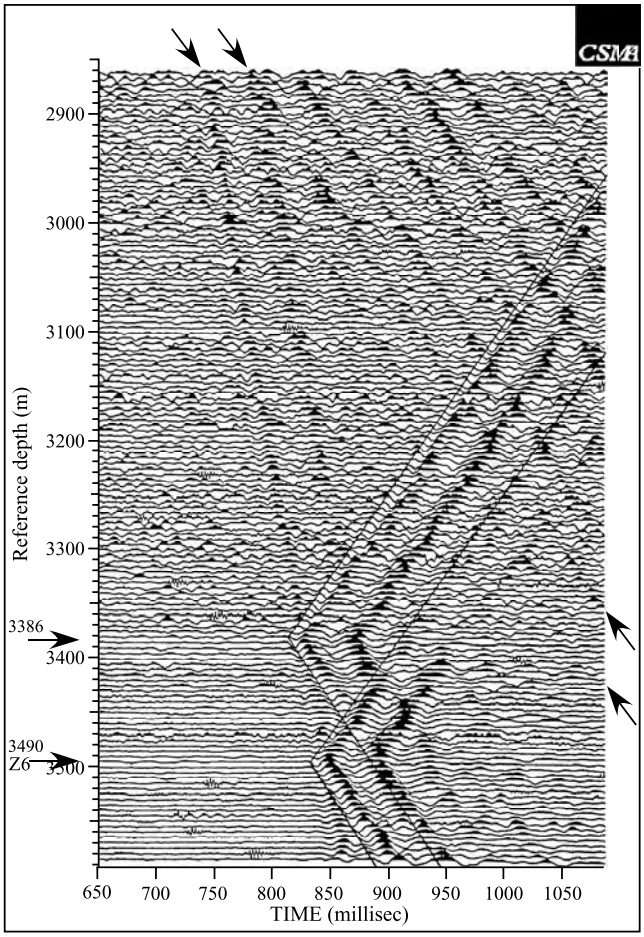

Figure 14. Seismic section obtained in GPK1 from the prestimulation (April 1993) VSP survey with the shot point in a water-filled pit some 350 m north of GPK1 wellhead. Two tube wave pairs can be seen in the lower section excited by the passing P waves (these are paired because of source characteristics.) The origin of the tube waves correlate with prominent fractures on the UBI reflectivity and electrical logs [*Sausse and Genter*, 2005]. An increase in noise level is also evident above the 3386 mRD fracture, indicating it to be a source of an upward ambient flow of fluid, which the temperature log in Figure 4 shows to be relatively hot (up-tailed positive temperature anomaly). This flow probably exits the borehole at a fracture near the top waveform that is the source of the tube waves indicated by the arrows. Both deep fractures were also sources of tube waves and ambient flow during the poststimulation VSP survey [*Evans*, 2001]. Modified from the original of *Jupe et al.* [1994].

open hole prior to any stimulation injection. Both fractures were the sole sources of strong tube waves, and they were also the primary sources of upward ambient flow under shut-in conditions, both before and after the stimulations [*Evans*, 2001]. Thus they are undoubtedly elements of the connected network of fractures/faults through which fluid moves through the rock mass under natural conditions. The fault at 3490 mRD did undergo a twofold decrease in hydraulic impedance from its original level defined in the 93JUN30 test, but the decrease appears to have occurred during the packer stimulation test 93OCT01, rather than the main injection, 93OCT11. This is suggested by the P-Q plot of zone 6 shown in Figure 7. The single lower-bound data point obtained in 93OCT01 before the packer failed lies close to the poststimulation, parabolic, impedance characteristic of the zone defined by the Q-P data points from both the 93OCT11 injection and the 1994 test series. Thus the impedance reduction appears to have occurred during the 93OCT01 injection, when the differential pressure reached only 5 MPa (before the packer failed), and was unchanged by the 93OCT11 injection, even though a differential pressure of 8.9 MPa was sustained for days, accompanied by substantial microseismic activity in the vicinity. The behavior of the fracture at 3386 mRD, whose prestimulation and poststimulation UBI reflectivity images are shown in Figure 15a, is just as surprising. Despite readily flowing under ambient conditions (Figures 4 and 13), it did not accept any detectable flow during the two injections, and ranked only as P? in the analysis of venting T logs (it is included as P in the database only because it is most certainly permeable). Both fracture zone structures appear to dip at 60–70° toward the west and almost certainly constitute the core zones of the major, hydrothermally altered, cataclastic shear structures illustrated in Figure 12. As such, their walls probably contain a major component of illite, a weak mineral with a low friction coefficient of 0.4 [*Morrow et al.*, 2000]. Both are almost optimally oriented for shear failure and require a friction coefficient in excess of 0.9 to maintain stability under ambient conditions [see *Evans*, 2005, Figure 4]). Under stimulation conditions, when both supported an internal overpressure of some 9 MPa, they would be expected to fail in shear if their strength were governed purely by friction and the resolved stresses were those derived from the stress characterization of the site. Comparison of prestimulation and poststimulation UBI travel time scans across the fracture at 3486 mRD does indeed suggest that it suffered a slip of 3–7 mm during the injections (Figure 15). The sense of slip is such that the east wall moves to the southeast with respect to the west wall, a direction that is different to the northwest orientation expected on the basis of the stress characterization. This may indicate that stress is perturbed in the vicinity of the fracture. There is also evidence that the stress is perturbed in the vicinity of the fracture at 3490 m (stress and stability aspects are dealt with in paper 2). Unfortunately, it could not be determined whether the fracture at 3490 mRD also underwent slippage during the injection since the prestimulation UBI log did not extend to this depth.

[33] Given the evidence that the fractures at 3386 m at 3490 m are both optimally oriented for shear, and that at least the fracture at 3386 m suffered shearing during the injections, the question arises as to why this did not translate to higher transmissivity. One possibility is that the strongly altered nature of these fractures suppressed dilation. *Sausse* [2002] noted that hydrothermal alteration resulted in a smoothing of small-scale fracture roughness, which would tend to suppress dilation due to shear dislocations of the order of millimeters. The weak nature of illite would also promote gouging and asperity indentation during sliding, perhaps producing clogging of apertures. This might partly explain why the stimulation process was so much more

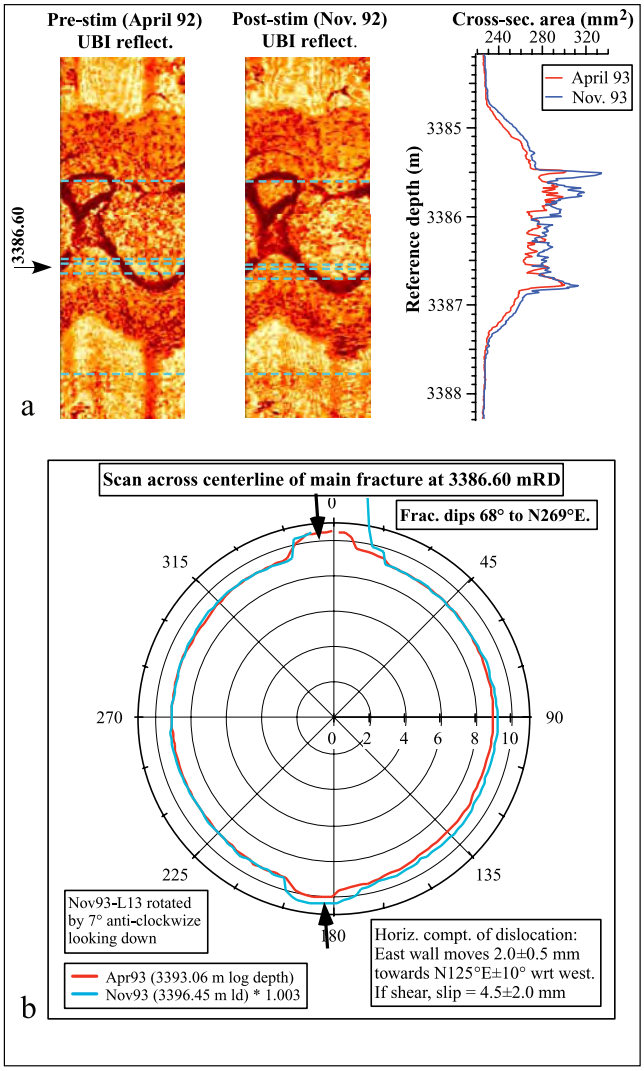

Figure 15. (a) Prestimulation and poststimulation UBI sonic reflectivity images of the major fracture at 3386 mRD. The profiles of cross-sectional area derived from the UBI logs are shown to the right and indicate that significant enlargement in the alteration zone about the fracture took place during drilling. (b) Prestimulation and poststimulation scans of the borehole geometry from the UBI travel time log taken near the centerline of the lower fracture. The curvature and detailed geometry of the walls match extremely well between the logs, indicating the walls remained intact during the stimulations. However, the fit requires that the fracture be dislocated such that the east wall move with respect to the west wall by 2 mm to the SE. If this resolved horizontal component of dislocation is interpreted as reflecting shear in the plane of the fracture, the slip of 5 mm is required.

effective for the shear zones that intersected the borehole above 3350 m, where the degree of alteration tended to be less than for the zones of the lower section [*Sausse and Genter*, 2005]. However, the strongly altered zone 4 at 3225 m did undergo transmissivity enhancement in the 93SEP01 injection, so there is no clear rule.

[34] The distribution of flowing fractures correlates quite well with the temperature profile of the borehole immediately after the 93SEP01 stimulation, as shown by the temperature log (CT13097) that was run 19 hours into the shut-in period at the end of the injection (Figure 9). The correlation is particularly striking between 2900 and 3100 m, where two sections that suffered markedly less cooling correlate precisely with an absence of flowing fractures, and also below 3330 m, where the temperature rises sharply at the lowermost major flowing fracture. These observations are qualitatively consistent with reduced penetration of advection-driven cooling during the cold water injection, because of the paucity of conducting fractures. It is also noteworthy that the shut-in temperature profile shows a distinct "warm nose" at 2956 m. This almost certainly reflects an active flow of warm fluid in the zone 2 fractures, which mark the sharp lower boundary of the section of relatively weak cooling. Below these fractures, rock temperatures plunge 25°C in only 15 m. As noted earlier, UBI travel time analyses of this zone indicate the borehole had split along a 10 m section during the stimulations, the axial fracture pair showing a widening of 0.5 cm (Figure 11). This fracture zone is most probably the outlet of a low-impedance flow path that extends more than 250 m down a steep, microseismically active shear structure, denoted by *Evans et al.* [2005] as the EL structure, and eventually merges with another low-impedance flow path that leads to the zone 4 outlet. However, these connected, relatively low-impedance flow paths appear to connect to the far field through relatively high-impedance linkage flow that account for most of the resistance to fluid exchange between the well bore and the far field, as described by the impedance characteristic curves of Figures 5 and 7 [*Evans et al.*, 2005].

[35] The results indicate that stimulation (i.e., permeability creation or enhancement) tends to be restricted to hydrothermally altered cataclastic shear zones, and that these contain the conduits through which fluid moves through the rock mass under both natural and forced fluid flow conditions. The pattern of microseismicity tends to support this view, since the majority of energy release tends to be confined to linear or planar structures [*Evans et al.*, 2005]. If the surface area swept by the primary flow under circulation of an HDR system is limited to the interior of the fracture zones, then the long-term thermal performance of the reservoir under circulation would depend on the degree of channeling within the fracture zones and the "intact" block size. For the Soultz reservoir, about 100 fracture zones have been recognized in 5500 m of borehole exposure from EPS1, GPK1, and GPK2. The zones themselves are found to be clustered and conform to a power law for intersection distances of between 20 and 300 m [*Genter and Castaing*, 1997]. Since the zones are invariably high angle, they are closer to each other than the distance between borehole intersections would suggest. We propose that separations of the order of 50 m are appropriate.

8. Conclusions

[36] Massive injections of water at high flow rates into 750 m long open hole section of a borehole in granite below 3 km depth produced a fifteenfold increase in the net

transmissivity. Prior to the injections, 17 fractures were identified as permeable from tube wave surveys and temperature logs. Following the injections, at least 95 fractures supported flow. Drilling-induced tension fractures, which extended almost continuously from 2900 m to 3250 m, did not accept flow, implying that well bore pressures remained below the minimum principal stress below 2900 m, and implicating shearing as the primary permeability enhancement mechanism.

[37] Permeability creation and enhancement was found to be limited to hydrothermally altered sections of the hole that denote its intersection with high-angle, cataclastic shear zones that are the principal, large-scale structures in the basement. Almost all fractures that were naturally permeable were located in these zones, indicating that the structures contain the conduits through which fluid moves through the rock mass under natural conditions.

[38] During the stimulation injections, 95% of the flow entered the rock mass at 10 discrete flow points. In most cases, these corresponded to naturally permeable fractures located in the core zones of the shear structures. These fractures suffered dislocations of millimeters to centimeters during the injections, mostly in shear, although several fractures in the upper section of the borehole showed a component of normal dislocation. The major flowing fractures were surrounded by swarms of newly permeable, minor-flowing fractures that also showed evidence of damage, probably through shearing. These represent failure of the minor fractures within the cataclastic shear zones. The fractures are altered and therefore weaker than those outside the zones.

[39] Major structures that showed a strongly developed alteration did not appear to be as susceptible to transmissivity enhancement through shear as lesser structures. This might be attributed to the effects of alteration in smoothing the fracture surfaces or to crushing of soft minerals such as illite, although the mechanism remain uncertain.

[40] The results indicate that major flow within the rock mass under circulation conditions is likely to be restricted to the shear zones which have a spacing of the order of 50 m.

[41] **Acknowledgments.** This work was mainly funded by the Swiss Federal Office of Education and Science as part of the Swiss contribution to the European HDR project at Soultz-sous-Forêts. The analysis of VSP and Stoneley wave logs was supported by the MTC/MURPHY International Collaborative Project (International Joint Research Grant) supported by NEDO and MESSC. The European HDR project at Soultz is supported mainly by the European Commission, BMBF (Germany), and ADEME (France). We are grateful to SOCOMINE for providing access to the data. Thanks are due to Rob Jones of VetcoGray and Kazu Tezuka of Japex for their help with the analysis of the tube wave logs. Chrystel Dezayes kindly gave permission to use Figure 1. The paper benefited from helpful reviews by the Associate Editor, André Revil, and Takatoshi Ito of Tohoku University.

References

Audigane, P., J.-J. Royer, and H. Kaieda (2002), Permeability characterization of the Soultz and Ogachi large-scale reservoir using induced microseismicity, *Geophysics*, *67*(1), 204–211.

Baumgärtner, J., R. Jung, A. Gérard, R. Baria, and J. Garnish (1996), The European Hot Dry Rock Project at Soultz sous Forêts: Stimulation of the second deep well and the first circulation experiments, paper presented at the 21st Workshop on Geothermal Reservoir Engineering, Stanford Univ., Stanford, Calif.

Baumgärtner, J., A. Gérard, R. Baria, R. Jung, T. Tran-Viet, T. Gandy, L. Aquilina, and J. Garnish (1998), Circulating the HDR reservoir at Soultz: Maintaining production and injection flow in complete balance, paper presented at the 23rd Workshop on Geothermal Reservoir Engineering, Stanford Univ., Stanford, Calif.

Bérard, T., and F. Cornet (2003), Evidence of thermally induced borehole elongation: A case study at Soultz, France, *Int. J. Rock Mech. Min. Sci.*, *40*, 1121–1140.

Brudy, M., and M. D. Zoback (1999), Drilling-induced tensile wall-fractures: Implications for determination of in-situ stress orientation and magnitude, *Int. J. Rock Mech. Min. Sci.*, *36*, 191–215.

Cornet, F. H., and R. H. Jones (1994), Field evidence on the orientation of forced water flow with respect to the regional principal stress directions, in *1st North American Rock Mechanics Symposium*, edited by P. P. Nelson and S. E. Laubach, pp. 61–69, A. A. Balkema, Brookfield, Vt.

Cornet, F. H., J. Helm, H. Poitrenaud, and A. Etchecopar (1997), Seismic and aseismic slip induced by large fluid injections, *Pure Appl. Geophys.*, *150*, 563–583.

Dezayes, C. T., T. Villemin, A. Genter, H. Traineau, and J. Angelier (1995), Analysis of fractures in boreholes of Hot Dry Rock Project at Soultz-sous-Forêts (Rhine Graben, France), *J. Sci. Drill.*, *5*(1), 31–41.

Drury, M. J., and A. M. Jessop (1982), The effect of a fluid-filled fracture on the temperature profile in a borehole, *Geothermics*, *11*(3), 145–152.

Esaki, T., K. Ikusada, A. Aikawa, and T. Kimura (1992), Surface roughness and hydraulic properties of sheared rock, in *Fractured and Jointed Rock Masses*, edited by L. R. Myer et al., pp. 393–398, A. A. Balkema, Brookfield, Vt.

Evans, K. F. (1998), Does significant aseismic slip occur on fractures in HDR systems under stimulation conditions?, paper presented at the 4th International Hot Dry Rock Forum, Eur. Union, Strasbourg, France.

Evans, K. F. (2000), The effect of the 1993 stimulations of well GPK1 at Soultz on the surrounding rock mass: Evidence for the existence of a connected network of permeable fractures, in *World Geothermal Congress*, edited by E. Iglesias et al., pp. 3695–3700, Int. Geotherm.Assoc., Morioka, Japan.

Evans, K. F. (2001), Determining the effect of stimulation injections on the rock mass around the well GPK1 from borehole data: Analysis of the 1993 injections, in *Data Analysis and Controls Towards Understanding Reservoir Behaviour and the Creating of a Conceptual Reservoir Models*, pp. 6–74, Swiss Fed. Inst. of Technol., Zürich.

Evans, K. F. (2005), Permeability creation and damage due to massive fluid injections into granite at 3.5 km at Soultz: 2. Critical stress and fracture strength, *J. Geophys. Res.*, B04204, doi:10.1029/2004JB003169.

Evans, K. F., T. Kohl, R. J. Hopkirk, and L. Rybach (1996), Studies of the nature of non-linear impedance to flow within the fractured granitic reservoir at the European Hot Dry Rock Project site at Soultz-sous-Forêts, France, report, Swiss Fed. Inst. of Technol./Polydyn. Eng., Zürich.

Evans, K. F., H. Moriya, H. Niitsuma, R. H. Jones, W. S. Phillips, A. Genter, J. Sausse, R. Jung, and R. Baria (2005), Microseismicity and permeability enhancement of hydrogeologic structures during massive fluid injections into granite at 3 km depth at the Soultz HDR site, *Geophys. J. Int.*, *160*, 388–412.

Fabriol, H., A. Beauce, A. Genter, and R. Jones (1994), Induced seismicity and its relation with natural fractures: The HDR example of Soultz (France), *Trans. Geotherm. Resour. Counc.*, *18*, 423–430.

Garnish, J., R. Baria, J. Baumgärtner, and A. Gérard (1994), The European Hot Dry Rock programme 1994–95, *Trans. Geotherm. Resour. Counc.*, *18*, 431–438.

Genter, A. (1989), Géothermie Roches Chaudes Sèches: Le granite de Soultz-sous-Forêts. (Bas-Rhin, France), Ph.D. thesis, Univ. d'Orléans, Orléns, France.

Genter, A., and C. Castaing (1997), Effets d'échelle dans la fracturation des granites (Scale effects in the fracturing of granite), *C. R. Acad. Sci.,Ser. IIa, Sci. Terre Planètes*, *325*, 439–445.

Genter, A., and H. Traineau (1992), Borehole EPS-1, Alsace, France: Preliminary geological results from granite core analyses from Hot Dry Rock research, *Sci. Drill.*, *3*, 205–214.

Genter, A., and H. Traineau (1996), Analysis of microscopic fractures in granite in the HDR geothermal well EPS-1, Soultz-sous-Forêts, France, *J. Volcanol. Geotherm. Res.*, *72*, 121–141.

Genter, A., H. Traineau, C. Dezayes, P. Elsass, B. Ledesert, A. Meunier, and T. Villemin (1995), Fracture analysis and reservoir characterization of the granitic basement in the HDR Soultz project (France), *Geotherm. Sci. Technol.*, *4*(3), 189–214.

Genter, A., C. Castaing, C. Dezayes, H. Tenzer, H. Traineau, and T. Villemin (1997), Comparative analysis of direct (core) and indirect (borehole imaging tools) collection of fracture data in the Hot Dry Rock Soultz reservoir (France), *J. Geophys. Res.*, *102*, 15,419–15,431.

Genter, A., C. Dezayes, S. Gentier, B. Ledesert, and J. Sausse (1998), Conceptual fracture model at Soultz based on geological data, *Geol. Jahrb., Reihe E*, *SE1*, 93–102.

Genter, A., H. Traineau, B. Ledésert, B. Bourgine, and S. Gentier (2000), Over 10 years of geological investigations within the HDR Soultz Project, France, in *World Geothermal Congress*, edited by E. Iglesias et al., pp. 3707–3712, Int. Geotherm. Assoc., Reykjavik, Iceland.

Gentier, S., D. Hopkins, and J. Riss (2000), Role of fracture geometry in the evolution of flow paths under stress, in *Dynamics of Fluids in Fractured Rock*, *Geophys. Monogr. Ser.*, vol. 122, edited by B. Faybishenko, P. A. Witherspoon, and S. M. Benson, pp. 169–184, AGU, Washington, D. C.

Henriksen, A. (2001), Fracture interpretation based on electrical and acoustic borehole image logs, *BRGM Rep. BRGM/RP-50,835–FR*, Bur. de Rech. Geol. et Miner., Orléans, France.

Hettkamp, T., J. Baumgärtner, R. Baria, A. Gérard, T. Gandy, S. Michelet, and D. Teza (2004), Electricity production from Hot Rocks, paper presented at 29th Workshop on Geothermal Reservoir Engineering, Stanford Univ., Stanford, Calif.

Jones, R. H., A. Beauce, A. Jupe, H. Fabriol, and B. C. Dyer (1995), Imaging induced seismicity during the 1993 injection test at Soultz-sous-Forêts, France, in *World Geothermal Congress*, edited by E. Barbier et al., pp. 2665–2669, Int. Geotherm. Assoc., Reykjavik, Iceland.

Jung, R. (1991), Hydraulic fracturing and hydraulic testing in the granitic section of borehole GPK1, Soultz-sous-Forêts, *Geotherm. Sci. Technol.*, *3*(1–4), 149–198.

Jung, R. (1993), Hydraulic tests in 1993 at the HDR Project, Soultz-sous-Forêts, France, report, Bundesans. für Geowis. und Rohstoffe (BGR), Hannover, Germany.

Jung, R., and R. Weidler (2000), A conceptual model for the stimulation process of the HDR-system at Soultz, *Trans. Geotherm. Resour. Counc.*, *24*, 143–147.

Jung, R., J. Willis-Richards, J. Nicholls, A. Bertozzi, and B. Heinemann (1995), Evaluation of hydraulic tests at Soultz-sous-Forêts, European Hot Dry Rock site, in *World Geothermal Congress*, edited by E. Barbier et al., pp. 2671–2676, Int. Geotherm. Assoc., Reykjavik, Iceland.

Jupe, A., R. J. Jones, J. Willis-Richards, B. Dyer, J. Nicholls, and P. Jacques (1994), Report on HDR Phase 4: Activity 4.1: Soultz experimental programme 1993/94, report, VetcoGray, Penryn, UK.

Keer, L. M., and S. H. Chen (1981), The intersection of a pressurized crack with a joint, *J. Geophys. Res.*, *86*, 1032–1038.

Keys, W. S. (1990), Borehole geophysics applied to ground-water investigations, *U.S. Geol. Surv. Tech. Water Resour. Invest.*, *Book 2, Chap. E2*, 149 pp.

Kohl, T., K. F. Evans, R. J. Hopkirk, R. Jung, and L. Rybach (1997), Observation and simulation of non-Darcian flow transients in fractured rock, *Water Resour. Res.*, *33*(3), 407–418.

Larroque, J. M., and P. Laurent (1988), Evolution of the stress field pattern in the south of the Rhine Graben from Eocene to the present, *Tectonophysics*, *148*, 41–58.

Morrow, C., D. E. Moore, and D. A. Lockner (2000), The effect of mineral bond strength and absorbed water on fault gouge frictional strength, *Geophys. Res. Lett.*, *27*(6), 815–818.

Murphy, H., D. Brown, R. Jung, I. Matsunaga, and R. Parker (1999), Hydraulics and well testing of engineered geothermal reservoirs, *Geothermics*, *28*, 491–506.

Niitsuma, H., et al. (1999), Current status of seismic and borehole measurements for HDR/HWR development, *Geothermics*, *29*, 475–490.

Pine, R. J., and A. S. Batchelor (1984), Downward migration of shearing in jointed rock during hydraulic injections, *Int. J. Rock Mech., Min. Sci. Geomech. Abstr.*, *21*, 249–263.

Poitrenaud, H. (1994), Application des mesures par 'ultrasonic borehole imager' à la determination de glissements sur fractures preexistants, Masters thesis, Inst. de Phys. du Globe de Paris, Paris.

Rummel, F. (1991), Physical properties of the rock in the granitic section of borehole GPK1, Soultz-sous-Forêts, *Geotherm. Sci. Technol.*, *3*(1–4), 199–216.

Sausse, J. (2000), Traitement graphique des données de forage: Caractérisation des relations fracturation-altérations: Application au granite de Soultz-sous-Forêts (Bas-Rhin, France), *C. R. Acad. Sci., Sér. IIa, Sci. Terre Planètes.*, *330*, 185–192.

Sausse, J. (2002), Hydromechanical properties and alteration of natural fracturee surfaces in the Soultz granite (Bas-Rhin, France), *Tectonophysics*, *348*, 169–185.

Sausse, J., and A. Genter (2005), Two types of fracture permeability in granite, in *Petrophysical Properties of Crystalline Rocks*, edited by P. K. Harvey et al., *Geol. Soc. Spec. Publ.*, *240*, 1–14.

Tezuka, K., and H. Niitsuma (2000), Stress estimated using microseismic clusters and its relationship to the fracture system of the Hijiori Hot Dry Rock reservoir, *Engineering Geology*, *56*, 47–62.

Tezuka, K., C. H. Cheng, and X. M. Tang (1997), Modelling of low-frequency Stoneley wave propagation in an irregular borehole, *Geophysics*, *62*(4), 1047–1058.

Wang, J. S. Y., T. N. Narasimhan, and C. H. Scholz (1988), Aperture correlation of a fractal fracture, *J. Geophys. Res.*, *93*, 2216–2224.

Weidler, R., A. Gérard, R. Baria, J. Baumgärtner, and R. Jung (2002), Hydraulic and micro-seismic results of a massive stimulation test at 5 km depth at the European Hot-Dry-Rock test site, Soultz, France, paper presented at the 27th Workshop on Geothermal Reservoir Engineering, Stanford Univ., Stanford, Calif.

Yeo, I. W., M. H. De Frietas, and R. W. Zimmerman (1998), Effect of shear displacement on the aperture and permeability of a rock fracture, *Int. J. Rock. Mech. Min. Sci.*, *35*(8), 1051–1070.

K. F. Evans, Engineering Geology, Department of Earth Science, Swiss Federal Institute of Technology (ETH), CH-8093 Zürich, Switzerland. (keith.evans@erdw.ethz.ch)

A. Genter, Unité Géo-énergie, BRGM, 3 Ave Claude Guillemin BP 6009, F-45060 Orleans Cedex 2, France. (a.genter@brgm.fr)

J. Sausse, UMR CNRS 7566 G2R, University of Nancy 1, BP239, F-54506 Vandoeuvre, France. (judith.sausse@g2r.uhp-nancy.fr)

APPENDIX 4(c)

Keith Evans, 2005, Permeability creation and damage due to massive fluid injections into granite at 3.5 km at Soultz: 2. critical stress and fracture strength, *J. Geophys. Res*., 110, B04204, doi:10.1029/2004JB003169, 2005.

Permeability creation and damage due to massive fluid injections into granite at 3.5 km at Soultz: 2. Critical stress and fracture strength

Keith F. Evans

Engineering Geology, Department of Earth Science, Swiss Federal Institute of Technology, Zürich, Switzerland

Received 10 May 2004; revised 24 December 2004; accepted 14 January 2005; published 22 April 2005.

[1] The stress acting on fractures in a 3.5 km deep borehole in granite is examined to place constraints on fracture strength and to evaluate whether permeable fractures tended to be "critically stressed." Two data sets consisting of some 500 fractures are analyzed. The first considers the permeable/impermeable fracture populations in their natural state. The second considers the populations after the hole had been subject to a prolonged, 9 MPa overpressure in two major injections which increased the number of permeable fractures from 18 to more than 95. For both data sets it is found that permeable fractures are critically stressed inasmuch as they support levels of shear stress that would be verging on failure if their strength were governed by a Coulomb friction law with a coefficient of 0.6–1.0. However, the vast majority of impermeable fractures are also critically stressed, implying that critical stressing is a necessary, but not a sufficient, condition for permeability to develop. Most permeable fractures showed evidence of shear failure after the injections and tended to occur in hydrothermally altered cataclastic shear zones, suggesting that they may have been relatively weak because of the presence of illite. To prevent failure of the impermeable fractures during the injections requires a cohesion of at least 6.5 MPa to augment a maximum allowable friction coefficient of 1.0. These are probably early mode 1 fractures that are sealed primarily with calcite. The strength of the shear zones appears to be significantly greater than the illite-rich fractures from which they are composed. This imposes constraints on their internal architecture.

Citation: Evans, K. F. (2005), Permeability creation and damage due to massive fluid injections into granite at 3.5 km at Soultz: 2. Critical stress and fracture strength, *J. Geophys. Res.*, *110*, B04204, doi:10.1029/2004JB003169.

1. Introduction

[2] In the companion paper by *Evans et al.* [2005a] (hereinafter referred to as paper 1) we describe the effects of massive fluid injections on the permeability of natural fractures intersecting a borehole in previously undisturbed granite. The borehole, denoted GPK1, is located at the Soultz-sous-Forêts Hot Dry Rock (HDR) project site in the Rhinegraben in France where the top of the basement lies at 1400 m depth. The hole is 3.6 km deep and is completed as $6\frac{1}{4}$ inch open hole below 2850 m. Of some 500 natural fractures imaged on a Schlumberger Ultrasonic Borehole Imager (UBI) log, 18 were found to be naturally permeable. Following the injections, this increased to at least 96 fractures, most of which showed evidence of shear dislocation. Knowledge of stress within the reservoir permits the maximum shear and normal stress components acting on fractures to be computed since their orientation is known. This in turn allows an assessment of whether the permeable fractures tend to be closer to shear failure conditions than nonpermeable fractures. *Barton et al.* [1995] first presented studies of this nature from several wells in different stress regimes. They found that permeable fractures tended to support shear stress levels which would be verging on failure if the strengths of the fractures were governed by a friction criterion with a coefficient of friction of between 0.6 and 1.0. Conversely, fractures that were not permeable were largely found to support shear stress levels that would render them stable under such a strength criterion. This led Barton et al. to postulate that the permeable fractures were permeable because they were active under the prevailing stress regime and had suffered shearing in the recent past. Such permeable fractures have become known in the literature as critically stressed. Since this pioneering work, several other studies have reported that permeable fractures within crystalline rock masses tend to be critically stressed [*Barton et al.*, 1998; *Hickman et al.*, 1998; *Ito and Zoback*, 2000; *Okabe and Hayashi*, 2000; *Okabe et al.*, 2002]. Both *Ito and Hayashi* [2003] and *Zoback and Townend* [2001] note that the stress state at Soultz reported in the literature implies that favorably oriented fractures within the rock mass would be critically

0148-0227/05/2004JB003169$09.00

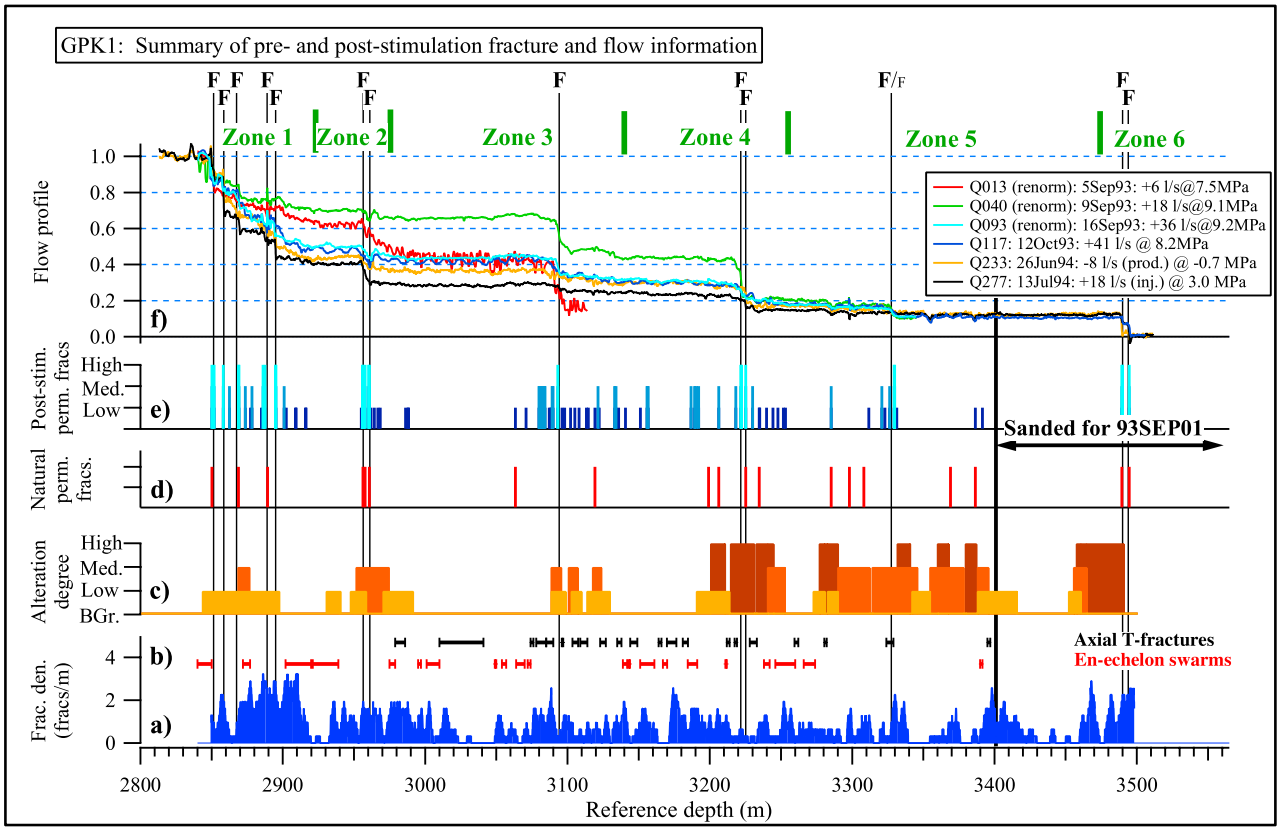

Figure 1. Summary of geological and hydraulic information for GPK1. (a) UBI-imaged natural fracture density; (b) axial and en echelon drilling-induced tension fractures; (c) hydrothermal alteration determined largely from cuttings; (d) location of naturally permeable fractures; (e) location and ranking of fractures that supported flow following the two stimulation injections; and (f) selection of flow profiles from spinner logs run during the stimulations and poststimulation characterization tests. The well was filled with sand to 3400 m for the 93SEP01 injection. Thus, to permit comparison of the flow profiles from this injection with later tests on the entire open hole, the 93SEP01 profiles have been normalized so as to give the same flow fraction at 3350 m (the bottom of most logs) as seen in the later tests. Major flowing fractures are denoted by F, and their corresponding six flow zones are as shown.

stressed. In this paper I evaluate whether the prestimulation and poststimulation sets of permeable fractures are more favorably orientated for failure than nonpermeable fractures. The results lead to the conclusion that critical stressing is a necessary but not a sufficient condition for fracture permeability to develop, at least for the Soultz reservoir, since many nonpermeable fractures are found to be critically stressed. Probable errors in the commonly used stress characterization and consideration of poroelastic stresses prevailing during the pressurization of the reservoir are shown to have little effect on the conclusion that the critically stressed, nonpermeable fractures have strengths significantly in excess of that which can be ascribed to friction. The strength of these fractures is ascribed primarily to the nature of the calcite filling and the absence of alteration. The permeable, critically stressed fractures largely occur in altered, cataclastic shear zones which serve to limit the strength of the rock mass. These zones are surprisingly strong given that the small-scale fractures from which they are composed contain an abundance of illite, a mineral that has a low fraction coefficient. The strength of the zones is attributed to their internal architecture and resides primarily in intact rock bridges and jogs between adjacent small-scale sheared fractures [*Zhang and Sanderson*, 2001].

2. Background

2.1. Key Results From Paper 1

[3] It is appropriate to summarize the background information and results from paper 1 that are used in this paper. The key hydrogeological results are summarized in Figure 1. Fracture density along the open hole is shown in Figure 1a, the location and extent of drilling-induced tension fractures, both en echelon and axial types, are shown in Figure 1b, the profile of alteration derived from cuttings is shown in Figure 1c, and the locations of naturally permeable fractures are shown in Figure 1d. The equivalent porous media (EPM) permeability of the rock mass penetrated by GPK1 before the major injections was similar to that measured on intact core, save for a fault at 3496 m which accounted for almost all the injectivity of the borehole. The hole was then subjected to two major injections of fresh water, each of approximately 20,000 m^3. The first injection, denoted 93SEP01, was conducted on the uppermost 550 m of open hole. In this injection, flow rate was stepped from 0.15 to

40 L s^{-1} over a 2 week period [*Evans et al.*, 2005a, Figure 2]. The second injection, denoted 93OCT11, was conducted on the entire open hole section. Flow rate was held at 40 L s^{-1} before being stepped to 50 L s^{-1} for the final day. Pressure-limiting behavior was observed in both tests, suggesting that jacking conditions were met somewhere along the open hole sections. The downhole well bore pressure excess above the natural formation pressure, hereafter referred to as the differential pressure, reached 9.2 MPa for the first injection and 8.9 MPa for the second. As a consequence of the injections, the injectivity increased fifteenfold for the entire borehole, and 200-fold for the uppermost 550 m that was open for the first injection. This difference reflects the effect of the fault at 3496 m. Spinner and temperature logs run during and following the injections indicated that at least 96 fractures supported flow to some degree following the injections, the vast majority in the section that was open to the first injection (Figures 1e and 1f). These fractures were organized into clusters spaced at approximately 100 m intervals along the well bore. Typically, each cluster contained one or two major flowing fractures surrounded by a swarm of newly permeable fractures that supported minor flow. The major flowing fractures were seen to have suffered dislocations of the order of millimeters to centimeters, and most showed evidence of permeability prior to the injections. The newly permeable, minor flowing fractures also showed evidence of damage, probably due to shearing. The clusters of permeable fractures occurred largely in hydrothermally altered sections of borehole (Figure 1c) that are believed to be the expression of major cataclastic shear structures that cut the borehole [see *Evans et al.*, 2005a, Figure 12]. This implies that the structures contain the flow conduits through which fluid moves through the rock mass under both natural and forced fluid flow conditions. It also indicates that permeability creation and enhancement (i.e., stimulation) was largely limited to the interior of these structures.

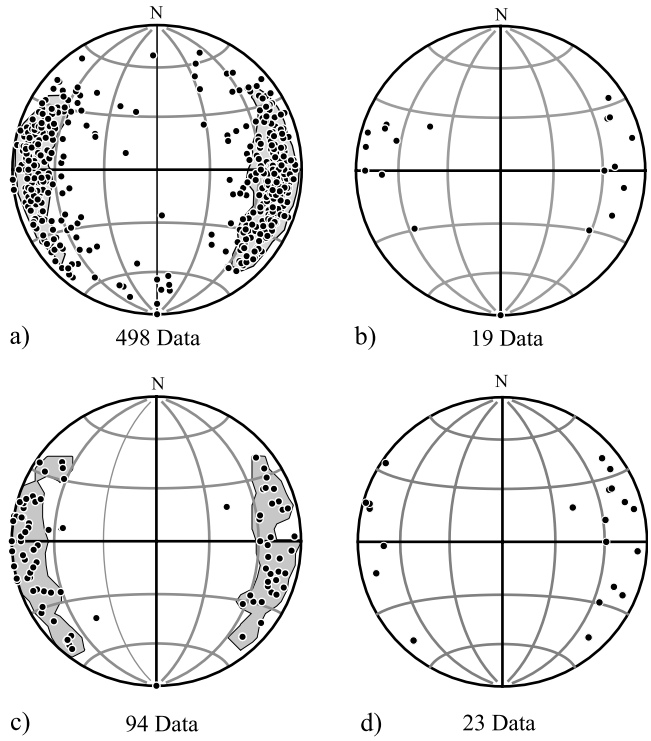

Figure 2. (a) Orientation distributions of poles to natural fractures identified on the UBI log run in the open hole section of GPK1 (lower hemisphere, equal-area projection); (b) poles to fractures recognized as being permeable prior to stimulation; (c) poles to fractures recognized as permeable following the stimulation (high confidence identification (see paper 1 for explanation)); and (d) poles to fractures that supported major flow following the stimulation injections.

2.2. Orientation Distribution of Fractures

[4] The poles to the 520 fractures imaged on the post-stimulation UBI log are plotted in Figure 2a. The fractures are almost all high angle with strikes varying within 45° either side of north. There is no obvious asymmetry in the population. The poles of the subset of fractures that were identified as being permeable before and after the stimulations are shown in Figures 2b and 2c, respectively. Both distributions are similar to that for all fractures. The poles to fractures that supported significant or major flow (designation of F or **F** in the ranking of flow described in paper 1) is shown in Figure 2d. Again, the distribution mimics the others except for a tendency for fractures to dip to the east. The cataclastic shear zone structures are high angle and tend to strike NNW-SSE [*Evans et al.*, 2005a, Figure 3d].

2.3. State of Stress

[5] Ideally, the analysis requires complete and accurate knowledge of the state of stress within the rock mass in question, which is the rock volume about the open hole section of GPK1. As in most situations, knowledge of the stress state is limited. However, in the Soultz case, there is also debate regarding the validity of published determinations. The data clearly show that the stress regime is consistent with the graben setting but do not unequivocally define whether it is predominantly strike slip or normal faulting type. Given the importance of stress for the analysis, it is appropriate to provide a summary of the constraints that the data place on the various attributes of stress. Hereafter, I will assume that one principal stress is vertical, although the presence of localized stacks of en echelon fractures indicate that local deviations from verticality are present [*Brudy and Zoback*, 1999]. As a starting point for the analysis, I will adopt the stress characterization reported most often in the literature [e.g., *Baria et al.*, 1995]. This will be referred to as the "standard stress state" and is defined by the following linear trends:

$$S_{Hmax}\ \text{orient} = \text{N}170^\circ\text{E} \pm 15^\circ \tag{1a}$$

$$S_{hmin}[\text{MPa}] = -5.9 + \{0.0149\ z[\text{m}]\} \tag{1b}$$

$$S_{Hmax}[\text{MPa}] = -25.3 + \{0.0336\ z[\text{m}]\} \tag{1c}$$

$$S_V[\text{MPa}] = -1.3 + \{0.0255\ z[\text{m}]\} \tag{1d}$$

$$P_p[\text{MPa}] = 0.90 + \{0.0098\ z[\text{m}]\} \tag{1e}$$

These trends are shown by the solid lines in Figure 3a.

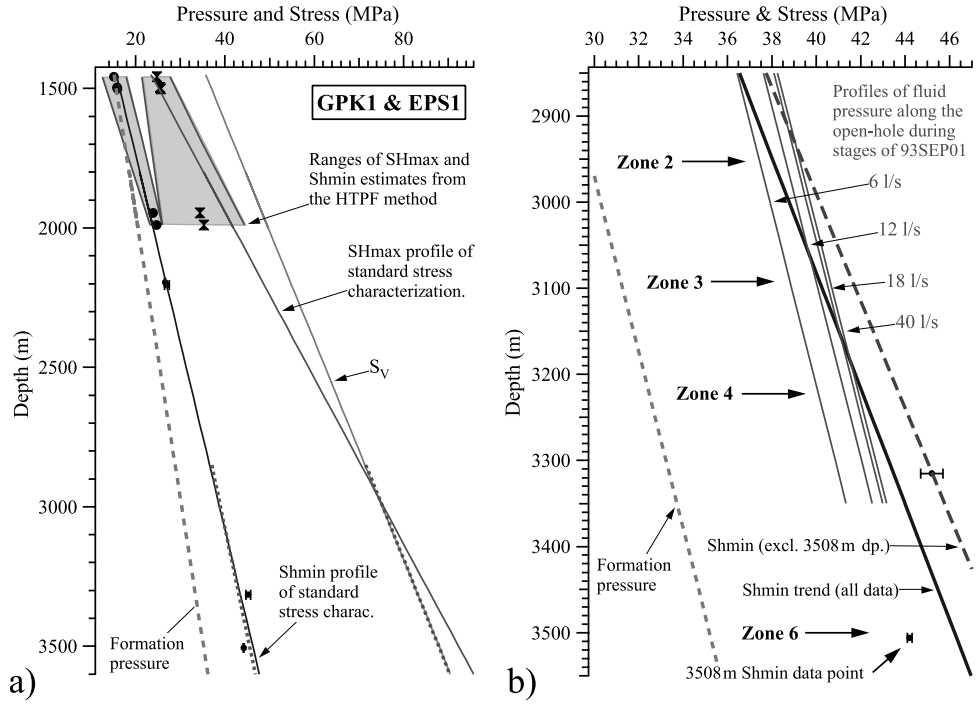

Figure 3. (a) Summary of stress magnitude information from tests in GPK1 and EPS1. The estimates obtained above 2000 m are from the HTPF method, whereas those below are from the hydrofracture method. The solid lines denote the linearized trends of the standard stress characterization. The dotted lines between 2850 and 3600 m denote the approximations to these trends used in the parameter studies. (b) Profiles of maximum differential pressure prevailing along the well bore during stages of the 93SEP01 stimulation injection. The bold line is the S_{hmin} profile of the standard stress state, and the dashed line is the preferred profile (see text for explanation).

[6] The orientation of S_{Hmax} is relatively well determined from extensive thermally induced tension fractures as N170°E ± 15° [*Bérard and Cornet*, 2003; *Brudy and Zoback*, 1999; *Cornet and Jones*, 1994]. This differs significantly from the regional trend obtained from inversion of focal mechanisms which suggests a more NW-SE orientation [*Plenefisch and Bonjer*, 1997]. It also differs from the orientation obtained from inversion of focal mechanisms of the microseismicity induced during the GPK1 injections which gives N124°E ± 24° [*Helm*, 1996]. *Cornet and Bérard* [2003] confirmed this discrepancy, and proposed that some of the microseismic events occurred at locations where stress was locally perturbed. For the present purposes, it is assumed that the mean stress orientation obtained from tension fractures is definitive, while recognizing that local variations within one standard deviation are likely.

[7] The profile of the magnitude of the minimum principal stress, S_{hmin}, is shown in Figure 3a. The estimates are derived from the Hydraulic Testing of Preexisting Fractures (HTPF) method above 2000 m by *Baumgärtner and Rummel* [1989] and several deeper hydrofracture tests reported by *Klee and Rummel* [1993]. The measurements, although sparse, are reasonably well approximated by the best fitting linear trend defined in the standard stress state. Figure 3b shows this linear trend together with the profiles of well bore pressure at several stages of the 93SEP01 injection. The S_{hmin} linear profile suggests that jacking conditions (i.e., well bore pressure exceeding the minimum principal stress) extended down to 3150 m at all stages above 18 L s^{-1}, when pressure-limiting conditions prevailed. However, there are good reasons to believe that jacking was limited to the rock mass about the uppermost 50–100 m of open hole. As shown in Figure 1a, axial or en echelon drilling-induced tension fractures (DITFs) were seen to extend almost continuously along the hole between 2900 and 3300 m prior to injection, yet they did not accept flow during the injections [*Evans et al.*, 2005a]. The apparent failure of these fractures to extend as hydrofractures during the injections implies that jacking was limited to above 2900 m. This is in accord with the conclusion reached by *Cornet and Jones* [1994] on the basis of a systematic change in the orientation of structures within the induced microseismic cloud. The absence of jacking below 2900 m indicates that the minimum principal total stress prevailing during the injections was greater than given by the standard stress state by 1.5 MPa at 2900 m. It is noteworthy that a single hydrofracture stress measurement at 3320 m indicates an S_{hmin} value that is 1.5 MPa higher than that given by the standard stress profile (Figure 3b). There is also a measurement at 3508 m which gave a value 2 MPa lower than the profile. However, this value probably represents a locally perturbed stress since the measurement was made only meters away from a major fracture zone (i.e., zone 6), and the strike of the induced vertical fracture was E-W rather than N-S [*Heinemann-Glutsch*, 1994]. Thus this measurement should be excluded from the data set used

to define the linear profile. The resulting S_{hmin} profile is shown by the dashed line in Figure 3b and is given by

$$S'_{hmin}[\mathrm{MPa}] = -8.1 + \{0.01608\ z[\mathrm{m}]\}. \quad (2)$$

The effect of excluding the 3508 m data point is to increase the S_{hmin} above that of the standard stress state by 1.2 MPa at 2850 m and 2 MPa at 3500 m. This profile is consistent with the hydrofracture stress measurement data and the inference that jacking occurred near the casing shoe. A similar profile was proposed by *Cornet and Bérard* [2003].

[8] Estimates of the maximum principal horizontal stress that are considered reliable are limited to the HTPF data above 2000 m. The deeper S_{Hmax} estimates of *Klee and Rummel* [1993] are unreliable since they are derived from the hydrofracture data using the reopening method, which is unlikely to yield correct results in the situation in question [*Ito et al.*, 1999; *Rutqvist et al.*, 2000]. Thus the linear S_{Hmax} trend of the standard stress profile is probably in error. Support for this is given by *Bérard and Cornet* [2003], who show that the S_{Hmax} and S_{hmin} profiles taken together imply that tension fracturing should occur in the lower section of the borehole, contrary to observation. The only reliable constraint on S_{Hmax} stems from the focal mechanisms of the microearthquakes induced during the injections, as deduced from recordings on a surface network [*Darnet*, 2000; *Gaucher*, 1998; *Helm*, 1996]. These indicate both normal and strike-slip mechanisms, suggesting that the magnitudes of S_{Hmax} and S_V are not greatly different. Thus the condition $S_{Hmax} = S_V$ is considered to represent a better working hypothesis for the S_{Hmax} profile than that of the standard stress state. As can be seen from Figure 3a, the S_{Hmax} and S_V profiles of the standard stress state coincide at 2850 m depth but diverge with depth so that S_{Hmax} exceeds S_V by 5 MPa at 3600 m.

[9] The vertical stress profile shown in Figure 3 is taken as equal to the overburden derived from density logs, and is linear with depth within the granite. The natural formation pressure gradient was derived by *Evans et al.* [1996] using downhole temperature and pressure data, and is appropriate for a hot brine with a molality of 1.76 mol kg^{-1}.

[10] Later, the effect of varying certain of the stress parameters will be considered. It will then prove convenient to approximate the stress trends defined by equations (1b), (1d), (1e), and (2) by linear trends that pass through the origin. The approximations were computed to give best fits over the depth range 2850–3500 m and are

$$S_{hmin}[\mathrm{MPa}] = 0.0130\ z[\mathrm{m}] \quad (3a)$$

$$S_V[\mathrm{MPa}] = 0.0251\ z[\mathrm{m}] \quad (3b)$$

$$P_p[\mathrm{MPa}] = 0.0100\ z[\mathrm{m}] \quad (3c)$$

$$S'_{hmin}[\mathrm{MPa}] = 0.0135\ z[\mathrm{m}] \quad (3d)$$

The approximations of S_{hmin} and S_V are shown by the dotted lines in Figure 3a. The discrepancy between the S_{hmin} profile of equation (3a) and that of the standard stress state (equation (1b)) is less than 0.6 MPa everywhere within the depth range 2580–3500 m.

3. Critical Stress Analysis

[11] The analysis consists of resolving the shear and effective normal stress components acting across members of the fracture populations, and plotting the results on a Mohr circle. The effective normal stress is obtained by subtracting the formation pressure at the depth of the fracture from the total normal stress. All stresses are normalized by dividing by the vertical stress at the depth of the fracture.

3.1. Standard Stress State: Prestimulation Permeable/Nonpermeable Fractures

[12] The prestimulation data set of permeable and nonpermeable fractures is the most directly comparable with the aforementioned published studies of critical stressing because the borehole at that time had not been subject to a major injection that radically changed the hydromechanical conditions in the rock mass. The maximum shear stress and effective normal stress resolved across the permeable fractures in this data set for the standard stress state are shown in the Mohr circle plot of Figure 4a. Both axes have been normalized by the vertical stress, S_V. If the profiles of S_{Hmax}, S_{hmin}, and S_V were all to pass through the origin when extrapolated upward to the surface (i.e., zero stress at zero depth), then the normalized Mohr circle representation of the stress state would be identical at all depths. However, the intercept of the S_{Hmax} and S_{hmin} profiles of the standard stress state with the stress axis is not zero. Hence the normalized Mohr representation is slightly depth-dependent. For this reason I show the Mohr circle stress representations for depths of 2850 m and 3500 m, which bracket the depth range of interest. Fortunately they do not differ greatly. The two dashed lines that pass through the origin denote the failure lines for an interface whose strength is governed by a Coulomb friction criterion with friction coefficients of 0.6 and 1.0. Laboratory experiments show these values represent conservative bounds for planar, interface strengths for all rock types, with the exception of some clay-type materials [*Byerlee*, 1978; *Zoback and Healy*, 1984]. The lines pass through the origin because the x axis denotes the effective normal stress, given by total normal stress minus the ambient formation pressure. The data points tend to plot between the two lines, indicating that the permeable fractures would be verging on failure if their strength were governed by friction. The permeable fractures are thus critically stressed. However, the complementary plot of nonpermeable fractures, shown in Figure 4b, indicates that the majority of these fractures are also critically stressed. Thus the results lead to the conclusion that critical stressing in a Coulomb friction sense is a necessary, but not a sufficient condition for a fracture to be permeable. It is also noteworthy that the shear stress level supported by all fractures is less than the failure limit for an interface strength governed by a friction coefficient of 1.0. This is consistent with generally held view that a friction coefficient of 1.0 appears to represent an upper bound for the large-scale strength of the crust

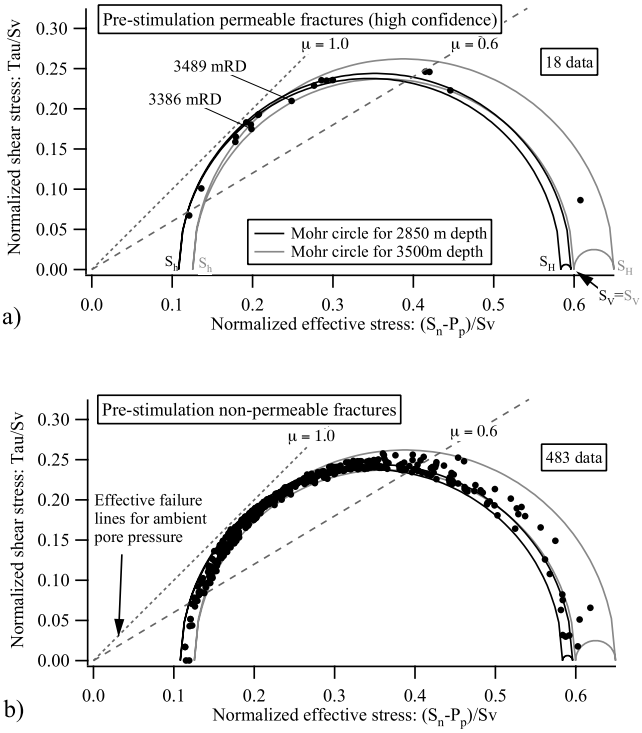

Figure 4. Shear and effective normal stress resolved on prestimulation (a) permeable and (b) impermeable fractures for the "standard" stress state under ambient conditions. Note that the stresses have been normalized by the vertical stress, S_V. The two Mohr circles depict the stress states at the depths of 2850 and 3500 m which bracket the range of interest. The failure lines are shown for a Coulomb friction criterion with friction coefficients of 0.6 and 1.0 under ambient formation pressure conditions. The permeable fractures shown in Figure 4a lie within the failure region of the Mohr circle representation of the stress state. However, so do the majority of fractures which are not permeable (Figure 4b).

[*Brace and Kohlstedt*, 1980; *Zoback and Townend*, 2001].

3.2. Standard Stress State: Poststimulation Permeable Fractures

[13] The stresses resolved across the fractures recognized as permeable or nonpermeable following the stimulation injections are shown in Figures 5a and 5b, respectively (these are the "high-confidence" data sets defined in paper 1). If the poroelastic effects of overpressure within the rock mass during the injections are ignored, and the pore pressure in the effective stress law for shear failure is taken as the ambient formation pressure, then the failure lines pass through the origin, and the same result holds as for the prestimulation data set; both permeable and nonpermeable fractures tend to be critically stressed. Similarly, the shear stress resolved on the fractures remains less than the failure limit for a friction coefficient of unity, which is the highest strength that can reasonably be ascribed to the fractures without adding a component due to cohesion. However, this limit is violated when the effects of fluid overpressures within the fractures are included.

[14] The consideration of an overpressure is warranted because the well was subject to a sustained overpressure of 9 MPa for 11 days during the 93SEP01 injection, and a further 5 days during the 93OCT11 injection. Thus it is highly probable that the pore pressure within all fractures around the well bore became elevated by up to 9 MPa during these injections. Consequently, the effective normal stress acting on the fractures would be reduced by 9 MPa, in accord with the effective stress law for shear failure [e.g., *Scholz*, 1990, p. 30]. For convenience, this modification is implemented in the Mohr plots by migrating the failure line to the right by 9 MPa, rather than migrating the circles to the left, as is more usual. Since the plots are normalized, the failure lines for ambient formation pressure must be translated by 9 MPa/S_V, where S_V is in megapascals. Hence the amount of translation is depth-dependent. For this reason, two sets of lines are plotted that define the translated failure limits at 2850 and 3500 m. It is evident that, regardless of depth, the shear stress levels supported by many fractures, permeable and nonpermeable alike, exceed the maximum value that can be supported by friction (i.e., the data

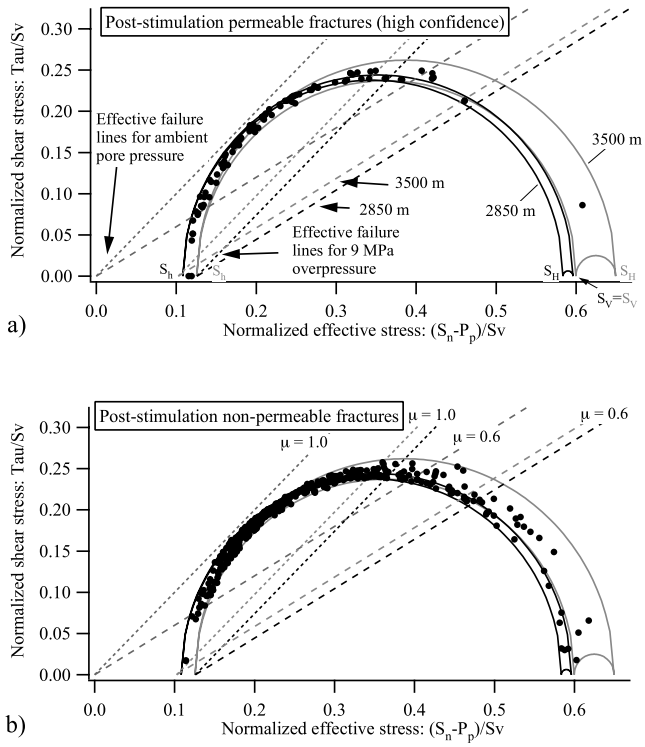

Figure 5. Shear and effective normal stress resolved on poststimulation (a) permeable and (b) impermeable fractures for the standard stress state under stimulation conditions. The Coulomb friction failure lines for ambient pore pressure conditions pass through the origin. The corresponding failure lines for fractures that host a 9 MPa fluid overpressure are translated to the right of the plot by an amount 9/S_V, where S_V is in megapascals (i.e., reduced effective normal stress). The two pairs of lines correspond to the extreme depths of 2850 and 3500 m. See text for further discussion.

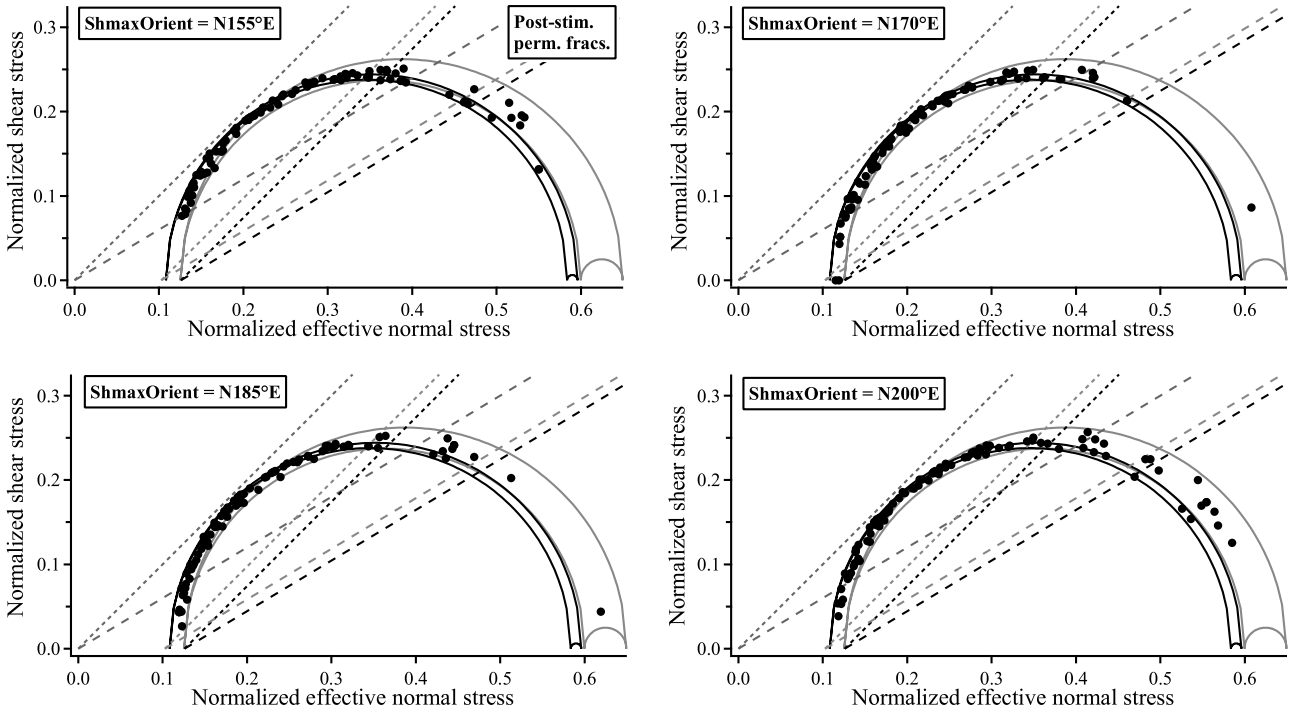

Figure 6. Mohr plot of the poststimulation permeable fracture data set (high confidence) using the standard stress state but with different values for S_{Hmax} orientation. The tightest clustering of the data points in the "most critically stressed" sector is obtained for S_{Hmax} orientations of between N170°E and N185°E which is in accord with the S_{Hmax} orientation from tension fractures. However, little change is seen in the number and degree to which the majority of data points lie above the failure line for $\mu = 1.0$.

points plot above the translated failure lines for $\mu = 1.0$). Most permeable fractures showed direct or indirect evidence of shearing during the injections (paper 1). Thus, for these it is possible that the excess shear stress was locally relaxed by slip to levels consistent with frictional strength, resulting in local stress perturbations such as reported by *Shamir and Zoback* [1992] and *Scotti and Cornet* [1994]. However, the vast majority of the nonpermeable fractures showed no evidence of damage or slip, which suggests they did not fail. If true, this implies that either the fractures have a cohesive component to their strength, or the standard stress state is not representative of the stress prevailing during injection. To estimate the minimum magnitude of the cohesive component required to prevent failure in the light of the uncertainties in the stress characterization, the effects of varying the stress parameters and of including poroelastic effects were examined.

3.3. Effect of Varying the Ambient Stress Parameters

[15] Parameter studies were conducted for the stress variables of S_{Hmax} orientation, S_{Hmax} magnitude and S_{hmin} magnitude. The effect of varying S_{Hmax} orientation between N155°E and N200°E in 15° steps is shown in Figure 6. The tightest clustering of the stress data points in the "most critically stressed" zone is obtained for S_{Hmax} orientations of N170°E and N185°E, corresponding to the S_{Hmax} orientation from drilling-induced fractures. However, little change is seen in the number and degree to which the majority of data points lie above the failure line for $\mu = 1.0$.

[16] The effect of varying S_{Hmax} magnitude was facilitated by replacing the standard stress profile of S_{Hmax} with the profile of S_V given by equation (3b) (see the section 2.3 for justification). The results of varying S_{Hmax} through values $0.6S_V$, $0.8S_V$, $1.0S_V$, and $1.2S_V$ are shown in Figure 7. Since the adopted profiles of S_V and S_{Hmax} pass through the origin (i.e., zero stress at zero depth), the normalized stresses are independent of depth. Reducing S_{Hmax} to $0.6S_V$ tends to produce a large cluster of data points with low shear stress near S_{hmin}. However, little change is seen in the number of data points that lie above the failure line for $\mu = 1.0$, except that the degree of excess becomes even greater as S_{Hmax} is increased beyond S_V. Indeed, for values of S_{Hmax} greater than S_V, the data points lie above the $\mu = 1.0$ line for ambient formation pressure conditions.

[17] The effect of varying S_{hmin} was performed using the approximation for S_{hmin} given by equation (3a) (Figure 3a). This permitted S_{hmin} to be expressed as a fraction of the vertical stress given by $S_{hmin} = 0.52S_V$. Figure 8 shows Mohr circle plots for S_{hmin} profiles of $0.4S_V$, $0.5S_V$, $0.6S_V$, and $0.7S_V$, all other parameters taking values given by the standard stress model. The value $S_{hmin} = 0.4S_V$ is the absolute minimum that can be adopted without hydrofracture occurring under ambient formation pressure conditions. Evidently, shear stress levels on most fractures now exceed the friction strength for $\mu = 1$ even for ambient pressure conditions. Increasing the minimum horizontal principal stress level to $0.5S_V$, close to the standard stress profile of $0.52S_V$, brings the shear stress levels

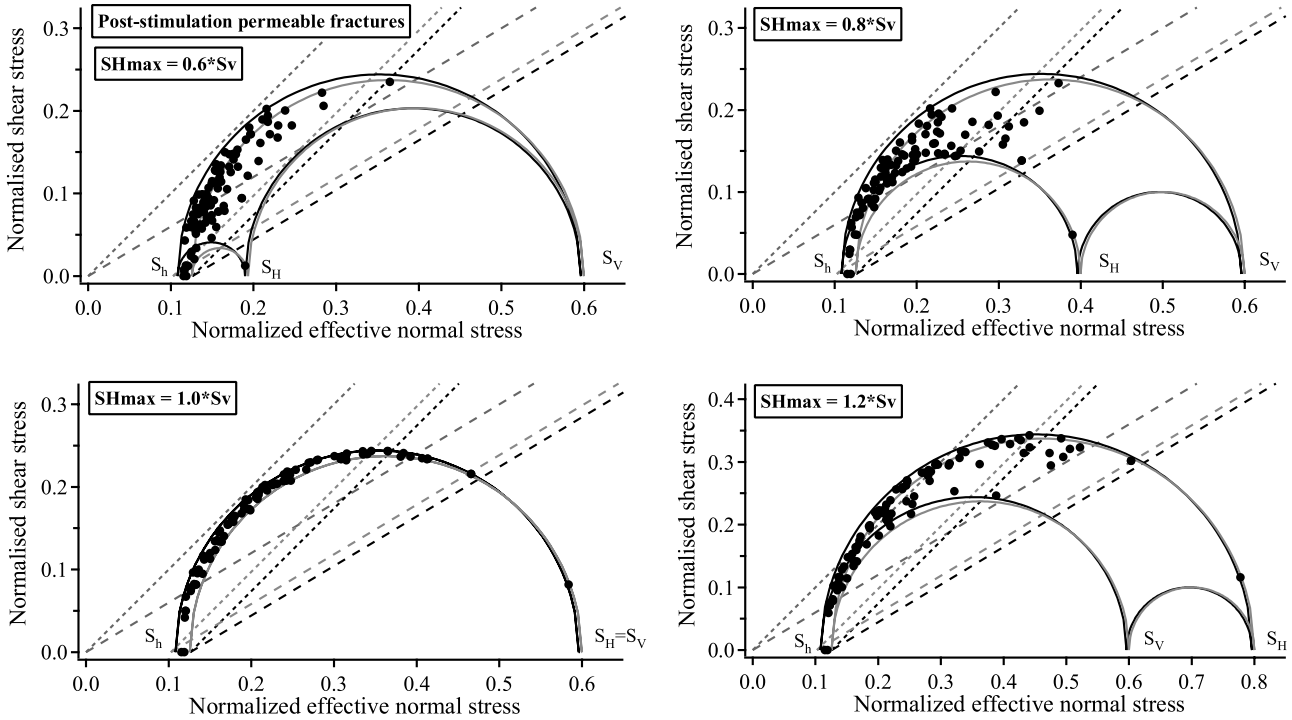

Figure 7. Results of critical stress analysis obtained using four different S_{Hmax} magnitude profiles, the other stress parameters taking the standard model values. See text for discussion.

down to below the $\mu = 1$ friction limit for ambient conditions, but not for the 9 MPa overpressure conditions. To meet the latter requires that the minimum stress level be increased to $0.6S_V$, the elevation of S_{hmin} values above those from the standard stress state then amounting to 5.7 MPa at 2850 m and 7.0 MPa at 3500 m. While there are grounds to believe that the standard stress profile modestly underestimates S_{hmin}

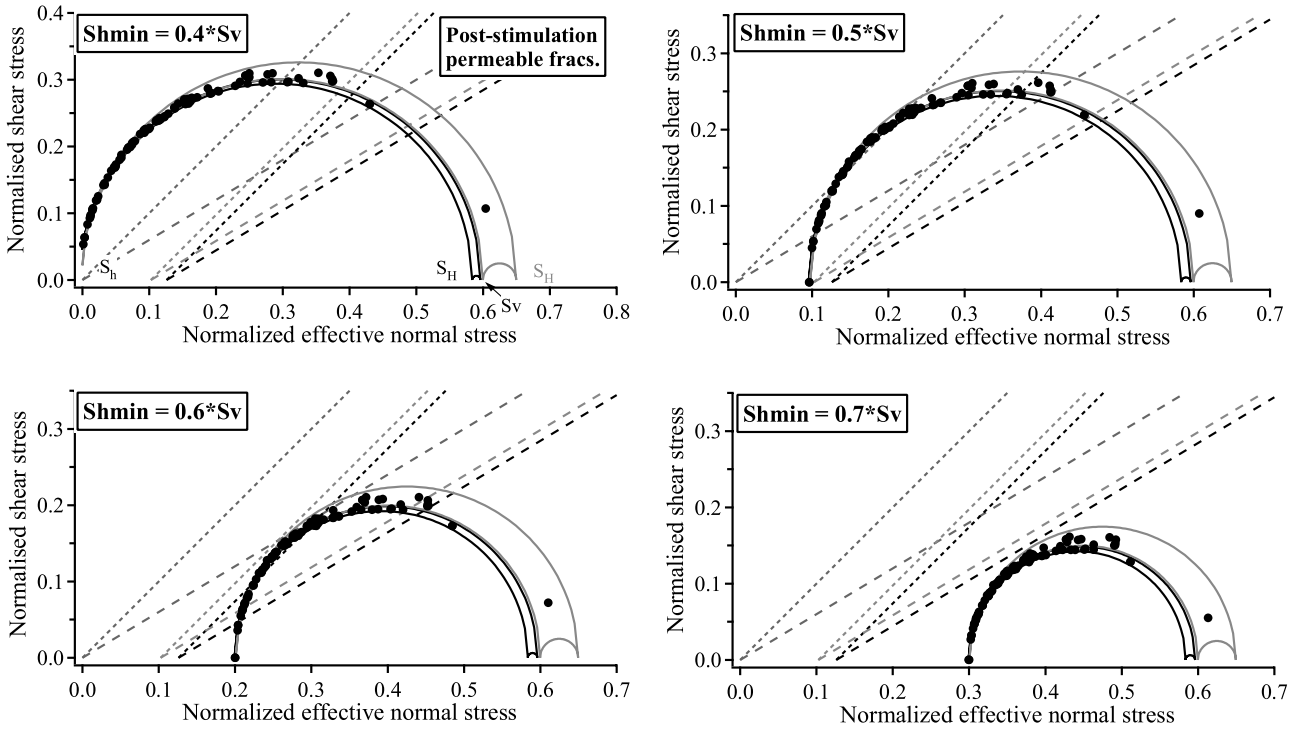

Figure 8. Results of critical stress analysis obtained using four different S_{hmin} magnitude profiles, the other stress parameters taking the standard model values. Increasing S_{hmin} to $0.6S_V$ results in all nonpermeable fractures lying below the failure line for $\mu = 1$ under pressured conditions, although then the permeable fractures are no longer critically stressed under ambient conditions.

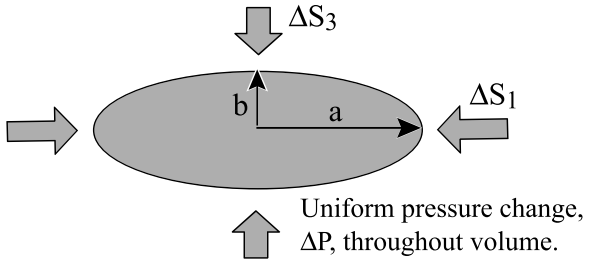

Figure 9. Oblate ellipsoidal geometry of rock volume in which pore pressure is raised uniformly by ΔP_p. The resulting perturbation of the total stress everywhere within the bounds of the ellipsoid are described by the principal perturbing stresses, ΔS_1, and ΔS_3 where $\Delta S_3 < \Delta S_1$. ΔS_3 acts normal to the plane of the larger dimension of the ellipsoid, "a."

over the depth range of interest, an underestimation of 6–7 MPa is not consistent with the data.

3.4. Consideration of Poroelastic Stress Effects

[18] The increase in pore pressure within the rock mass about the well during stimulation perturbs the in situ stress field from that which prevails under ambient conditions. Thus the total stress acting on the fractures will be different during injection. The foregoing analysis assumed that the perturbation was negligible. Support for this view comes from the observation of pressure-limiting behavior during the injections which suggests that jacking occurred. If true, then the poroelastically induced increase in S_{hmin} must be less than 2 MPa since values larger than this would suppress jacking everywhere along the open hole section (Figure 3b). Nevertheless, it is of interest to estimate the poroelastic perturbation expected, and evaluate the impact on the critical stress analysis.

[19] The precise form of the perturbation depends upon the effective Biot constant, α_b, of the rock mass and, most importantly, the geometry of the perturbed volume. *Segall and Fitzgerald* [1998] give expressions for computing the poroelastic stress arising from a uniform pressure increase of ΔP_p within a volume embedded within a uniform, isotropic, poroelastic medium. For the case where the volume has the shape of an oblate ellipsoid of maximum and minimum half axes, a and b, respectively (Figure 9), the change in total stress within the volume is the same everywhere and is described by the perturbing principal stresses:

$$\Delta S_1 = E_1\ \alpha_b\ \Delta P_p \tag{4a}$$

$$\Delta S_3 = E_3\ \alpha_b\ \Delta P_p \tag{4b}$$

where ΔS_1 and ΔS_3 act in plane and normal to the plane of elongation of the ellipsoid. E_1 and E_3 are the Eshelby shape factors whose values are plotted by *Segall and Fitzgerald* [1998] for various aspect ratios, b/a. In reality, the rock volume about the well is not uniformly pressured. Nevertheless, a useful upper bound on the magnitude of the stress perturbation can be obtained by assuming the well bore overpressure of 9 MPa extends to the limits of the microseismic cloud. Figure 10 shows the microseismic cloud resulting from the 93SEP01 stimulation [*Evans et al.*, 2005b]. The geometry of the cloud corresponds reasonably well to an oblate ellipsoid that has its short axis oriented horizontal toward N65°E. Thus the principal horizontal axes of the stress perturbation, ΔS_1 and ΔS_3, are oriented N25°W and N65°E, respectively. Two ellipsoids are shown in Figure 10. The larger has half axes 650 × 650 × 185 m giving an aspect ratio of 1:3.5, and the smaller has half axes 300 × 300 × 150 m giving an aspect ratio of 1:2. From *Segall and Fitzgerald* [1998], the corresponding Eshelby shape factors are $E_1 = 0.55$, $E_3 = 0.22$ for the large ellipsoid, and $E_1 = 0.53$, $E_3 = 0.35$ for the small ellipsoid. Since the small ellipsoid gives the largest stress perturbation, and we are interested here in obtaining an upper bound for the perturbation, this was used in the calculations. Biot's constant was taken as 0.75, again a value considered to be an upper bound. From equations (4a) and (4b), the resulting principal stress magnitudes are $\Delta S_1 = \Delta S_2 = 3.6$ MPa, and $\Delta S_3 = 2.7$ MPa. ΔS_3 is horizontal and oriented N65°E. This perturbation must be added tensor-wise to the ambient stress state to obtain the upper bound on the perturbed stress state. The ambient stress is assumed to be the standard stress state with S_{Hmax} taken as S_V. The effects of the poroelastic component on the stresses resolved on the poststimulation nonpermeable fractures are shown in Figure 11. The inclusion of poroelastic stress in the analysis reduces the cohesive component of strength required to prevent the fractures failing in shear, although it remains 6.5 MPa at 2850 m. Since the poroelastic component used in the calculation was an upper bound, and is probably too large given that it implies jacking would be suppressed throughout the depth range of the open hole, it is concluded that poroelastic stress cannot account for the stability of the fractures.

4. Discussion

[20] The analysis indicates that during the injections, the shear stress acting on the majority of the fractures intersecting the borehole exceeded that which can be supported by friction alone. Almost all of the 95 fractures that were found to be permeable following the injections showed direct or indirect evidence of shearing, consistent with the relaxation of the excess shear stress through slip. However, some 400 fractures showed no evidence of supporting flow or damage. One explanation is that these fractures did indeed fail, but failure did not extend significantly from the well bore. If the radius of the fractures remained small, then slip magnitude and hence dilation would be small, resulting in limited permeability. Moreover, small radius fractures would have less chance of intersecting a network, as required to support flow and produce a detectable temperature perturbation. While this may be true of some of the nonpermeable fractures, it is considered unlikely to apply to most of them since the vast majority showed no evidence of damage on the UBI reflectivity log, in contrast to the permeable fractures (see paper 1). Thus it is concluded that these fractures are stronger than can be ascribed to friction alone. A cohesive component of at least 6 MPa is required to augment a friction coefficient of 1.0 to prevent failure. This value assumes the minimum principal total stress during the injections is 2 MPa greater than given by the standard stress state, due either to error in the ambient stress estimates or to the poroelastic

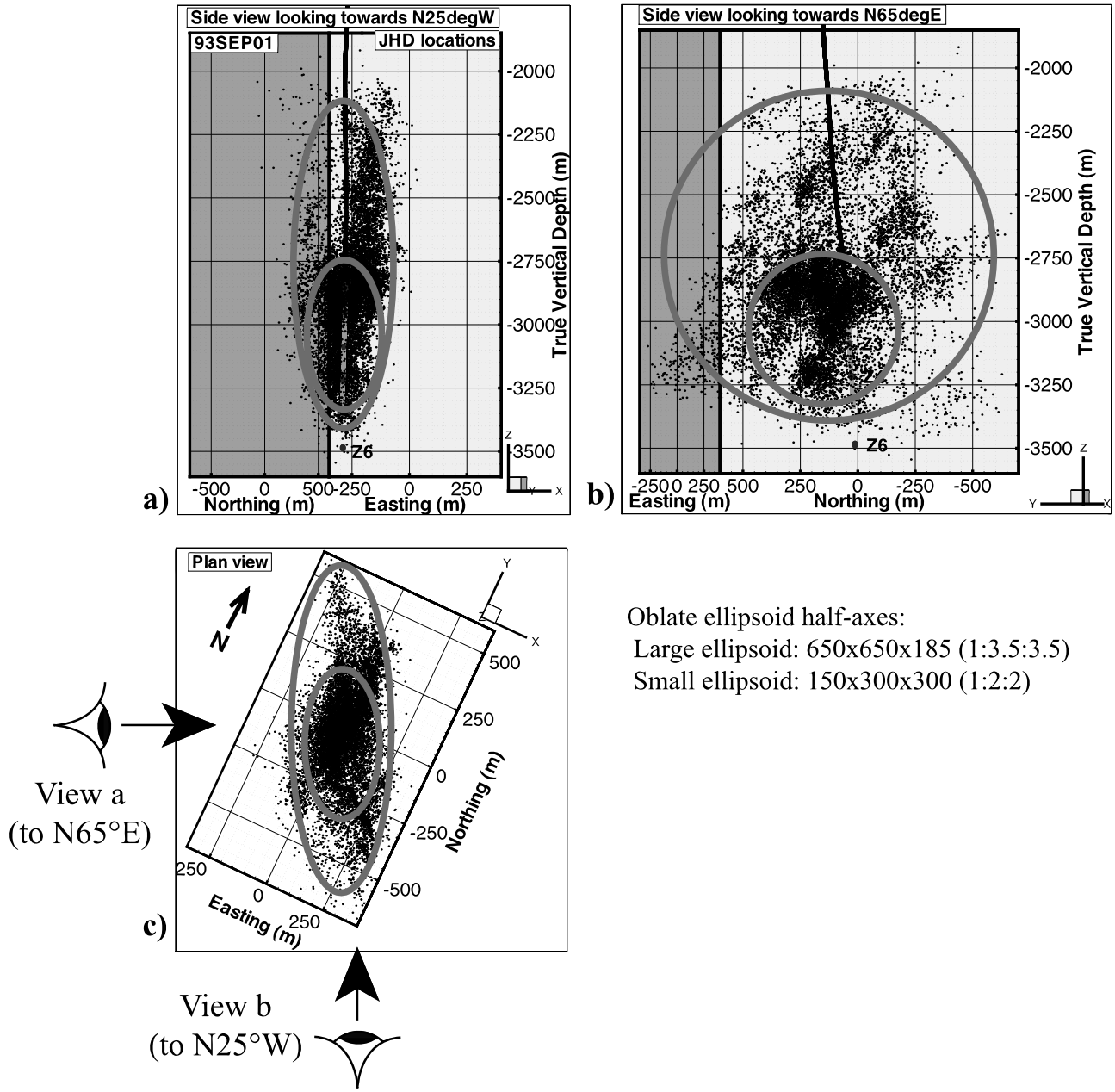

Figure 10. Geometry of microseismic cloud induced during the 93SEP01 injections (see *Evans et al.* [2005b] for details) and the two oblate ellipsoids used to compute the poroelastic stress perturbation.

perturbation (Figure 11). The cohesive component increases to 8.5 MPa if the S_{hmin} profile of the standard stress state is used. Even larger cohesion components are required if lower friction coefficients are assumed. Such strengths suggest well-cemented, fully sealed fractures.

[21] The clustered organization of the permeable fractures and their coincidence with zones of hydrothermal alteration determined from cuttings (Figure 1) suggests that they define the intersection of the well with hydrothermally altered, cataclastic shear zones that are the primary large-scale structural features in the basement (paper 1). Such structures were identified from core from a nearby well and were commonly found to include smaller-scale fractures that were hydrothermally altered and slickensided. The alteration was characterized primarily by the production of illite with minor quartz which is occasionally geodic [*Genter and Traineau*, 1996]. The presence of illite would be expected to weaken the fractures since the friction coefficient of illite at the appropriate pressure and temperature conditions is reported to be approximately 0.4 [*Morrow et al.*, 2000, 1992]. In contrast, most other fractures belong to an older population of isolated, mode 1 type fractures that are narrow and completely filled with calcite with minor chlorite [*Genter and Traineau*, 1996]. As such they are likely to be stronger in shear than the hydrothermally altered fractures. It is reasonable to identify the mode 1, calcite-filled fractures with the impermeable fractures that did not fail during the injections, and to associate the permeable fractures that sheared with the hydrothermally altered fractures that are internal to the

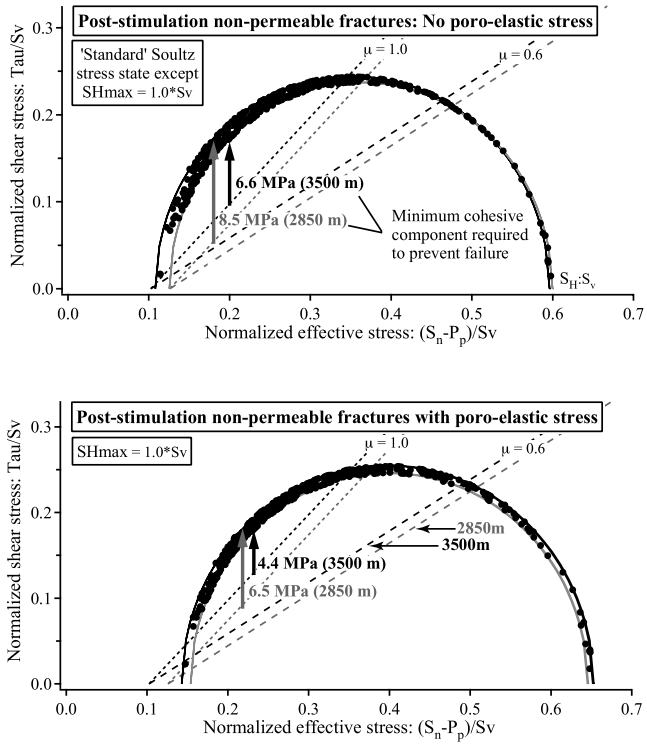

Figure 11. Effect of including the upper bound on the poroelastic stress on the stress analysis. The cohesive component of strength required to augment a friction coefficient of 1.0 in order to prevent failure of the nonpermeable fractures is reduced from 8.5 to 6.5 MPa at 2850 m.

shear zones. Unfortunately, it is not possible to critically evaluate this hypothesis on a fracture-by-fracture basis without core. The profile of alteration shown in Figure 1 is derived from cuttings whose source depth estimates are affected by transit and mixing in the drilling mud, and the frequency of sampling. The resultant smoothing prohibits resolution of alteration on the fracture scale. Nevertheless, it is of interest to use the alteration profile to segregate the fractures into those that occurred within and outside alteration zones, and assess the degree to which critically stressed, permeable fractures tend to be located within alteration zones. The analysis was conducted for the interval 2850–3400 m, which was open during the 93SEP01 injection. The results are shown in Figure 12. For fractures located in altered zones, the fraction of permeable to nonpermeable fractures is 34%, whereas for nonaltered zones, the fraction is 18%. Thus, although permeable fractures tend to be located in altered zones, there are also many impermeable fractures in alteration zones, and some permeable fractures in unaltered zones. The former is not surprising since the mode 1 calcite-filled fractures predate and are possibly precursor fractures of the shear structures and hydrothermal alteration [*Kim et al.*, 2004]. Hence this population of fractures is present in altered and nonaltered zones alike. However, the presence of permeable fractures in unaltered zones must be ascribed to the low resolution of the alteration profile, which would not show the presence of narrow alteration bands around fractures that were outliers to the main structures. All things considered, it seems probable that fractures, which were permeable during the injections, either naturally, or as a consequence of failure, were components of hydrothermally altered, shear structures, and those

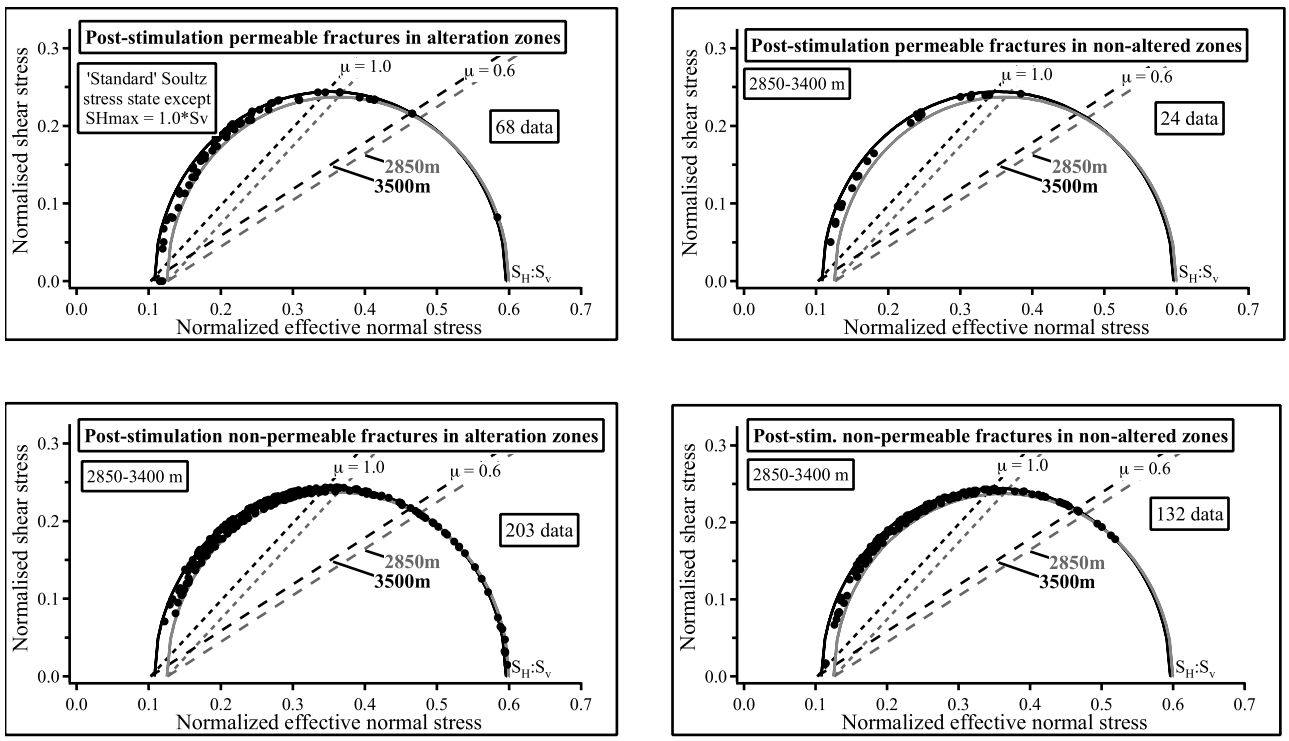

Figure 12. Mohr circle plots of fractures located in (left) altered and (right) nonaltered zones to 3350 m depth as identified from cuttings and indicated in Figure 1c of paper 1.

that remained impermeable did not fail, because they had a higher strength due to the well-sealed nature of their calcite filling.

[22] The stress data indicate that the basement at Soultz is in a critical stress state and hosts high ambient shear stress levels. Expressed in terms of a Coulomb friction strength criterion, a friction coefficient of almost 1.0 is required to prevent failure of the rock mass. The strength is limited by the hydrothermally altered, cataclastic shear zones that are the primary large-scale structures in the basement. Exposures in core and logs show they have widths of centimeters to tens of meters, and are high-angle features that trend mostly NNW-SSE [*Genter and Traineau*, 1996]. As such, they are close to optimally oriented for failure. Most of the 18 naturally permeable fractures in GPK1 are probably core elements of such structures. Two of the most prominent examples are found at depths of 3385–3387 m and 3489–3497 m depth. The latter constitutes flow zone 6 and is shown in Figure 13 (see Figure 15 of paper 1 for the former). The two zones were the sole sources of tube waves in a prestimulation VSP survey and also of upward ambient flow under shut-in conditions (Figure 14 of paper 1). Thus they are likely to be part of the network of connected structures through which fluids move through the basement under natural conditions. Both zones are bounded by prominent, parallel fractures with extensive alteration halos. These, and the other internal fractures, almost certainly contain an abundance of illite, a mineral that has a friction coefficient of 0.4–0.5 [*Morrow et al.*, 2000, 1992]. The stress components resolved across the bounding fractures are indicated in Figure 4a. For both zones, the bounding fractures, and by inference, the parent structures whose large-scale orientation the bounding fractures are taken to indicate, are optimally oriented for shear failure in the standard stress state, and support stress levels that require friction coefficients of almost 1.0 to maintain equilibrium. While there is evidence to suggest that the stress in the vicinity of the zones is perturbed because of shear stress relaxation through slip, it is doubtful that the shear stress is reduced to the levels appropriate for a friction coefficient of 0.4, at least for the lower zone: For a single hydrofracture test at 3508 mRD, some 10 m below the zone, yielded an estimate of S_{hmin} that was 2 MPa lower than that given by the standard stress state, suggesting higher, rather than lower, levels of shear stress (Figure 3b). Thus the evidence suggests that the shear zones have relatively high strength, whereas the illite-rich fractures that constitute them should have low strength. *Zhang and Sanderson* [2001] examined the hydromechanical properties of cataclastic shear zones under critical stress conditions using a numerical code. They found that the apparent strength of the zones was generally higher than the frictional strength of the fractures within them. The additional strength was derived from the cohesion of the intact rock at jogs within throughgoing failure surfaces, and at rock bridges separating the ends of neighboring, slipped, fractures. This provides a reasonable framework for explaining the present observations. However, the presence of the illite could lead to strength contrasts between the fractures and the intact rock that are far more extreme than considered by *Zhang and Sanderson* [2001]. If fractures do have strengths appropriate for illite-coated interfaces, then they cannot have large spatial extent. The

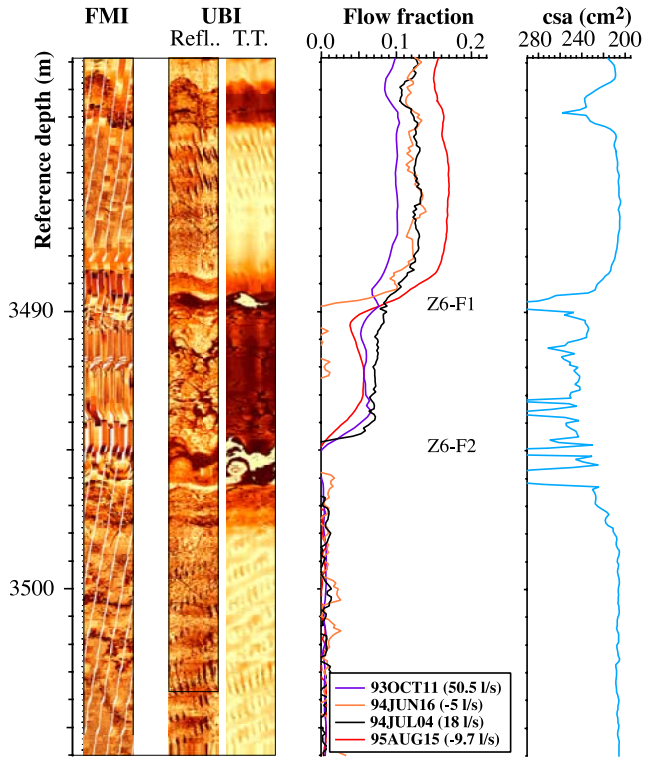

Figure 13. Selection of logs across the shear structure that constitutes flow zone 6. The logs are, from left to right, prestimulation FMI (Formation Micro Imager), poststimulation ultrasonic reflectivity (Refl.), and travel time (TT) from a UBI log, a selection of flow logs for a variety of production and injection tests, and the profile of borehole cross-sectional area (CSA). The flow logs have been corrected for variations in CSA and show that flow takes place predominantly at the subparallel, bounding fractures. These dip at 60–75° to N245–270° and coincide with major borehole spalling, which generally indicates strong hydrothermal alteration. The entire zone has suffered significant alteration.

absence of large, throughgoing, planar slip surfaces is supported by studies of waveforms from microseismic events which indicate an upper limit on the scale of coherent slip of some 10 m [*Evans et al.*, 2005b; *Moriya et al.*, 2002]. Two factors could moderate the effect of the illite in reducing the shear strength of the fractures. One is that illite formation may be restricted to only a fraction of the fracture plane, reflecting channeling of old flow paths during the alteration events. The other is that roughness within the plane of the individual fractures could lead to the weak illite being scraped from asperities under shear, leaving relatively unaltered granite in contact. However, the illite would still be present elsewhere on the fracture surface and thus might still be effective in reducing the friction coefficient of the fracture surface taken as a whole. Regardless of the strength of the individual fractures, it is probable that the strength of the shear structures resides primarily in intact rock bridges and jogs that bring the cohesion of the intact rock into play. The presence of fractures with very low shear strengths would be expected to lead to strong stress heterogeneity within the shear zones.

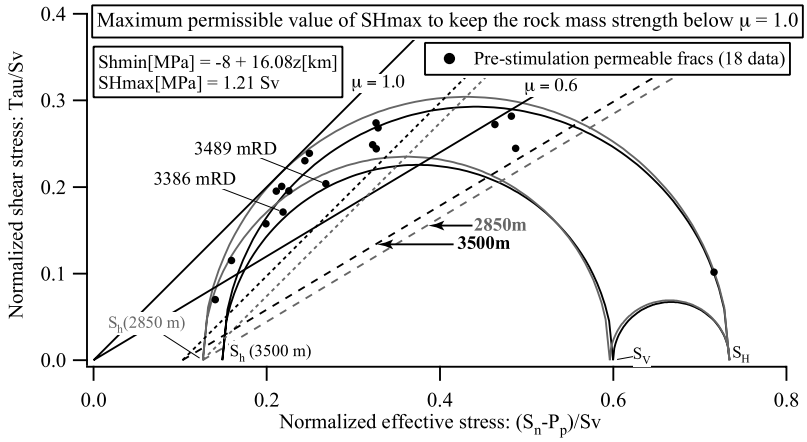

Figure 14. Mohr representation of the stress state that gives the maximum permissible value of S_{Hmax} which is consistent with a crustal strength given by a Coulomb friction law with a friction coefficient of 1.0. The value of S_{hmin} is also the maximum value that is consistent with the data (excluding the data point at 3508 m) and the inference that jacking occurred at the casing shoe for the 12 L s^{-1} and later injection stages. The maximum value of S_{Hmax} is $1.21S_V$.

[23] Acceptance that an upper bound on the strength of the crust is given by optimally oriented faults whose strength is governed by friction with a maximum coefficient of 1.0 places constraints on the maximum value that the maximum horizontal stress can take. It is of interest to compute this since the profile of S_{Hmax} in the Soultz basement is currently uncertain. Using the approximations to the standard stress state given by equations (3a), (3b), and (3c), the limit on S_{Hmax} is $1.10S_V$. If the revised S_{hmin} profile given by equation (3d) is used, then the limit is $1.21S_V$ (Figure 14). S_{Hmax} values greater than these result in ambient shear stress levels on some naturally permeable fractures that require a cohesive component of strength to prevent failure.

5. Conclusions

[24] The crystalline basement at Soultz supports very high shear stress levels that require a rock mass strength equivalent to a Coulomb friction law with a friction coefficient approaching 1.0 to remain stable under ambient conditions.

[25] All naturally permeable fractures (18) were found to be critically stressed. However, so were the vast majority of nonpermeable fractures (some 500). This implies that critical stressing of fractures in a Coulomb friction sense is a necessary but not a sufficient condition for permeability to develop.

[26] Following injections where pressure was maintained at 9 MPa above ambient for up to 11 days, a further 78 fractures were identified as newly permeable. These lay within alteration zones defined from cuttings that are believed to reflect the intersection of the borehole with high-angle, cataclastic shear structures. The newly permeable fractures represent the failure under reduced effective normal stress of small-scale (meters to decameters) fractures that comprise the altered shear structures. These fractures, which tend to be filled predominantly with illite, a mineral that has a low frictional strength, showed evidence of shear, and were critically stressed. However, some 400 fractures did not become permeable during the injections, most likely because they did not fail. To prevent failure requires that their shear strength include a cohesive component of at least 6.5 MPa which augments a maximum allowable frictional coefficient of 1.0. These fractures are thought to be a population of early, mode 1 fractures that predate the shear structures and tend to be completely filled with calcite with minor chlorite. As such, they would be stronger in shear than the altered fractures.

[27] Although the shear structures are composed of fractures that might be expected to have low shear strengths as a consequence of the illite filling, the structures themselves are strong. Their strength is best explained by an internal architecture that involves small-scale fractures connected by relatively intact rock bridges and jogs.

[28] The results are consistent with the view that the strength of the crust is limited by the strength of faults and major structures. However, to keep the strength of the basement at Soultz below the friction limit imposed by a friction coefficient of 1.0 requires that the maximum principle horizontal stress be less than 1.21 times the vertical stress.

[29] An upper bound on the large-scale poroelastic stress induced during reservoir pressurization is given by $\Delta S_1 = \Delta S_1 = 3.6$ MPa, and $\Delta S_3 = 2.7$ MPa. In actuality, the inference that jacking occurred suggests that the minimum principal poroelastic stress was less than 1.5 MPa.

[30] **Acknowledgments.** This work was funded by the Swiss Federal Office of Education and Science as part of the Swiss contribution to the European HDR project at Soultz-sous-Forêts, which is supported mainly by the European Commission, BMBF (Germany), and ADEME (France). I am grateful to SOCOMINE for providing access to the data. Thanks are due to Takashi Okabe of GERD, Tokyo, for discussion and especially to Takatoshi Ito of Tohoku University for discussion and a careful review.

References

Baria, R., J. Garnish, J. Baumgärtner, A. Gérard, and R. Jung (1995), Recent developments in the European HDR Research programme at Soultz-sous-Fôrets (France), in *World Geothermal Congress*, edited by E. Barbier et al., pp. 2631–2637, Int. Geotherm. Assoc., Reykjavik, Iceland.

Barton, C. A., M. D. Zoback, and M. D. Moos (1995), Fluid flow along potentially active faults, *Geology*, *23*(8), 683–686.

Barton, C. A., S. Hickman, R. Morin, M. D. Zoback, and R. Benoit (1998), Reservoir-scale fracture permeability in the Dixie Valley, Nevada, Geothermal Field, paper 47371 presented at SPE/ISRM Eurock '98, Soc. of Pet. Eng., Trondheim, Norway.

Baumgärtner, J., and F. Rummel (1989), Experience with 'fracture pressurization tests' as a stress measuring technique in a jointed rock mass, *Int. J. Rock Mech. Min. Sci. Geomech. Abstr.*, *26*, 661–671.

Bérard, T., and F. Cornet (2003), Evidence of thermally induced borehole elongation: A case study at Soultz, France, *Int. J. Rock Mech. Min. Sci.*, *40*, 1121–1140.

Brace, W. F., and D. L. Kohlstedt (1980), Limits on lithospheric stress imposed by laboratory experiments, *J. Geophys. Res.*, *85*, 6248–6252.

Brudy, M., and M. D. Zoback (1999), Drilling-induced tensile wall-fractures: Implications for determination of in-situ stress orientation and magnitude, *Int. J. Rock Mech. Min. Sci.*, *36*, 191–215.

Byerlee, J. (1978), Friction of rocks, *Pure Appl. Geophys.*, *116*, 615–626.

Cornet, F. H., and T. Bérard (2003), A case example of integrated stress profile evaluation, in *3rd International Symposium on Rock Stress*, edited by K. Sugawara, Y. Obara, and A. Sato, pp. 23–24, A. A. Balkema, Brookfield, Vt.

Cornet, F. H., and R. H. Jones (1994), Field evidence on the orientation of forced water flow with respect to the regional principal stress directions, in *1st North American Rock Mechanics Symposium*, edited by P. P. Nelson and S. E. Laubach, pp. 61–69, A. A. Balkema, Brookfield, Vt.

Darnet, M. (2000), Caractérisation microseismique d'un massif hydrauliquement stimulé, Mémoire de DEA thesis, Univ. Louis Pasteur, Strasbourg, France.

Evans, K. F., T. Kohl, R. J. Hopkirk, and L. Rybach (1996), Studies of the nature of non-linear impedance to flow within the fractured granitic reservoir at the European Hot Dry Rock Project site at Soultz-sous-Forêts, France, report, Swiss Fed. Inst. of Technol./Polydyn. Eng., Zürich.

Evans, K. F., A. Genter, and J. Sausse (2005a), Permeability creation and damage due to massive fluid injections into granite at 3.5 km at Soultz: 1. Borehole observations, *J. Geophys. Res.*, B04203, doi:10.1029/2004JB003168, in press.

Evans, K. F., H. Moriya, H. Niitsuma, R. H. Jones, W. S. Phillips, A. Genter, J. Sausse, R. Jung, and R. Baria (2005b), Microseismicity and permeability enhancement of hydro-geologic structures during massive fluid injections into granite at 3 km depth at the Soultz HDR site, *Geophys. J. Int.*, *160*, 388–412.

Gaucher, E. (1998), Comportement hydroméchanique d'un massif fracturé: Apport de la microseismicité induite, Ph.D. thesis, Univ. de Paris 7, Paris.

Genter, A., and H. Traineau (1996), Analysis of microscopic fractures in granite in the HDR geothermal well EPS-1, Soultz-sous-Forêts, France, *J. Volcanol. Geotherm. Res.*, *72*, 121–141.

Heinemann-Glutsch, B. (1994), Results of scientific investigations at the HDR test site, Soultz-sous-Forêts, Soultz, France.

Helm, J. A. (1996), The natural seismic hazard and induced seismicity of the European HDR (Hot Dry Rock) geothermal energy project at Soultz-sous-Forêts, France, Ph.D. thesis, Univ. Louis-Pasteur, Strasbourg, France.

Hickman, S., M. D. Zoback, and R. Benoit (1998), Tectonic controls on fault-zone permeability in a geothermal reservoir at Dixie Valley, Nevada, paper 47213 presented at SPE/ISRM Eurock '98, Soc. of Pet. Eng., Trondheim, Norway.

Ito, T., and K. Hayashi (2003), Role of stress-controlled flow pathways in HDR geothermal reservoirs, *Pure Appl. Geophys.*, *160*, 1103–1124.

Ito, T., and M. D. Zoback (2000), Fracture permeability and in-situ stress to 7 km depth in the KTB Scientific Drillhole, *Geophys. Res. Lett.*, *27*(7), 1045–1048.

Ito, T., K. Evans, K. Kawai, and K. Hayashi (1999), Hydraulic fracture reopening pressure and the estimation of maximum horizontal stress, *Int. J. Rock Mech. Min. Sci.*, *36*(6), 811–826.

Kim, Y.-S., D. C. P. Peacock, and D. J. Sanderson (2004), Fault damage zones, *J. Struct. Geol.*, *26*, 503–517.

Klee, G., and F. Rummel (1993), Hydrofrac stress data for the European HDR research project test site Soultz-sous-Forêts, *Int. J. Rock Mech. Min. Sci. Geomech. Abstr.*, *30*, 973–976.

Moriya, H., et al. (2002), Detailed fracture system of the Soultz-sous-Forêts HDR field evaluated using microseismic multiplet analysis, *Pure Appl. Geophys.*, *159*, 517–541.

Morrow, C., B. Radney, and J. Byerlee (1992), Frictional strength and the effective pressure law of montmorillonite and illite clays, in *Fault Mechanics and the Transport Properties of Rocks*, edited by B. Evans and T.-F. Wong, pp. 69–88, Springer, New York.

Morrow, C., D. E. Moore, and D. A. Lockner (2000), The effect of mineral bond strength and absorbed water on fault gouge frictional strength, *Geophys. Res. Lett.*, *27*(6), 815–818.

Okabe, T., and K. Hayashi (2000), Estimation of stress field by using drilling-induced tensile fractures observed at well TG-2 and a study of critically-stressed shear fractures based on stress field, in *World Geothermal Congress*, edited by E. Iglesias et al., pp. 1533–1538, Int. Geotherm. Assoc., Reykjavik, Iceland.

Okabe, T., T. Kajiwara, H. Nakata, K. Hayashi, S. Yokomoto, and S. Miyazaki (2002), In-situ stress field and permeable fractures in the Akinomiya Geothermal Field, Japan, *Trans. Geotherm. Resour. Counc.*, *26*, 237–243.

Plenefisch, T., and K.-P. Bonjer (1997), The stress field in the Rhine Graben area inferred from earthquake focal mechanisms and estimation of frictional parameters, *Tectonophysics*, *275*, 71–97.

Rutqvist, J., C. F. Tsang, and O. Stephansson (2000), Uncertainty in the maximum principal stress estimated from hydraulic fracturing measurements due to the presence of the induced fracture, *Int. J. Rock Mech. Min. Sci.*, *37*, 107–120.

Scholz, C. H. (1990), *The mechanics of Earthquakes and Faulting*, 439 pp., Cambridge Univ. Press, New York.

Scotti, O., and F. H. Cornet (1994), In-situ evidence for fluid-induced aseismic slip events along fault zones, *Int. J. Rock Mech. Min. Sci. Geomech. Abstr.*, *31*, 347–358.

Segall, P., and S. D. Fitzgerald (1998), A note on induced stress changes in hydrocarbon and geothermal reservoirs, *Tectonophysics*, *289*, 117–128.

Shamir, G., and M. D. Zoback (1992), Stress orientation profile to 3.5 km depth near the San Andreas fault at Cajon Pass, California, *J. Geophys. Res.*, *97*, 5059–5080.

Zhang, X., and D. J. Sanderson (2001), Evaluation of instability in fractured rock masses using numerical analysis methods: Effects of fracture geometry and loading direction, *J. Geophys. Res.*, *106*, 26,671–26,687.

Zoback, M. D., and J. H. Healy (1984), Friction, faulting and "in situ" stress, *Ann. Geophys.*, *2*, 689–698.

Zoback, M. D., and J. Townend (2001), Implications of hydrostatic pore pressures and high crustal strength for the deformation of intraplate lithosphere, *Tectonophysics*, *336*, 19–30.

K. F. Evans, Engineering Geology, Department of Earth Science, Swiss Federal Institute of Technology (ETH), CH-8093 Zürich, Switzerland. (keith.evans@erdw.ethz.ch)

APPENDIX 5 - hydraulics

APPENDIX 5 (a)

Reinhard Jung, Torsten Tischner, Jörg Baumgärtner, Dimitra Teza, Patrick Nami and Marion Schindler, 2008, Review of hydraulics stimulation tests and hydraulic experiments at Soultz, *paper presented at the EHDRA Scientific Conference, Soultz-sous-Forêts*, September 24-25, 2008.

EC Contract SES6-CT-2003-502706

PARTICIPANT ORGANIZATION: BGR……

Related with Work Package……WP1/WP5

Related with Working Group……WG4

REVIEW OF HYDRAULICS STIMULATION TESTS AND HYDRAULIC EXPERIMENTS AT SOULTZ

Jung R*., Tischner T.**, Baumgärtner J.***, Teza D.***, Nami. P.****, Schindler M.**

**JUNG-GEOTHERM, Isernhagen, Germany*

***Federal Institute for Geosciences and Natural Resources (BGR), Hannover, Germany*

****BESTEC GmbH, Kandel, Germany*

*****Leibniz Institute for Applied Geophysics (GGA-Institut), Hannover, Germany*

e-mail: jung.geotherm@googlemail.com

EXTENDED SUMMARY

A great number of hydraulic tests had been performed in the crystalline basement of the Soultz test-site in the period 1988 to 2008. The tests were performed in 3 different depth levels 1400 m – 2000 m, 2800 m – 3600 m and 4400 m – 5000 m and comprised pre-frac injection and production tests for determining the natural hydraulic properties of the granite, massive water frac-tests for creating or stimulating large fracture systems in the granite, post-frac injection and production experiments for studying the hydraulic properties of the created fracture systems and hydraulic circulation tests for studying the hydraulic connection between the boreholes established by these fracture systems. The most important results of the hydraulic investigations can be summarized as follows:

PRE-FRAC INJECTION AND PRODUCTION TESTS

Water transport in the granite at the Soultz test site was dominated by a few discrete faults with transmissivity values ranging from about 10-13 m^3 to some 10-11 m^3.
The effective permeability of the granite without these faults was some 10-17 m^2 with no obvious decrease with depth. This value is representative for an open hole length of almost 4000 m. It is about two orders of magnitude higher than the permeability of the granite matrix and may be attributed to the contribution of several thousand of joints and tens of faults or fracture zones identified in the uncased sections of the boreholes.
The formation fluid pressure at all depths levels was in balance with the hydrostatic head produced by the fluid coulomb in the boreholes when these were filled with formation fluid in thermal equilibrium with the surrounding rock. This indicates that the hydraulically dominant faults are open to the surface.

WATER FRAC TESTS

All massive water frac-tests performed at different depth levels in 4 boreholes showed remarkable similarities in the following aspects:

- Single discrete structures had been activated in shear mode as was indicated by the spatial distribution and the waveform of induced seismicity.
- The size of these structures was proportional to the water volume injected during the tests and was roughly 1km^2 per 10,000 m^3 of injected fluid.
- All seismically activated structures were almost vertical. Their strike directions of 135º to 180º are all in the region most suitable for strike slip movement if an orientation of the maximum horizontal stress of 170º ± 15º is assumed.
- Flow logs performed during the tests showed that in all cases the majority of the injected water was consumed by only a few discrete fractures. In at least one case a long axial fractures was created extending for several hundred meters along the borehole wall thus proofing, that despite of the presence of hundreds of joints fresh fractures can be created.
- Some of the seismically activated structures had straight boundaries in one or the other direction. This may indicate intersections with major faults hindering the structure to grow further in this direction.
- The injection pressure was almost constant when the flow rate was constant and increased only moderately or remained constant when the flow rate was increased. It increased significantly with depth.

In summary these observations show, that “stimulation” is a stress and (injected) volume controlled process and is not directly dependent on the a priori hydraulic properties of the fractured rock provided no major (hydraulically dominant) fault is involved in the process. Yet it is not quite clear whether the activated structures are natural discontinuities or fresh fractures being created during the stimulation process. Since natural discontinuities with appropriate orientations may in most cases be present in the rock this question is not of major practical concern.

POST FRAC INJECTION TESTS

All post-frac injection or production tests demonstrated that the hydraulic properties of the activated structures achieved at the end of the frac-tests were perfectly pre-served during depletion of the fluid pressure. Specifically the injectivity index determined by post-frac injection tests proofed to be equal to the injectivity index at the end of the frac-test. This differs completely from the classical hydro-fracturing models used in the oil- or gas industry. These tensile fracture models assume that fractures will deflate and will finally close when the fluid pressure in the fracture drops below the normal stress acting on the fracture plane and that proppants have to be placed within the fractures to keep them open. The different behavior of the fractures produced

during massive water-frac tests in granite can be explained by a self propping effect resulting from the mismatch of the two opposite rough and uneven fracture surfaces after shearing.

The fracture transmissivities derived from the post-frac tests were between 10-13 and some 10-12 m^3. These values are at the upper limit for propped fractures and show that the application of proppants in granite is not necessary or may even be harm full in terms of fracture transmissivity. Nevertheless the fracture transmissivities achieved in Soultz are still too low if flow rates in the range of 100 l/s are to be obtained with one or only a few fractures.

All post-frac tests showed a square-root or fourth-root of time behavior of the pressure. The same is normally ob-served after conventional hydro-fracturing tests in oil- and gas reservoirs and is characteristic for linear or bilinear fracture flow. For fractures in oil- or gas-reservoirs where the fracture-length is generally much higher than its height this behavior is to be expected. In the granite at Soultz where the height of the fractures is similar to their length and where their interceptions with the boreholes is rarely longitudinal this clear flow characteristic is surprising and needs to introduce rather long highly conductive flow channels connecting the boreholes to the fractures. Those channels are also required to explain the very long duration of the linear or bilinear flow period at Soultz.

For the upper HDR-systems in the depth range 2800 m to 3600 m a constant pressure boundary was determined from the post-frac test results indicating that the activated fractures had been connected to a highly permeable fault several hundred meter distant from the borehole. For the lower system (4400 m – 5000 m) this was not the case and it seems likely that here the activated fractures are completely imbedded in the rock mass.

CIRCULATION TESTS

The results of the circulation tests agreed quite well with the fracture-transmissivities derived from the single well tests. Indeed was the hydraulic connection slightly better than was predicted from the single well results. This proofs that there is no hydraulic barrier between the factures activated from one borehole and those activated from the other(s) or even that both fracture sets are identical. The only exception was the rather poor connection between GPK4 and the two other wells GPK3 and GPK2 in the deeper system.

Borehole interference tests showed a relatively high storage coefficient of the interconnecting fractures of about 10-9 m/Pa. This value is too high for one a few discrete fractures. On the other hand tracer tests yielded a quite low break-through volume, which could be explained by assuming a single fracture between the boreholes with an aperture of about 1 cm or less. Combining both observations we conclude that flow between the boreholes takes place either on discrete fractures with a seam of broken or altered rock or on fractures with a step-like path, consisting of shear and tensile elements.

APPENDIX 5 (b)

Keith Evans, Robert Hopkirk, Reinhard Jung, Patrick Nami, Marion Schindler, Dimitra Teza and Torsten Tischner, 2008, Milestone events & key observations in thermics, stress and hydraulics at Soultz (1987-2002), *paper presented at the EHDRA Scientific Conference, Soultz-sous-Forêts,* September 24-25, 2008.

EC Contract SES6-CT-2003-502706

PARTICIPANT ORGANIZATION NAME: ETH Zurich

Related with Work Package 5 +

Related with Working Group 4

MILESTONE EVENTS & KEY OBSERVATIONS IN THERMICS, STRESS AND HYDRAULICS AT SOULTZ (1987-2002)

Keith Evans[1], Robert Hopkirk[2], Reinhard Jung[3], Patrick Nami[4], Marion Schindler[5], Dimitra Teza[5], Torsten Tischner[6]
1) Dept. of Earth Sciences, ETH-Zürich, Switzerland
2) Polydynamics Engineering, Männedorf, Switzerland
3) JUNG-GEOTHERM, Isernhagen, Germany
4) Leibniz Institute for Applied Geosciences (GGA), Hannover, Germany
6) Bestec GmbH, Kandel, Germany
6) Federal Institute for Geosciences and Natural Resources (BGR), Hannover, Germany
e-mail: keith.evans@erdw.ethz.ch

ABSTRACT

In 2007 EHDRA decided that each Workgroup should produce a timeline-structured summary of key events and milestones in their area of expertise that have impacted the Soultz project since its inception. Here we present the current version of the summary of observations pertaining to thermics, stress and hydraulics prepared by Work Group 4 (Seismo-hydraulics). The work is still in progress: The task of expanding and writing commentary to the initial base-listing of events and observations has so far only reached 2003. Furthermore, Figures have yet to be included; and a thematic discussion section added. These elements will be developed during the next year.

EVENTS & MILESTONES

1987: GPK1 drilled to 2002 (582 m open hole) and stimulated

A surprise in drilling this first test hole into granite at the Soultz site was that the temperature at 2 km was only 140℃, instead of the 200℃ that were expected from the thermal gradient in the first km (100℃/km). Althou gh not recognised until later, this reflected active convection in the granite basement.
The ~600 m of open hole which extends almost to the granite top, was subjected to a comprehensive series of hydraulic tests using packers to isolate intervals. The program and results are reported in (Jung, 1991). Most facets of rock mass hydraulic behaviour seen in later, deeper project phases were manifest in the tests.
Difficulty was encountered with the use of inflation packers which tended to have short operational lifetimes owing to a combination of temperature and aggressive formation fluid (Rummel and Baumgärtner, 1991, Jung, 1991). This problem essentially prohibited the use of inflation packers in later phases of the project and led to the development of aluminium packer technology (Klee and Hegermann, 1995).
Pre-stimulation tests (e.g. 88MAY02) showed a reservoir production impedance of 1.7 MPa/l/s, with almost all production derived from a fracture zone at 1813 m. The remainder of the well had an impedance of less than 17 MPa/l/s, corresponding to an equivalent porous media (EPM) permeability of $< 3x10^{-17}m^2$. During testing, accidental overpressuring of the well led to a further zone near the bottom of the hole becoming active. Temperature logs suggest this zone consists of a 24 m long newly-induced axial fracture that intersects a natural fracture zone. The collective zone had an initial production impedance of 3.3 MPa/l/s (Jung, 1991?), and was subject to three focussed stimulation injections through a packer over a 2 year period, with progressively larger volumes and flow rates of 3 l/s (88DEC13), 7 l/s (91JUL11) and 15 l/s (91JUL18). In all three cases, the peak downhole overpressure was 6.0-6.5 MPa, indicating pressure-limiting behaviour. As a consequence of the injections, the production impedance of the zone was progressively increased to 0.24 MPa/l/s at 0.9 MPa drawdown, representing a tenfold increase.
Analysis of well test transients and the observation that pressure perturbations dissipated within a day indicated that the well was connected to a fault or fracture zone of large capacity that acted as a constant potential boundary. The well-test transients also showed that the impedance to both production and injection was non-Darcy, and had a turbulent-like component (Jung, 1992).
The shut-in pressure of injections suggested the minimum principal horizontal stress, Shmin is about 50% of the vertical stress (Rummel and Baumgärtner, 1991, Jung, 1991), which is typical of graben situations (Jamison and Cook, 1980). This implies a critical stress state where only small increases in pore pressure are required to produce shearing of optimally-oriented fractures (Barton et al., 1995, Evans, 2005). Breakouts and drilling-induced tension fractures indicated S_{Hmax} was oriented approximately N-S (Tenzer et al., 1992). Fault plane solutions to microearthquakes were a mix of strike-slip and normal, suggesting that $S_{Hmax} \approx S_V$.

1991 EPS1 drilled down to 2200 m depth and cased to 2007 m (193 m open hole)

The well was not tested until 1994 and was never stimulated. The initial reservoir impedance of the ~200 m open hole section to injection at 3 MPa was 15.4 MPa/l/s (94Apr08), but this decreased with higher pressure in later tests, particularly when downhole overpressure exceeded 4 MPa (Jung, field report?). This is close to the overpressure of 4.7 MPa required for jacking (Evans et al., 1996), as indicated by stress measurements. Four flow zones were identified in the well. Aluminium packers were successfully used for the first time to conduct hydraulic fracture stress tests at two locations near the hole bottom (Klee and Rummel, 1993). The results support the view that S_{hmin} is about 50% of the vertical stress.

1992 GPK1 extended to 3590 m (740 m open hole) and stimulated.

The temperature gradient continued to decline with depth averaging less than 10°/km between 2000 and 3000 m, before increasing again in the lowermost few hundred metres. This essentially confirmed that convection was taking place within the granite (Le Carlier et al., 1994, Pribnow and Schellschmidt, 2000). The bottom-hole temperature at 3.6 km was 160°.

Practically all facets of hydraulic behaviour observed in the shallow tests to 2001 m also apply to this deeper interval. Prior to stimulation, evidence of natural permeability was seen at seven or so hydrothermally-altered fracture zones (HAFZ) that crossed the well every 50-100 m, although not all HAFZs were detectably permeable (Evans et al., 2005a). However, only the lowermost of these at 3480 m depth was hydraulically significant and accounted for almost all flow in well tests. The zone had large capacity and an injection impedance of ~1.4 MPa/l/s for flow rates up to 0.4 l/s (Jung et al., 1995b). At higher rates the impedance became turbulent-like and thus impedance increased with flow rate (Evans et al., 1996). The overlying 650 m section of hole that contained six flow points produced negligible flow and had an EPM permeability of ~10^{-17} m^2 (Evans et al., 2005a).

Attempts to perform focussed stimulations using mechanical packers were hampered by packer flow-by (93AUG19, 93OCT01). Eventually, the well was sanded back to 3400 m, and the upper, low-permeability section was stimulated by injecting 20,000 m^3 of water at progressively higher flow rates from 0.15 l/s to 34 l/s (93SEP01). Pressure-limiting behaviour was observed, the maximum downhole overpressure of 9.0 MPa being attained by the 18 l/s stage. Well breakdown began almost immediately, and accelerated once the over pressure exceeded 6 MPa, the onset of detected microseismicity (Evans et al., 2005a, Baria et al., 1995). The breakdown during the early stages reflected progressive impedance reduction of individual flow zones throughout the depth range of the open hole, but this became focussed at the uppermost part of the hole once the limiting pressure was reached (Jones et al., 1995). At this time, jacking conditions were attained near the casing shoe and upward growth of microseismicity commenced. However, at greater depth, the wellbore pressure remained less than Shmin throughout the injection, suggesting shearing accounted for the impedance reduction in the lower section (Evans et al., 2005a). Systematic changes in the geometry of the microseismic cloud with depth are consistent with this (Cornet and Jones, 1994). A second stimulation was performed on the whole well by injecting 20,000 m^2 of water at 40 & 50 l/s (93Oct11). Initial injection pressure was ~1 MPa less than prevailed at the end of the earlier injection despite comparable flow rates at the flow zones, indicating some change had taken place during the 1 month shut-in.

Low-pressure step-rate injection and step-pressure production tests performed after the stimulations showed that the well impedance was the same for both production (94JUN15) and injection (94JUL04), and was governed by turbulent-like losses. Transient modelling demonstrated that the non-Darcy impedance was not just limited to the immediate vicinity of the wellbore, implying that flow paths within the rock mass had low divergence to maintain high flow velocities (Kohl et al., 1998). Modelling also demonstrated that the flow paths led to structures of large hydraulic capacity (i.e. constant potential features) (Jung et al., 1995b, Kohl et al., 1997). Spinner logs identified six flow zones, all of which showed turbulent-like impedance characteristics (Evans et al., 1996, Evans et al., 2005b). Some 50% of the flow occurred in a complex 80 m zone extending below the casing shoe, and the remainder was distributed between five discrete zones spaced every 100-150 m along the well. Importantly, the flow profile differed between injection and production tests, even though the wellhead impedance was the same, more flow entering the rock mass at a zone at 2950 m during injection at the expense of flow at a zone near 3225 m. This observation implies that a flow diversion between two zones 275 m apart was occurring which not change the net impedance. It follows that the two zones must be linked by a flow path of negligible impedance, possibly defined within a major microseismic structure that extends over 300 m near the zones, and that the impedance governing fluid exchange between these zones and the far-field must be common to both and lie beyond these zones, as shown in Figure 1 (Evans et al., 2005b).

The injection flow profile defined by this distribution did not change with injection pressure and was essentially the same as prevailed at the end of the simulation injections, suggesting that a relatively stable 'propped' network of flow paths had been created. The injectivity of the well increased 15 fold as a consequence of the injections, and 200 fold for the uppermost 650 m. The injectivity of the major HAFZ at 3480 m that was dominant prior to the stimulation increased by a factor of 2.

Five of the six major flow zones correspond to HAFZs that were determined to be permeable before stimulation. This suggests that the stimulated flow paths developed within existing, hydraulically-active structures. Repeat ultrasonic televiewer logs indicate that all major flowing fractures suffered dislocations of millimeters to centimetres, both in shear (Poitrenaud, 1994, Cornet et al., 1997), and opening mode (Evans, 2001, Evans et al., 2005a). The major flowing fractures tend to be accompanied by swarms of newly-permeable fractures that lie within the band of vein alteration about the major flowing fracture. These fractures support only minor flow, and show evidence of damage, most likely through shearing since they are critically-stressed (Evans et al., 2005a). There is little evidence for hydrofracture propagation from the well. Drilling-induced tension fractures occur more or less continuously from the casing shoe to 3250 m in the pre-stimulation fracture imaging logs (Bérard and Cornet, 2003). Despite this, almost all flow during stimulation enters the rock mass at the HAFZs.

Several wells sampling pore pressure near the top of the granite showed a reaction during the stimulation injections suggestive of communication through diffusion.

1995 GPK2 drilled to 3876 m (665 m open hole) some 450 m SSE of GPK1 and stimulated

During drilling, a HAFZ intersected at 2110 m proved so transmissive that mud laden with cuttings ascending the annulus flowed into the feature rather than to the surface. No cuttings or fluid were recovered from below 2110 m, demonstrating the enormous capacity that fracture zones within the granite can have.

The initial EPM permeability of the hole was determined before and after running the 7" casing when the open hole lengths were 2454 m and 665 m respectively. Prior to casing, a 15 l/s injection (95FEB02) was performed on the interval 1422 m - 3876 m. Temperature logs indicated more than 95% of the flow entered the rock mass at the fracture zone at 2110 m where the differential pressure was 0.53 MPa, implying a transmissivity of 3.7e-4 m^2/s (Jung, field report, 1995). The injection impedance of the entire 2454 m open-hole section of 0.03 MPa/l/s implies an EPM permeability of 5e-15 m^2. This compares with an EPM permeability for the 1766 m long section below the zone of less than 2e-16 m^2.

After casing the well to 3211 m, two 50 minute injections (95FEB10) were performed at 8.3 l/s to test the casing seal. Hydraulic data for these tests were not recorded, but it is reported that wellhead pressure rose to 8.0 and 8.6 MPa, and was probably still rising at shut-in (Socomine progress report, 1995). These data imply impedance of the 665 m open-hole section was at least 1 MPa/l/s. Spinner logs run

during these tests indicated 14% of flow entered the formation at a double-fracture at 3245 m, 18% in a continuous zone extending 30 m below the fracture, ~13% at 3370 m, 12% between 3460 and 3480 m, and 13% below this point. Thus, relatively little flow entered in the lower half of the well. Several months later, a step-rate injection that attained steady-state was performed on the open hole at rates of 0.6 and 1.0 l/s and a maximum differential pressures of 1.55 and 2.75 MPa respectively (95JUN10), implying the reservoir impedance at these flow rates was Darcian and equal to 3 MPa/l/s, or an EPM permeability of 1.4e-16 m^2 (Jung et al., 1995a, Evans et al., 1996). This value is a lower limit of the natural impedance since it is possible that stimulation occurred during the earlier, relatively high pressure injection. The flow profile

A novel stimulation technique that used a heavy brine to begin the injection was first tried on GPK2. The intention was to increase the hydrostatic gradient along the open-hole section thereby maximising the pressure attained at deeper intervals during the 'fracture initiation' phase. Thus a 'pre-pad' injection of 208 m^3 of heavy brine (ρ=1.18 gm/cc) was followed by 316 m^3 of formation brine (ρ=1.06 gm/cc) at 31 l/s (95JUN14). After a brief shut-in, injection resumed with 10,000 m^3 of formation fluid grading to 18,000 m^3 of fresh water injected at flow rate steps increasing from 13 l/s to 55 l/s (95JUN16). The well GPK1, which was shut-in, reacted almost immediately. Spinner logs in GPK2 indicate that at the end of the stimulation, flow entered the formation primarily at three zones: ~30% near the top of the open hole between 3215 and a prominent double fracture at 3237 m (25%), 30% across a broad zone with many flow points between 3300-3350 m; and 40% below 3448 m with 15% entering at a 2 m long vertical fracture that became progressively more active during the stimulation. Flow logs could not be run below 3470 m because of an obstruction. Identification of the nature of these extended zones of permeable fractures was hampered by the absence of cuttings.

A step-rate injection test conducted after stimulation (95JUL01) indicated the impedance to flow had been substantially reduced but was now turbulent-like (Kohl et al., 1996). Remarkably, the pressure-flow relation was very similar to that of GPK1, which had been stimulated with comparable volumes and maximum flow rates, although more flow entered in the lower part of the hole than was the case for GPK1. At 1.5 MPa downhole overpressure, the flow rate prior to stimulation was 0.6 l/s, and 12.5 l/s afterwards, indicating a 20-fold improvement in impedance.

The GPK1-GPK2 system was subjected to several trial circulations using GPK2 as the injection well and GPK1 as the production well. In the first test, GPK1 was produced under buoyancy drive through a choke at a flow rate of 15 l/s and GPK2 injected first for 6 days 15 l/s and then 9 days at 21 l/s (95JUL09). The test was terminated by a leak at the GPK2 wellhead assembly. The GPK1 production rate remained constant, in contrast to the decline observed in an earlier production tests without GPK2 injection (94JUN15). A downhole pump was then deployed at 380 m in GPK1 and a balanced circulation conducted for 9 days at the higher flow rate of 21 l/s (95AUG01). The circulation was terminated by the development of a leak at the GPK2 casing shoe. A stable drawdown in the pressure of GPK1 of ~2.5 MPa was reached after about 7 days.

GPK2 was subject to a further stimulation in 1996 with the injection of 27,000 m^3 of water at rates of 25, 46 and 78 l/s (96SEP18). Pressure at the casing shoe increased above the expected level of Shmin by 2-3 MPa. However, the excess is not large and essentially consistent with jacking with small entrance losses. Spinner logs, which could now be run to 3600 m because of the removal of an obstruction, showed that the flow profile remained largely unchanged from that prevailing at the end of the 1995 stimulation. Some 40% of the flow continued to enter below 3448 m, although the vertical fracture at 3448 m took a higher fraction of that flow (~25%). A step-rate test (96SEP29) following the stimulation showed the impedance remained turbulent-like, but had been reduced by a further 30% such that a 3.6 MPa downhole overpressure drove 25 l/s rather than 19 l/s following the 1995 stimulation, and 1.3 l/s using the initial Darcian impedance of 3 MPa/l/s.

1997 4 month circulation tests (97Jul12)

In summer 1997, the 3.0-3.5 km system was subject to a 4 month long, more-or-less continuous closed-loop, balanced circulation at ~ 24 l/s. Fluid was produced from GPK2 through a downhole pump that produced an estimated downhole drawdown of 3.0 MPa. Surface pressure was maintained at ~1.2 MPa to prevent scaling and CO2 outgassing before passing through the GPK1 reinjection pump.

Remarkably, reinjection pressure declined from 4.5 MPa at the start of the test to 2.0 MPa at the end, reflecting a decrease in injection impedance. Most of this decrease occurred in an episode lasting a few days in the middle of the test, although a gradual decline was evident throughout the test. The latter was primarily due to a gradual reduction in the impedance of a flow zone at 3250 m, possibly due to the effects of cooling stresses which could widen fracture apertures at the borehole and thus reduce entrance losses. However, the large, mid-test drop in injectivity is more complicated. The decline began shortly after the termination of the practice of adding an anti-scaling agent (Aquaprox) to the fluid prior to reinjection. A possible explanation of this coincidence is that the agent had somehow led to the build-up of deposits on the walls of the fracture entry points during the first part of the test, and this build-up precisely masked an increase in aperture resulting from the cooling stresses. Termination of the supply of Aquaprox led to the gradual depletion of the deposits, thereby eliminating the masking of the accrued effects of increased aperture on entrance losses. The impedance drop associated with the event occurred at both the flow zone at 3250 m that showed the gradual decline, and also a permeable fracture at 2860 m which is known to have suffered 2 cm of shear during the 1993 stimulation program (Evans et al., 1998). The impedance drops at these points resulted in increased focussing of flow and hence a change in the injection flow profile of the well, the first to have occurred since the 1993 stimulations. Although the impedance drops appear to indicate significant cooling-promoted reductions in pressure drops along flow paths leading from the well, it is unclear how far along the paths the implied aperture-increases extend.

The net impedance following the event produced a circulation impedance at the surface of 0.1 MPa/l/s, which the first time that this long-standing commercial target has been attained in any EGS system, and then for the largest well separation of 450 m ever attempted.

The production temperature increased throughout the circulation from 130℃ to reach 142℃ by the end. T he increase probably reflects heating of the cooled rock volume around the well which had been cooled by the earlier stimulation injections. The productivity of GPK2 declined only slightly during the circulation, perhaps reflecting higher entrance losses due to thermo-elastic effects on the producing fractures. The usable thermal power produced assuming an injection temperature of 40℃ attained ~11 MWt at the end of the test. The salinity of the production fluid increased during the test, reflecting a progressively larger fraction of formation water was present. This, together with the relatively small quantities of tracer recovered from tests indicates that production was accessing fluid stored in the 'far-field', probably in the network of major fracture zones and faults present in the rock mass. Nevertheless, the tracer results also showed a rapid response, indicating that at least some of the principal flow paths linking the wells were direct.

1999 GPK2 extended to 5024 m TVD (638 m open hole) and stimulated in 2000 (00JUN30)

Development of the 5 km deep system began in spring 1999 when the existing well GPK2 was extended from 3876 to 5084 m with open hole below 4431 m (all depths are measured along the hole from ground level). Prior to extension, the existing casing was removed and a downhole pump plus 150 m of tubing which had been lost in spring 1995 were fished. In addition, the major loss zone at 2110 m that had taken all cuttings during the initial drilling was plugged using a HMR (High Magnesium Resistant) cement which had been developed for the high temperature and high salinity conditions of Soultz. The success of the operation was demonstrated by the termination of the sensitivity of pressure in neighbouring well EPS1 to operations in GPK2. Leak-off into the stimulated fractures of the 'upper reservoir' between 3200 and 3600 m was not large enough to require remedial action. The hole was then reamed and extended to 5048 m with an 8-1/2 inch bit, and a 3 m core taken. A 33 m long 6-1/4 inch pilot bore was drilled at the hole bottom with the intention of conducting hydrofracture stress measurements. However, these were never conducted due to hole stability fears. Wireline logs including temperature, spectral gamma, ARI and UBI were run, the latter 3 only above 4650 m because of temperature limitations. The hole was sanded back and a 7 inch casing run with the shoe at 4431 m. The casing weight was supported by metal packers set above the casing shoe and ~260 m of cement. This was overlain by 460 m of fly-ash, the annulus being open above ~3740 m, just below the 'upper reservoir'. The sand was cleaned-out to 5069 m MD leaving 638 m of open hole.

A wireline gyro survey revealed that the hole becomes progressively deviated from vertical below 3870 m, the deviation reaching 26° at 4450 m before declining to 16° at TD. The deviation is consistently to the NW, suggesting it is controlled by a rock mass attribute. Severe spalling also occurred near the start of the deviation producing a cave between 3866 and 3891 m. A temperature log run six months after completion showed a bottom hole temperature of 202°C and a gradient in the lower kilometer of 30°C/km. Geological information from cuttings indicate major HAFZs at 4580-4600 and 4775 m, but no significant mud losses were noted at these depths (Genter et al., 1999). There are numerous other minor HAFZs defined by the presence of alteration minerals of illite and calcite, as in the upper reservoir.

Stress information from depths greater than the original bottom is sparse, because the UBI log was severely affected by stick-slip movement arising from the borehole irregularity.

Several hydraulic tests were performed without downhole pressure sensors prior to the stimulation in order to characterize the undisturbed formation and formation water: slug tests (99AUG02) yielded a near-field EPM permeability of 5-13e-17 m^2 (Weidler, 1999); a 5 week pump-assisted production test (99OCT25) conducted at 0.25 l/s attained steady-state and indicated a productivity index of 0.1 – 0.3 l/s/MPa, implying an EPM permeability of 4-12e-17 m^2 (Weidler and Jung, 2000); and a low rate injection test (00FEB25) conducted for 5 days at rates between 0.26 and 0.5 l/s attained quasi steady state conditions in several hours and indicated an injectivity index of 0.2 l/s/MPa, indicating an EPM permeability of 8e-17 m^2. Thus, all tests indicate the EPM permeability of the entire open hole section is of the same order as observed in the upper reservoir. The geochemical composition of the production fluid was also similar to that found in the upper reservoir, and the attainment of steady-state conditions in only a few hours indicates the existence of a large-capacity, hydraulic feature(s) close to the well - again a feature of the upper reservoir. It is of note that although wellhead pressure during the injection test did not exceed 2 MPa, irregularities in the pressure record were observed that suggest stimulation processes were being activated, possibly reflecting shearing on natural fractures. However, no evidence of microseismic emission was detected by a hydrophone in EPS1. None of the observation wells showed a pressure response to the injection which indicates the tightness of casing and the hydraulic isolation of the upper and lower reservoirs.

Attempts to identify flow points along the open hole during the low-rate injection were hampered by difficulty in running the P-T sonde past an enlarged zone at 4680 m. All that could be determined was that a flow entry point exists just below the casing shoe.

The entire open hole section was subjected to a major stimulation injection (00JUN30). Microseismicity was monitored by both an expanded surface network (Cuenot et al., 2008), and also an expanded and renovated downhole network (Dyer, 2001). A total volume of 23,400 m^3 of fluid was injected during 6 days in steps of 31, 41, and 51 l/s (Weidler, 2000). The main injection was preceded by a pad of 800 m^3 of heavy brine (1200 kg/m^3) injected abruptly at 32 l/s to reduce the pressure gradient along the open hole and thus maximise the pressure near hole bottom. The density of the brine was progressively reduced over a 6 hr period by mixing with stored formation water until fresh water injection commenced. All injected fluid was tagged by tracers. The 31 l/s and 41 l/s steps each lasted for ~1 day. Pressure at the casing show rose quickly and peaked at 12 MPa after 6 hrs during the brine-transition, before declining slightly. However, during the final stage, which lasted 4 days, differential pressure slowly but continually increased reaching 13.5 MPa at shut-in. This maximum pumping pressure is only slightly higher than required for stimulation of the upper reservoir and indicates both are critically-stressed (Hettkamp et al., 1998). The pressure decline upon shut-in was much longer than observed for the stimulations of the shallow reservoir, suggesting that either the reservoir has hydraulically-tighter boundaries, as also suggested by the pattern of microseismicity, or it has a larger storage capacity. As in the pre-stimulation tests, no hydraulic response was observed in the other wells, again suggesting hydraulic isolation of the upper and lower reservoirs (Weidler, 2000).

Only one spinner log was successfully performed to TD. This was run during the 30 l/s-step and indicated outlets near 4430 m (10 %), 4780 m (20 %), 4890 m (17 %) and below 4950 (52 % (Baria et al., 2002). However, the absence of a caliper profile below 4610 m, and the inference from logging that hole irregularity is significant severely degrades the confidence in these flow fractions. Nevertheless, the flow zone as 4780 m coincides with the HAFZ at ~4775 m inferred from drill cuttings, although the other major HAFZ at 4580-4600 m does not appear to have accepted significant flow.

Seismic activity was high throughout the injection with about 30,000-40,000 triggered events of which up to 14,000 were located (Dyer, 2001, Asanuma et al., 2001b). First events were located directly below the casing shoe, and around and below 4800 m, with predominantly downward migration. Seismic activity persisted after shut-in, even when the wellhead pressure approached its initial level. The primary microseismic structure defined by the events is a planar feature that strikes ~N155°E and dips 80° that intersects GPK2 at 4700 m (Asanuma et al., 2001a, Weidler, 2000).

The PTS sonde remained parked in the open hole at 4550 m for most of the stimulation. A flow/temperature log (TP20150) was run 6 days after shut-in on 12th July and the sonde re-parked at 4550 m. This was the last log run in the well. Shortly thereafter it was noticed that the sonde could not be moved upwards, and attempts to free it failed when the wireline snapped leaving 700 m of cable above the sonde. Camera inspection of the source of the problem in June 2002 showed that the casing had partially collapsed at 3904 m, leaving the sonde and cable trapped below. The collapse occurred near a cave zone, and it is thought to have been provoked when the casing was extending of the casing

that was occurring due to warm-up after the stimulation, was blocked at the wellhead. However, it has also been suggested that the collapse was induced by shearing of a major structure that cuts the wellbore at the spall zone.
To characterise the improvement in reservoir productivity, an step-rate injection test (00JUL13) was performed one week after the stimulation, before the reservoir had returned to equilibrium. The test featured one-day stages of 15, 25 and 30 l/s, but was terminated midway through the 30 l/s stage due to the rising level of seismic activity. Steady-state conditions were not reached in any stage from which an injectivity could be estimated, although it was clearly higher than before the stimulation (Weidler, 2000).
In 2000 and 2001, a series of four production tests were conducted, two of which were long term with a cumulative volume of 4000 m^3. Steady-state conditions were not reached after 3 weeks. Chemical analyses of the produced fluid indicated that 40% was fresh water from the stimulation. Two further production tests with volumes of 450 and 253 m^3 were performed mainly for geochemical investigations. At the end of the fourth production test, the freshwater content was 19 % in contrast to the first production in 2000 where it was 46 %.
In June 2002, an investigation of the obstruction at 3904 m revealed that the casing had collapsed, trapping the sonde below, but that a 3 inch aperture to the hole below remained. A short injection test (2002JUN13) of 120 m^3 was performed at various flow rates to confirm the well was open, but the stages were too short to estimate the injectivity. This deficiency was addressed in a further injection test (03JAN23) conducted after GPK3 had been drilled and shut-in but not stimulated. GPK2 was injected with fresh water at 15 l/s for 7 days, with pressure monitored by a gauge 3500 m. (Tischner et al., 2007) analysed the shut-in pressure decline curve and estimated an injectivity of 0.35 l/s/bar. Wellhead pressure of GPK3 reacted immediately to the injection in GPK2 which indicates hydraulic coupling. Furthermore, the pressure in GPK1 also reacted, in contrast to earlier tests prior to the drilling of GPK3.
Examination of the core from the hole bottom indicated fractures filled with calcite, a mineral that is also known to be present in fractures both within and outside of HAFZs. To try to dissolve this mineral, an acidizing operation (03FEB12) was performed during a convention stimulation in which 5800 m^3 of fresh water was injected at a base flow rate of 15 l/s over 4 days. Four 6 hr pulses of 30 l/s were spaced over the 4 days. During the 2nd/3rd pulses 2/3 m^3 of HCl was added to 300/700 m^3 of water respectively (Hettkamp et al., 2004). A marked drop in injection pressure of 0.7 MPa occurred as soon as the first acid pulse reached the open hole, the second pulse having no clear effect. Comparison of the first and transient pressure histories for the fourth pulses showed that a reduction in the near-field impedance of the well had occurred.
(Tischner et al., 2006) summarize the hydraulic behaviour of GPK2 with a formation linear flow regime. A turbulent skin is observed as well as a high storage of 20 m^3/MPa and a high conductive fracture which is connected to the borehole. The productivity is 5.0 l/s/MPa after two days declining to 4 l/s/MPa after 4 days.

2003: Drill GPK3 to 5000 m TVD and stimulate (03May27) with simultaneous injection into GPK2

- One dominant fracture zone at 4760 m depth (total mud losses during drilling and flow log before stimulation show that production came only from this fracture).
- 03JAN23 15 l/s injection into GPK2 - GPK3 reacts almost immediately.
- 03Feb12 15/30 l/s inject into GPK2 with acidising. Reduces near-well impedance.
- Turbulent flow in GPK2 casing after collapse (possibly because of restriction in wellbore)
- 03May27 stimulation: Starting different than previous stimulation
- Characteristics of the pressure curve looks like normal hydraulic testing on a permeable feature at the beginning
- Downhole overpressure: 170 bars, high flow rate for 2 h: around 90 l/s
- No significant increase of injectivity after stimulation. (?)
- 03Jun24 15 l/s circulation between GPK2&3.
- It worked!
- Tracer return after 3 days suggest a relatively direct connection (probably along the fracture)
- Circulation on a distance of 600 m

2004 Drill GPK4 to 5000 m TVD and stimulate (04Sep13 & 05Feb04*)*

- Acidization improvements in injectivity and communication with GPK3.
- Hydraulic stimulation with lower rates and lower volumes
- Initial injectivity very low: 0.01 l/s/bar, corresponding to an apparent porous media permeability of around 10-20 mD
- Maximum pressure higher in the second stimulation than in the first one
- HCl injection did not significantly improve the injectivity in the open-hole section (?)
- Flow log after RMA shows changes in the flow profile in the open-hole section and improvement of the injectivity (?)
- Improved connection to GPK3
- Casing leaks seen to develop (4360, 4712 MD). Possible explanation is that casings have been sheared by slip on a fracture zone (surprising USIT log did not see strong evidence of deformation)
- Image logs are recommended
- Real breakdown pressure with possibly a hydraulic axial fracture

REFERENCES

Asanuma, H., Ishimoto, M., Jones, R.H., Phillips, S. & Niitsuma, H., 2001a. A variation of the collapsing method to delineate structures inside a cloud. *Bull. Seis. Soc. Am.*, **91,** 154-160.

Asanuma, H., Mochizuki, S., Nakazato, K., Soma, N., Niitsuma, H. & Baria, R., 2001b. Data acquisition and analysis of microseismicity for simulation of deep reservoir by the MTC/Murphy International Collaborative Project. *Geothermal Resources Council Transactions*, **25,** 161-165.

Baria, R., Garnish, J., Baumgärtner, J., Gérard, A. & Jung, R., 1995. in World Geothermal Congress. Florence, Italy, pp. 2631-2637

Barton, C.A., Zoback, M.D. & Moos, D., Year. in Mechanics of Jointed and Faulted Rock. Vienna, pp. 381-387

Bérard, T. & Cornet, F., 2003. Evidence of thermally induced borehole elongation: a case study at Soultz, France. *Int. J. Rock Mech. Min. Sci*., **40,** 1121-1140.

Cornet, F.H., Helm, J., Poitrenaud, H. & Etchecopar, A., 1997. Seismic and aseismic slip induced by large fluid injections. *Pure Appl. Geophys*., **150,** 563-583.

Cornet, F.H. & Jones, R.H., Year. in 1st North American Rock Mechanics Symposium. Austin, Texas, pp. 61-69

Cuenot, N., Dorbath, C. & Dorbath, L., 2008. Analysis of microseismicity induced by fluid injections at the Hot Dry Rock site od Soultz-sous-Forêts (Alcace, France):

Implications for the characterization of the geothermal reservoir. *Pure and Applied Geophys*., **165,** 797-824.

Dyer, B.C., 2001. Soultz GPK2 stimulation (June/July 2000) seismic monitoring report., Report to Socomine, Semore Seismic, Falmouth, UK.

Evans, K.F., 2001. Determining the effect of stimulation injections on the rock mass around the well GPK1 from borehole data: analysis of the 1993 injections, Final report to the Swiss Department of Education and Science (BBW) under contract BBW 98.0008-1, Swiss Federal Institute of Technology.

Evans, K.F., 2005. Permeability creation and damage due to massive fluid injections into granite at 3.5 km at Soultz: Part 2 - Critical stress and fracture strength. *Journal of Geophysical Research*, **110,** 14 pp.

Evans, K.F., Genter, A. & Sausse, J., 2005a. Permeability creation and damage due to massive fluid injections into granite at 3.5 km at Soultz: Part 1 - Borehole observations. *Journal of Geophysical Research*, **110,** 19 pp.

Evans, K.F., Kohl, T., Hopkirk, R.J. & Rybach, L., 1996. Studies of the nature of non-linear impedance to flow within the fractured granitic reservoir at the European Hot Dry Rock Project site at Soultz-sous-Forêts, France, Final report to the Swiss Department of Education and Science (BBW) under contract BBW 93.0010, Swiss Federal Institute of Technology/Polydynamics Engineering.

Evans, K.F., Kohl, T. & Rybach, L., 1998. Analysis of the hydraulic behaviour of the 3.5 km deep reservoir during the 1995-1997 test series, and other contributions to the European Hot Dry Rock Project, Soultz-sous-Forêts, France, Final Report to the Swiss Department of Education and Science (BBW) under contract number BBW 95.0673-2, Swiss Federal Institute of Technology.

Evans, K.F., Moriya, H., Niitsuma, H., Jones, R.H., Phillips, W.S., Genter, A., Sausse, J., Jung, R. & Baria, R., 2005b. Microseismicity and permeability enhancement of hydrogeologic structures during massive fluid injections into granite at 3 km depth at the Soultz HDR site. *Geophys. J. Int*., **160,** 388-412.

Genter, A., Homeier, G., Chèvrement, P. & Tenzer, H., 1999. Deepening of GPK-2 HDR borehole, 3880-5090 m (Soultz-sous-Forêts, France): Geological Monitoring, Public report, BRGM.

Hettkamp, T., Baumgärtner, J., Baria, R., Gérard, A., Gandy, T., Michelet, S. & Teza, D., Year. in 29th Workshop on Geothermal Reservoir Engineering. Stanford University, Stanford, California, pp. 184-193

Hettkamp, T., Klee.G. & Rummel, F., 1998. in Pre-conference proc. of 4th Int. Hot Dry Rock Forum. Strasbourg, France, pp.

Jamison, D.B. & Cook, N.G.W., 1980. Note on measured values for the state of stress in the Earth's crust. *Journal of Geophysical Research*, **85,** 1833-1838.

Jones, R.H., Beauce, A., Jupe, A., Fabriol, H. & Dyer, B.C., 1995. in World Geothermal Congress. Florence, Italy, pp. 2665-2669

Jung, R., 1991. Hydraulic fracturing and hydraulic testing in the granitic section of borehole GPK1, Soulz-sous-Forets. *Geothermal Sci. and Tech*., **3,** 149-198.

Jung, R., 1992. Connecting a borehole to a nearby fault by means of hydraulic fracturing. *Trans. Geotherm. Resources Council*, **16,** 433-437.

Jung, R., Reich, W., Engelking, U., Hettkamp, T. & Weidler, R., 1995a. Hydraulic tests in1995 at the HDR Project, Soultz-sous-Fôrets, France, Field Report, Bundesanstalt für Geowissenschaften und Rohstoffe (BGR), Hannover, Germany.

Jung, R., Willis-Richards, J., Nicholls, J., Bertozzi, A. & Heinemann, B., 1995. in World Geothermal Congress. Florence, Italy, pp. 2671-2676

Klee, G. & Hegermann, P., 1995. World Geothermal Congress. Florence, Italy, pp. 2559-2561

Klee, G. & Rummel, F., 1993. Hydrofrac stress data for the European HDR research project test site Soultz-sous-Forêts. *Int. J. Rock Mech. Min. Sci. & Geomech*. Abst., **30,** 973-976.

Kohl, T., Evans, K.F., Hopkirk, R.J., Jung, R. & Rybach, L., 1997. Observation and simulation of non-Darcian flow transients in fractured rock. *Wat. Resourc. Res*., **33,** 407-418.

Kohl, T., Evans, K.F. & Rybach, L.R., 1998. in Pre-conference proc. of the 4th Int. Hot Dry Rock Forum. Strasbourg, France, pp.

Kohl, T., Jung, R., Hopkirk, R.J. & Rybach, L., 1996. in Proc. 3rd Int. Hot Dry Rock Forum. Santa Fe, New Mexico, pp. 85-87

Le Carlier, C., Royer, J.J. & Flores, E.L., 1994. Convective Heat Transfer at the Soultz-sous-Forêts geothermal Site: implication for oil potential. *First Break*, **12,** 553-560.

Poitrenaud, H., 1994. Application des mesures par 'ultrasonic borehole imager' à la determination de glissements sur fractures preexistants, Masters Thesis (Rapport de DESS) in French, Institut de physique du globe de Paris.

Pribnow, D. & Schellschmidt, R., 2000. Thermal tracking of Upper Crustal flow in the Rhine Graben. *Geophys. Res. Lett*., **27,** 1957-1960.

Rummel, F. & Baumgärtner, 1991. Hydraulic fracturing stress measurements in the GPK1 borehole, Soultz-sous-Forêts. *Geotherm. Sci. and Tech*., **3,** 119-148.

Tenzer, H., Mastin, L. & Heinemann, B., 1992. Determination of planar discontinuities and borehole geometry in the crystalline rock of borehole GPK-1 at Soulz-sous-Forets. *Geothermal Sci. and Tech*., **3,** 31-68.

Tischner, T., Pfender, M. & Teza, D., 2006. Hot Dry Rock Projekt Soultz: Erste Phase der Erstellung einer wissenschaftlichen Pilotanlage Final report to Bundesministerium für Umwelt, Naturschutz und Reaktorsicherheit for period: 1.04.2001-31.03.2005., Bundesanstalt für Geowissenschaften und Rohstoffe (BGR)

Tischner, T., Schindler, M., Jung, M. & Nami, P., Year. in Thirty-second Stanford Workshop on Geothermal Reservoir Engineering. Stanford University, pp. 322-328

Weidler, R., 1999. Slug test in the non-stimulated 5 km deep well GPK-2, Bundesanstalt für Geowissenschaften und Rohstoffe (BGR) Hannover.

Weidler, R., 2000. Hydraulic stimulation of the 5 km deep well GPK-2, Report to Socomine, Bundesanstalt für Geowissenschaften und Rohstoffe (BGR) Hannover.

Weidler, R. & Jung, R., 2000. Production test in the non-stimulated 5 km deep well GPK-2, Report to Socomine, Bundesanstalt für Geowissenschaften und Rohstoffe (BGR) Hannover.

APPENDIX 6 - modelling

APPENDIX 6 (a)

Clément Baujard, Thomas Kohl, Thomas Mégel, M. Rosener, Dominique Bruel, Sandrine Portier, Emmanuel Stamatakis, Hans Sulzbacher, Michael Kühn, Xavier Rachez and Michel Rabinowicz, 2007, Modelling of the Soultz reservoir: different approaches and possible benefits, *paper presented at the EHDRA Scientific Conference, Soultz-sous-Forêts,* June 28-29, 2007.

"MODELLING OF THE SOULTZ RESERVOIR: DIFFERENT APPROACHES AND POSSIBLE BENEFITS"

C. Baujard[1], T. Kohl, T. Mégel, M. Rosener, D. Bruel, S. Portier,
E. Stamatakis, H. Sulzbacher, M. Kühn, X. Rachez, M. Rabinowicz

[1] GEOWATT AG
Dohlenweg 28
CH-8050 Zürich; Switzerland

e-mail: baujard@geowatt.ch

ABSTRACT

This paper gives an overview of numerical models developed and used around the reservoir of Soultz-sous-Forêts. We focus here only on reservoir modeling numerical codes (no fracture/pore scale numerical code). The main mathematical features and physical processes taken into account, as well as an application example and major bibliography about each code are presented.

INTRODUCTION

Many numerical codes have been developed and used since the experiments began in Soultz-sous-Forêts, in 1989. Indisputable advances have been released in this domain during the past years. The modeling group, the last years chaired by T. Kohl, coordinates work of several scientific teams over Europe.

A state-of-the-art of modeling activities in Soultz is presented. Instead of adopting a classical scientific paper shape, we give here an overview of the different codes existing and used for scientific investigations in Soultz.

To that purpose, a form has been sent to recent contributors of the modeling group in order to shortly describe their numerical code. The main fields of the form that was sent are:

- Author(s)
- Institution
- Code
- Mathematical algorithm
- Physical Processes and interactions
- Special features
- One application example
- Future developments
- Benefits for Soultz Project
- References

Each author that answered and filled in the form is an author of this paper. This overview is voluntarily limited to reservoir modeling codes. Many other codes (mainly fracture/pore scale simulation code, inverse modeling or economical modeling) were written and used but are voluntarily not referenced in the following pages.

In the following, the codes are presented by alphabetical order of the code name.

Author(s):	**Peter Cundall, Mark Christianson, Jose Lemos, Branko Damjanac**
Institution	**ITASCA Consulting Group**
Code:	**3DEC**
Mathematical algorithm:	3D Distinct Element
Physical Processes:	Thermo-Hydro-Mechanical modelling of fractured rock masses Discontinuous medium modelled as an assemblage of convex or concave polyhedra. Discontinuities treated as boundary conditions between blocks.
Physical Interaction:	Motion along discontinuities governed by linear and non-linear force displacement relations for movements in both the normal and shear direction (friction, dilatancy, cohesion, rugosity, stiffnesses) Material models include: elastic, anisotropic, Mohr-Coulomb, Drucker-Prager, bilinear plasticity, strain softening, creep, and user-defined. Joint fluid flow (flow in fractures is laminar and obeys a cubic law ; blocks are impermeable) Heat conduction in blocks, thermal convection in fractures filled with moving fluid
Special features	Internal macro-language that allows building complex models, hooking 3DEC to any other software, performing parameter studies, etc. Joint fluid logic and thermal calculations implemented for BRGM needs. Specific hydro-mechanical coupling developed by BRGM, dedicated to simulate the behaviour of fractured rock masses during hydraulic tests.
One application example	Influence of the stress field on the hydromechanical behaviour of the rock mass during the stimulation of GPK4. 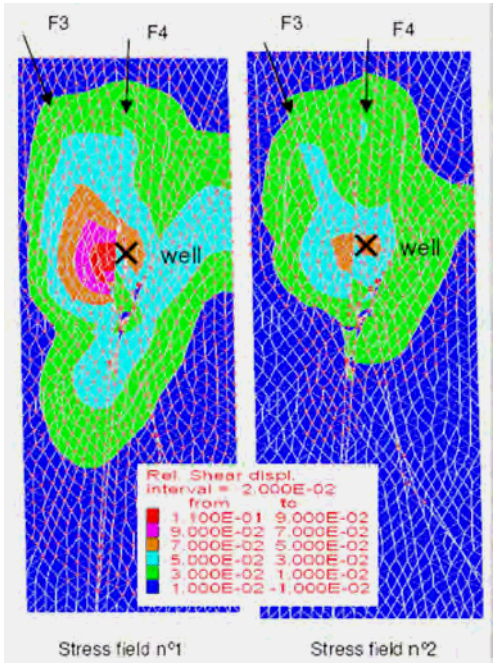 *Shear displacements contours in one of the main fracture during injection in GPK4 (for 18.3 MPa overpressure stage), for 2 given stress fields*
Future developments	New flow boundary logic for limiting the flow extension of a given fracture. Procedures for automatically coupling 3DEC and FRACAS (code developed by ARMINES – D. BRUEL) in order to solve coupled hydromechanical problems where the role of the mechanics on the hydromechanical behaviour is either “strong” (3DEC case) or “light” (FRACAS case).
Benefits for Soultz Project	Helps understanding the hydro-mechanical behaviour of the fractured rock mass during hydraulic tests.
References	Gentier, S., Rachez, X., Dezayes, C., Blaisonneau A. and Genter, A. (2005). How to understand the effect of the hydraulic stimulation in term of hydro-mechanical behaviour at Soultz-sous-Forêts (France) in Geothermal Energy – The World’s Buried Treasure (Proceedings of the GRC 2005 Annual meeting, Reno, USA, September 2005) Rachez, X., Gentier, S. and Blaisonneau, A (2006) “Hydro-mechanical behaviour of GPK3 and GPK4 during the hydraulic stimulation tests – Influence of the stress field” (Proceedings of the European Hot Dry rock Association Scientific conference, Soultz-sous-Forêts, France, 15&16 June 2006).

Author(s):	**Daniel Billaux, Caroline Darcel**
Institution	**ITASCA Consultants SAS**
Code:	**3FLO**
Mathematical algorithm:	Finite Element; 3D
Physical Processes:	Flow in fracture networks, represented by a 3D network of 1D channels. Flow in porous media using Galerkine or Mixed-Hybrid 3D finite elements Flow in interacting fractures and porous media Pollutant transport, simulated by the particle tracking method Geochemistry, coupled or not with solute transport, taking into account most types of reactions
Physical Interaction:	Conductivity (1D channel), permeability (3D element), porosity, aperture, storativity, dispersivity, diffusion, etc.
Special features	Internal macro-language that allows building complex models, hooking 3FLO to any other software, performing parameter studies, etc. Advanced fracture tool, adapted for BRGM needs, that allows mixing 1D channels and 3D finite elements.
One application example	A flow and transport model of the Soultz reservoir is under progress. Its aim is to reproduce the in-situ tracer test that has been performed during the fluid circulation test conducted between the injection well GPK3 and the production wells GPK2 and GPK4.  *Perspective view of the model exchanger*
Benefits for Soultz Project	Will help understanding the in-situ tracer tests
References	Billaux, D., J. P. Chilès, K. Hestir and J. Long (1989) - « Three-Dimensional Statistical Modelling of a Fractured Rock Mass — An Example From the Fanay-Augères Mine » Int. J. Rock Mech. & Min. Sci., 26 (3-4), 281-299. Billaux, D., and S. Gentier (1990) - « Numerical and Laboratory Studies of Flow in a Fracture » in Proceedings of the International Conference on Rock Joints (Loen, Norway, 1990), pp. 369-374. Rotterdam: A. A. Balkema.

Author(s):	**S. Ollivella, J. Vaunat ; M. Rosener**
Institution	**ETC - UPC, Barcelone ; EOST, Strasbourg**
Code:	**Code_Bright**
Mathematical algorithm:	Finite element method is used for the spatial discretization while finite differences are used for the temporal discretization ; 1D to 3D
Physical Processes:	Hydraulic (linear, non-linear); Thermal (linear, non-linear); Mechanic (linear),
Physical Interaction:	diffusive/ dispersive flux, advective flux caused by fluid motion, advective flux caused by solid motion (depending on activated governing equations)
One application example	Different fault zone geometries were built and tested to look at the hydraulic and thermal behaviour of the structure. Special configurations like a sealed gauge zone were tested too. 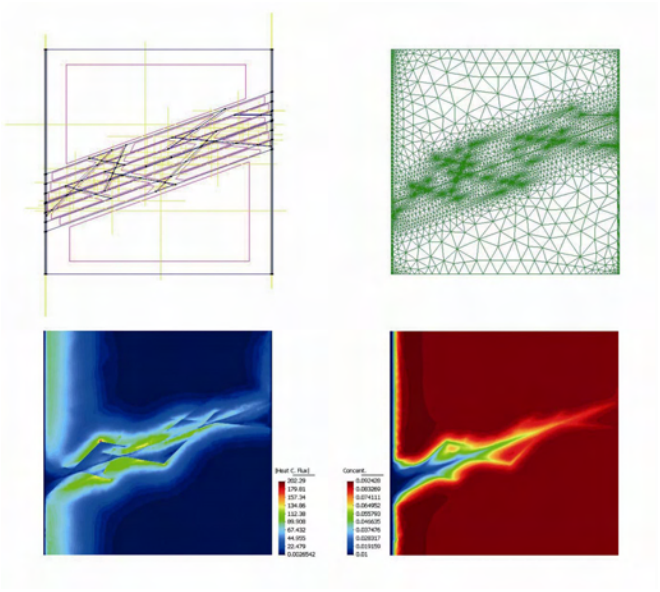 *Geometry, grid, heat flux and Total Dissolved Matter distribution*
Future developments	Chemical evolution
Benefits for Soultz Project	Estimation of the damage zone impact on heat and mass transfer in a fault zone during geothermal exploitation
References	Rosener M., Géraud Y., Vaunat J. and Fritz B. 2007 Damage zone integration into fault models : implication on heat and mass transfer during geothermal exploitation, EHDRA Scientific Meeting, Soultz-sous-Forêts.

Author(s):	Michel Rabinowicz
Institution	Observatoire Midi-Pyrénées Toulouse
Code:	Convection
Mathematical algorithm:	Finite 3-D difference for the thermal equation, 2-D spectral for the flow equation
Physical Processes:	Darcy flow and convection in a porous media
Physical Interaction:	Variable permeability and viscosity
Special features	2-D flow-fields in vertical gouges coupled with the 3-D thermal field within the walls and gouges
One application example	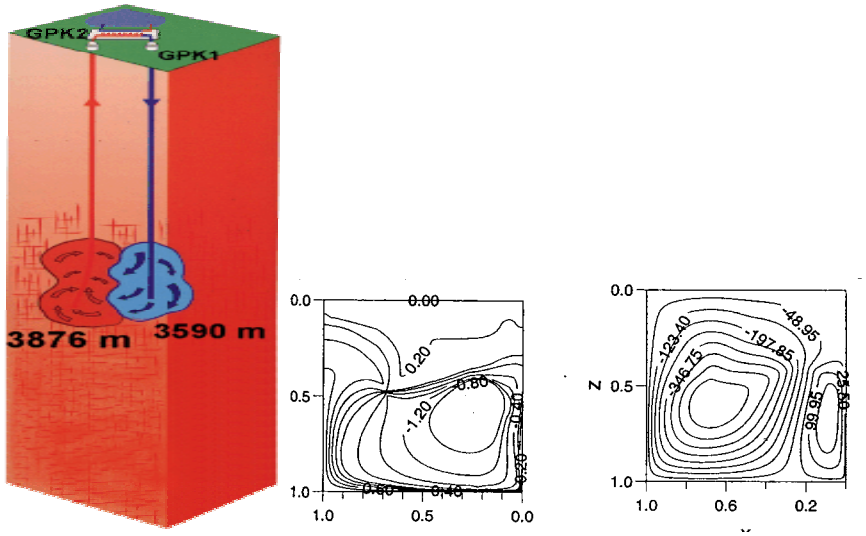 We inject cold water in a well and produce it warm in another one both being in hydraulic connection with a vertical stimulated gouge. The temperature and flow evolutions during 30 years of production are computed.
Benefits for Soultz Project	Prediction of production temperature of Soultz Plant
References	Bataillé A., P. Genthon, M. Rabinowicz, B. Fritz: Modeling coupled free and forced convection in a vertical permeable slot: implications for the heat recovery of a geothermal plant, Geothermics, 35, 654-682, 2006. Tournier, C.; P. Genthon, M. Rabinowicz: The onset of natural convection in vertical fault planes; consequences for the thermal regime in crystalline basements and for heat recovery experiments. Geophysical Journal International. 140; 3, 500-508, 2000. Rabinowicz, M., J. Boulegue, P. Genthon: Two- and three-dimensional modeling of hydrothermal convection in the sedimented Middle Valley segment, Juan de Fuca Ridge. Journal of Geophysical Research, B, 103, 10, 24,045-24,065, 1998.

Author(s):	**D. Bruel, C. Baujard**
Institution	**Paris School of Mines - Geosciences**
Code:	**Fracas**
Mathematical algorithm:	Finite Volume, Stochastic Discrete Fracture Network
Physical Processes:	Hydraulic (linear, non-linear); Thermal coupling (*); Non-miscible fluid flow (*); Fracture mechanics (normal; shear and irreversible post rupture dilation) (*) Not both at the same time
Physical Interaction:	Advection; Buoyancy; Viscosity for thermal coupling Density-driven flows for biphasic flow. Permeability (function of pressure; stress; fracture parameters)
Special features	Stochastic Generation of a Discrete Fracture Network with Deterministic Faults segments and Fracture zones.
One application example	The hydraulic stimulation of GPK2, GPK3, and GPK4 were successfully reproduced (see figure below) in terms of well pressure response and hydraulic diffusivity of Soultz reservoir. Tracer tests were used to calibrate the reservoir volume and an estimation of reservoir volume invaded by injection fluid during long-term circulation test of summer 2005 was proposed. 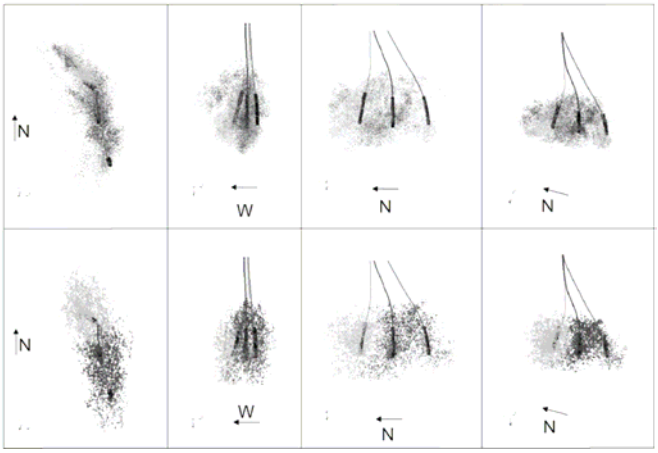 *On top, recorded microseismic events; on bottom, computed shear events with Fracas*
Future developments	Seismic magnitude events, thermal coupling with Non-miscible fluid flow
Benefits for Soultz Project	Forecast of stimulation events and accessible gains in hydraulic properties Evaluation of fluid density impact during stimulation; Forecast of tracer breakthrough curves and thermal behaviour of the stimulated reservoir
References	Baujard, C. and Bruel, D., 2007. Numerical study of the impact of fluid density on the pressure distribution and stimulated volume in the Soultz HDR reservoir. Geothermics, 35: 607-621. Bruel, D., (2007) Using the migration of the induced seismicity as a constraint for fractured hot dry rock reservoir modelling. Int. J. Rock. Mech. Min. Sci. & Abstr., 2007, in press. Bruel D., (2002), Impact of induced thermal stresses during circulation tests in an engineered fractured geothermal reservoir. Example of the Soultz sous Forêts, European hot fractured rock geothermal project, Rhine Graben, France, Oil & Gas Science and Technology, Rev. IFP, vol. 57, n°5, p. 459-470.

Author(s)	**S. Portier with the contributions of L. André; D. Bächler; P. Durst; T. Kohl; V. Rabemana; and F-D. Vuataz.**
Institution	**CREGE, Neuchâtel with the collaboration of GEOWATT AG, Zürich**
Code	**FRACHEM**
Mathematical algorithm	The 3D finite element code FRACTure (Kohl and Hopkirk, 1995) and the 3D finite volume code CHEMTOUGH (White, 1995) were coupled. The characteristics of the Soultz system, such as the high salinity of the fluids and the re-injection of the fluid after production, preclude the use of the original geochemical model implemented in CHEMTOUGH. Durst (2002) made several modifications: implementation of the new method to calculate activity coefficients (Pitzer model), the reaction kinetics subroutines for the minerals, modification of the calculation of the reaction surface areas and the permeability changes, as well as introduction of the possibility to simulate re-injection processes.
Physical Processes	Hydraulic processes; thermal processes; chemical reactions; advective transport of chemical species and variation of porosity and permeability.
Physical Interaction	Thermodynamic equilibrium; species concentration; precipitation/dissolution; brine-rock interactions; kinetic model; reaction rates; porosity changes; permeability changes, reaction mineral surface area changes.
Special features	1D or 2D deterministic fracture sets are mapped onto a finite element mesh.
One application example	The circulation of injected cold brine in the 5000-m deep Soultz reservoir was modelled. After a brine circulation of 1800 days, calcite appeared to be the most reactive mineral with about 1300 kg dissolved in the first 50 meters of the fractured zone and about 1500 kg precipitated in the second half of the fracture. Silicates and aluminosilicates tended to precipitate near the injection well but in small quantities. A consequence of these reactions was a change in reservoir porosity and permeability. In the vicinity of the injection well, porosity increased by about 30 %, mainly due to calcite dissolution, while porosity decreased by 5 % near the production well. Carbonate reactions seemed to control the porosity of the reservoir, at least during the first 1800 days of circulation. Carbonate behaviour in the deep Soultz reservoir seemed to be in coherence with the results observed for the shallow reservoir. 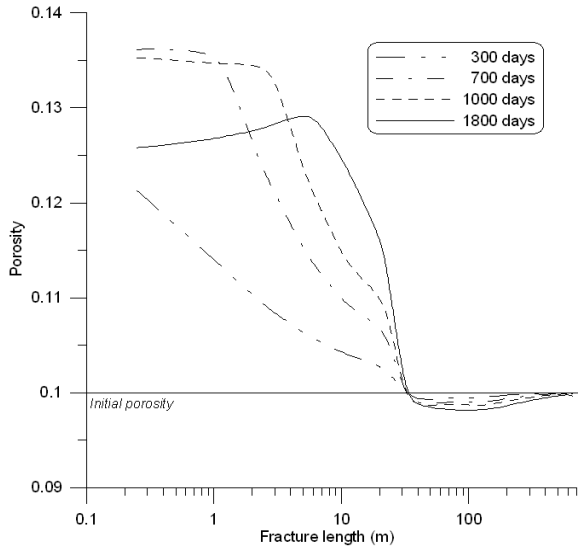 *Increase of porosity in the vicinity of the injection well due to carbonates dissolution during injection of supersaturated brine at 65 °C.*
Future developments	Sensitivity studies; fracture geometry; redox processes; chemical speciation.
Benefits for Soultz Project	Forecast of chemical and thermal evolution of produced fluid; forecast of minerals behaviour and resulting porosities evolution due to mineral reactions and forecast the effectiveness of the chemical stimulations to enhance the reservoir porosity/permeability. The code appears to be a good tool for investigating the impact of the geochemical processes on reservoir properties.
References	André L., Rabemanana V. and Vuataz F.-D., 2006, Influence of water-rock interactions on fracture permeability of the deep reservoir at Soultz-sous-Forêts, France. Geothermics 35, 507–531. André L., Spycher N., Xu T., Pruess K. and Vuataz F.-D., 2006, Modelling brine-rock interactions in an Enhanced Geothermal System deep fractured reservoir at Soultz-sous-Forêts (France): a joint approach from two geochemical codes: FRACHEM and TOUGHREACT. Lawrence Berkeley National Laboratory, Berkeley. LBNL-62357 Collaboration Report. Bächler D., 2003, Coupled Thermal-Hydraulic-Chemical Modelling at the Soultz-sous-Forêts HDR reservoir (France). PhD thesis, ETH-Zürich, Switzerland, 151 p. Durst P., 2002, Geochemical modelling of the Soultz-sous-Forêts Hot Dry Rock test site: coupling fluid-rock interactions to heat and fluid transport. PhD thesis, University of Neuchâtel, Switzerland, 128 p. Portier S., André L. and Vuataz F.-D., 2007, Modelling the impact of forced fluid-rock interactions on reservoir properties at Soultz-sous-Forêts EGS geothermal site. Proc. European Geothermal Congress, Unterhaching, Germany.

Author(s):	**E. Stamatakis[a,b], A. Stubos[a], C. Chatzichristos [b] and J. Muller [b]**
Institution	**[a]National Centre for Scientific Research Demokritos, Greece** **[b]Institute for Energy Technology, Norway**
Code:	**gPROMS**
Mathematical algorithm: (discretization)	Axial domain: 2nd order Centered finite difference method; Radial domain: 2nd order Orthogonal collocation on finite elements
Physical Processes:	heat transfer mass transfer chemical reactions
Physical Interaction:	fluid velocity, fluid composition, pressure and temperature
Special features	radial dependency of velocity, temperature and concentrations
One application example	Scale tube length:60 cm; scale tube radious:1.25 cm; inlet flowrate: 0.005 kg/s; Pressure: 20 bar; Initial fluid temp: 120°C; inlet Ca: 100 mols/m^3; inlet $CaCO_3$:0 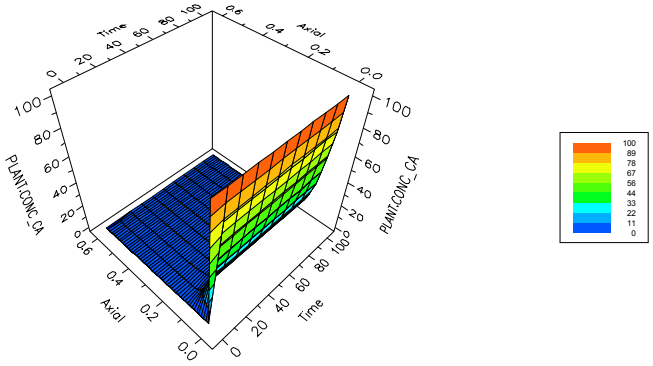 *Consumption of Ca at the inlet of the scale tube*
Future developments	Parameter estimation; objective function; optimization
Benefits for Soultz Project	Forecast of precipitation events; optimal design and operation of the plant
References	Stamatakis E., Bjørnstad T., Muller J., Chatzichristos C., Stubos A., "Simulation of mineral precipitation in geothermal installations: The Soultz-sous-Forëts case", presented during the Workshop 3 ENGINE – ENhanced Geothermal Innovative Network for Europe, Kartause Ittingen, Zürich, Switzerland, June 29 – July 1, (2006). Stamatakis E., Bjørnstad T., Chatzichristos C., Muller J., Stubos A., "Scale Detection in Geothermal Systems: The Use of Nuclear Monitoring Techniques", *presented during the Launching Conference of the European Project: Enhanced Geothermal Innovative Network for Europe (ENGINE),* Orleans, France, 13-15, February (2006). Stamatakis E., Muller J., Chatzichristos C., Haugan A., "Real-time monitoring of calcium carbonate precipitation from geothermal brines", *presented during the European Hot Dry Rock Association (EHDRA) Scientific Meeting*, Soultz-Sous-Forêts, France, 17-18 March (2005).

Author(s):	**T. Mégel**
Institution	**GEOWATT AG, Zurich**
Code:	**HEX-B2, Version 1.1, Borehole simulator**
Mathematical algorithm:	Finite Difference; 1D / 2D cylindrical
Physical Processes:	Navier-Stokes equation, mass conservation and pipe friction in the borehole; radial thermal diffusion in the borehole completion and rock mass
Physical Interaction:	Advection of NaCl-molality and temperature; buoyancy; density, viscosity and heat capacity as a function of temperature, pressure and NaCl-molality;
Special features	Calculation of pressure and temperature profiles from wellhead measures. Exit-/Entry points with specific time histories of temperature/NaCl-molality in different depths can be defined. Arbitrary borehole diameters and well completion.
One application example	Borehole models have been built and calibrated for the three deep wells of Soultz GPK2 GPK3 and GPK4. These models were used to calculate pressure and temperature profiles during injection or production in boreholes. 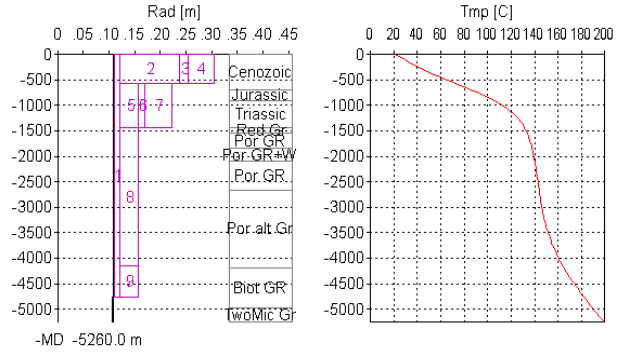 *HEX-B2 Well model for well GPK4, right: initial temperature*
Future developments	Understand better transient processes, especially for shut-in phases which sometimes show gaps between measured and calculated values
Benefits for Soultz Project	- Prediction of production temperature dependence with flowrate of wells GPK2 and GPK4, effect of entry-points - Pressure values when fracture failure occurs - Making test data comparable - It may not be necessary to use downhole sensors for each injection/production experiment in Soultz, as calculated HEX-B2 values can be used for interpretation
References	Mégel, T., Kohl, T. and Hopkirk, R.J., 2007. The potential of the use of dense fluids for initiating hydraulic stimulation. Geothermics, 35: 589-599.

Author(s):	**T. Kohl; T. Mégel**
Institution	**GEOWATT AG, Zurich**
Code:	**HEX-S**
Mathematical algorithm:	Finite Element; 3D
Physical Processes:	Hydraulic (linear, non-linear); Thermal (linear, non-linear); Elastic (linear), Fracture mechanics (normal; shear)
Physical Interaction:	Advection; Buoyancy; viscosity Poroelasticity (*); Thermoelasiticity (*); Permeability (function of pressure; stress; fracture parameters) (*) not yet activated
Special features	Deterministic and stochastic fracture sets are mapped onto a finite element mesh
One application example	The hydraulic stimulation of GPK4 in September 2004 was simulated using the available information of stress field. The model includes 15 major deterministic fractures of GPK2-GPK4 and accounts for stochastic fracture distribution at larger distance. 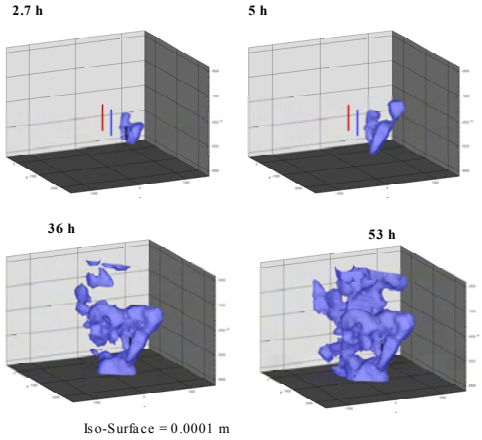 *Increase of permeability due to normal compliance and shearing during injection in GPK4*
Future developments	Parameter studies; Poroelasticity; Thermoelasiticity
Benefits for Soultz Project	Forecast of stimulation events; Can be used for stimulation design
References	Kohl T., Mégel T., 2007, Predictive modeling of reservoir response to hydraulic stimulations at the European EGS site Soultz-Sous-Forêts, Int. J. of Rock Mechanics, In press Kohl T., Baujard C., Mégel T., 2006, Conditions for Mechanical Re-Stimulation of GPK4, Soultz Scientific Meeting, Synthetic 2nd year report Kohl T. Mégel T., 2005, Coupled Hydro-mechanical modelling of the GPK3 reservoir stimulation at the European EGS site Soultz-sous-Forêts, Proc. 31th Workshop on Geothermal Reservoir Engineering; Jan. 31-Feb. 2, 2005, Stanford University, CA, USA.

Author(s):	**H. Sulzbacher; R. Jung**
Institution	**Leibnitz Institute for Applied Geoscience, Hannover**
Code:	**Rockflow**
Mathematical algorithm:	Finite Element; 3D
Physical Processes:	thermal, hydraulic and mechanic coupled processes (THM $_{plus}$)
Physical Interaction:	Advection; Conduction; Viscosity
Special features	Stimulated fractures, connected to the boreholes and an interconnecting natural fault zone are mapped onto a finite element mesh.
One application example	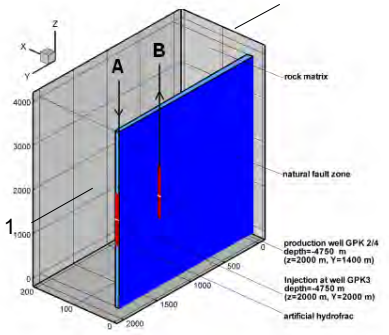 *Deep reservoir in Soultz. Numerical model of the heat exchanger. Due to symmetric reasons only a quarter of the model has to be considered. A: GPK3, B: GPK4 or GPK2. The Cartesian coordinate system is oriented parallel to the strike of the model. Z=2000 m corresponds to a depth of 4750 m.* 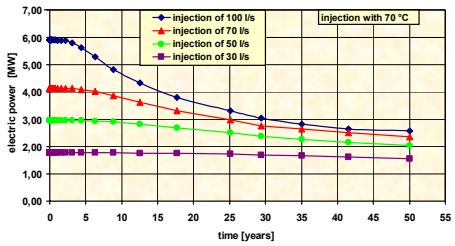 *Production of electric power with different injection rates. Injection temperature is 70°C.* The long term production temperature and electric power of the deep heat exchanger has been computed for different fracture lengths, injection temperatures and circulation flow rates. The results show that due to the presence of the stimulated fractures the thermal performance and the lifetime of the system are significantly improved and are of commercial interest even if fluid flow is restricted to the relatively narrow fault zone.
Future developments	Calibration of the model with data from tracer experiments
Benefits for Soultz Project	Forecast of production temperature and production power
References	Grecksch,G., H. Sulzbacher, R. Jung (2003b): Hydraulic Modeling of the Deep Geothermal Reservoir in Soultz– ZIP Vorhaben "*Hot-Dry-Rock-Project Soultz – Hydrogeothermische Modellierung des HDR-Wärmetauschers" (Förderkennzeichen: 0327109B), "Hot Dry Rock Energy" (EC contract ENK5-CT-2000-00301)* Jung, R, S. Röhling,N.Ochmann, S.Rogge, R.Schellschmidt, R.Schulz, T.Thielemann (2002): Abschätzung des technischen Potentials der geothermischen Stromerzeugung und der geothermischen Kraftwärmekopplung (KMW) in Deutschland. *Studie im Auftrag des Büros für Technikfolgeabschätzung beim deutschen Bundestag (TAB)*

Author(s):	**M. Blumenthal, M. Kühn, H. Pape, V. Rath, C. Clauser**
Institution	**Applied Geophysics and Geothermal Energy** **RWTH Aachen University**
Code:	**SHEMAT**
Mathematical algorithm:	Finite Difference; 2D
Physical Processes:	Flow, heat, transport
Physical Interaction:	Flow and heat coupled via density, viscosity, compressibility, thermal conductivity, and thermal capacity (function of temperature and pressure). Temperature dependence of thermal rock properties.
One application example	The tracer test performed in 2005 was used to calibrate a simplified 2D horizontal model of the deep reservoir in Soultz. The model is based on known structural units: (1) two fracture families in the host rock; (2) mechanically stimulated zones around the wells; (3) a direct hydraulic connection between the wells. 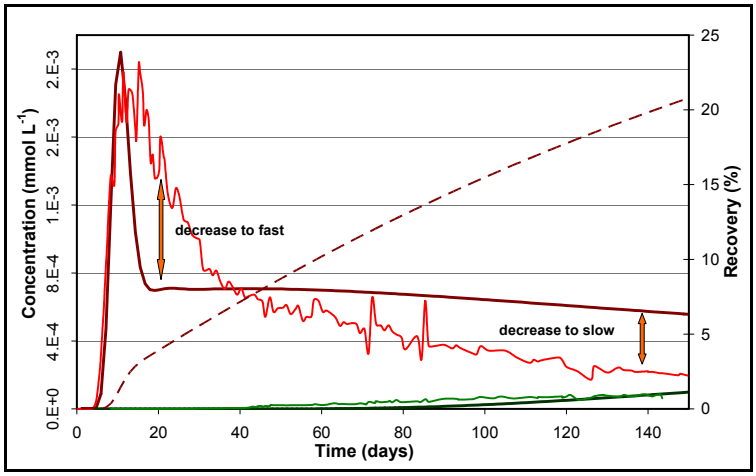 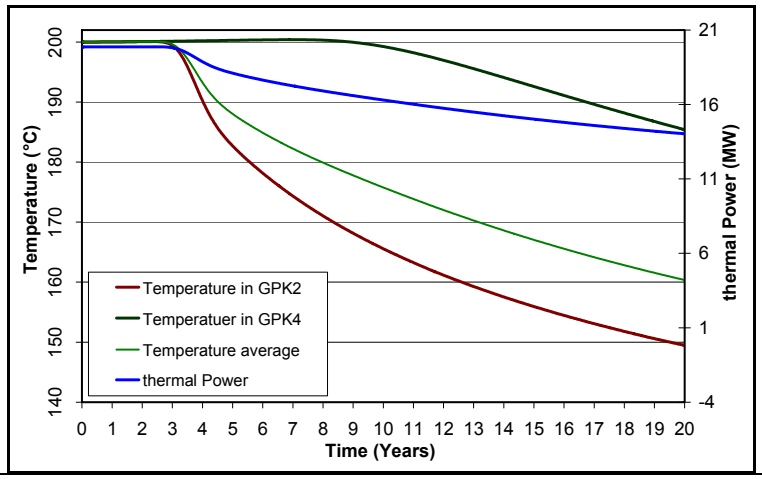
Future developments	3D model, water-rock interaction, chemical stimulation test, multiple porosity/permeablity module
Benefits for Soultz Project	Interpretation of tracer tests. Evaluation of hydraulic concepts. Forecast of heat extraction process under varying constraints (e.g. pumping rates).
References	Blumenthal M., Kühn M., Pape H., Rath V., Clauser C. (2007) Numerical simulation of a tracer test from the EGS test site Soultz-sous-Forêts. Jahrestagung der Deutschen Geophysikalischen Gesellschaft. 26.-29. März 2007, Aachen Kühn M., Pape H., Rath V., Wolf A., Clauser C. (2007) Interaction of a multi-fractured rock system with fluid flow, mass and heat transport, and chemical reactions. Jahrestagung der Deutschen Geophysikalischen Gesellschaft. 26.-29. März 2007, Aachen Pape H., Rath H. (2006) Simulation of reactive transport in a stimulated “hot dry rock” system with mass exchange between fracture systems of various thermal gradient, In: Proc. EHDRA Scientific Conference. June 15-16, 2006, Soultz-sous-Forêts, France

APPENDIX 6 (b)

Thomas Kohl and Clément Baujard, 2008, Overview of the modelling workgroup activities, *paper presented at the EHDRA Scientific Conference, Soultz-sous-Forêts,* September 24-25, 2008.

EC Contract SES6-CT-2003-502706

PARTICIPANT ORGANIZATION NAME: Geowatt

Related with Work Package: WP5

Related with Working Group WG5

OVERVIEW OF THE MODELING WORKGROUP ACTIVITIES

Kohl Th. and Baujard C.
Geowatt, Zürich, Switzerland
e-mail: kohl@geowatt.ch

ABSTRACT

It was foreseen in the second phase of the European EGS project Soultz-sous-Forêts to summarize the activities in the different project history performed in the framework of the different workgroups. This paper proposes such an overview for the Workgroup Modeling (WG 5). A brief description of the activities, tools developed, achieved goals and unresolved challenges is presented in the following.

INTRODUCTION

The covering of a wide range of research fields is probably the major characteristic of the modeling Workgroup WG5. Indeed, besides skills in computer programming and mathematical algorithms required for numerical modeling the different teams also have to understand physical processes and their interactions when they intend to simulate the complexity of EGS fields. Consequently, the workgroup WG5 is a constructive instrument to share and acquire new data, but also to explain – or debate – the understanding of physical processes occurring in the reservoir.
Three main research fields were investigated in the framework of the workgroup:

- (thermo-)hydro-mechanical processes,
- (thermo-)hydro-chemical processes
- hydro-thermal processes

Though several economical modeling tools exist and were used in Soultz, this branch of activities was rarely discussed in the workgroup.

NUMERICAL APPROACHES

Various numerical approaches have been developed to study the Soultz reservoir in the framework of the modeling Workgroup WG 5. The main goals were the diagnosis of methods to develop permeabilities and the optimization of test efficiencies. A special issue in Geothermics was published mostly from contributions of WG 5 in January 2007.
Models are at different stage of development and resulted in an individual support of the Soultz experiments. The following list provides an overview of the codes applied in the current phase by various scientific groups (see more extensive summary in Baujard et al., 2007).

- "3DEC" Code for Thermo-Hydro-Mechanical modelling of fractured rock (BRGM - Orléans, F)
- 3FLO" Code for Flow in fracture networks (BRGM - Orléans, F)
- "Code_Bright" for diffusive-advective transport (EOST - Strasbourg, F)
- "Convection" Code for Darcy flow and convection in a porous media (OMP - Toulouse, F)
- "Fracas" Code for hydraulic, thermal, solute and fracture mechanics (ENSMP Paris, F)
- "FRACHEM" Code for hydrothermal processes with chemistry (CREGE, Neuchâtel CH)
- "gPROMS" for heat, mass transfer and chemical reactions (NCSR "DEMOKRITOS", GR)
- "HDREC", thermal code for economical modeling (GTC Kappelmeyer, DE)
- "HEX-B2" Borehole simulator for hydrothermal and NaCl transport (GEOWATT Zürich, CH)
- "HEX-S" Code for hydrothermal processes and fracture mechanics (GEOWATT Zürich, CH)
- "Rockflow" Code for advection; conduction and viscosity effects (GGA Hannover, D)
- "SHEMAT" Code for coupled flow and heat transport (RWTH Aachen, D)

RESERVOIR MODELS: CHRONOLOGICAL DEVELOPMENT

The models mostly used at Soultz are the so-called reservoir models, which have for purpose to suggest interpretations or even predict the test results (stimulation, production, injection, circulation…) lead in the Soultz reservoirs. This family of codes improved in several ways these last years.
The modeled geometry of the reservoir taken in account went through several steps. The main milestones concerning the model geometries can be exposed so:

- Single Fracture models
- Large-scale 2D / 3D porous media models; dual porosity models
- Discrete fracture network (deterministic/stochastic)
- Simplified 3D reservoir models (porous/fractured media)

In parallel to the discretization structure the numerical codes must have the ability to account for numerous physical processes and individual constitutive laws and interactions:

- Linear / non linear hydraulics
- Non-miscible fluid flow
- Transport (thermal or tracers)
- Mohr-Coulomb criteria for hydro-mechanical interactions
- Thermo- poroelasticity
- Plastic deformation

FOCUSES AND MAIN ACHIEVEMENTS

The main focus of the numerical developments was on the reservoir behavior and on the evaluation of field tests. Generally, the model complexity increases with the number of physical mechanisms to consider. Major achievements in

the reservoir assessment are linked to mechanical interactions. The numerical codes used in this perspective integrate strong hydromechanical couplings to quantify the results of stimulation campaigns performed at Soultz. For the first time, the reservoir behavior was reproduced in numerical models before and during stimulation of the reservoir. Different kinds of data were used and the following goals were achieved:

Hydraulic stimulation

- For the first time, Graben-type reservoir behavior simulated before and during stimulation of the reservoir.
- It was showed that tensile fracturing can occur under certain conditions (stress field, low transmissivity)
- The technique of multi-well stimulation was investigated and models demonstrated its potential.
- Simulators could reproduce the evolution observed in the flowlogs due to mechanical stimulation of the reservoir

Use of seismic data

Microseismic events distribution in space, magnitudes and frequency of the seismic events were intensively used by different modeling teams:

- Several models reproduced accurately the derived hydraulic diffusivity computed with the development of the seismic cloud in time and space.
- The impact of the density of injected fluid on stimulation was discussed and modeled; it was shown that the use of heavy brine during stimulation can be important in the initial phase.
- The Gutenberg-Richter relation could be numerically reproduced.
- With models calibrated on GPK2 and GPK3 and flow-logs of GPK4, the stimulation of GPK4 in September 2004 (pressure response of the well and location / extension of seismic events) could be predicted

The use of hydrochemical couplings with simplified geothermal reservoir models allowed predicting the long-term reservoir behavior influenced by chemical reactions occurring in the reservoir.

Evaluations of the downhole parameters from single borehole (GPK3; GPK4) tests and from circulation tests in summer 2005 (production GPK2 and GPK4; injection GPK3) have been performed. It was shown that results from single borehole tests significantly differ from multi borehole tests. Discussion on the borehole simulator HEX-B applied to derive downhole pressure and temperature data from surface measurements were conducted in a dedicated workgroup meeting. It was concluded that a numerical simulation could hardly reproduce the critical relaxation periods of the well (“shut-in phases”) that may be of interest for scientists. But the reliable corrections obtained for injection or production phases (thus allowing the injectivity/productivity index evolution), demonstrated that the use of such a tool is complementary to downhole pressure and temperature measurements, and could participate to costs reduction. The results obtained with HEX-B during 2005-2007 were supplied to the members of WG 5.

UNRESOLVED CHALLENGES

In spite of the efforts of the different modeling teams, several scientific questions remained open and no satisfactory results could be obtained until now:

- The problem of the structure isolating GPK4 from the well-connected boreholes GPK2-GPK3 was deeply investigated in the modeling workgroup, but no satisfactory explanation could be found, as both assumptions (drain or cemented zone) could partially fit the data.
- Temperature prediction still remains problematic (single / multiple fracture models)
- The processes that could result from the geometries being established in the geological GoCad reservoir models have not been quantified. This should be realized in a following-up phase of the investigations in Soultz

Except the cooperation with the seismo-hydraulic workgroup (WG4), the links with the other existing workgroup have the potential for to be more extensively used by WG5. It is a major task of this Workgroup to quantify the analyses and proposed scenarios of other experts.

PERSPECTIVES

One of the first fields of research where modeling activities could bring an interesting contribution is the behavior of the reservoir under production conditions:

- Modeling of tracer tests/results
- Investigation of flow paths in the reservoir
- Temperature field evaluation
- Interaction between stress and fluid injections, influence of thermal stress

Numerical simulations also offer a great opportunity to investigate the long-term behavior of the reservoir:

- Evaluation of sustainable flow
- Long term behavior in pressure / flowrate / temperature

The influence of GPK4 or of additional boreholes on the system could also be investigated.

REFERENCES

C. Baujard, T. Kohl, T. Mégel, M. Rosener, D. Bruel, S. Portier, E. Stamatakis, H. Sulzbacher, M. Kühn, X. Rachez, M. Rabinowicz, 2007, "Modelling of the Soultz Reservoir: Different Approaches And Possible Benefits", EHDRA Scientific Meeting 2007